INTEGRATION OF OSCILLATING WATER COLUMN WAVE ENERGY CONVERTERS WITHIN MULTI-USE MARITIME STRUCTURES

by

Damon Peter Howe, BEng. (OE)(Hons)

National Centre for Maritime Engineering and Hydrodynamics
Australian Maritime College

Submitted in fulfilment of the requirements for the degree of Doctor of Philosophy

Supervisors:
Dr Jean-Roch Nader
Associate Professor Gregor Macfarlane

University of Tasmania
August, 2020

I declare that this thesis contains no material which has been accepted for a degree or diploma by the University or any other institution, except by way of background information and duly acknowledged in the thesis, and that, to the best of my knowledge and belief, this thesis contains no material previously published or written by another person, except where due acknowledgement is made in the text of the thesis.

Signed: ______________________

Damon Peter Howe

Date: 13/08/2020

Signed: ____________________

Damon Peter Howe

Date: 13/08/2020

Statement of Co-Authorship

The following people and institutions contributed to the publication of the work undertaken as part of this thesis:

Candidate: Damon Peter Howe, National Centre for Maritime Engineering and Hydrodynamics, Australian Maritime College, University of Tasmania

Author One: Jean-Roch Nader, National Centre for Maritime Engineering and Hydrodynamics, Australian Maritime College, University of Tasmania

Author Two: Gregor Macfarlane, National Centre for Maritime Engineering and Hydrodynamics, Australian Maritime College, University of Tasmania

Author Three: Jarrah Orphin, National Centre for Maritime Engineering and Hydrodynamics, Australian Maritime College, University of Tasmania

Contribution of work by co-authors for each paper:

Paper One (Chapter 3):

D. Howe and JR. Nader. "OWC WEC Integrated within a Breakwater Versus Isolated: Experimental and Numerical Theoretical Study". *International Journal of Marime Energy. 2017;20:165-182*

Author Contributions
Candidate: Conceived and Designed Experiment, Performed Experiment, Analysed the Data, Wrote the Manuscript, Reviewed the Manuscript
Author 1: Conceived and Designed Experiment, Contributed Reagents, Materials, and Analysis Tools, Reviewed the Manuscript

Paper Two (Chapter 4):

D. Howe, JR. Nader and G. Macfarlane. "Experimental Investigation of Multiple Oscillating Water Column Wave Energy Converters integrated in a Floating Breakwater: Energy Extraction Performance". *Applied Ocean Research. 2020 (Under Review)*

Author Contributions
Candidate: Conceived and Designed Experiment, Performed Experiment, Analysed the Data, Wrote the Manuscript, Reviewed the Manuscript
Author 1: Conceived and Designed Experiment, Contributed Reagents, Materials, and Analysis Tools, Reviewed the Manuscript
Author 2: Conceived and Designed Experiment, Contributed Reagents, Materials, and Analysis Tools, Reviewed the Manuscript

Paper Three (Chapter 5):

D. Howe, JR. Nader and G. Macfarlane. "Experimental Investigation of Multiple Oscillating Water Column Wave Energy Converters integrated in a Floating Breakwater: Wave Attenuation and Motion Characteristics". *Applied Ocean Research. 2020 (Under Review)*

Author Contributions
Candidate: Conceived and Designed Experiment, Performed Experiment, Analysed the Data, Wrote the Manuscript, Reviewed the Manuscript
Author 1: Conceived and Designed Experiment, Contributed Reagents, Materials, and Analysis Tools, Reviewed the Manuscript
Author 2: Conceived and Designed Experiment, Contributed Reagents, Materials, and Analysis Tools, Reviewed the Manuscript

Paper Four (Chapter 6):

D. Howe, JR. Nader and G. Macfarlane. "Performance Anlysis of a Floating Breakwater integrated with Multiple Oscillating Water Column Wave Energy Converters in both Regular and Irregular Seas". *Applied Ocean Research. Special Issue: Wave Energy Utilization 2020 (Under Review)*

Author Contributions
Candidate: Conceived and Designed Experiment, Performed Experiment, Analysed the Data, Wrote the Manuscript, Reviewed the Manuscript
Author 1: Conceived and Designed Experiment, Contributed Reagents, Materials, and Analysis Tools, Reviewed the Manuscript
Author 2: Conceived and Designed Experiment, Contributed Reagents, Materials, and Analysis Tools, Reviewed the Manuscript

Paper Five (Appendix C):

D. Howe, JR. Nader, J. Orphin and G. Macfarlane. "The Effect of Lip Extrusion on Performance of a Breakwater Integrated Bent Duct OWC WEC". In: *Proceedings of the 12th European Wave and Tidal Energy Conference. Vol. 2017, p. 1-9*

Author Contributions
Candidate: Conceived and Designed Experiment, Performed Experiment, Analysed the Data, Wrote the Manuscript, Reviewed the Manuscript
Author 1: Conceived and Designed Experiment, Contributed Reagents, Materials, and Analysis Tools, Reviewed the Manuscript
Author 2: Conceived and Designed Experiment, Contributed Reagents, Materials, and Analysis Tools, Reviewed the Manuscript
Author 3: Conceived and Designed Experiment, Performed Experiment, Reviewed the Manuscript

Paper Six (Appendix D):

D. Howe, JR. Nader and G. Macfarlane. "Experimental Analysis into the Effects of Air Compressibility in OWC Model Testing". In: *AWTEC 2018 Proceedings. National Taiwan Ocean University, 2018, p. 449*

Author Contributions
Candidate: Conceived and Designed Experiment, Performed Experiment, Analysed the Data, Wrote the Manuscript, Reviewed the Manuscript
Author 1: Conceived and Designed Experiment, Contributed Reagents, Materials, and Analysis Tools, Reviewed the Manuscript
Author 2: Conceived and Designed Experiment, Contributed Reagents, Materials, and Analysis Tools, Reviewed the Manuscript

Paper Seven (Appendix E):

D. Howe, JR. Nader and G. Macfarlane. "Integration of Wave Energy Converters within Floating Offshore Structures". In: *Proceedings of the Australasian Coasts and Ports Conference. Hobart, Tasmania, 2019.*

Author Contributions
Candidate: Conceived and Designed Experiment, Performed Experiment, Analysed the Data, Wrote the Manuscript, Reviewed the Manuscript
Author 1: Conceived and Designed Experiment, Contributed Reagents, Materials, and Analysis Tools, Reviewed the Manuscript
Author 2: Conceived and Designed Experiment, Contributed Reagents, Materials, and Analysis Tools, Reviewed the Manuscript

Papers One, Two, Three and Four are peer-reviewed journal publications whose contents are fundamental to the research conducted throughout this thesis. Subsequently, the contents of these papers can be found in Chapters 3, 4, 5 and 6 respectively, which have been altered from their published form to adhere to the thesis guidelines. Papers Five, Six and Seven were additional works conducted by the candidate which were published as peer-reviewed conference papers. While the contents of these papers pertain to the works conducted throughout this research project, they consist of preliminary and/or complementary research which aided the works presented throughout this thesis. These papers have been included in their published form as Appendices C, D and E.

We the undersigned agree with the above-stated proportion of work undertaken for each of the published and/or submitted peer-reviewed manuscripts contributing to this thesis.

Signed: ______________________________

Doctor Jean-Roch Nader

Primary Supervisor

National Centre for Maritime Engineering and Hydrodynamics

Australian Maritime College

University of Tasmania

Date: 13/08/2020

Signed: ______________________________

Associate Professor Gregor Macfarlane

Secondary Supervisor

National Centre for Maritime Engineering and Hydrodynamics

Australian Maritime College

University of Tasmania

Date: 13/08/2020

Signed: ______________________________

Doctor Vikram Garaniya

Head of School

National Centre for Maritime Engineering and Hydrodynamics

Australian Maritime College

University of Tasmania

Date: 13/08/2020

ABSTRACT

Ocean energy presents arguably one of the most rich renewable energy solutions currently under exploration, and consists of a variety of potential resources including tidal barrages, salinity gradients and ocean thermal energy. However two sources, tidal currents and ocean waves, are considered by many as the most promising and have subsequently observed the greatest development in recent decades. Ocean waves offer a predictable, dense and virtually untapped energy resource with potential to significantly contribute towards the rising global energy demands. A number of prototype failures and subsequent lack of long term commercial deployments has consequently impacted the development of Wave Energy Converter (WEC) technologies, such that the technologies are considered immature and currently economically uncompetitive with renewable energy counterparts such as wind and solar. To combat the economic argument, a number of solutions have been devised to reduce the high costs currently associated with ocean wave energy, one of which is integration within maritime structures to create synergistic multi-purpose platforms.

While concepts have been formulated for the integration of various WEC technologies, the Oscillating Water Column (OWC) WEC is favoured as a predominant devices for implementation due to its rigid design, capability for incorporation within solid edifices, and relative ease of maintenance due to all moving parts above water. The OWC device's operational principle, in its most elementary form, utilises incident wave interaction to oscillate a trapped column of water inside the chamber, subsequently operating in a 'piston-type' motion to force air in and out of a turbine. The economic benefits of OWC device integration encompass both the capital and operating expenditure, from costs shared during the construction, through to the reduction in maintenance and grid connection costs, ultimately making the concept more competitive within the renewable energy sector. With some full scale demonstration cases and commercial devices currently operational, the vast majority of maritime structure integrated WECs target bottom-mounted breakwaters, which are typically depth limited due to the economic constraints associated with deep water construction. This type of integration restricts the operational range of the concept to onshore/nearshore regions; however, with the expansion of many blue economy industries into offshore regions, opportunities arise for exploration of wave energy conversion to serve in deeper waters. In order to migrate from the nearshore integrated concepts, integration within floating offshore structures, such as breakwaters and offshore platforms, must be explored for viability from both economic and

operational perspectives. Understanding the hydrodynamic performance of OWC devices integrated within maritime structures, both fixed and floating, is the focus of this research project.

Initial stages of the research project considered a detailed model scale experimental investigation regarding integrated OWC device performance, which was conducted to explore two specific parameters respective impact on OWC device energy absorption; firstly, the cross-sectional geometry, and secondly, breakwater integration. An isolated OWC device of rectangular cross-section was compared to a previously researched device with a circular cross-section of equivalent area to explore the impact on energy absorption, where negligible difference in performance was observed between the geometrically varying devices. Following this realisation, both respective devices were incorporated within a model scale, gravity-based breakwater to compare the extraction efficiency of the devices between both isolated and integrated configurations. The results obtained indicated that the energy absorption capacities of the OWC devices are significantly improved through breakwater integration, with the rectangular OWC device recommended due to its orthogonal construction allowing for less complex incorporation. This research provided a foundation for the performance of OWC device integrated maritime structures, and enhanced the potential for OWC device integration within floating offshore structures.

Development of the project generated a second comprehensive model scale investigation designed to establish a proof-of-concept for a floating breakwater integrated with multiple OWC devices. A generic π-type, soft-moored breakwater was integrated with a modular number of OWC devices and subjected to both regular and irregular sea states to analyse how variations to device configuration, breakwater width, pneumatic damping, wave height and motion constraints impact two overarching parameters; the energy absorption of the integrated OWC devices, and the performance of the floating breakwater. The investigation yielded substantial insights regarding the beneficial impact OWC device integration can have on the motion characteristics of the floating breakwater, while minor reduction was simultaneously observed for wave transmission and reflection. The investigation also highlighted the importance of device spacing with respect to OWC device performance, where insufficient spacing was found to have a detrimental impact on energy absorption where destructive device-device interference was observed. Through specific configuration of the aforementioned design parameters, the WEC/breakwater concept was able to obtain total device conversion efficiencies of up to approximately 80% at resonance in regular waves, and observed equivalent performance in irregular waves. This project reveals that maritime structure integration of OWC WECs provides significant benefits to the hydrodynamic performance of the integrated devices, which in association with the previously established economic benefits, further strengthens the viability of the concept, and provides foundation for future development.

ACKNOWLEDGMENTS

My project has provided me with the privilege and pleasure of working with many people that deserve acknowledgement, however there are a number of important people I must explicitly display thanks toward.

I wish to sincerely thank my supervisory team; Dr Jean-Roch Nader and Assoc. Prof. Gregor Macfarlane, for the support, guidance and mentorship you have both provided me with throughout the duration of my PhD project. Your supervision and expertise was invaluable, and you helped create an environment which made my time during this PhD enjoyable. I would also like to acknowledge the Australian Maritime College's renewable energy team for their support and contributions towards my project.

I acknowledge the technical support provided during my project by the model test basin and towing tank staff; particularly Mr Kirk Meyer, Mr Tim Lilienthal, Mr Liam Honeychurch, Mr Adam Rolls, Mr Tristan Bauer and Dr Nick Johnson. If not for your assistance during the design, construction and setup stages of the experimental investigations, this project would not have been possible. Similarly, I acknowledge and convey thanks to those who played small but important roles during my experiments; Robert Daly, James McGregor, Yon Chen Ling, Chun Ken Thum, Jason Burns, Thomas Fallon, Hayden Chrzanowski, Marc Holstenkamp and Steven Ogbebor.

To my AMC colleagues, and fellow PhD candidates in the research hub, thank you for your contributions toward making my project a great experience. In particular, thanks to Jarrah Orphin for your ongoing support throughout this project, along with your insights and feedback regarding the intricacies of wave energy.

Last but not least, I wish to thank and share appreciation for the support provided by my family throughout my PhD research. To my wife to be Caitlin, your support, encouragement and love has allowed me to pursue my aspirations and I am forever grateful for all you have done for me throughout this time. To my parents Bronwyn and Simon, my nan and pop Marlene and Bernie, my sisters Brielle and Teegan and the rest of my family, thank you for your ongoing love and encouragement which has helped me towards completing this project.

In Loving Memory of

Deon Timothy Howe

(26/03/1965 - 26/01/2001)

TABLE OF CONTENTS

LIST OF TABLES

LIST OF FIGURES

NOMENCLATURE

Greek Symbols

Symbol	**Description**	**Units**
δ	Pneumatic Damping Coefficient	kg/m^{4}s
η_0	Incident Wave Amplitude	m
η_d	Diffracted Wave Amplitude	m
η_{OWC}	OWC Chamber Free Surface Amplitude	m
$\overline{\eta_{OWC}}$	Mean OWC Chamber Free Surface Amplitude	m
η_r	Reflected Wave Amplitude	m
η_t	Transmitted Wave Amplitude	m
λ	Incident Wave Length	m
ρ	Mass Density of Fluid	kg/m^3
ϕ	Incident Wave Phase	rad
ω	Incident Wave Frequency	rad/s

Roman Symbols

Symbol	Description	Units
A	Transverse Cross-Sectional Area of Basin	m^2
$A_{\eta_{OWC}}$	OWC Chamber Free Surface Amplitude	m
$A_{\overline{\eta_{OWC}}}$	Mean OWC Chamber Free Surface Oscillation Amplitude	m
A_m	Six Degree of Freedom Motion Amplitude	m or °
A_p	OWC Chamber Dynamic Pressure Amplitude	Pa
$A_{\overline{v_s}}$	OWC Chamber Free Surface Mean Velocity Amplitude	m/s
A_{v_s}	Free Surface Velocity Amplitude	m/s
A_x	Submerged Transverse Cross-Sectional Area	m^2
C	Wave Celerity	m/s
C_g	Wave Group Velocity	m/s
D	OWC Inlet Height	m
d	Draft of Breakwater	m
e	OWC Chamber Lip Extrusion	m/s
f_n	Natural Frequency	Hz
f_p	Peak Frequency	Hz
g	Gravitational Acceleration	m/s^2
H	Incident Wave Height	m

h	Water Depth	m
h_b	Height of Breakwater	m
h_p	Height of Breakwater Pontoon	m
H_s	Significant Wave Height	m
l_b	Length of Breakwater	m
P	Hydrodynamic Power Absorbed	W
p_c	OWC Chamber Dynamic Pressure	Pa
P_h	Mean Hydrodynamic Power Absorbed	W
P_{h_t}	Total Mean Hydrodynamic Power Absorbed	W
P_I	Incident Wave Power	W
Q	Volume Flux	m^3/s
S_c	OWC Device Cross-Sectional Area	m^2
S_{η_0}	Linear Incident Wave Spectrum	m^2/Hz
S_{η_m}	Linear Motion Spectrum	m^2/Hz
$S_{\eta_{OWC}}$	Linear OWC Free Surface Elevation Spectrum	m^2/Hz
T	Incident Wave Period	s
T_e	Wave Energy Period	s
t	Time	s
t_c	OWC Chamber Wall Thickness	m

v_s	OWC Chamber Free Surface Velocity	m/s
$\overline{v_s}$	Mean OWC Chamber Free Surface Velocity	m/s
W	OWC Inlet Width	m
w_b	Width of Breakwater	m
w_p	Width of Breakwater Pontoon	m

Dimensionless Numbers

Symbol	Description	Definition
$A_{Q'}$	Non-Dimensional Volume Flux Amplitude	$\frac{A_{\overline{\eta_{OWC}}}}{\eta_0}$
c_R	Coefficient of Wave Reflection	$\frac{\eta_r}{\eta_0}$
c_T	Coefficient of Wave Transmission	$\frac{\eta_t}{\eta_0}$
E'	Normailised Error	$\frac{S_{\eta_{mes}} - S_{\eta_{est}}}{max(S_{\eta_{mes}})}$
$H_{\eta_{AF}}$	Wave Amplification Factor	$\frac{\eta_{OWC}}{\eta_0}$
k'	Diffraction Coefficient	$\frac{\eta_d}{\eta_0}$
$\tilde{L}_{pc}$	Non-Dimensional Capture Width	$\frac{P_h}{P_I W}$
$\tilde{L}_{pc_m}$	Mean Non-Dimensional Capture Width	$\frac{\sum_1^n \tilde{L}_{pc_n}}{n}$
m	Blockage Parameter	$\frac{A_x}{A}$
p'_c	Non-Dimensional Pressure	$\frac{p_c}{\rho g H}$
Q'	Non-Dimensional Volume Flux	$\frac{\overline{v_s} S_c}{\omega \eta_0 S_c}$
γ	Peak Enhancement Factor	-
ϵ	Hydrodynamic Power Absorption Efficiency	$\frac{P_{h_t}}{P_I L}$

ABBREVIATIONS

AMC	Australian Maritime College
BBDB	Backwards Bent Duct Buoy
CAPEX	Capital Expenditure
DoE	Design of Experiment
DOF	Degree of Freedom
DRE	Data Reduction Equation
FEM	Finite Element Method
IQR	Inter-Quartile Range
ITTC	International Towing Tank Conference
IWP	Incident Wave Probe
LCOE	Levelised Cost of Energy
LDV	Linear Damping Value
LIMPET	Land Installed Marine Power Energy Transmitter
LRET	Large Renewable Energy Target
MTB	Model Test Basin
OPEX	Operational Expenditure
ORE	Ocean Renewable Energy
OWC	Oscillating Water Column
PTO	Power Take-Off
PWP	Phase Wave Probe
RAO	Response Amplitude Operator
RWP	Reflection Wave Probe
TRL	Technology Readiness Level
TWP	Transmission Wave Probe
WEC	Wave Energy Converter

Chapter 1

Thesis Introduction

1.1 Current Status of Ocean Wave Energy

1.1.1 Ocean Renewable Energy

As global political and environmental climates change, so too does investment in energy production. Many countries are actively committing towards reducing their carbon footprint by evolving from carbon-producing fossil fuel generated power, to investing in sustainable renewable energy resources. This considerable shift from fossil fuel derived energy has resulted in a significant rise in research and development for renewable energy systems; from the more established technologies such as hydropower and wind, through to emerging fields such as ocean energy. In the current global energy market, trajectories indicate that reliance upon fossil fuel generated electricity is set to decrease, while renewable energy generated electricity will increase and fill the void [1]. While the environmental benefits are apparent, the economic benefits of energy resources that do not deplete over time are often insufficiently recognised [2]. As of the end of 2018, the global energy share between non-renewable and renewable energy resources was estimated at 73.8% and 26.2% respectively [3], with hydropower (60.3%), wind (21.0%) and solar (9.2%) accounting for approximately 90.3% of the renewable energy share. Other resources identified as key contributors towards renewable energy generation include bioenergy, geothermal energy and ocean energy, whose respective technologies are reviewed in the Special Report on Renewable Energy Sources and Climate Change Mitigation (SRREN) [4], which was produced and published by the Intergovernmental Panel on Climate Change (IPCC). Installation of onshore wind and solar projects continue to increase annually despite the geographical spatial requirements associated with commercial scale farms [5, 6], and the impact of public perception [7–9]. These factors may lead toward a reduction in future installation rates, potentially opening the door for other renewable energy sources such as ocean wave energy to contribute towards the global renewable energy share.

Ocean Renewable Energy (ORE) provides one of the most profuse, predictable and dense renewable energy resources worldwide; yet to date, is virtually untapped relative to the vast resource it presents [10–13]. ORE is often subdivided into categories pertaining to the variety of differing renewable resources encompassed within the ocean, which include; tidal barrages, salinity gradient and ocean thermal energy to name a few [14], however tidal stream and ocean wave energy present two of the most promising resources for ocean energy extraction [15]. The estimated value for the oceans technical energy potential, considering all aforementioned subcategories of ORE, is 91 944 TWh [16, 17]. For perspective, the global electricity demand for 2018 was approximately 22 200 TWh [18], less than a quarter of the estimated potential ocean energy, illustrating the immense resource the ocean could provide. Though it is unrealistic to contemplate meeting global electricity demands solely via ocean energy, there is significant potential for ORE to provide support in the ever-growing renewable energy sector. Considering specifically ocean wave energy, the worldwide theoretical resource has been estimated to be approximately 32,000 TWh/yr [4], however the technical potential is predicted to be substantially less and is dependent upon wave energy conversion technology development. More recent estimates indicate the resource to be approximately 18 480 TWh/yr [19], with a number of region specific resource assessments highlighting the potential for ocean wave energy worldwide [20–27]. Australia, being an island nation, has one of the largest ocean wave energy resources of any country [20], with a recent assessment indicating an approximate value of 1796 - 2730 TWh/yr [28]. For perspective, Australia's total electricity generation for the 2018 calendar year, considering both renewable and non-renewable generation sources, was estimated to be 261 TWh [29]. With 90% of the Australian population living within 100 km of the coastline [30], harnessing the significant available resource in close proximity to the dense populous could provide a number of environmental and economic benefits. Figure 1.1a illustrates the wave energy available to Australia, while Figure 1.1b highlights the Australian population distribution.

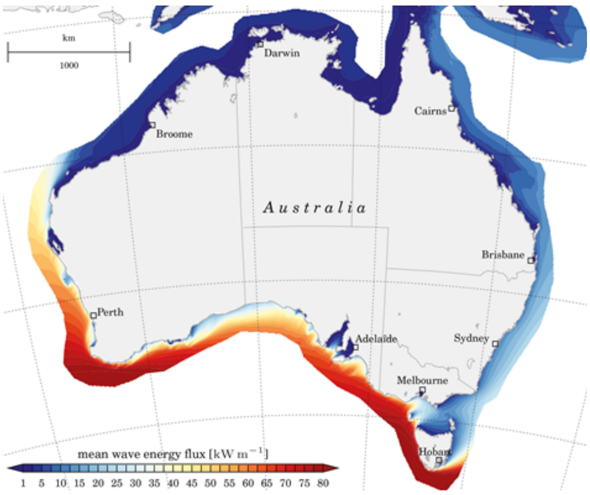

(a) Annual Mean Wave Energy Flux [28]

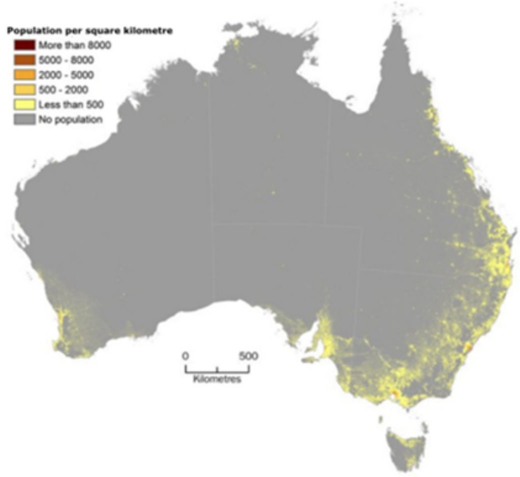

(b) Population Density 2018 [31]

Figure 1.1: Australian maps indicating wave energy potential and population distribution

Currently, the Australian Government has committed to 33,000 GWh/yr of renewable energy generation by 2020 as part of the Large-scale Renewable Energy Target (LRET), the value of which was downgraded from 41,000 GWh/yr in 2015 [32]. While the LRET was met in September 2019 [33], Australia has no current policy to govern the renewable energy target beyond 2020; however, with commitment to the Paris Agreement, Australia has vowed to reduce greenhouse gas emissions to 26 - 28% below 2005 levels by 2030 [34]. To achieve this, further commitment to increasing the presence of renewable energy generation within the Australian market will be required, providing opportunity for development of ocean wave energy technologies.

Unlike the technology developed for wind and solar energy conversion, ocean wave energy is yet to converge on a universal technology for conversion [35]. Despite a large variation in concept designs, WECs can generally be categorised into three predominant types [36];

1. **Attenuators:** which are positioned perpendicular to the wave crest and 'ride' the waves.
2. **Point Absorbers:** which are of small dimensions relative to wave length and typically heave up and down either on or below the water surface.
3. **Terminators:** which typically operate parallel to the wave crest and physically intercept waves.

Each of the aforementioned WEC types can then be subdivided into classes based upon their mode of operation, by which they are more commonly recognised. A number of WEC technology reviews identify these classes to be; submerged pressure differential devices, oscillating wave surge devices, oscillating water column devices, overtopping devices and oscillating body devices [12, 36–38], and provide detailed characterisation regarding the mode of extraction and examples of pre-commercial concepts that adopt the operation. Figure 1.2 categorises a number of wave energy converter devices with respect to operational principle and region of operation, highlighting the diversity of current technology. The potential for variation amongst these classes has resulted in over 100 different wave energy converter technologies to be developed; yet, few have been tested at pre-commercial or full scale.

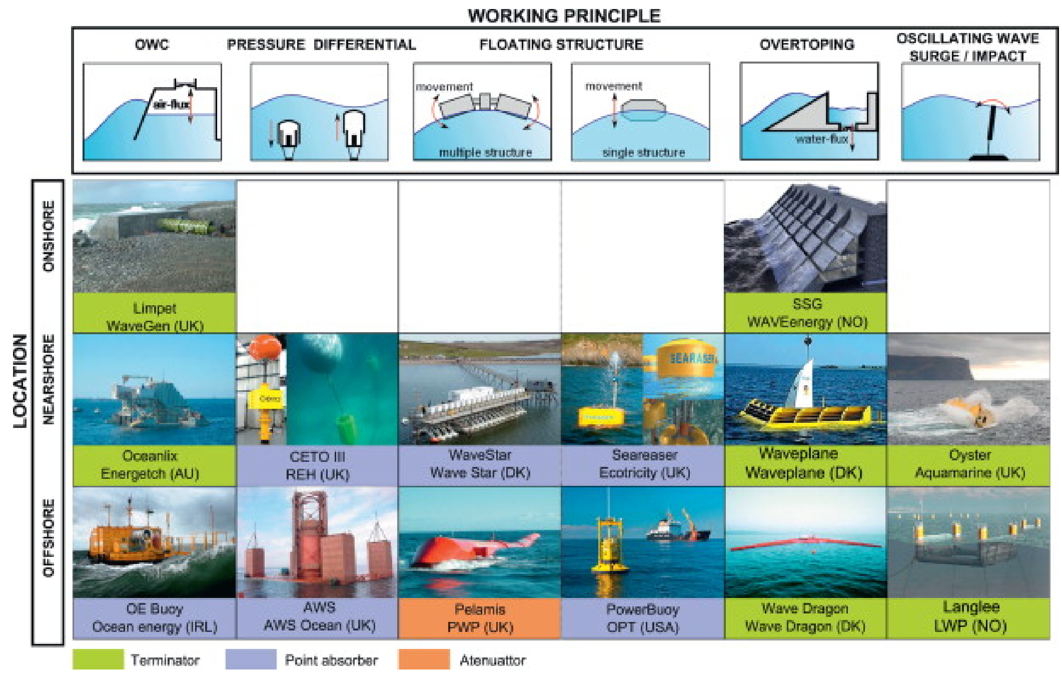

Figure 1.2: Wave energy conversion technology classified by mode of operation and region of operation. Image credit: [36]

1.1.2 Applications for LCOE Reduction

While a world-class wave resource is readily available for Australia, very little has been achieved by means of commercial scale wave energy development. A number of pre-commercial prototype failures, as well as failure to meet stakeholder deliverables, has had a detrimental impact on the public perception of ocean wave energy's capability to provide sustainable energy generation. As a consequence, development of WEC technology within Australia observed a period of reduced activity. The major challenge that ocean wave energy currently faces is the high costs affiliated with WEC technology [12, 37]. Currently, the first commercial scale ocean wave energy array is expected to have a Levelised Cost of Energy (LCOE), a metric which relates lifetime energy production to capital and operational costs, of approximately USD$120 - $1058 per MWh [39, 40]. In comparison, the 2022 predictions for wind and solar are approximately USD$55.8/MWh and USD$73.7/MWh respectively [41], which are considerably less than that predicted for ocean wave energy. The large LCOE value range presented for ocean wave energy is in relation to an offshore array configuration of devices, and results from lack of commercially available and proven concepts from which valuable input data can be obtained, along with the generalised immaturity of the technologies across the sector attributes to the significant variation in values, hence providing a relatively unfair comparison. Consequently, most existing studies regarding LCOE predictions for wave energy rely on "hypotheticals" to devise evaluations [42–45]. Hence, in order for future development and commercialisation of wave energy to occur, significant reduction in the high associated costs is necessary.

To combat the high LCOE of ocean wave energy, two major applications have been derived and considered for WECs. The first of which are array configurations; which entails implementing the devices in a structured grid formation to produce an array or 'farm' of devices that work in synchronisation to harness wave power and convert it into a usable form of energy. This application of the technology is yet to be implemented at the prototype scale of testing, however an increase in research regarding this concept by means of theoretical, numerical [46–50], and experimental investigations [51–55] provides a foundation for the future development of the concept. A review of numerical modelling for arrays of wave energy converters was conducted by Folley et al. [56], highlighting the aims, underlying principles, pros and cons, and results of the main numerical methodologies utilised for this application.

The second application that provides potential for LCOE reduction, and the foundational concept for this research project, is the integration of WECs into pre-existing or in-development maritime structures, such as harbours or breakwaters. Successful integration of WECs within breakwater design (both fixed and floating) allows the concept to synchronously achieve the traditional operational purpose of environmental protection, in terms of leeside sheltering, with the additional benefit of renewable energy generation, subsequently creating a multi-purpose platform. In addition to the aforementioned benefits, these multi-purpose structures can also provide valuable 'space' in the maritime environment capable of supporting topside infrastructure. Above-water area presents a significant commodity for many maritime industries, particularly in the offshore region, and has potential to assist on-water operations such as material/consumable storage and accommodation among other industry specific requirements. The reduction in LCOE through integration of WECs within maritime structures encompasses both the CAPEX costs, where costs can be shared during construction, and OPEX costs, where accessibility associated with a nearshore or onshore maritime structure could reduce the costs affiliated with maintenance and grid connection. Feasibility studies of breakwater integrated WEC systems have been conducted, which identified that the total additional cost increment for WEC integration would be approximately 4% of the total breakwater cost, where the OWC breakwater represents appoximately 30% of the breakwater structure, and the predominant cost influence was the non-commercialised Power Take-Off (PTO) system requirements [57, 58]. The benefits of maritime structure integration are not exclusively economic. Devices also observe improved reliability and extended lifetime due to the additional strength and support provided by the breakwater during heavy wave and/or storm conditions.

1.1.3 The Oscillating Water Column WEC

Of the aforementioned WEC classes, the oscillating water column WEC presents one of the most promising technologies for maritime structure integration. This is attributed primarily to; its rigid construction, allowing for reduced complexity associated with integration into solid edifices, and the positioning of all moving parts above the waterline, which increases reliability and reduces maintenance costs. The OWC WEC is one of the most researched and developed technologies utilised to harness ocean wave energy, with literature of the concept first published by Masuda in 1971 [59], and origins dating back as far as 1910 [13]. Following this, Evans published a paper describing the operation and efficiency of Masuda's floating type OWC WEC by means of analytical and theoretical analysis [60], providing the foundation for wave energy extraction via the OWC device, and leading to development and refinement of the operating principles in the early years of the concept [61–63]. Typical OWC device operation considers a trapped column of water within the device chamber moving in a piston-type motion when excited by incident wave interaction. The fluctuating water column interacts with a trapped pocket of air in the pneumatic chamber, subsequently generating an oscillatory airflow, which is harnessed to produce electricity as it passes through the PTO system, typically an air turbine coupled with an electric generator. Figure 1.3 illustrates the power and information flow for a generic bent duct type OWC device.

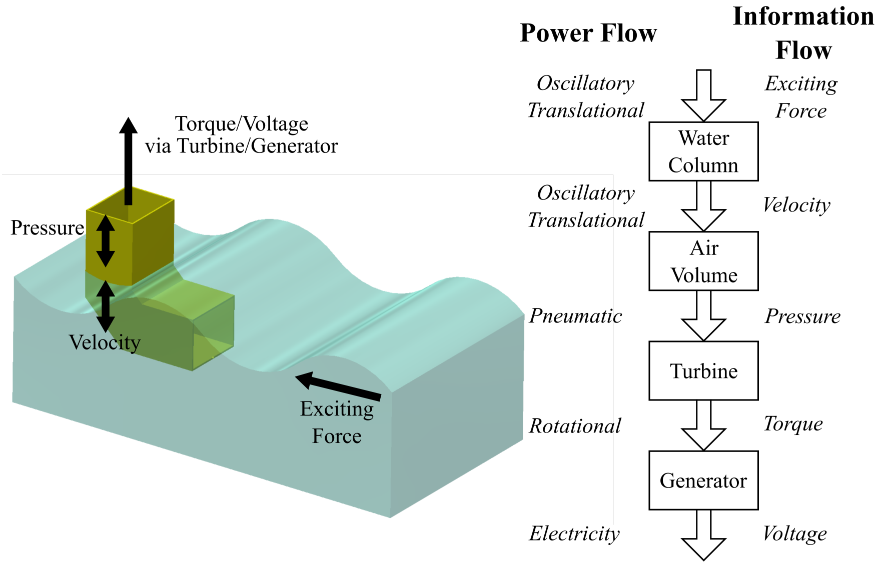

Figure 1.3: Power and information flow for mode of operation for an oscillating water column device.

Of the OWC WEC variations, the bent duct type OWC device presents a well researched and developed concept explored for both fixed and floating configurations. The bent duct type OWC device is a geometrically shaped chamber that has vertical, horizontal and diagonal sections. The cross-sectional geometry of the devices, (rectangular and circular utilised throughout this research project), follow a predetermined swept path to form the chamber of the device, as is later illustrated in Section 2.1.1. The vertical section of the device pierces the waterline to create a free surface within the chamber, whilst the remainder of the device is submerged. There are currently two OWC devices that are referred to as a bent duct type OWC device, the first of which is the Backward Bent Duct Buoy (BBDB) as found in [64–70], which was developed by Yoshio Masuda [71]. This device is constructed as a floating buoy device tethered to the seabed, which is positioned so the inlet of the device faces in the same direction as the incident wave propagation. The operating principle of the device remains the same as other OWC devices in that a volume flux of air created by wave interaction drives a turbine to produce electrical power. However, in this case the relative motions, heave, surge and sway are enhancing factors for energy production and therefore the technology is inappropriate for fixed breakwater implementation, yet could be considered for floating breakwater integration if motions were not a governing design constraint. Currently, one particular technology adopting the BBDB design, the OE buoy [72], which completed 1:4 scale testing in Galway Bay, Ireland in 2011 [73], is in the final stages of development as a pre-commercial unit rated at 1.25 MW is set to be tested at the US Navy Wave Energy Test Site on the coast of O'ahu, Hawaii.

The second bent duct device is the fixed bent duct OWC concept, such as that used throughout this research, and also found in [74–81]. It is constructed as was previously described, which results in the formation of a rigid structure. The device is then fixed in position so the inlet of the device faces the incoming waves with the upper section of the device piercing the water surface. A key aspect of the fixed bent duct type OWC device is that the natural frequency of the device can be varied through the extension and reduction in the length of the submerged duct, subsequently varying the length of the swept path. This is an advantage as it can be customised to suit site-specific wave patterns and conditions to optimise the extraction efficiency. As of 2019, an Australian wave energy company, Wave Swell Energy, is planning to deploy their 200 kW Uniwave® OWC device, which adopts the bent duct type profile, on the South-East coast of King Island, Tasmania. The isolated, full-scale prototype is a gravity-based structure which sits on the seabed with an inlet facing the direction of incoming incident wave propagation, and offers the world's first 'vented' OWC concept, utilising only one stroke of the internal free surface oscillation, which is discussed further in Section 1.1.4.

Regarding the hydrodynamic power absorption capacity of an OWC device, a number of key parameters in design of an OWC device have been identified, which include; the internal chamber pressure and the power take-off damping. These parameters have been numerically [82–86], and experimentally [87–89], explored for their influence on OWC device energy extraction. Results of these studies indicate that turbine damping was the factor that most significantly affected the performance of the OWC device, even more so than tidal variations and wave conditions [87]. Hence, manipulation of the turbine damping to tune the device results in significant changes in the hydrodynamic efficiency of the OWC device, as the mean power output of the device is directly related to both the PTO damping coefficient, and the internal pressure. The damping characteristics of a turbine, which indicates the relationship between internal chamber pressure and volume flux of air, can vary from a linear relationship as observed for the Wells type turbine, through to a quadratic or non-linear relationship displayed by impulse turbines.

The development of fixed, stand-alone OWC devices has resulted in a number of full scale demonstration cases to be deployed. Typically these devices have been shoreline power plants that operate through incorporation of a concrete caisson with an open bottom to the sea, subsequently creating an air chamber. The devices are often built into recesses in rocky cliffs or on the sea floor, surrounded by vertical cliffs or open ocean. The operational capacity of these types of devices, as with other OWC devices is dependant upon the design of the device, and the sea state in which the device operates. Given the operating environment characteristics, the operational capacity of devices can range from a few hundred kW up to a few MW, with demonstration case devices proven to operate within this range. The first device of this type to be deployed at full scale was a demonstration plant built in Toftestallen, Norway. The plant was constructed in 1985 and operated on a cliff face recess for approximately three years before it was damaged by a severe storm, subsequently resulting in decommission shortly thereafter. The device had a 500 kW operational capacity, and represented one of the first fixed structure onshore plants to operate [90, 91]. Following the installation of this device was the construction of two more recognised fixed onshore OWC devices, namely the Pico OWC plant operating in Pico, Azores, Portugal, and the LIMPET device in Islay, Scotland, UK. The first of these two devices to be constructed was the Pico plant in 1999. The device is a bottom standing OWC situated adjacent to a vertical cliff that offers several rocky shoreline gully formations, which provides a natural energy concentrating characteristic. Although construction was completed in 1999, the device only ran its first tests in 2005 due to technical issues; however, as a result of these issues the device had been significantly improved whereby it performed at an operational rating of 400 kW [92–94], up until it ceased operation in October 2018.

Figure 1.4: LIMPET OWC device installed on the island of Islay, Scotland. Image Credit: [95]

The LIMPET (Land Installed Marine Power Energy Transmitter) plant, pictured in Figure 1.4, completed construction and was commissioned in 2000 originally equipped with 500 kW Wells turbine, however was downgraded to a 250 kW version [96]. The device was constructed in a recess carved into a rocky cliff, and was operational from its inception up until 2018 when it was decomissioned. While sustaining some commercial energy generation, the LIMPET device was primarily used as a test facility for turbine design by Voith Hydro Wavegen, where they develop their commercial concepts. Due to the turbine testing, the facility logged over 60 000 hours of turbine operation, and the concept design provided foundation for other full scale OWC device installations including the Mutriku breakwater. Review of the LIMPET devices design, construction and operation can be found in [97, 98]. In addition to these original full-scale prototypes, a number of other fixed structure devices have been constructed and deployed including OSPREY (Scotland) [99, 100], greenWAVE (Australia) [101, 102] and Trivandrum OWC (India) [103].

1.1.4 Power Take-Off Systems

OWC WECs typically utilise airflow on both the up-stroke (exhalation) and down-stroke (inhalation) of the free surface to extract hydrodynamic energy. To achieve this, OWC devices generally require an air turbine with the capacity to observe unidirectional rotation while under the influence of this bidirectional airflow. While a number of differing turbine options have been developed for OWC devices, the two most common are the Wells' type [104], and impulse type [105] turbine variations. The Wells type turbine was invented and patented by Dr. Alan Arthur Wells (1924-2005) in 1976. The design presented one of the first concepts of a self-rectifying turbine that allowed for oscillatory airflow without the need for a system of non-return valves. The turbine is considered one of the simplest and most economical turbines for wave energy conversion. Although being quite economical, previous studies have identified that the turbine has some inherent disadvantages, the most prominent of which are low efficiency at high flow coefficient and poor starting characteristics [106–108]. A favourable characteristic of the Wells turbine is the approximately linear relationship the turbine has between the internal pressure of the device and volumetric flow. Variations in the design to improve the disadvantages have been proposed [109–111], which look to reduce the noise and maintenance due to high rotational speed associated with Wells turbines. A comprehensive review of Wells turbines was published in 1995 detailing the application for wave energy conversion [112]. The Wells turbine has also been adopted/tested in a number of full scale demonstration cases, such as in the LIMPET device on the Isle of Islay, Scotland, pictured in Figure 1.5a [92, 113, 114].

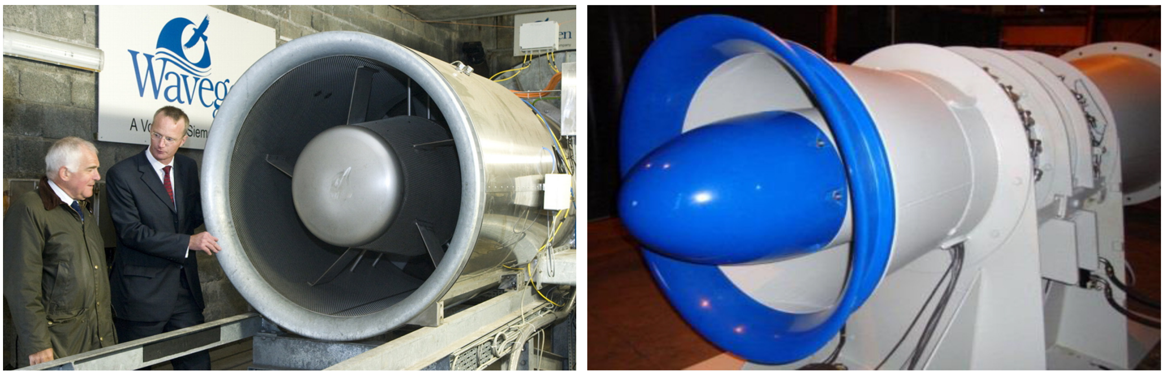

(a) Wells Tubine - LIMPET. Image Credit: [115]   (b) Impulse Turbine - OE Buoy. Image Credit: [95]

Figure 1.5: Commonly adopted bi-directional air turbines variations for OWC devices.

The second of the two most frequently adopted turbines for wave energy conversion is the self-rectifying impulse turbine as found in Figure 1.5b, which observes a quadratic damping relationship, differing from the linear relationship observed for the Wells turbine. Many variations in the design of impulse turbines have been produced since their inception to the wave energy extraction field as can be found in [116]. The advantages of the impulse turbine include; improved starting characteristics in comparison to the Wells turbine, widened range of flow rates at which suitable efficiencies are delivered, and lower operational speeds, hence reduced noise levels and maintenance issues compared to Wells turbines. A common type of impulse turbine includes a variable pitch mechanism for the guide vanes and/or rotor blades, an example of which can be found in [117]. However, the inclusion of variable pitch mechanisms inherently requires robust mechanical design and higher associated costs. Though the operational flow range of the impulse turbine is improved compared to the narrow range of the Wells turbine, the peak efficiency of the impulse turbine rarely exceeds 50%, whereas the Wells turbine has been proven to achieve a peak efficiency of approximately 75% under laboratory conditions [95]. Mean conversion efficiencies of the Wells type and impulse type turbines have been found to be approximately 30% and 47% respectively [117]. However, recently developed 'vented' OWC devices (as mentioned in Section 1.1.3), which exploit only the down-stroke of water column motion, have utilised one-way air turbines with typical efficiencies of 77.5%, resulting in performance equivalent to the bidirectional devices [118]. This type of device is able to target the inhalation process on the down-stroke through specially designed flap valves, which open during the up-stroke, allowing for undamped water column rise, subsequently increasing the magnitude of the down-stroke, allowing for unidirectional air flow, and integration of traditional air turbines.

1.1.5 OWC Device Integration - Breakwaters

The aforementioned benefits of OWC device integration within maritime structures has resulted in the development of a number of full scale demonstration and commercial device deployments, covering both fixed and floating structures. While only a few remain currently operational, the knowledge gained from these cases provided a foundation for the development of future concepts. Pushes for industries such as aquaculture and offshore wind to expand operations into deeper waters presents the opportunity for further expansion of the breakwater integrated WECs from traditional fixed structures, which have been adopted in most full-scale demonstration cases, into floating breakwater concepts. Excluding the stand-alone floating type OWC devices, which rely predominantly on device motions under incident wave interaction for energy extraction, few studies have been conducted regarding the integration of wave energy conversion devices within floating breakwaters, where structure motion is desirably minimal. Mustapa et al. conducted a review on breakwater integrated WEC systems which highlights OWC devices as the most common WEC technology for integration [119].

Fixed

Fundamental theoretical and experimental research into the fixed OWC device was conducted by Maeda [120], detailing the absorption characteristics of generic caisson type device using linear theory. The first prototype scale concept to utilise this research was constructed in the Sakata Port, Japan. The prototype employed the design principles of the caisson breakwater to convert wave energy into electrical power. The caisson was 20 m in width, and integrated with five cells that operated as OWC devices by providing an air chamber between the waterline and the devices turbines. The plant was commissioned for operation in 1989, and became operational at a grid-connection stage from 1991 to 2000, before being decommissioned. A review of the construction phase of the Sakata Port OWC breakwater can be found in [121], and preliminary results from the experimental phase of the plant's operations have been published [122]. The caisson type breakwater is a common maritime structure employed in coastal protection engineering, which is comprised of a rigid structure that can contain a hollow chamber or air pocket dependent upon the design. To utilise this structure for wave energy extraction, the formation of openings across the entirety of the structure allowed the propagating wave patterns to interact with the free surface within the chamber, creating the OWC device.

Following this, further investigations have been conducted into OWC devices implemented either into, or as the breakwater structure. The planned installation of a OWC device intended for the head of a breakwater in the mouth of the Douro river is described by Martins et al. [123]. As an extension of this, Boccotti [124] followed a similar design principle as that presented for both the Sakata Port and Douro River, where a caisson type breakwater was modified to create a generic OWC device. Both theoretical [124], and experimental [125] investigations were performed to validate and expand on the effectiveness and efficiency of the implemented OWC devices. Most of the devices studied analytically and numerically for this application are two dimensional, hence limiting the relative capture width to 1 for the caisson style OWC device [62]. Further works on integrated OWC devices include analytical and numerical solutions developed for a cylindrical OWC device at the tip of a breakwater and along a straight coast by Martins-Rivas and Mei in [126, 127] respectively, where it was found that the performance of these simple units was found to exceed those of the caisson type and the offshore devices with a relative capture width reaching 2 and greater resulting from the reflection incurred by the design.

As a result of these analytical, numerical and experimental investigations into integrated OWC devices, and after the prototype investigation in Sakata Port, full scale pre-commercial and commercial devices have been planned and/or constructed, the most notable of which is the OWC power plant located in Mutriku, Basque Country, Spain, as found in Figure 1.6. The

Mutriku Wave Power Plant was both the world's first multi-turbine facility to be installed into a breakwater. A detailed report of the conceptual design, planning and construction phases of this device can be found in [128]. Severe storms impacted construction of the power plant resulting in commissioning delays until the summer of 2009; however, another severe storm hit the structure in January 2009 resulting in substantial structural damage to a number of the OWC cells. Speculation and conjectures into the specific failure mechanism of the plant under these severe storms has been published [129], with the plant eventually commissioned by the Spanish utility Ente Vasco de la Energia (EVE) in July 2011. The plant consists of 16 air chambers that house 16 individual Wells turbines, each rated at 18.5 kW. With a total capacity of approximately 300 kW, the plant has the potential to power 250 houses, and will reduce carbon emissions by 600 t per annum. While still currently operational, in July 2016 the plant achieved the milestone of generating over 1 GWh of clean energy since its inception [128].

Figure 1.6: The Mutriku OWC breakwater in Basque Country, Spain presents one of the current commerical applications for OWC device integrated fixed-breakwater concepts. Image Credit: [130]

More recently, the development of the technology, known as 'U-OWC' or 'REWEC3', led to the design of a full-scale prototype U-OWC breakwater in 2012, aimed for installation in the harbour of Civitavecchia, Italy [131, 132]. The progression of the concept investigated the wave climate conditions at the installation location, and also explored a secondary location in Pantelleria, Italy. Preliminary results regarding the energy absorption capacity of the devices, which utilised data obtained from a wave buoy located in close proximity to the location, were released in 2013 [133], with more recent results by Arena et al. indicating the device absorbed between 76% - 96% of the available wave energy [134, 135]. Development of mathematical models to predict and investigate paramaters that impact performance have been produced [136–138], while a number of additional full-scale projects adopting the REWEC3 concept have been planned for the harbour of Salerno, Italy and marina of Roccella Jonica, Italy.

Floating

Floating breakwaters are maritime structures which have the primary operational function of wave attenuation to provide environmental protection, which is achieved through partial dissipation and reflection of the incident wave, leaving a reduced level of energy to be transmitted beyond the floating breakwater. Incident wave energy is reflected, and dissipated through eddy generation at the sharp edges of the breakwater, as well as damping and frictional loss contributions [139]. Unlike fixed breakwaters (excluding potential diffraction effects), floating breakwaters are unable to completely remove incident wave action. In locations of deep water, poor foundation or high tidal variation, floating breakwaters are often preferred over rigid fixed breakwaters as the economic feasibility of fixed breakwaters is significantly reduced [140–142]. Floating breakwaters also provide flexibility of configuration as their design, contingent upon mooring arrangement, allows for relatively simple portability.

The first consideration for a structure floating at the water surface for wave attenuation was by Joly in 1905 [143], after which little progress was made until necessity fuelled innovation during World War II, when Great Britain developed two floating structures to aid in safely progressing men and supplies from the water onshore. Extensive reviews of floating breakwater structures have been conducted, including by Hales [140], who looked to categorise floating breakwaters into 11 classifications based upon geometric and functional similarities. McCartney [144] continued the categorisation of floating breakwaters, which was achieved through distribution into the four general categories of; box, pontoon, mat and tethered floats. Biesheuvel [145] conducted a performance review of floating breakwaters with varying mooring configurations using experimental data obtained from literature, and compared this to fixed breakwater structures, of which the major findings indicated the application of existing wave transmission theories yields results of good/reasonable agreement to experimentally obtained data. Most recently Dai et al. [146] conducted a literature review on the recent research and developments of floating breakwaters, categorising them by shape in the same vein as McCartney [144].

The development of floating breakwaters has led to a series of differing designs suited for various applications [140, 144, 147], including but not limited to the Y-Frame floating breakwater [148] and its evolution to a cage floating breakwater [149], the spar buoy floating breakwater [150], the H-type floating breakwater [151], variations of flexible porous type breakwaters [152–155] and traditional rectangular pontoon type floating breakwaters [156–158], with the two latter design representing the most extensively researched in the current market. Two important parameters for consideration in floating breakwater design are wave attenuation and motion response, where good designs achieve both high wave attenuation and low motion response [159]. One benefit floating breakwater integration presents is the operational range in which the structure can be viably deployed, where unlike the depth limited fixed breakwaters, the floating breakwater range encompasses the onshore, nearshore and offshore regions.

Floating breakwater integrated WEC systems can be distinguished as one of two specific categories, namely; floating wave energy converter modules that can be connected to form floating breakwater structures, and floating breakwater structures designed to incorporate wave energy conversion devices. Across both classes of floating breakwater WEC systems, there has ultimately been no full-scale demonstration cases to-date, with all full-scale floating WECs considering isolated devices providing minimal environmental protection, a few of which can be found in [95, 160, 161]. The closest example to a breakwater integrated OWC WEC structure was a prototype tested in 1976, named Kaimei, which was deployed off the coast of Yura, Tsuruoka City in Japan's Yamagata Prefecture. The device was a floating barge of dimensions 80 m $\times$ 12 m, weighing 820 tonnes, which housed 13 OWC open bottom chambers within the hull [162]. The device was designed and deployed by Yoshio Masuda and represented the first large-scale wave energy converters deployed at sea [163, 164]. The concept operated more similarly to a floating type OWC device, which relies on structure motion to harness energy, as opposed to fixed and/or breakwater integrated devices. Subsequently, the concept was not to be explored for its environmental protection characteristics. Due to the technological status of wave energy conversion considered to be in its infancy at the time of testing, the power production results of the Kaimei testing program were not considered very successful. Although no full-scale concepts have been created for OWC WEC integrated floating breakwater structures, a number of studies have been conducted at model scale.

1.1.6 Model Scale Experimental Testing

Model scale hydrodynamic experimentation is a key component in the development of wave energy conversion technology, and provides an efficient and relatively inexpensive platform for both concept validation and progression through Technology Readiness Levels (TRLs). The TRLs, originally developed at NASA during the 1970's, and modified for renewable energy systems by the National Renewable Energy Laboratory (NREL), refer to a set of best practices and guidelines contributing toward a systematic development plan for wave energy converter technologies, which is governed by nine distinct levels across the following five developmental stages [165].

- **Stage 1: Concept Validation** *(TRL 1-3)*: Encompasses small scale physical model testing (scale $\approx$ 25-100) to validate the performance of the concept. Optimisation of performance is typically explored, and performance in irregular sea states is evaluated.

Investigations may also explore the mooring and PTO systems to establish a baseline before survivability is explored.

- **Stage 2: Design Validation** *(TRL 4)*: Medium scale (scale $\approx$ 1:10-25) physical model experimentation to address the known unknowns in the design. Generally entails more extensive performance evaluation in realistic sea states, while investigations into PTO control strategies and mooring/anchorage systems are expected. Survival loading and extreme motion behaviour should be explored.

- **Stage 3: Systems Validation** *(TRL 5-6)*: Large scale (scale $\approx$ 1:3-10) physical model testing of a fully operation electricity generating device. Investigation into PTO design and systems testing conducted prior to full system sea trials, where deployment and recovery methods and environmental monitoring is considered.

- **Stage 4: Device Validation** *(TRL 7-8)*: Prototype scale (scale $\approx$ 1:1-2) testing in both sheltered and exposed sites to validate power production, power quality, PTO control strategies and prove the engineering of all systems.

- **Stage 5: Economics Validation** *(TRL 9)*: Final stage at 1:1 scale investigating the economic feasibility and evaluating the performance and interaction effect of multiple units in 'array'. Environmental impact should be explored while also ensuring compliance of all operations with existing legal requirements.

Adopting this standardised approach to technology development evaluation presents a sequential process aimed at reducing the risk associated with concept development as complexity and costs increase. Much focus on the development of OWC devices, both fixed and floating types, has been conducted to investigate the influence of various design parameters on the optimisation of conversion efficiency and survivability. While considerable research has been conducted regarding onshore and nearshore OWC devices, little research has been conducted into floating breakwater WEC systems. Of the aforementioned categories, the majority of research conducted regarding floating WEC systems has focused on the class which considers the whole breakwater structure to act as a WEC device, while very little has been conducted regarding floating breakwaters integrated with WEC devices, and more specifically OWC devices.

Fixed Breakwater Integrated

The continued development of breakwater integrated oscillating water column wave energy converters has seen few experimental investigations regarding the performance characteristics of the embedded devices, along with studies proposing optimised structural compositions and configurations. Vyzikas et al. [166] undertook an experimental investigation to compare the influence of OWC chamber geometry on the performance characteristics of the devices. The experiments evaluated the 'U-OWC' device against a generic caisson OWC device, and also investigated the impact of submerged slope leading to the device inlet. The results concluded that the U-OWC outperformed the traditional caisson OWC device, however it was found that the slope was found to benefit the performance of the traditional device. A similar experiment was conducted by Ashlin et al. [167] which investigated how the bottom profile of the integrated OWC device impacted the hydrodynamic performance. The investigation concluded that the OWC device with a circular curved bottom achieved greatest extraction capacity compared with the others tested. A number of studies have proposed variations to the traditional caisson type OWC device, and have utilised experiments to examine the efficiency of the concept [168–170], with most considering an opening at the bottom, close to the seabed and/or toe of the breakwater.

Caisson type OWC devices have also been subjected to larger scale testing within experimental facilities, as was conducted by Viviano et al. [171]. The investigation considered an approximately 1:5 - 1:9 scale generalised OWC devices tested in a large wave channel, which were installed across the entire width of the channel. The devices were subjected to random waves, and data was recorded to examine the wave reflection and wave loadings on the structure, in particular the front wall, rear wall and internal ceiling of the OWC devices. Results of the experiments illustrate the influence of PTO damping on the reflection coefficient of the structure, where wave reflection was most greatly reduced when the optimum PTO system for energy extraction was equipped. The results of the wave loadings highlighted similarities to those previously observed for Jarlan-type breakwaters; however, the results of the ceiling wave loadings detected spikes in pressure located in the rear corners of the chamber resulting from jets of water interacting with the surface in higher wave heights, and was highlighted as an area of design improvement which should be considered.

Ashlin et al. extended the work conducted regarding OWC chamber bottom geometry to integrate an array of the devices within an offshore detached breakwater [172]. The experimental setup considered five devices arranged side-by-side, centrally located within the rubble mound style detached breakwater. The investigation considered the independent variables of wave height, wave steepness and device spacing, which were varied to assess their impact on the performance of the integrated devices. The results of the experimental investigation illustrated that the devices observed reduced hydrodynamic performance as wave height and wave steepness increased. Regarding device spacing, it was found that optimal spacing was a function of wave length, subsequently for the concept considered during the investigation, the optimal spacing occurred when the parameter kS=2.27, where k represents the predominant wave length, and S is the device spacing. Finally, it was observed that a concentration of wave energy due to three-dimensional effects in front of the breakwater resulted in higher energy absorption for an array of devices relative to a single device. Though a number of breakwater integrated experiments have been conducted, no comparison between an isolated versus breakwater integrated study has been conducted to isolate the breakwater influence on energy absorption.

Floating Breakwater Integrated

A number of experimental studies have considered WEC-type floating breakwaters [173–176], with majority of these concepts adopting pontoon type breakwaters, either pile restrained or moored. Ning et al. investigated the hydrodynamic performance of a pile-restrained, pontoon-type floating breakwater using a 1:10 scale model in a wave flume, where it was established the concept had a conversion efficiency of approximately 24%, while keeping the wave transmission coefficient below 0.5 [177]. This concept was further expanded to investigate a two-pontoon system where one structure is stationary while the second is floating. This investigation yielded results indicating that this proposed configuration was able to improve the performance of the concept, and expand the effective operational range of the device [178]. Another example of a WEC-breakwater concept tested at model scale is the DEXA device, developed and patented by DEXA Wave Energy ApS, which is a wave activated body type WEC utilising relative movement of different parts for energy production. This device was explored as a potential solution for environmental protection through an experimental investigation exploring its wave attenuation characteristics [179, 180]. Similarly, WEC technologies have been integrated onto, or within, floating breakwaters and experimentally investigated to exploit a synergistic ocean wave energy extraction system, and example of which is found in [181], which considers multiple OWC devices configured in front of a floating breakwater.

Considering previous works in which OWC devices have been integrated into floating breakwaters, He et al. [182] investigated a floating rectangular breakwater both with and without pneumatic chambers integrated through model scale hydrodynamic experimentation to explore the integration impact on the performance characteristics of the breakwater. The 1:15 scale model was semi-constrained using a catenary mooring within a wave flume and subjected to a series of differing wave periods and operational drafts. The data acquisition included 6-degree of freedom motions via Qualisys video motion capture system, and pressure data from the chambers, and both reflected and transmitted wave characteristics. The results of the study indicated that the pneumatic chamber integration had positive effects on both the motion and wave attenuation capacities of the breakwater, however the energy extraction performance of the rear pontoon was less efficient due to the reduction in wave energy of the transmitted wave after dissipation due to the forward chamber. He et al. [159]

continued with concept development to explore asymmetrically designed pneumatic chambers to improve energy extraction of the devices. The pneumatic chamber alteration led to a minor increase in the heave response of the breakwater relative to the aforementioned symmetrically designed device, yet the overall energy extraction performance increased at shallower drafts with no reduction in wave attenuation performance of the breakwater. A more comprehensive evaluation of the device performance, with comparisons between the symmetric and asymmetric models was conducted by He et al. [183]. Though examples of OWC device integrated floating breakwater concepts are present in current literature, most studies in the field have only focused on concepts where the breakwater pontoons act as a single WEC unit, with far less research looking at multi-device integration and the impacts this may have on energy extraction and breakwater performance.

1.2 The Problem

1.2.1 Problem Definition

Currently, the major obstacle facing the commercialisation of wave energy is the high associated costs linked to the technology. The levelised cost of electricity for ocean wave energy is currently considered uncompetitive with other renewable energy sources such as wind and solar, which stems from lack of full-scale deployments from which valuable operational data can be acquired. While providing a rich, dense and predictable resource, the destructive power of ocean waves has also contributed to the stagnation of full-scale deployment, as many of those that have tried have fallen victim to statistically unlikely storms, either during construction and/or deployment, as well as other points of failure including deployment, grid connection and mooring failure. Of the two previously mentioned applications for reducing the LCOE of wave energy, breakwater integration yields the most promising, with a small number of full-scale commercial and demonstration cases currently operational, and greatest development through the WEC technology readiness levels. While some research has been conducted regarding the integration of OWC devices within breakwater/harbour structures, majority focus on caisson type devices, and do not consider the implications of integration on both the device performance, and the performance characteristics of the breakwater. Further understanding of these interrelated characteristics could provide validation for the OWC device's capacity to extract energy efficiently, and similarly, it's propensity for integration to create synergistic multi-purpose maritime structures. If the research indicates that the OWC device integration is beneficial for both device and structure, greater levels of confidence in the technology should be achieved, which when combined with the previously established economic benefits of integration, should ultimately increase the competitiveness of ocean wave energy.

The estimated future expansion of economic activities related to oceans, seas and coasts, known as the 'blue economy', also provides a platform for the rapid development of ocean wave energy. To continue at the current growth rate of the sector, a number of industries will be required to expand operations into deeper waters, as regulation and spatial limitations restrict the potential for expansion in coastal and near-shore regions. With industries moving further offshore, and the economic feasibility of WEC integrated bottom-mounted breakwaters becomes unachievable, the necessity for development of floating multi-purpose maritime structures as a means to reduce the high associated costs will become increasingly important. With very little research conducted into the integration of OWC devices within floating offshore structures, a significant knowledge gap is identified, subsequently much is required to determine whether such a concept is feasible; firstly from an operational perspective, as will be investigated in this research, and then from an economic perspective, which will not be covered.

This PhD focuses on two main areas of research regarding OWC WECs integrated within maritime structures; the impact of integration on the performance characteristics of OWC devices, and the influence of integration on the performance characteristics of a floating breakwater. Establishing the impact of integration on OWC device performance will provide an early indication of the operational feasibility of the concept, whereby an improvement in performance associated with integration would have beneficial ramifications regarding confidence in the concept, and subsequently result in further development of the concept through the predefined technology readiness levels. While investigating structure integration is the fundamental component of the project, the hydrodynamic performance of multiple device integration is also investigated, as to the authors knowledge, no such investigation has been conducted for a WEC integrated floating structure.

Following a preliminary study of a fixed, bottom-mounted breakwater, this project utilised the lessons and knowledge acquired to develop a proof-of-concept for a floating breakwater integrated with multiple oscillating water column wave energy converters. Establishing the hydrodynamic performance of such a concept was central to the research project, with investigations conducted into array interaction, configurational optimisation and realistic sea state analysis to establish operational feasibility, and establish a foundation of knowledge to aid future development.

1.2.2 Research Questions

This research project addresses the following research questions:

- What impact, and to what extent, does breakwater integration, both fixed or floating, have on the hydrodynamic performance of an OWC device?

- Conversely, what impact does OWC device integration have on the traditional hydrodynamic performance parameters of a fixed or floating breakwater?
- When considering multi-device OWC integration within a breakwater, is device-device interaction observed, and if so, to what extent is it beneficial and/or detrimental?

1.3 Approach

To achieve the objectives and research questions proposed by this research project, a number of physical model scale hydrodynamic experiments were designed and conducted. While a number of numerical methods have been derived to evaluate the performance of OWC devices, the candidate opted to elect physical model scale experimentation as the elementary method of investigation. As this thesis primarily considers a proof-of-concept investigation, the lack of understanding regarding the complex hydrodynamics and motions of the model warranted an experimental campaign which could then be used to validate future numerical tools if developed and adopted. A finite element method model was however utilised when possible throughout the experimental investigation for design and validation purposes for developing the isolated and fixed, bottom-mounted breakwater.

Two independent model scale hydrodynamic experimental investigations were devised to assist in answering the research questions proposed for this research project. The initial set of experiments were considered as a baseline study, from which the results acquired could be employed in the development of a second, more comprehensive set of experiments. With a focus on the integration of OWC WECs within breakwaters, both fixed and floating, the details of experimental campaigns conducted are as follows:

1) The preliminary experimental investigation sought to establish the impact of breakwater integration on the performance of an OWC WEC. The candidate was provided access the Australian Maritime College's Model Test Basin facility to conduct this initial experiment. Comparisons between isolated and fixed breakwater integrated OWC devices were conducted, from which the results were utilised to assess the feasibility of progressing the concept to incorporate OWC WECs within a floating breakwater. The study also sought to identify the influence of OWC chamber geometry on power absorption capacity, which further contributed to the design of the WEC/floating breakwater.

2) The results of the initial experimental campaign culminated in the design and development of a floating breakwater integrated with multiple OWC WECs, which aimed to provide answers to all of the research questions proposed for this research project. The WEC/floating breakwater model, whose design was governed by the initial experimental study as well as supplementary numerical studies, sought to explore the potential

for OWC WEC integration within floating maritime structures. The Model Test Basin facility was once again employed for the experimental investigation, in which the device was subjected to a comprehensive set of tests which targeted Stage 1 of the aforementioned TRLs for concept validation. The tests encompassed both OWC device and breakwater performance across regular and irregular waves to thoroughly analyse the impact that OWC device integration has on the performance of the floating breakwater, and how OWC WECs in multi-device configurations interact and impact hydrodynamic absorption.

1.3.1 Contributions

The design and execution of all physical model scale experiments discussed within the thesis was completed by the candidate, with guidance from the supervisory team. Similarly, the design of the physical scale models was performed by the candidate; however, construction of the models was outsourced to the technical support staff of the Australian Maritime College. All other tasks associated with the physical experiments were intently led by the candidate, with guidance and assistance provided by technical staff when training and/or safety procedures were required. Majority of the theory and a number of components of the physical scale configurations were common across the experiments, subsequently, much of the in-depth methodology adopted for this research is detailed in Chapter 2, with the pertinent configurational variations related to specific objectives detailed within each relevant chapter.

1.4 Novel Components

This thesis provides significant contribution to the existing knowledge of the OWC WEC, specifically regarding the application of maritime structure integration. The study contributes the following novel aspects to the ever growing field of OWC WEC development:

1) Physical scale model hydrodynamic experimentation detailing direct comparison between hydrodynamic performance of a generic bent-duct type OWC device when installed in isolation, and both fixed and floating breakwater integrated configurations.

2) Identifying the influence of OWC chamber geometrical cross-section on the power extraction efficiency of both isolated and breakwater integrated models.

3) Proof-of-concept investigation by means of physical model scale experiments conducted in realistic sea state for a free-floating offshore structure integrated with bent duct type OWC devices.

4) Identifying the influence of OWC device integration on the relative motions and wave attenuation characteristics of a generic π-type breakwater.

5) Conducting the first comprehensively published experimental investigation of a floating breakwater integrated with an array of integrated OWC devices.

6) Identifying the influence that device-device interaction has on the hydrodynamic performance of a floating breakwater integrated with multiple OWC devices, in both regular and irregular sea states.

7) Evaluating how design parameters of the integrated breakwater structure impact the hydrodynamic performance of the installed OWC devices.

1.5 Thesis Outline

To achieve overall target of evaluating the feasibility of bent duct OWC device integration within maritime structures from an operational perspective, two comprehensive experimental investigations were designed and conducted. The chapters of this thesis adhere to the sequential process followed to investigate and understand the hydrodynamic performance potential for OWC device integrated multi-use maritime structures. Following Chapter One which has presented a review of the literature pertaining to current status of ocean renewable energy and highlights the research questions, approach and novel components of this thesis, the contents of each chapter are as follows:

Chapter Two presents the theoretical framework applicable across the experimental investigations, detailing the hydrodynamic considerations for the performance of the OWC devices, as well as the relative theory for floating breakwater performance. A generic experimental setup is detailed, illustrating the common configuration adopted across the two suites of experiments.

Chapter Three details the methodology and findings of the initial investigation regarding the influence of breakwater integration on the performance of a generic bent duct type OWC device. A comparison between the performance characteristics of two geometrically varying cross-sections are also examined to establish the impact of this design feature on performance. The results obtained from the experimental investigation are compared to those derived from an hydrodynamic finite element model for model validation, and to explore optimal pneumatic damping characteristics to assess the optimal device performance in each of the tested configurations.

Contributing Paper (Paper One): Howe D, Nader JR. OWC WEC Integrated within a Breakwater Versus Isolated: Experimental and Numerical Theoretical Study. *International Journal of Marine Energy. 2017;20:165-182*

Chapter Four focuses on the hydrodynamic energy absorption pertaining to the extensive experimentation into the proof-of-concept investigation of a generic π-type floating breakwater integrated with multiple OWC devices in regular waves. A number of design parameters including; breakwater width, OWC configuration, motion constraint and PTO damping are investigated for their influence on the energy extraction capacity of the installed OWC devices. Key areas of interest and trends are identified regarding multi-device integration and the impact of device spacing is highlighted to optimise hydrodynamic energy absorption.

Contributing Paper (Paper Two): Howe D, Nader JR, Macfarlane G. Experimental Investigation of Multiple Oscillating Water Column Wave Energy Converters integrated in a Floating Breakwater: Energy Extraction Performance. *Applied Ocean Research. 2020 (Under Review)*

Chapter Five details the secondary component of the proof-of-concept experimental investigation which explored the impact of OWC device integration on the wave attenuation and motion characteristics of the π-type floating breakwater. While subjected to regular waves, the wave attenuation performance with respect to wave transmission and wave reflection, as well as the relative heave, pitch and surge motions of the multi-purpose structure are compared with and without OWC devices integrated to establish the impact on the breakwaters primary modes of operation.

Contributing Paper (Paper Three): Howe D, Nader JR, Macfarlane G. Experimental Investigation of Multiple Oscillating Water Column Wave Energy Converters integrated in a Floating Breakwater: Wave Attenuation and Motion Characteristics. *Applied Ocean Research. 2020 (Under Review)*

Chapter Six presents the final component of the proof-of-concept investigation, which explores the hydrodynamic energy absorption and relative motions of the multi-purpose floating structure in irregular sea states. A number of varying irregular wave spectra are investigated to develop a performance matrix for the concept, while comparisons for relative motion with and without OWC devices integrated is explored. Comparisons are made between non-dimensional performance parameters in regular and irregular sea states, and the use of linear superposition of regular wave data for irregular sea state performance prediction is explored. The feasibility of the concept from a performance perspective is discussed, with the current progression through the relevant technology readiness levels recognised.

Contributing Paper (Paper Four): Howe D, Nader JR, Macfarlane G. Performance Analysis of a Floating Breakwater integrated with Multiple Oscillating Water Column Wave Energy Converters in both Regular and Irregular Seas. *Applied Ocean Research. Special Issue: Wave Energy Utilization 2020 (Under Review)*

Chapter Seven: Provides a summary of the research completed contributing towards this thesis and offers the subsequent conclusions developed and suggestions for future works.

Appendices: Appendix A details the conditional variation information for the experiments discussed in Chapters 4, 5 and 6. Appendix B describes the methodology employed for the uncertainty analysis conducted. Appendices C–E present other published work completed by the candidate during the course of the PhD research project (Papers Five–Seven).

Chapter 2

Theory and Methodology

2.1 Theory

2.1.1 General

A thin wall bent duct type OWC device facing the direction of incoming incident wave propagation is considered. The generic device is surface piercing and operates in a constant water depth, h. In all cases, unless otherwise specified, the device adopts a rectangular cross-sectional area, denoted S_c, as governed by the inlet width, W, and inlet height, D, as derived using Equation 2.1.

$$S_c = WD \tag{2.1}$$

The swept path formed by s_1, s_2, s_3 and s_4 defines the geometrical construction of the OWC chamber, along with the thickness, t_c, where applicable, as illustrated in Figure 2.1. The submerged chord length, s_1 - s_3, governs the natural period of the device. A preliminary study which utilised an in-house linear hydrodynamic FEM model, described further in Section 3.2.3, yielded results to indicate that when the total submerged chord length remained constant and adhered to a 45° constraint (see Figure 2.1), the natural resonance period of the device remained constant for all variations of the parameters s_1 - s_3. While no change in the natural period was observed, the magnitude of absorbed power decreased as the draft, d, increased.

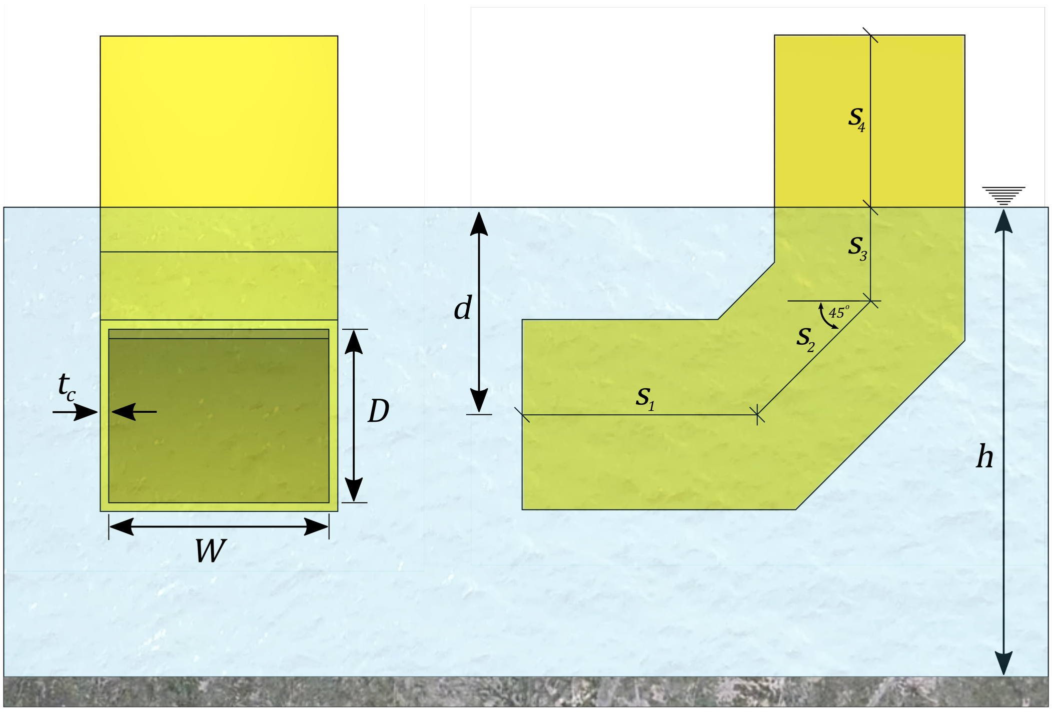

Figure 2.1: Schematic diagram of generic OWC device illustrating front and side view, and illustrating theoretical geometric parameters governing design.

These criteria were chosen such that the volume of air and water at rest inside the OWC chamber and the depth of inlet centre remain constant during the experimental investigation. Altering these criteria would change the device inner performance properties (cf. [184]). The integration of OWC devices within maritime structures introduces additional design parameters contributing to the performance of the OWC device which are specifically detailed when relevant throughout this thesis. Generally, unless otherwise specified, the maritime structures consisted of a flat vertical face, into which the OWC device inlet was integrated such that the inlet lip was co-located on the same plane as the structure face, as illustrated in Figure 2.2.

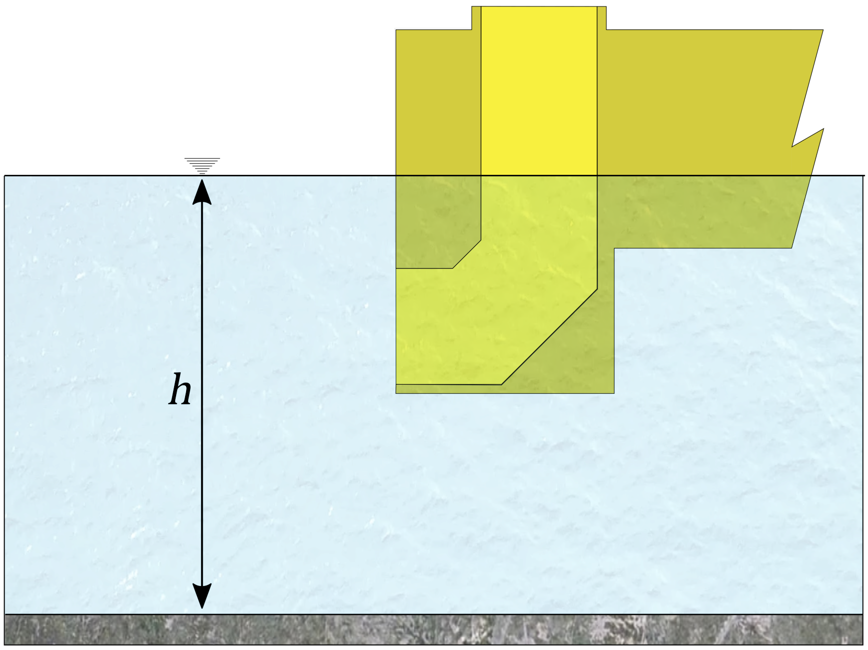

Figure 2.2: Schematic diagram of generic OWC device within a floating maritime structure illustrating side view.

The explicit dimensions of the models used in each respective experimental investigation are presented as required in the designated chapters.

2.1.2 Theoretical Hydrodynamic Consideration

Linear water-wave theory with irrotational and inviscid flow is considered, in which small amplitude waves are assumed. During investigations in which the devices are subjected to regular waves, a monochromatic incident wave plane of amplitude η_0 and frequency ω propagates in a constant direction toward the device. For irregular wave investigations, a JONSWAP spectrum defined by a significant wave height, H_S, peak frequency, f_p and peak enhancement factor, γ, is considered to propagate directly toward the device.

The interaction of the waves with the device creates a volume flux, Q, inside the chamber.

Due to the power take-off system, the turbine, a dynamic pressure, p_c, is created which oscillates around the mean atmospheric pressure. In this thesis, a linear relationship between volume flux and pressure, such is the approximated correlation for the Wells' turbine, is considered, governed by Equation 2.2,

$$p_c = \delta Q \tag{2.2}$$

where δ is the pneumatic damping coefficient. As opposed to the quadratic relationship typically utilised through use of orifice plate damping, the linear relationship was employed such that direct comparison could be made between the experimental results and those acquired via a linear hydrodynamic FEM model. The relationship is the same as in used in [48, 185–192]. Further studies have demonstrated that air compressibility within the chamber can generate a time lag between p_c and Q with significant impact on the power absorption [47, 62, 126, 127, 184, 193]. However, this effect requires large air chamber volumes, as has been found in previous numerical and experimental investigations with bent duct type OWC devices of small scale [194] (as found in Appendix D. The air chamber volumes of the OWC devices utilised throughout this research project were sufficiently small enough for this effect to be disregarded.

Volume Flux, Q

The volume flux within the OWC chamber can be defined as,

$$Q = \iint\limits_{S_c} \frac{\partial \eta}{\partial t} ds = \iint\limits_{S_c} v_s ds \tag{2.3}$$

where v_s is the velocity of the free surface within the chamber. Under the assumption that the free surface will move uniformly, Equation 2.3 can be written as,

$$Q = \overline{v_s} S_c \tag{2.4}$$

where $\overline{v_s}$ is the mean free surface velocity. Spatial averaging has been utilised where applicable to reduce the uncertainties associated with the free surface uniformity assumption. The non-dimensional volume flux, Q', with respect to the incident wave can be defined as presented in Equation 2.5.

$$Q' = \frac{\overline{v_s} S_c}{\omega \eta_0 S_c} \tag{2.5}$$

For the purpose of this thesis, the amplitude of the non-dimensional volume flux, $A_{Q'}$, was compared to display the amplification effect of the chamber on incident waves. The amplitude of the non-dimensional volume flux can therefore be defined as,

$$A_{Q'} = \frac{A_{\overline{v_s}}}{\omega \eta_0} = \frac{\omega A_{\overline{\eta_{OWC}}}}{\omega \eta_0} = \frac{A_{\overline{\eta_{OWC}}}}{\eta_0} \tag{2.6}$$

where $A_{\overline{\eta_{OWC}}}$ is the mean amplitude of free surface oscillation within the chamber, and $A_{\overline{v_s}}$ is the mean amplitude of free surface velocity.

Mean Hydrodynamic Power Absorption

The instantaneous power absorbed by the OWC device is able to be determined through the use of Equation 2.7, where the power at a given time, t, is derived as the product of the dynamic internal chamber pressure and the volume flux of air.

$$P(t) = p_c(t)Q(t) \tag{2.7}$$

The mean hydrodynamic power absorption, P_h, can be determined using Equation 2.8,

$$P_h = \frac{1}{T}\int_0^T p_c(t)Q(t)dt \tag{2.8}$$

where T is the incident wave period. This relationship is utilised as a quantitative tool in comparing extraction efficiency of the OWC devices utilised during this research under varying experimental configurations and conditions. The final power output of the device needs to include losses from the PTO system. These losses are not covered throughout this study where only the hydrodynamic behaviour of the devices are investigated. By introducing Equation 2.2 into Equation 2.8, and assuming linear wave theory, the power absorption can be rewritten as,

$$P_h = \frac{1}{T}\int_0^T \frac{p_c^2}{\delta}dt = \frac{1}{2}\frac{A_p^2}{\delta} \tag{2.9}$$

where A_p represents the amplitude of the dynamic internal chamber pressure as defined in Equation 2.10.

$$A_p = \frac{max(p_c) - min(p_c)}{2} \tag{2.10}$$

Compared to Equation 2.8, Equation 2.9 was considered the primary method of mean hydrodynamic power calculation throughout the study when considering regular waves as it yields lower uncertainties on the results (as seen in Chapter 4).

The power outputs are non-dimensionalised with respect to the power of the incident wave interacting directly with the water column. The incident wave power of crest width equivalent to the device inlet is derived using Equation 2.11,

$$P_I = \frac{1}{2}\eta_0^2 \rho g C_g \tag{2.11}$$

where ρ is the water density, g is the gravitational acceleration and C_g is the group velocity which is derived as,

$$C_g = nC \tag{2.12}$$

where C is wave celerity, as expressed in Equation 2.13, and n is a constant derived using the dispersion relationship as presented in Equation 2.14,

$$C = \frac{gT^2}{2\pi} \tanh\left(\frac{2\pi h}{\lambda}\right) \tag{2.13}$$

$$n = \frac{1}{2}\left[1 + \frac{\frac{4\pi h}{\lambda}}{\sinh(\frac{4\pi h}{\lambda})}\right] \tag{2.14}$$

where λ represents the incident wave length.

The non-dimensionalisation of mean hydrodynamic power absorption of the device is represented by the non-dimensional capture width, $\tilde{L}_{pc}$, which relates power absorbed to incident wave power and is derived as shown in Equation 2.15.

$$\tilde{L}_{pc} = \frac{P_h}{P_I W} \tag{2.15}$$

It should be noted that while the non-dimensional capture width, $\tilde{L}_{pc}$, is similar to efficiency, it is possible to have a value for $\tilde{L}_{pc}$ greater than 1 as the devices are able to absorb more energy than interacts directly across the width of the device.

2.2 General Experimental Configuration

Commonalities are present across both the methodologies and experimental configurations adopted for the various experimental campaigns undertaken during this research. To avoid repetition in the proceeding chapters, the shared components, including experimental considerations, facilities and instrumentation, of each experiment are presented in this section, with the topic specific elements of each investigation covered in the respective chapters.

2.2.1 Experimental Considerations

Mean hydrodynamic power absorption output of the OWC models has a direct correlation to the pressure and volume flux of the air in the chamber, and the damping of the turbine. To compare the results of experimental tests in regular waves, calibrated and phase averaged (described in Section 2.2.4) data for pressure and volume flux were utilised to determine the mean hydrodynamic power absorbed for the devices under a given model condition, incident wave frequency and wave height.

Incident Wave

To establish the available incident wave energy during experimental tests, resistance type wave probes were installed within the shallow water basin during wave calibration tests without the experimental models present. These probes were set up in locations corresponding to positions in which the OWC chambers would be situated during experimentation so that any spatial variability in incident wave power across the basin would not influence the results obtained.

Volume Flux, Q

Two assumptions were made with regards to the volume flux and amplitude of the non-dimensional volume flux during the experimental investigations. Firstly, the amplitude of the free surface within the OWC chamber, η_{OWC}, as measured by the internal wave probe/s is considered approximately equal to the mean amplitude of the free surface, proposing that the free surface oscillates uniformly in the vertical chamber as defined in Equation 2.16.

$$A_{\eta_{OWC}} \approx \overline{\eta_{OWC}} \tag{2.16}$$

Secondly, it was assumed that the free surface velocity was approximately equal to the mean free surface velocity as shown in Equation 2.17, indicating that the free surface again oscillates uniformly.

$$A_{v_s} \approx \overline{v_s} \tag{2.17}$$

The volume flux, as defined in Equation 2.3, requires the velocity of the free surface, which was not measured during the experimental investigation. As such, a numerical derivation was required to provide an approximate value for the mean free surface velocity to be used when evaluating the volume flux air within the chamber. By acquiring the data for free surface elevation within the chamber; the numerical velocity derivation was performed by phase averaging the elevation data for a time sequence from 0 to T, from this each phase-averaged elevation point was derived to produce a velocity measurement, through the use of Equation 2.18,

$$v_s = \frac{\eta_{OWC}(2) - \eta_{OWC}(1)}{t(2) - t(1)} \tag{2.18}$$

where, $\eta_{OWC}(1)$ and $\eta_{OWC}(2)$ represent consecutive elevation data points, and $t(1)$ and $t(2)$ are the corresponding time data points. By evaluating Equation 2.18 for each data point in the phase averaged elevation vector, the resulting velocity vector of the OWC chambers free surface across one period is produced, from which the average free surface velocity, $\overline{v_s}$, can be determined. The velocity vector can subsequently be multiplied by the cross-sectional area of the chamber to produce a phase averaged vector with approximate values for Q across the time interval 0 to T.

It is understood that the assumptions made, along with the numerical derivation of experimental data can induce non-negligible errors. The assumptions of uniform free surface elevations and velocities are approximations, and do not truly represent the complexity of the dynamic system within the OWC chamber. The assumptions were a necessary step in the process of evaluating the numerical derivation, consequently, the approximate results produced for volume flux do not provide a realistic representation of the air flow emanating in and out of the chamber. Elhanafi et al. [195] conducted a comparison between air flow derived using the aforementioned assumption, and a direct measurement at the PTO. It was found that for fixed structures where two wave probes were used for spatial averaging, the difference in the volume flow rate between the two methods was less than 2% for a stationary structure, however increased to 11% for a floating structure. Elhanafi et al. subsequently introduced a third wave probe, which reduced the error between the approximation method and direct measurement to less than 4% for the floating structure. Hence, where applicable, spatial averaging has been utilised to reduce the uncertainty associated with the volume flux assumption. Notwithstanding, the numerically derived volume flux was solely used in the calculation of the pneumatic damping coefficient to determine the characteristics of the porous mesh for PTO simulation.

Damping, δ

The linear damping characteristics of a Wells turbine allows for relatively accurate predictions of the expected power outputs [196]. In order to determine the damping coefficient for the systems investigated, it was necessary to replicate the linear relationship between pressure and volume flux. O'Gorman [197] conducted a series of experiments into the use of various meshes to simulate the linear damping of a Wells turbine, concluding that the damping could be replicated through the use of a fabric mesh material, as it was able to replicate representative pressures and airflows within the OWC device. The mesh utilised in all experiments conducted is a 100% polyester porous fabric product called Enviro Cloth, which could be incrementally layered to increase the damping of the system. The Enviro Cloth mesh can be found installed on one of the tested devices in Figure 2.3.

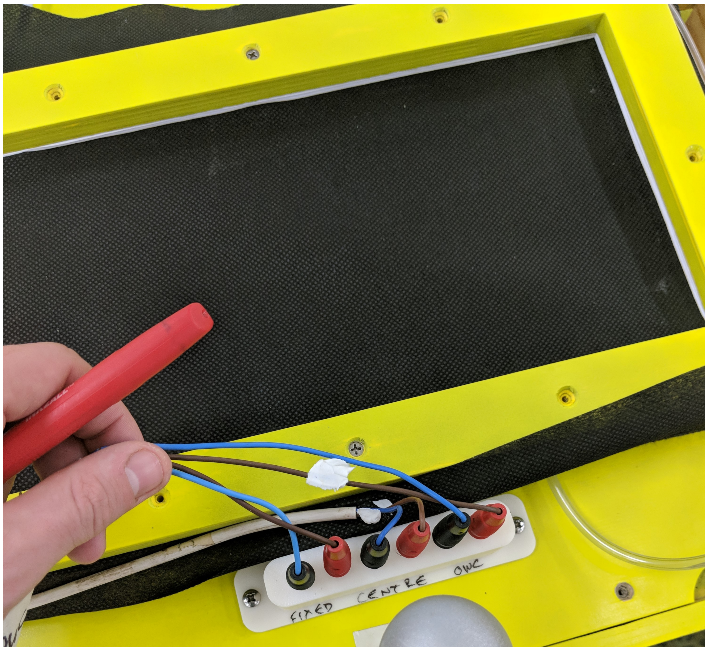

Figure 2.3: Enviro Cloth Mesh installed on one of the operational OWC chambers investigated throughout the experimental campaign.

The pneumatic damping coefficient is the gradient of the pressure versus volume flux plot, an example of which can be found in Figure 2.4. As such, for each condition tested it was necessary to plot this data for all incident wave frequencies tested, and then produce a linear fitted equation encompassing all test frequencies to establish the damping coefficient. Each respective experimental investigation followed this methodology, and the respective results can be found within the dedicated chapters. Once the linear relationship had been established across all test frequencies, and the equation for the relationship found, the damping coefficient is determined and subsequently allows for calculation of the mean hydrodynamic power absorption of the device under each frequency through use of Equation 2.9.

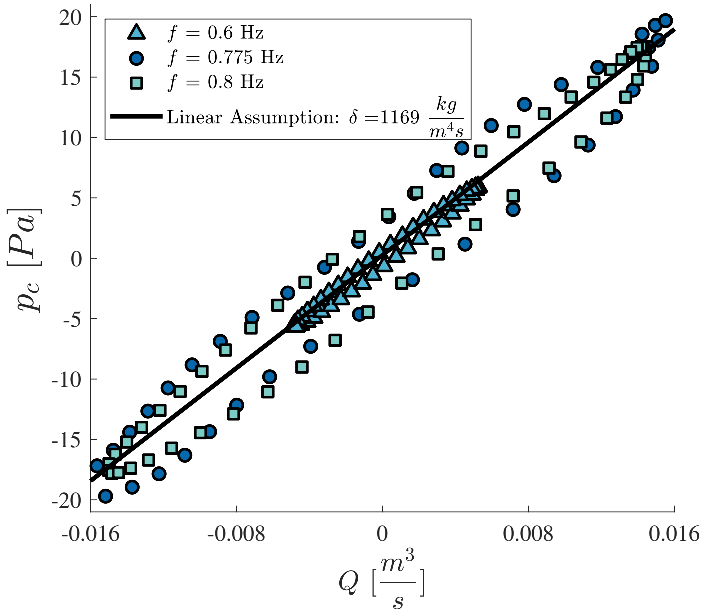

Figure 2.4: An example of the frequency independent pressure versus volume flux relationship derived from experimental data, which indicates the assumed linear relationship for the frequencies displayed. All frequencies were used in the derivation of the pneumatic damping however, only three were chosen to be presented for figure clarity. Further evidences can be found in Figure 3.5, Figure 4.6 & Figure 6.1.

2.2.2 Experimental Facility

All physical scale model experimental investigations presented within this thesis were conducted within the Australian Maritime College's (AMC) Model Test Basin (MTB). The facility contains a 35 m × 12 m × 1 m shallow water wave basin equipped with 16 individual piston-type wave paddles capable of producing regular waves, short-crested and long-crested irregular waves and focus waves. The opposing end of the basin houses a wave damping beach which serves the purpose of reducing the reflection of waves during experimental testing, and similarly, dissipates energy from the system between experimental runs. The electronically operated wavemaker receives inputs for frequency and wave height in regular waves, and spectrum parameters of peak period, significant wave height and enhancement factor for irregular JONSWAP spectra. The wavemakers did not have active absorption capabilities to mitigate the impact of reflected waves, however, wave reflection was managed via data processing methods (see Section 2.2.4). Where applicable, all experimental runs were randomised with respect to frequency, sea state (regular and irregular) and wave height. This is in compliance with the Design of Experiment (DoE) guidelines as specified by the International Towing Tank Conference (ITTC) [198, 199].

Figure 2.5: Australian Maritime College's Model Test Basin facility

2.2.3 Instrumentation

The experimental investigations carried out during this research project utilised two common pieces of instrumentation to acquire the desired data. Water surface elevation was key to the assessment of hydrodynamic performance for the maritime structure integrated WEC devices, and it was necessary to capture both the water surface elevation internally within the OWC chamber, and the external wave surface elevation to establish incident wave parameters. To measure water surface elevation, resistance type wave probes were configured to a multi-channel wave probe monitor manufactured by HR Wallingford. The wave probes were built in-house at the Australian Maritime College, and customised to suit configuration specific deployment, with an example of the probes presented in Figure 2.6. The resistance type wave probes are installed such that the two vertical wires pierce the water surface. A constant high frequency alternating voltage is used to excite the wire, inducing a current which allows the resistance of the water between the parallel rods to be measured. This resistance is linearly proportional to the immersion depth of the wave probes, subsequently providing an accurate means of measuring free surface elevation [200], an example of which can be found in Figure 2.7. Reviews of resistance type wave probes can be can be found in [201, 202].

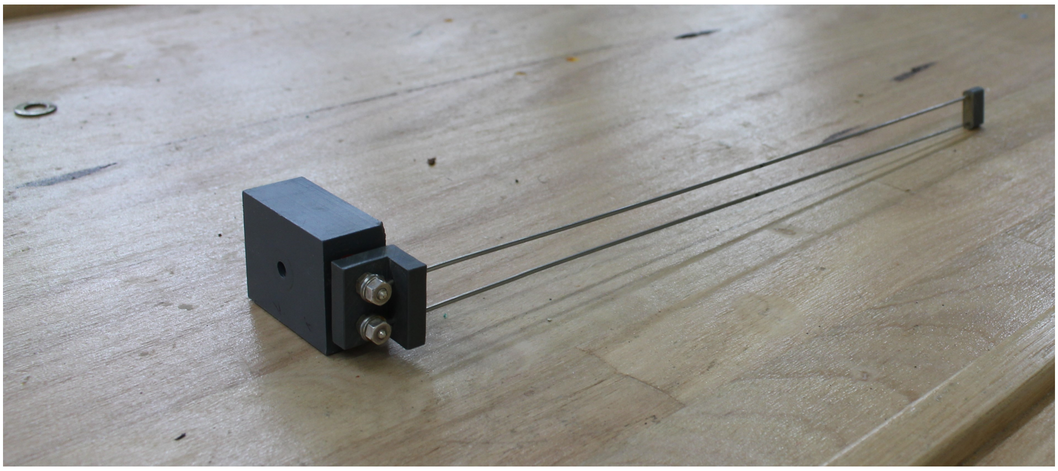

Figure 2.6: 300 mm resistance type wave probe built in-house at the Australian Maritime College

Each investigation undertaken had differing water surface measurement requirements and configurations; as such, specifications regarding location and amount of probes utilised in each experiment are described in the relevant chapter. All experiments were subjected to wave calibration tests, in which the physical scale model was removed from the basin, and wave probes were installed in the model location to acquire baseline data sets for the incident wave at the model location.

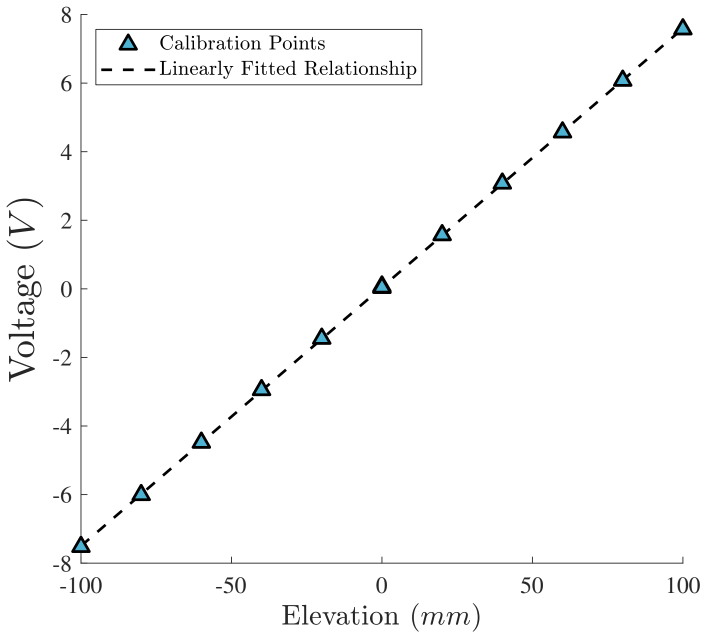

Figure 2.7: An example of the calibration data associated with the 300 mm resistance type wave probe built in-house at the Australian Maritime College

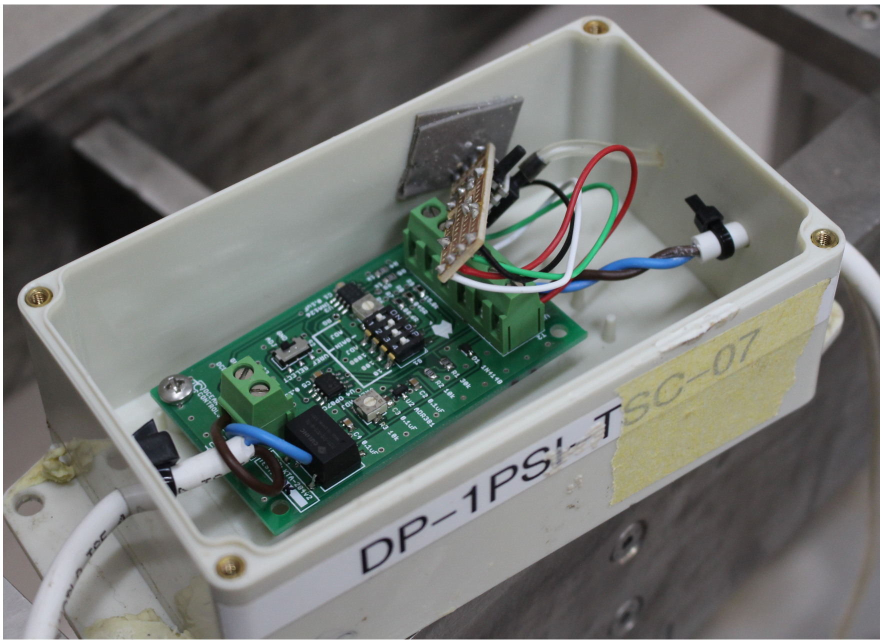

Figure 2.8: Pressure sensor utilised during experimentation to acquire the dynamic pressure data from the OWC chamber

The second piece of instrumentation common across all experiments was a pressure sensor. To capture the dynamic pressure fluctuating as a result of incident wave interaction, the experimental apparatus employed Honeywell Controls TruStability board mount pressure sensors connected to Ocean Controls KTA-284 instrumentation amplifiers, as can be found pictured in Figure 2.8. Each operational OWC chamber utilised during experiments was configured with one of these sensors, whilst also generally fitted with a small diffuser that connected to the sensor to prevent water entering and/or becoming lodged within the pressure probe tap. Similarly to the wave probes utilised, the differential pressure sensors yield a linear relationship as illustrated via the calibration data shown in Figure 2.9.

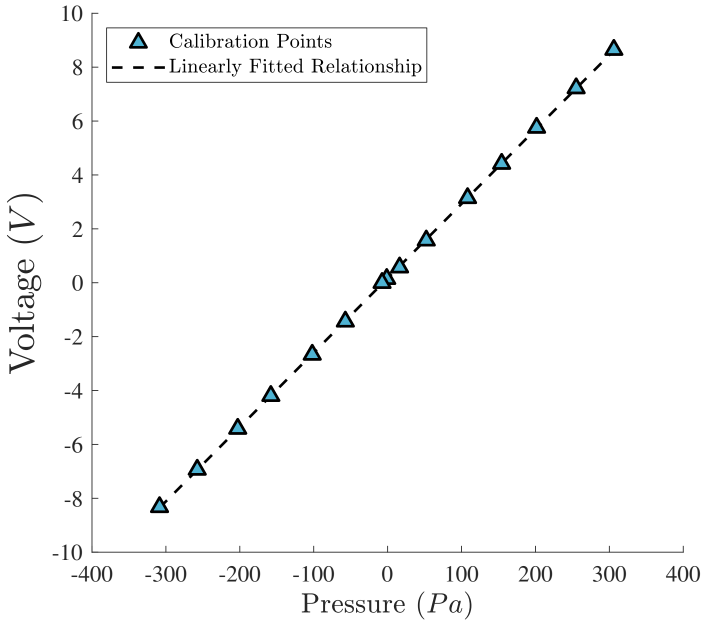

Figure 2.9: An example of the calibration data associated with the differential pressure sensors utilised to measure the dynamic pressure within the OWC chamber.

Both aforementioned instruments were sampled at 200 Hz during all experiments, while the gain, filtering and calibration settings were experiment specific, and are highlighted where appropriate.

2.2.4 Data Processing

Phase Averaging

The experimental testing of the OWC models provided data for both the wave oscillations of the incident, phase and OWC wave probes, and data for the OWC pressure probe. This data was of an oscillatory nature due to the frequency of the regular waveforms interacting with the probes in the Model Test Basin.The necessity for reliable data to justify the hypotheses of this experimental research, in culmination with the limitations of time allocated for experimental investigations established the need to produce a phase averaging program to analyse the experimental data. The data produced is sinusoidal in nature; hence, the application of phase averaging vastly improves the accuracy by segmenting the data into separate vectors comprised of one full period of oscillation. These vectors are then superimposed over one another across the time range 0 to T, from which one average oscillatory waveform can be derived to produce a singular averaged data range of the incident wave profile. Fleming et al. employed this method of data analysis on experiments involving OWC devices previously as in [77–79]. Firstly, it was necessary to select the region of the raw data that would yield the most accurate results. This was in the stationary region where the effects of reflection and diffraction had not yet adversely affected the data and after the transition period where the waves first interact with the devices and configurations. Figure 2.10 displays the raw data of an experimental test where the frequency was set to 0.9 Hz, the target wave height was 0.02 m and a rectangular OWC device was implemented in the breakwater with the mesh damping applied. The selected data was taken from a region of stationary wave forms as shown. This provided the most accurate representation of the desired interaction between the incident waves and the device. It should be noted that the reflection region illustrated in Figure 2.10 was measured during the fixed, bottom-mounted breakwater experiments described in Chapter 3. Experiments described in Chapters 4, 5 and 6 utilised a floating breakwater structure which observed far less reflectivity than the fixed breakwater, subsequently the reflection region was recognised to be of lower magnitude.

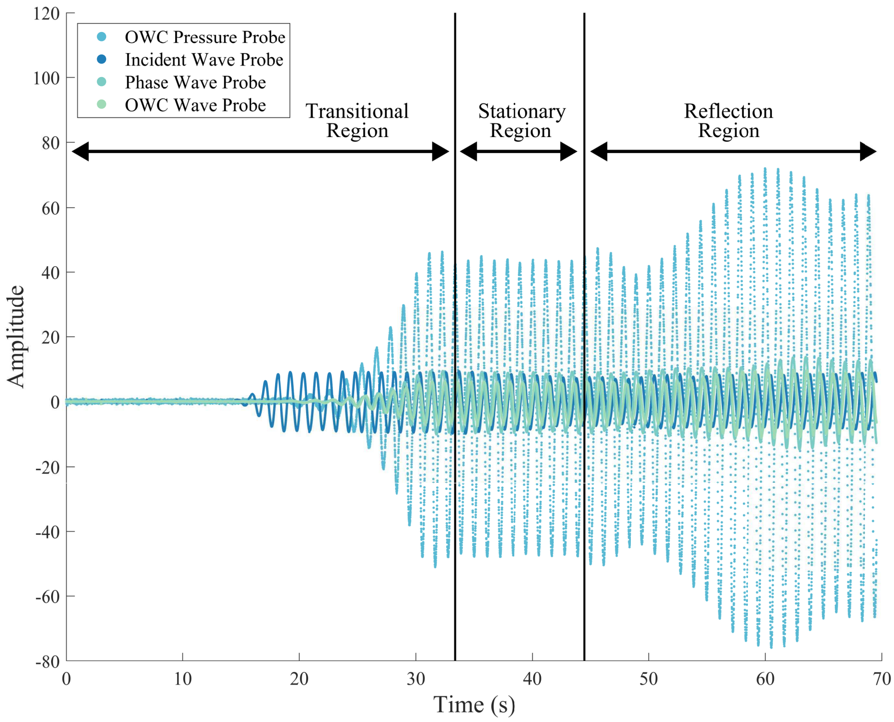

Figure 2.10: Raw data selection process with data taken from the fixed breakwater mounted rectangular OWC device subjected to 20 mm wave heights at 0.9 Hz

The procedure to calibrate the raw experimental data into phase averaged data sufficient for analysis is concisely outlined as follows, and is justified with the use of the equations governing the procedure. Firstly the period was divided into a defined number of points, or repeating cycles as explained in [78], which was 50 for this data analysis, where t_r represents a time point correlating to a data point within the repeating phase-averaged cycle. The first and last points were calculated separately, before being plotted independently on the graph to their respective positions on the vector T. This averaged data can now be considered as the mean data from repeatable runs, hence improving the accuracy of the data without having to repeat the experiment numerous times. The resultant pressure plot of the phase averaging process can be found in Figure 2.11. The raw pressure data obtained from the stationary region was split into respective wave periods, then superimposed over each other with the phase-averaged data representing the mean values for amplitudes.

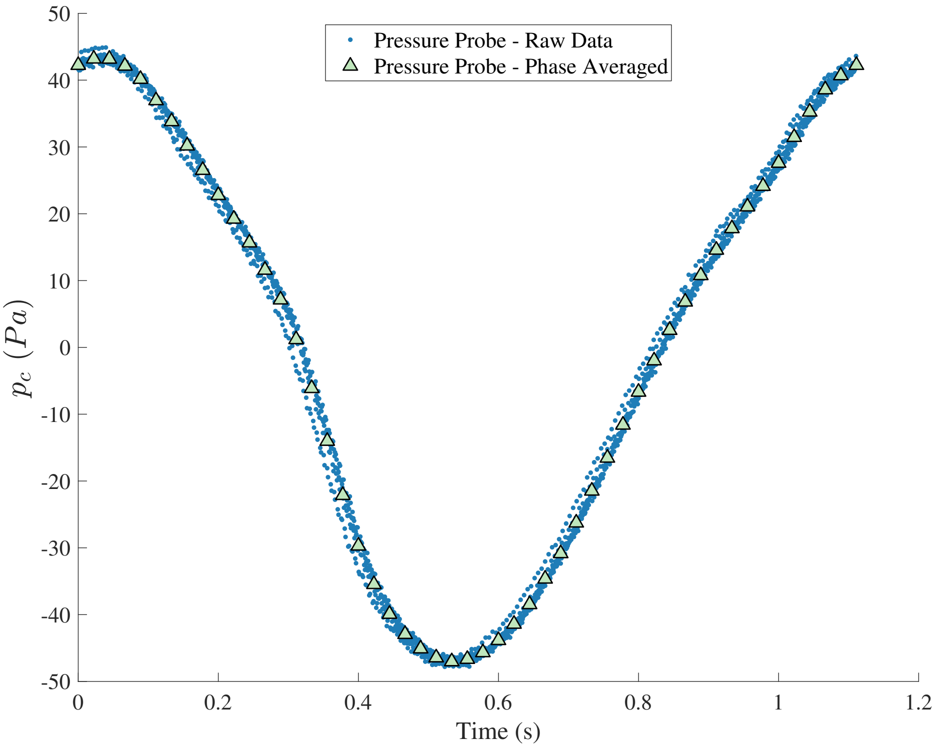

Figure 2.11: Phase averaged pressure data from the fixed breakwater mounted rectangular OWC device subjected to 20 mm wave heights at 0.9 Hz

The phase difference was calculated via the use of linear theory where the wave profile is described as shown in Equation 2.19.

$$\eta_0 = \frac{H}{2}\cos(\omega t + \phi) \tag{2.19}$$

Given data sets A and B, ϕ_A and ϕ_B are the respective phases. In order to find the phase difference, it is necessary to find $\phi_A - \phi_B$. The phase difference can therefore be calculated through the use of the time difference between two data points, those being the respective maximums and minimums of the data sets ($T_{A_{max}}$, $T_{B_{max}}$, $T_{A_{min}}$, $T_{B_{min}}$).

2.2.5 Generic Experimental Setup

The commonalities regarding experimental configuration present across the investigations conducted throughout this research campaign can be found displayed in Figure 2.12, with additional details regarding common instrumentation, calibration and methodologies provided. Experiment specific details will be provided within the relevant chapters.

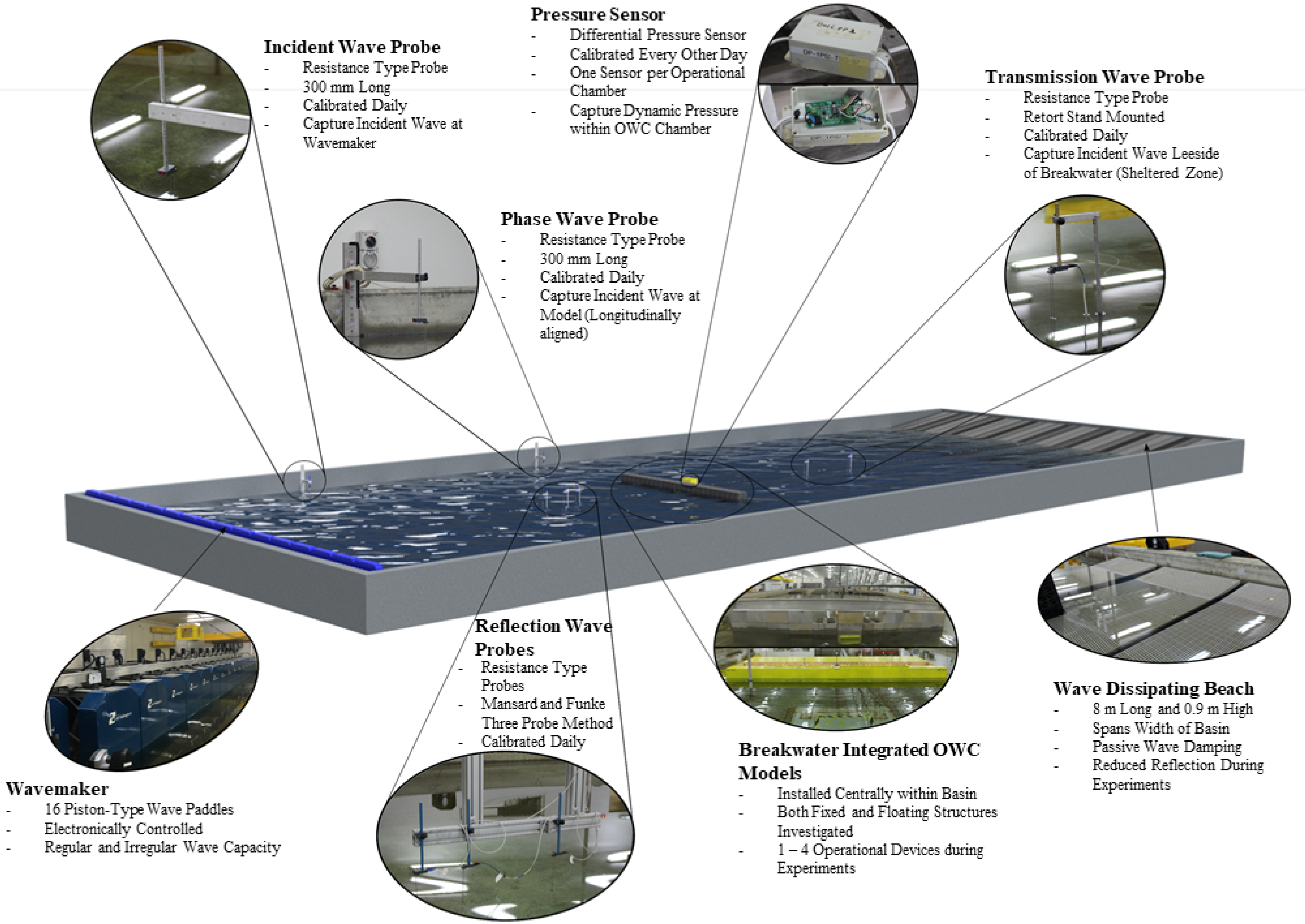

Figure 2.12: Schematic of the Australian Maritime College's Model Test Basin facility outfitted with common instrumentation, models and systems utilised across the experimental campaigns.

CHAPTER 3

Gravity-based Breakwater Mounted OWC WEC

3.1 Introduction

The purpose of this experimental research investigation presented in this chapter is to determine two significant distinctions in an OWCs power extraction. Firstly, the effect that OWC device inlet geometry has on the power output of the device is explored, and secondly, the effect of implementing an OWC device into a flat-faced breakwater is investigated. The results of both these experimental studies are compared with respect to the power extraction capture width. Limits in the research undertaken are noted as follows. The effect of the breakwater on the wave propagation parameters such as reflection, diffraction and forces is not examined as the research is specifically devoted to the energy extraction capacities of the devices both when implemented and isolated. In other words, this research is on the energetic property of the devices across different conditions rather than on the maritime structure.

The investigation was undertaken as a preliminary or 'baseline' study which sought to identify the influence of breakwater integration on the performance of a bent duct type OWC device. Establishing the impact that breakwater integration has on the energy absorption capacity of the OWC devices can potentially improve the viability of the concept, as a greater energy yield improves confidence in the device, while possibly benefiting the economic feasibility as concept development continues. The results of this study would subsequently contribute to assessing the suitability of OWC WEC integration within a floating breakwater, as is considered in the latter chapters of this thesis.

3.2 Theory

3.2.1 General

Two different cross-sectional shapes are considered as seen in Figure 3.1, one circular shape of diameter D and one rectangular shape of length W and width D. The swept path formed by s_1, s_2, s_3 and s_4 is kept the same. Furthermore, the cross-sectional area S_c for the two cases is also preserved,

$$S_c = \pi \left(\frac{D}{2}\right)^2 = DW \tag{3.1}$$

meaning that

$$W = \pi \frac{D}{2} \tag{3.2}$$

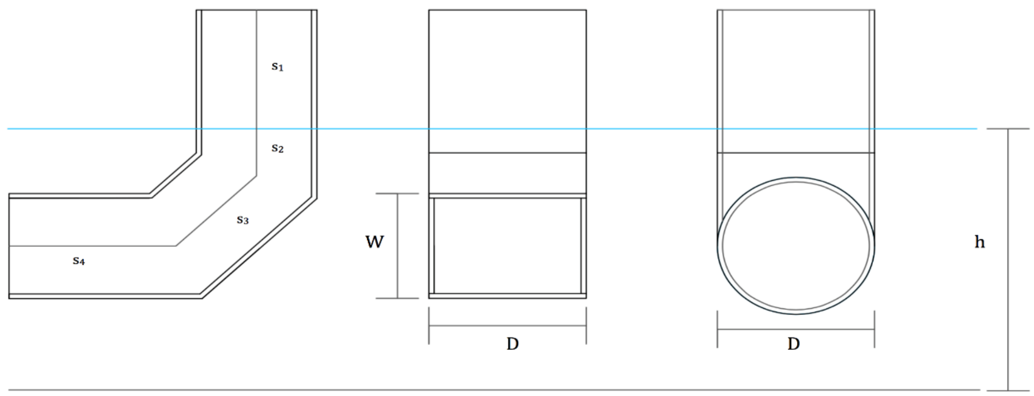

Figure 3.1: Schematic diagrams depicting side view of both devices (left), front view of the rectangular device (middle) and front view of the circular device (right)

These criteria were chosen so that the volume of air and water at rest inside the OWC chamber, the depth of the opening centre and the opening width remain the same between the two types of device. In addition to the shape, two different configurations of the devices were considered. The device is first considered in isolation and secondly integrated into a breakwater structure represented by a flat vertical wall (cf. Figure 3.2), where the front of the device extrudes from the breakwater by distance e. The dimensions for the model testing, which remained fixed throughout the experiments, can be found in Table 3.1.

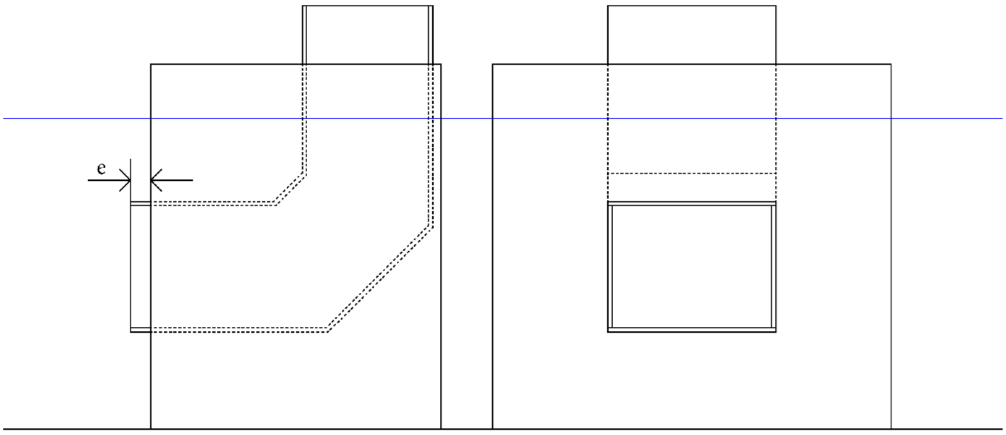

Figure 3.2: Schematic diagram of the rectangular breakwater integrated OWC device

Table 3.1: Model scale factor and design governing dimensions

Scale Factor 1:20	
Variable	Measurement (mm)
D	300
W	236
e	38
s_1	260
s_2	103
s_3	217
s_4	318

3.2.2 Theoretical Hydrodynamic Consideration

The assumptions and considerations applicable to this experimental investigation follow those outlined in Section 2.1.2, specifically with respect to internal volume flux of air passing through the PTO system, the pneumatic damping applied by the PTO simulant, the dynamic pressure within the OWC system and the subsequent energy absorption capacity of the OWC devices.

Non-dimensional capture width, as defined by Equation 2.15, was utilised to compare the performance of the OWC devices across both the configurational and geometric variations investigated during this study. The power absorbed by the OWC devices was determined by evaluating Equation 2.9, which utilised the pressure directly measured during the experiments, and the derived pneumatic damping coefficient of the PTO representative mesh.

3.2.3 Numerical Model

The results from the experiment is compared to the FEM numerical hydrodynamic model as previously developed in [47, 48, 184, 203]. Compared to [47], the model was adjusted for the breakwater configurations in order to take into account the no flow boundary condition

$$\frac{\partial \phi_b}{\partial x} = 0 \tag{3.3}$$

at any point on the breakwater wall and the reflected velocity potential by modifying the incident velocity potential to

$$\phi_{inc} = -2\frac{ig}{\omega}\eta_0 \frac{\cosh k(z+h)}{\cosh kh} \cos(kx) \tag{3.4}$$

The mesh was generated using ANSYS® [204] meshing tool and exported into Matlab to apply the FEM model. The domain was discretised by employing tetrahedron elements with a node at each vertex and at the middle of each edge. Half of the domain was discretised to take advantage of the symmetry and the element sizes refined around the OWC device and free surface. The element sizes were taken as invariable throughout the volume of the domain and adjusted to have minimum of ten elements per wavelength. Figure 3.3 presents an example of these meshes for each of the different configurations. Typically, a mesh for the isolated devices comprised of around 65000 elements and 90000 nodes. A lower number of elements (≈35000) and nodes (≈50000) was needed for the breakwater integrated device due to the smaller domain.

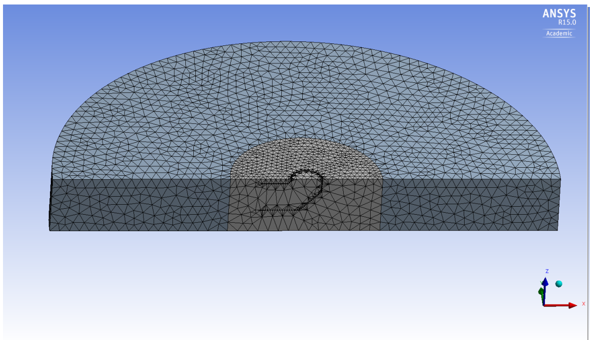

(a) Isolated Circular OWC Device

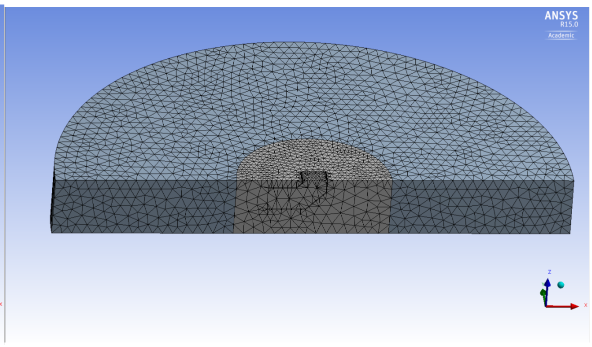

(b) Isolated Rectangular OWC Device

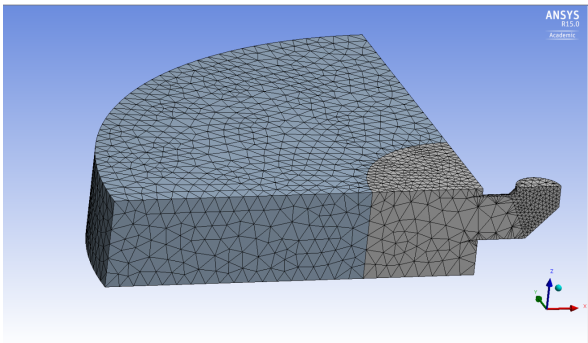

(c) Breakwater Mounted Circular OWC Device

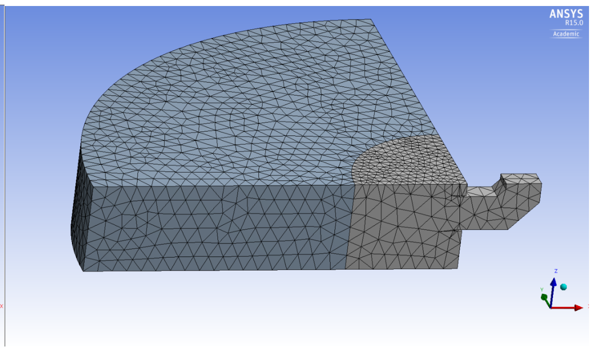

(d) Breakwater Mounted Rectangular OWC Device

Figure 3.3: Mesh examples for the different configurations

3.3 Experimental Setup

3.3.1 Experimental Considerations

Volume Flux Q

The assumptions made for this experimental investigation regarding volume flux adhere to those described in Section 2.2.1. Similarly, it is understood that due to the complexity of the system being examined, the assumptions made will induce non-negligible errors. However, these assumptions were a necessary step in the process of evaluating the OWC device performance. When comparing the non-dimensional volume flux between the devices and configurations, the relationship stated in Equation 2.6 was utilised, where the values for $A_{\overline{\eta_{OWC}}}$ and η_0 were taken directly from the amplitudes recorded by the respective wave probes.

Damping δ

The linear damping of a Wells turbine was replicated through the use of a mesh material, as it was able to produce representative pressures and airflows within the OWC device. The mesh can be seen pictured in Figure 3.4.

Figure 3.4: Circular OWC model with porous fabric mesh damping applied

The volume flux is plotted as a function of pressure in Figure 3.5, showing the typical shape of the relationship, how all test frequencies superimpose over each other, and where a linear fitted line would be applied to find the relationship between pressure and volume flux. Once the linear relationship has been established across all test frequencies and the equation for the relationship is found, the damping coefficient can be determined, hence allowing for the calculation of the mean hydrodynamic power absorption of the device under each frequency when using the relationship for power with respect to pressure and pneumatic damping. Conducting the analysis into the damping characteristics of the devices yielded a valuable and interesting conclusion, being that the damping of the system was not dependent upon frequency. This meant that the damping coefficient could be applied uniformly across all frequencies when power analyses were conducted. Other studies in which a porous membrane has been used to simulate PTO systems for WEC devices relate applied damping to the relative thickness of the membrane [190]. The current study did not vary damping, and subsequent membrane thickness, as such only a single layer of the porous mesh was utilised.

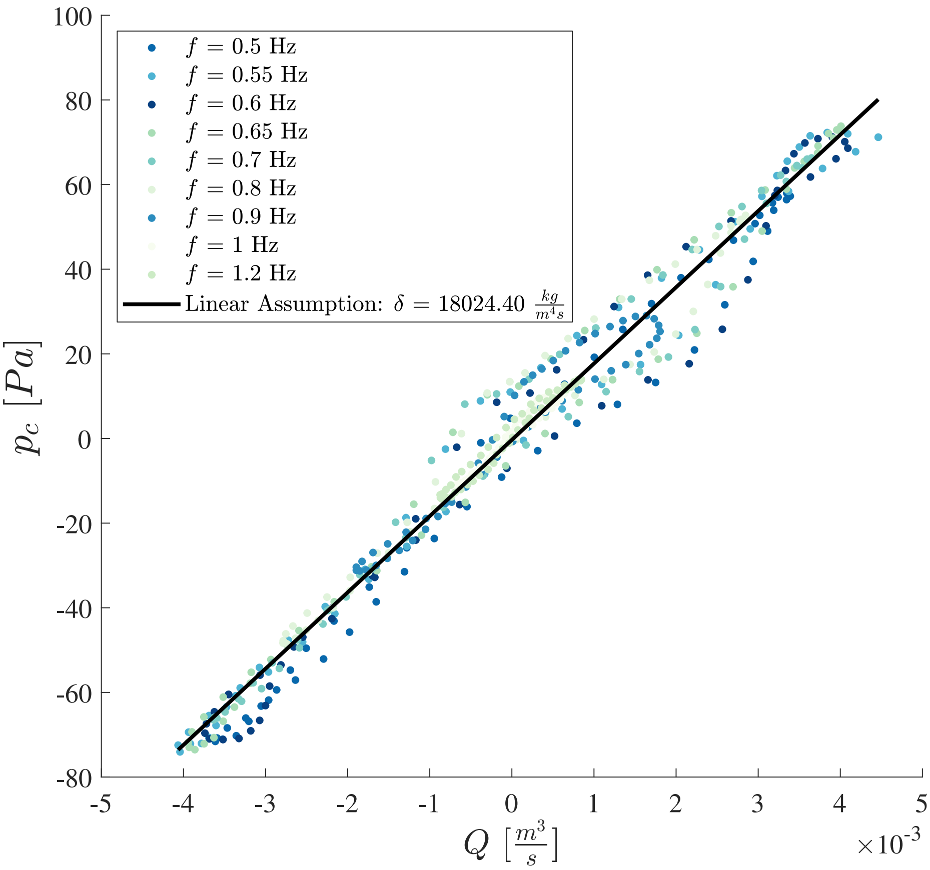

Figure 3.5: A p_c versus Q plot for the circular OWC device in isolation with the linear fitted damping coefficient superimposed

3.3.2 Model Test Basin

The experimental model investigation was conducted within the Australian Maritime College's Model Test Basin, the details of which are presented in Section 2.2.2. The model breakwater was positioned symmetrically across the longitudinal axis and was located a distance of 14 m from the 16 wavemaker paddles. Acrow props were secured between the ceiling of the facility and the top of the breakwater to provide additional stability to the structure, and aid in the rigidity when under the influence of the wave propagation. Similarly, an Acrow prop was used to situate the OWC device in the correct position in both the breakwater mounted and isolated states. A scaled schematic of the experimental test apparatus can be found in Figure 3.6. The electronically operated wavemakers received inputs for frequency and wave height to produce the desired waveforms for testing and would run indefinitely, however each run was ceased after approximately 90 seconds as this allowed enough time for the necessary data to be acquired.

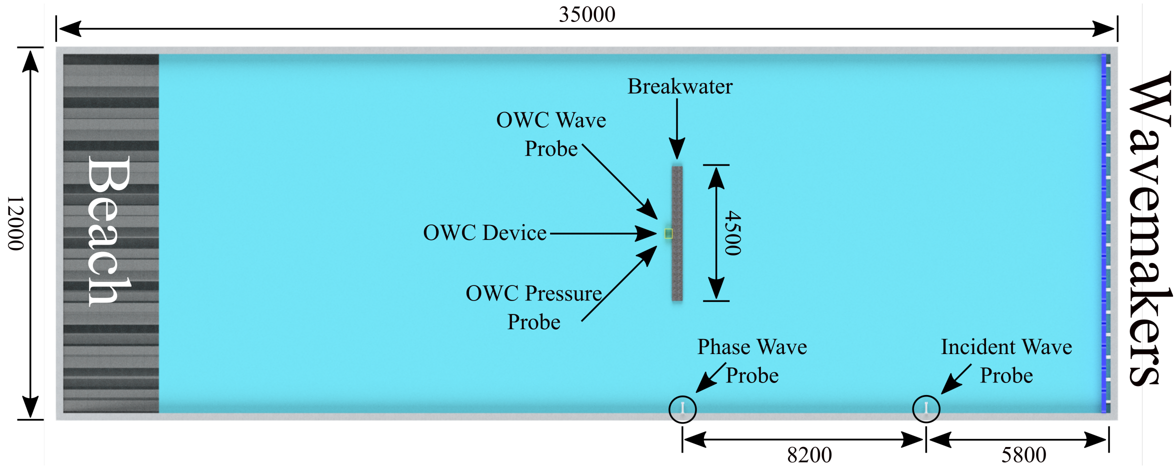

Figure 3.6: Scaled schematic of the test apparatus within the AMC MTB. All units in mm.

3.3.3 Models

The experimental setup for the OWC device study consisted of two separate model configurations; these were the implementation into a breakwater, and in isolation. Each configuration was subjected to four different conditions respectively, which were the rectangular OWC device with and without damping, and the circular OWC device with and without damping. The two models were constructed in-house at the Australian Maritime College, where dimensions of the rectangular OWC model were based upon the diameter and cross-sectional area of the circular model which had previously been constructed. This allowed for direct comparison of volume flux and power outputs of the separate devices. The models can be found in Figure 3.7 configured in isolation, and in Figure 3.8 implemented into the model breakwater.

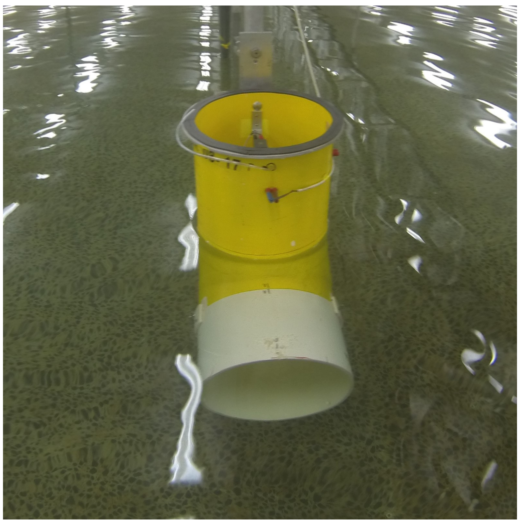

(a) Circular OWC Device

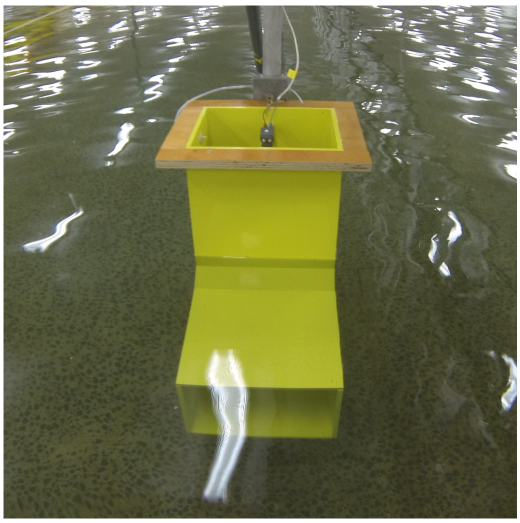

(b) Rectangular OWC Device

Figure 3.7: Geometrically varying OWC devices installed in isolated configuration

(a) Circular OWC Device

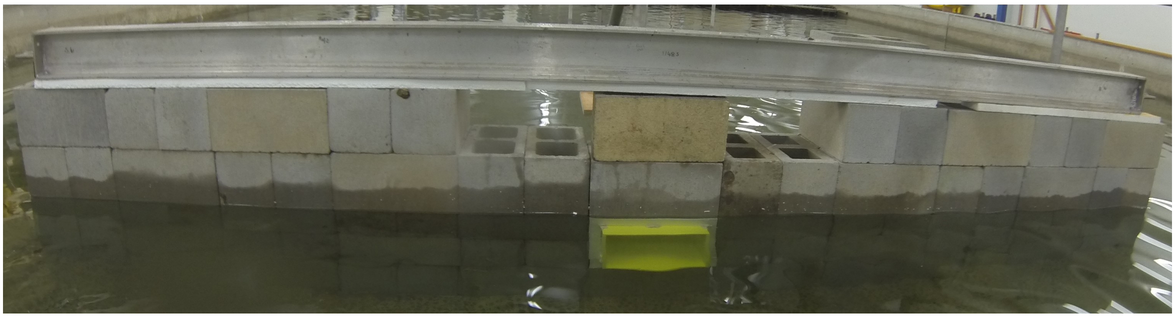

(b) Rectangular OWC Device

Figure 3.8: Geometrically varying OWC devices integrated within the model breakwater

3.3.4 Instrumentation

There were four sensors used during the experimental testing procedure, these were three wave probes and a pressure probe. The wave probes were configured as an incident and phase probe located close to the wavemakers and in line with the OWC model respectively, and finally the third probe was located in the OWC chamber to measure the elevations of the free surface. The pressure probe was located in the side of the devices and was utilised when the damping condition was applied. The positioning of the phase and OWC wave probes were configured to allow for direct comparison between the elevations of the incident waves and the wave oscillations within the chamber to determine the magnification effect the chamber had on the waves. Table 3.2 shows the specifications designated for each probe.

Table 3.2: Sensor Properties

Sensor	Range	Sensitivity	Output (VDC)
Incident Wave Probe	± 50 mm	0.2 $^{VDC}/_{mm}$	± 10
Phase Wave Probe	± 50 mm	0.2 $^{VDC}/_{mm}$	± 10
OWC Wave Probe	± 120 mm	0.083 $^{VDC}/_{mm}$	± 10
Pressure Probe	± 400 Pa	25 $^{mVDC}/_{mm}$	± 10

3.3.5 Calibration

The probes were calibrated daily, with incident and phase probes to a range of ± 50 mm, allowing for variations in the experimental test facility, and ensuring that the expected 20 mm wave heights were accurately captured. Similarly, the OWC wave probe was calibrated to ± 120 mm in order to capture the magnified oscillatory motion of the free surface within the chamber resulting from incident wave interaction. The pressure probe was calibrated to ± 400 Pa despite the maximum captured pressure being approximately 120 Pa, guaranteeing that all pressure values were recorded. The sampling rates for probes were allocated at 200 Hz, with the gain set to 2.5, and the low-pass filter value set to 10 kHz for all probes.

3.3.6 Test Regime

Variations in the experimental tests came from the conditions to which the experimental setup was devised, and the frequency of the oncoming waves. Target wave height and incident wave frequency ranges were kept constant at 20 mm and 0.5-1.2 Hz respectively across all the conditional variation during the investigation. The full breakdown of conditional information for the testing along with the variables can be found in Table 3.3. The data received from the probes allocated to the test was then processed, analysed and subsequently presented in Section 3.4 to provide comparisons and recommendations on the potential for each device to extract power, and the effect of incorporating the devices within a maritime structure on power extraction.

3.4 Results and Discussion

The aim of the experimental investigation conducted was to firstly compare the effects that the inlet geometry of the OWC device would have on the production characteristics, such as the volume flux, damping coefficient and power output. Similarly, the secondary aim looked to compare the same production characteristics when the device was both implemented in the breakwater, and in isolation. An OWCs capability as a renewable energy device is not a function of its peak magnitudes in power output or volume flux, but its capacity to produce over a spectrum of frequencies. Subsequently the testing performed on the devices was investigated over a frequency band spanning from 0.5 Hz to 1.2 Hz to provide data of the devices capability to utilise an array of incident wave conditions. The resulting data was used to compare the devices production over this range to determine which geometrical device performed best under a given construction condition so that recommendations could be provided into the design and implementation of OWC devices.

Table 3.3: Conditional Testing Information

Set Up	Information	Target Wave Height (mm)	Test Frequencies (Hz)
1	No Mesh/Damping: Circular in Breakwater	20	0.5, 0.55, 0.6, 0.65, 0.7, 0.8, 0.9, 1, 1.2
2	Porous Mesh: Circular in Breakwater	20	0.5, 0.55, 0.6, 0.65, 0.7, 0.8, 0.9, 1, 1.2
3	No Mesh/Damping: Rectangular in Breakwater	20	0.5, 0.55, 0.6, 0.65, 0.7, 0.8, 0.9, 1, 1.2
4	Porous Mesh: Rectangular in Breakwater	20	0.5, 0.55, 0.6, 0.65, 0.7, 0.8, 0.9, 1, 1.2
5	No Mesh/Damping: Rectangular Isolated	20	0.5, 0.55, 0.6, 0.65, 0.7, 0.8, 0.9, 1, 1.2
6	Porous Mesh: Rectangular Isolated	20	0.5, 0.55, 0.6, 0.65, 0.7, 0.8, 0.9, 1, 1.2
7	Porous Mesh: Circular Isolated	20	0.5, 0.55, 0.6, 0.65, 0.7, 0.8, 0.9, 1, 1.2
8	No Mesh/Damping: Circular Isolated	20	0.5, 0.55, 0.6, 0.65, 0.7, 0.8, 0.9, 1, 1.2

3.4.1 Damping

Through the four separate damped cases conducted, it was determined that the pneumatic damping coefficient was consistent around the value of $\delta = 17{,}715\ \frac{kg}{m^4 s}$, which was the mean average of the four cases, subsequently this value was employed during numerical simulations.

3.4.2 Volume Flux

The results for variations in the amplitude of non-dimensional volume flux between the respective conditions and models are presented in Figure 3.9 with the plots displaying the volume flux across the test frequency band for each respective test condition. For this, both the volume flux and the frequency were non-dimensionalised; hence, the resulting plots shown as Figure 3.9 depict the non-dimensional volume flux amplitude against kh. From Figure 3.9, it can be seen that the OWC devices implemented into the breakwater produce larger non-dimensional volume flux amplitudes when compared to the respective device implemented in isolation. Subsequently, the breakwater appears to enhance the magnitude to which the incident wave is amplified within the OWC chamber. This is an interesting result and may be attributed to the fact that, due to wave reflection from the breakwater, a greater amount of energy is present in front of the OWC inlet, subsequently allowing the device to attract more energy through resonance. As power can be determined with respect to the volume flux, it can be hypothesised that the results drawn from the volume flux under each condition would indicate that the power output of the OWC devices would be of larger magnitude when implemented in a breakwater than when deployed in isolation.

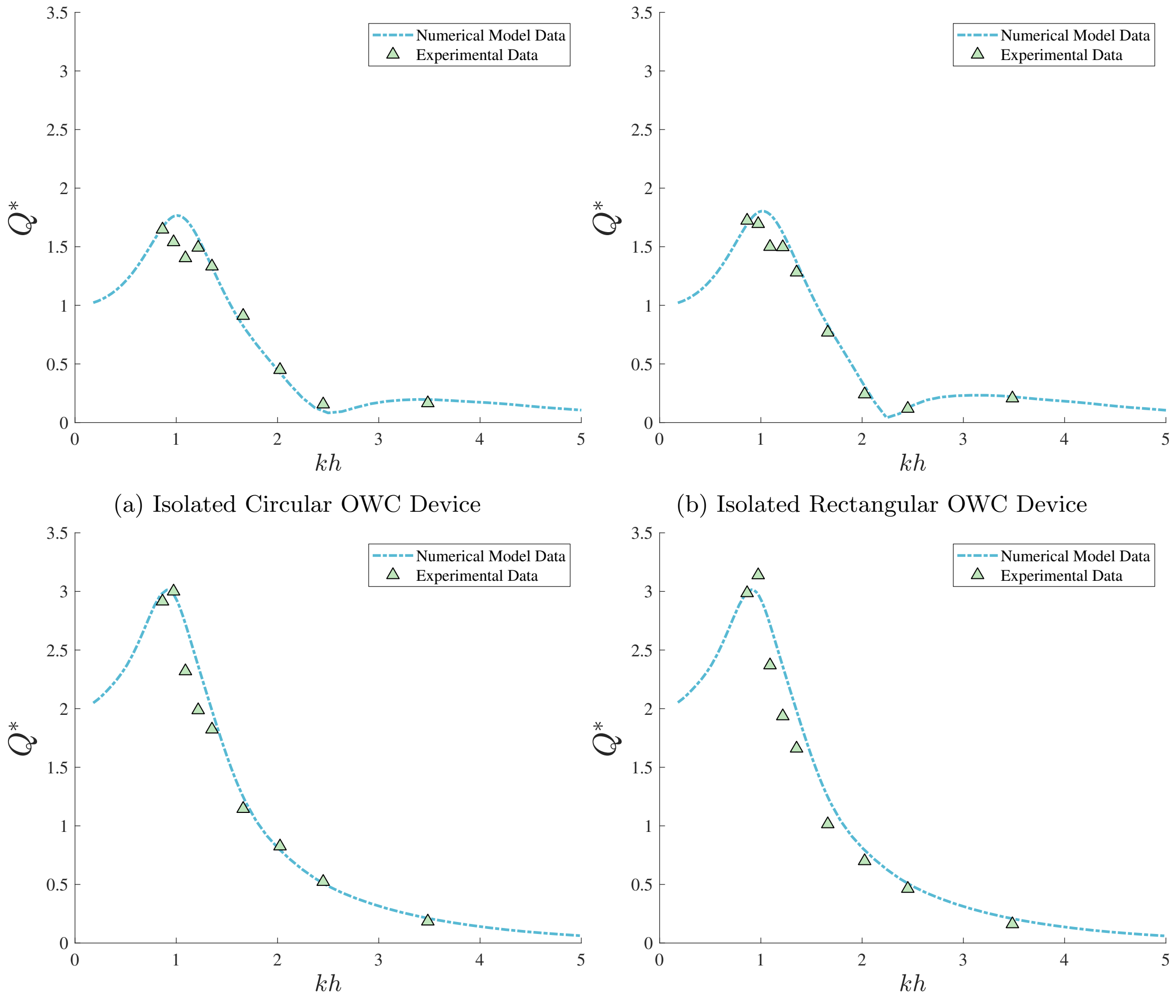

(a) Isolated Circular OWC Device (b) Isolated Rectangular OWC Device

(c) Breakwater Mounted Circular OWC Device (d) Breakwater Mounted Rectangular OWC Device

Figure 3.9: Experimental and numerical non-dimensional volume flux amplitude presented as a function of kh

Figure 3.9 also depicts that whilst the rectangular OWC device appears to display the highest peak value for non-dimensional volume flux amplitude at approximately 3.1, the circular OWC device produces at a greater capacity over the spectrum of test frequencies. This trend is present in the damped condition when implemented both in isolation, and in the breakwater. In relation to the power output potential, this would indicate that the circular OWC device would perform best at producing power over the range of test frequencies hence would provide the most suitable design as an OWC concept. All the conditions targeted the same resonance frequency at 0.6 Hz, however during the experiments, a resonance frequency closer to 0.55 Hz was observed. This is evident in both damping conditions as can be noted by the peak magnitudes. The interaction with the breakwater did not appear to effect the location within the frequency band at which resonance occurred, but did affect the magnitude of the volume flux in the chamber.

The numerical model results for each condition can be found superimposed over each plot in Figure 3.9. The numerical simulation conducted for the damped conditions yielded results that correlated well in the highest test frequencies; however, for the frequencies around resonance the experimental results provided varying magnitudes. This contrast in the data is a result of the limitations regarding the applicability of turbulence and viscous forces in the numerical model. These effects were therefore not considered during the numerical analysis, as further research must be done into the viscous force that is present in OWC device technology, and is subsequently recommended for future works to provide more conclusive evidence of the relationship. The experimental investigation was limited around the lower frequencies due to the capabilities of the wavemakers to produce the incident waves, and although the correlation between the model and experimental data amongst the higher frequencies was positive, further investigation is required to determine the differences in the results around the lower and resonance frequencies. This limitation is addressed in Chapters 4, 5 and 6 where devices were design to resonate at approximately 0.775 Hz.

3.4.3 Power

The power results were produced using the method explained previously, and were used for comparative and verification purposes to justify the accuracy of the numerical model against the experimental data. Similarly, to the volume flux results, Figure 3.10 displays both the numerical and experimental data to provide a visual representation of the correlation between the results.

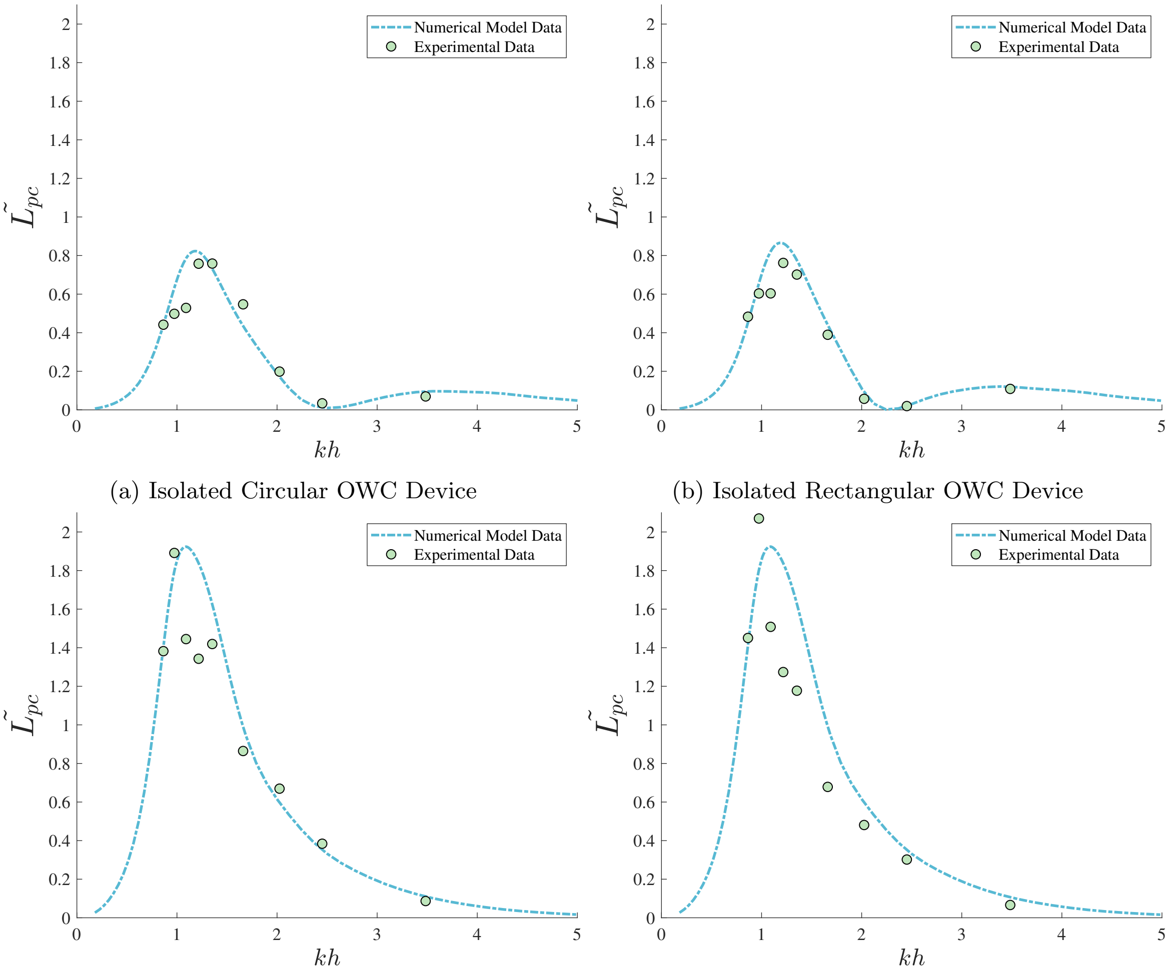

(a) Isolated Circular OWC Device (b) Isolated Rectangular OWC Device

(c) Breakwater Mounted Circular OWC Device (d) Breakwater Mounted Rectangular OWC Device

Figure 3.10: Experimental and numerical non-dimensional capture width presented as a function of kh

As displayed in Figure 3.10, the numerical model data yielded results for each condition that correlate well for the isolated cases with the data acquired from the experimental investigation. Similarly, the numerical model data for the breakwater conditions correlates well in the higher frequencies as displayed, where the value is within an acceptable error to that of the experimental data. The discrepancies in the data around resonance could again be related to the damping characteristics of the system, in culmination with the turbulence and viscous forces that were not modelled. The variation in the magnitude of the non-dimensional capture width between the model and experiment is similar to that of the volume flux. A comparison of the results for the different geometries under the same condition indicated that the variation in the OWC device geometry does not greatly vary the magnitude of the capture width; as such, a definitive conclusion to the optimal geometry was not made as the pair produce similar results.

It should be noted that the capture width and subsequent potential to absorb power presented in the results are not the optimal magnitude for each device. Although the non-dimensional capture width approached 0.6 for the isolated and 1.8 for the breakwater conditions respectively, the damping for each device was not optimised in the experimental investigation meaning the maximum capture width was not provided, therefore in practice under conditions of optimal damping, the devices would have the potential for higher power absorption capacities.

The comparison between the same devices under different conditions provided results that showed a significant increase in the capture width of the device when implemented into the breakwater. This increase in capture width suggests an indicative improvement in the potential for power absorption of an implemented device. The potential for power extraction close to shore, however, is less than that in an offshore region, which subsequently indicates that in practice the OWC device placed in isolation offshore has the possibility to absorb more energy than an onshore device implemented into a maritime structure. The increase in the potential power absorption of a device that is implemented into a breakwater or harbour does imply a capacity to increase the feasibility of the concept, as there is a reduction in costs associated with installation closer to shore, transportation of the electricity produced and maintenance of the device.

It is recommended that in order to further improve the results produced for this experimental investigation conducted on the OWC device implementation a study should be conducted into determining both the viscous coefficient and the effect it has through means of experimental comparison to a numerical model. This could further aid in the feasibility of OWC device implementation into a maritime structure and the optimisation of the power extraction capabilities.

3.4.4 Power Optimisation

A comparison was conducted between the numerical data produced using the experimental test variables, and numerical data produced using an optimal damping coefficient in order to determine the optimal potential power output of the OWC devices across a range of wave frequencies. Figures 3.11a and 3.11b display the numerical OWC data using test condition variables with the optimised data superimposed for the circular and rectangular devices respectively. It is illustrated that the power output of all devices could be increased dramatically around resonance by reducing the damping of the system, whereas, areas away from resonance would require more damping in order to produce more power than what was extracted during testing. The point at which the damping would be optimal to produce the maximum power across all the test frequencies is where the optimal power data is tangential to the numerical data in the plot.

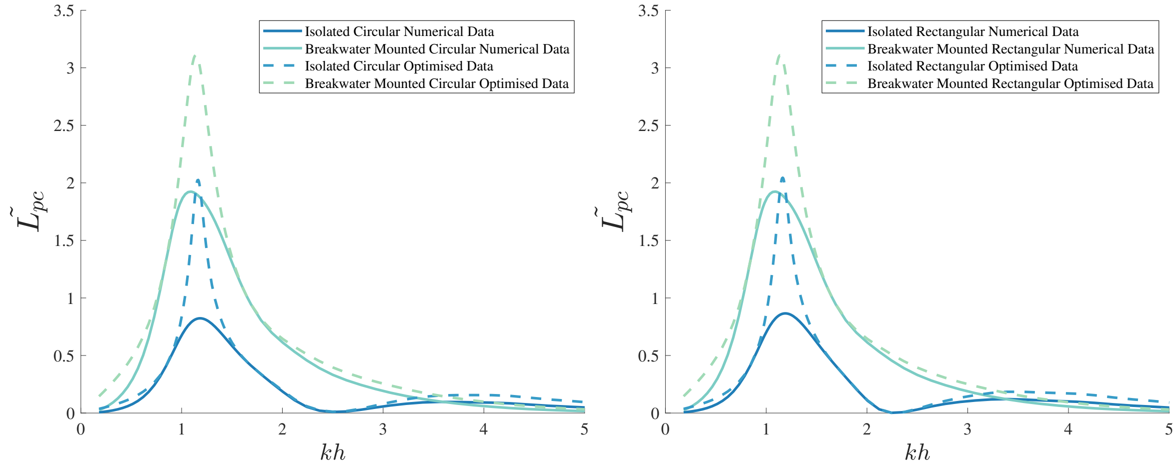

(a) Circular OWC Device

(b) Rectangular OWC Device

Figure 3.11: Numerical OWC power data plotted against optimised damping power data to display potential power output through varied damping coefficients

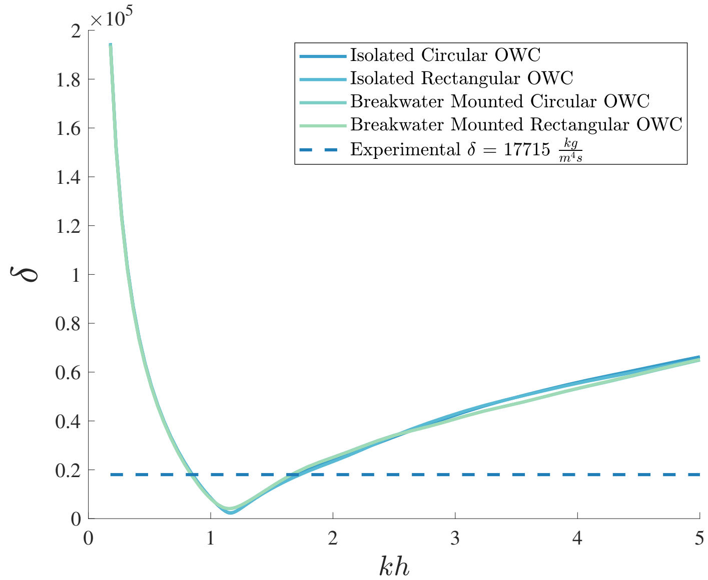

Figure 3.12: Numerical OWC damping data plotted with optimised damping line to display optimal damping coefficient for OWC devices

Figure 3.12 displays the change in optimal damping coefficient with respect to kh. It can be observed in this figure that the optimisation line intersects the optimal damping data at a value of approximately 18000 $\frac{kg}{m^4 s}$, which is comparable to that which was used during testing. Figure 3.12 also supports the data displayed in Figure 3.11, which shows that in order to increase the power output the damping should be decreased around resonance and contrarily increased outside of the resonance.

3.5 Conclusions

The objective of the presented paper was to establish whether chamber geometry and breakwater integration would have an effect on device performance. Through the use of FEM numerical hydrodynamic modelling and hydrodynamic experimental investigations, results were produced for volume flux, pneumatic damping and mean hydrodynamic power absorption. These results were used as quantitative tools in the analysis, comparisons and conclusions drawn regarding the design variations. The results regarding device chamber geometry, and its effect of the extraction efficiency presented results that indicated there was no discernible variation in the potential for power absorption between the two geometrically differing devices. This led to the conclusion that the chamber geometry of an OWC device had a negligible effect on performance. Although no optimal design was selected in regards to the performance characteristics of the device, when considering constructability and maritime structure integration, the rectangular device presents a more viable design solution. The comparison into the isolated and breakwater integrated devices produced results that showed a significant increase in the potential power absorption of the integrated device. The non-dimensional capture width of the integrated device could be seen as more than twice that of the isolated device at frequencies around resonance, with the non-dimensional capture width increasing across almost all of the test frequencies in comparison to the isolated device. In conclusion, it was determined that by integrating a bent duct OWC WEC into a maritime structure such as a harbour or breakwater, a significant increase could be achieved regarding the extraction efficiency of the device. This provides evidence that increases the feasibility of such a concept being developed in the future, however further research into the effects of viscosity and damping optimisation, along with air compressibility and losses related to the PTO system should be investigated to provide a more robust analysis of the integration effect. Similarly, realistic sea states including direction, crest length and irregularity should be investigated to provide representative analysis of the system performance.

Chapter 4

Energy Extraction Performance

4.1 Introduction

Chapter 3 illustrated the benefits to performance observed following breakwater integration of OWC devices, with the model scale experiments comparing an identical device both in isolation and breakwater integrated indicating that the device performed almost twice as effectively at resonance when integrated within a fixed breakwater. Pushes for industries such as aquaculture and offshore wind to expand operations into deeper waters presents the opportunity for further expansion of the breakwater integrated WECs from traditional fixed structures into floating breakwater concepts. Excluding the stand-alone floating type OWC devices discussed in Sections 1.1.3 and 1.1.5, which rely predominantly on device motions under incident wave interaction for energy extraction, few studies have been conducted regarding the integration of wave energy conversion devices within floating breakwaters, where structure motion is desirably minimal.

For the purpose of this proof-of-concept, a pontoon floating breakwater, specifically a Π-type, was selected as the most suitable structure for WEC integration. The unique shape of the breakwater aided in the ease of device incorporation within the rigid structure, allowing the OWC devices to achieve complete encapsulation within the forward pontoon of the breakwater. The Π-type breakwater was first proposed by Günaydin and Kabdaşli [205], an extension of work investigating the inverse U-type breakwater [206]. A comparison of the two design types highlighted the reduction in wave transmission and reflection, and increase in wave energy dissipation observed by the solid Π-type relative to the U-type [205] in both regular and irregular waves. These characteristics are preferable for a floating breakwater, as the performance of a breakwater is often evaluated as a function of its wave attenuation capacity and motions [159]. As the primary purpose of this concept will be to perform effectively as a floating breakwater, these characteristics were a governing factor during design selection. Further analysis into the π-type floating breakwater has resulted in the development of a formula to estimate the transmission characteristics of the structure [207, 208], as well as the evaluation of mooring stiffness on the behavior of the breakwater [209].

The purpose of the research presented in this experimental study is to provide a proof-of-concept for a floating breakwater integrated with bent duct type OWC devices, and how various design and incident wave parameters impact the energetic properties of the installed devices. As this is considered a baseline study, a soft mooring arrangement (see Figure 4.5) was employed during the experiments to simulate a free floating condition, subsequently eliminating the influence of mooring arrangement from the results and allowing future investigations to explore this component of the design. The results of the variational changes are compared with respect to both the non-dimensional capture width as defined in Section 2.1.2, and also as an efficiency relative to the incident wave energy interacting with the breakwater. The scope of the research presented in this chapter is centered solely around the hydrodynamic performance of the integrated OWC devices under the influence of monochromatic wave trains. Subsequently, the reflection and transmission properties and structure motions are covered in Chapter 5 and irregular wave analysis is covered in Chapter 6.

4.2 Theory

4.2.1 General

This research considers bent-duct type OWC devices governed by the dimensions described in Section 2.1.1, and illustrated in Figure 4.1. The rectangular cross-sectional area was maintained across all chambers, derived using Equation 2.1.

Maintaining the cross-sectional area and swept path dimensions across all devices ensured the volumes of air and water within the chambers and the inlet draft were consistent across devices, subsequently governing the extraction response. Common construction also allowed the interaction effects observed throughout the experimental investigation to be isolated, as all devices were expected to perform equivalently.

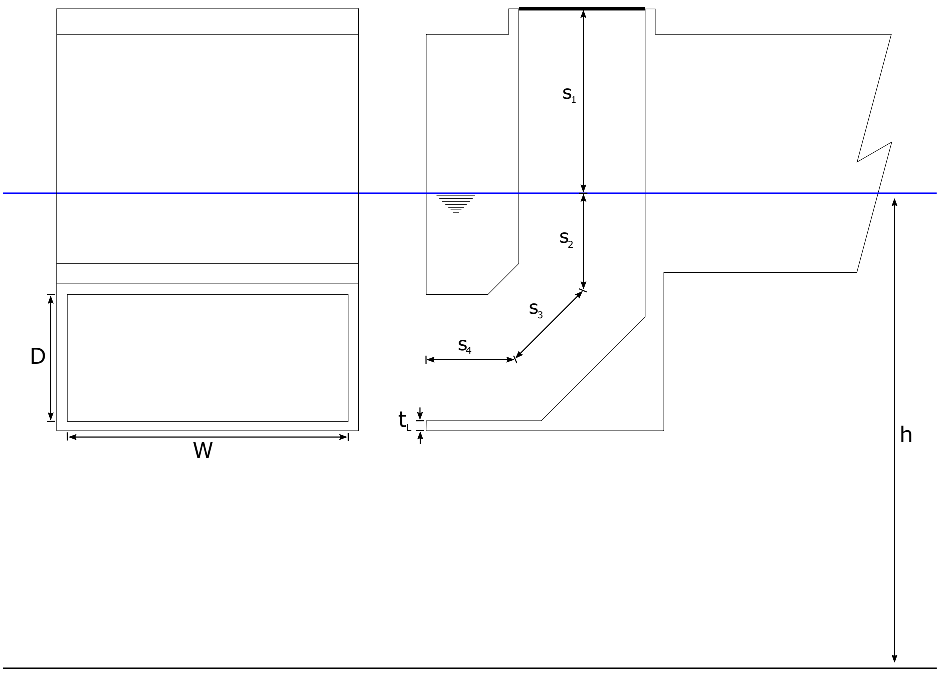

Figure 4.1: OWC device schematic detailing theoretical parameters, with model-scale PTO simulant (thick line) presented at outlet of device (not to scale)

4.2.2 Theoretical Hydrodynamic Consideration

Volume Flux and Damping

In the same vein as Chapter 3, the theoretical hydrodynamic considerations applicable to this research investigation are outline in Section 2.1.2. The experiments adopts the same PTO simulant as used in Chapter 3, which observed a linear damping relationship. Subsequently the volume flux, pneumatic damping, dynamic pressure and energy absorption characteristics of the integrated OWC devices are evaluated equivalently. As previously, the air chamber volume of the model OWC devices were selected small enough such that the effects of air compressibility were not observed during testing. Elhanafi et al. [210] proposes that performance estimates based on model scale testing where air compressibility is not modelled can result in an overestimation of approximately 12% at full scale. While this research considers a proof-of-concept, and does not extrapolate to predict full scale performance, it is understood that a simple correction can be applied to these estimates to reduce the extrapolated pneumatic power results accordingly.

Power and Performance

The performance of the individual OWC devices integrated within the floating breakwater were evaluated in terms of the non-dimensional capture width, as derived in Chapter 2. This provided a metric illustrating the power absorbed by the device relative to the incident wave power entering the inlet of the OWC device. As the WEC/breakwater model considered operation of multiple OWC devices, a second performance comparison concentrated on the mean non-dimensional capture width of the operating OWC devices, denoted as $\tilde{L}_{pc_m}$, and defined in Equation 4.1

$$\tilde{L}_{pc_m} = \frac{\sum_{i=1}^{n} \tilde{L}_{pc_i}}{n} \tag{4.1}$$

where n represents the number of operational devices. Finally, to establish the performance of the entire multi-device floating structure, the efficiency, ϵ, of the module was derived using the relationship presented in Equation 4.2

$$\epsilon = \frac{P_{h_t}}{P_I L} \tag{4.2}$$

where L represents the length of the breakwater and the total mean hydrodynamic power absorbed, P_{h_t}, is given by,

$$P_{h_t} = \sum_{i=1}^{n} P_{h_i} \tag{4.3}$$

where n again represents the number of operational chambers. This considers the total mean hydrodynamic power absorbed by the operational devices relative to the incident wave power interacting across the length of the breakwater.

4.3 Experimental Setup

4.3.1 Experimental Considerations

Volume Flux Q

As with previous experimental investigations conducted using bent duct type OWC devices (cf. Chapter 3 and [89, 187–189, 194]), two assumptions were made regarding the volume flux. Firstly, it is understood that the dynamic oscillation within the OWC chamber will induce different excitation modes of the free surface. In an effort to capture these variations in free surface elevation, three wave probes were installed within each chamber at varying locations. The OWC chamber free surface amplitude, (η_{OWC}), is considered approximately equal to the mean amplitude of the free surface as determined via spatial averaging of measured data from three internal wave probes, hence proposing the free surface oscillates uniformly within the vertical chamber. Secondly, the free surface velocity is assumed to be approximately equal to the mean free surface velocity also indicating the free surface moves uniformly. The equations governing these assumptions can be found in Chapter 2.

4.3.2 Model Test Basin

The Australian Maritime College's Model Test Basin was the hydrodynamic experimentation facility utilised for these experiments, with an operational water depth of 600 mm employed for this investigation.

The configuration devised for the experiments is illustrated in Figure 4.2. It displays the locations of the instruments within the basin as well as the MTB dimensions. It should be noted that the incident wave probe (IWP) and phase wave probe (PWP) were located 300 mm from the starboard side wall. Similarly, the floating breakwater/WEC was positioned centrally within the basin such that the sides of the breakwater were positioned 3.75 m from the basin walls.

In Figure 4.2, the structure to the left of the WEC/breakwater device is the damping beach outfitted in the MTB, while the blue structure to the right of the device represents the 16 piston-type wave paddles that generated the regular waves in this experimental investigation. Mooring lines are not observed in Figure 4.2 as a soft mooring was utilised during the experiments.

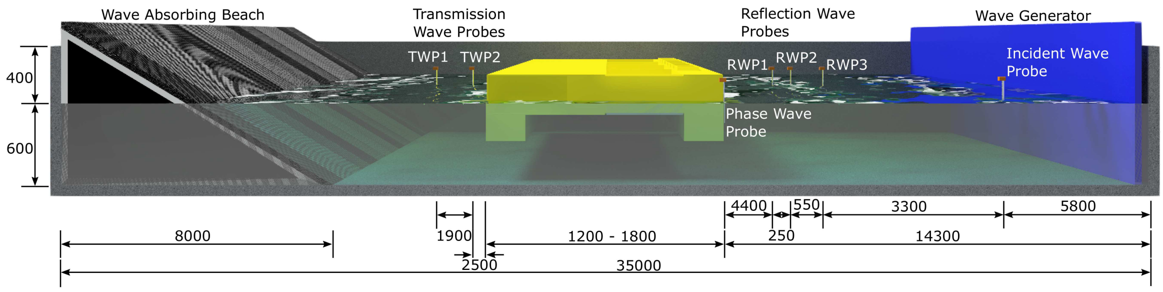

Figure 4.2: Side view of experimental configuration within AMC MTB, all units in mm (not to scale)

4.3.3 Model

AMC Model 18-17 was constructed in-house at the AMC, predominantly of marine grade plywood and finished with epoxy coating and paint. The OWC device dimensions can be found presented in Table 4.1, where the dimensions s_1-s_4 were determined through the use of the linear hydrodynamic FEM model detailed in Chapter 3 to ensure resonance would be observed at approximately 0.775 Hz, while W and D were selected as these were the maximum possible dimensions which allowed the OWC chambers to be completely incorporated within the front pontoon of the floating breakwater. When compared to the devices in Chapter 3, the resonant frequency was increased from 0.6 Hz to 0.775 Hz to increase data acquisition for frequencies below resonance. The floating breakwater/WEC device represents a 1:20 scale model, indicating an intended full-scale module size of 90m long, 36 m wide, 6 m draft and a freeboard of 4 m using Froude Similitude for the largest (1800 mm) width variation. Two key design requirements were the necessity to easily manipulate both the width of the breakwater, and also the configuration of the operational OWC devices. The first of these requirements was met through the integration of a sliding mechanism which allowed the bow pontoon to separate from the stern portion of the breakwater, subsequently increasing the width. To fill the void left by the pontoon separation, two spacing modules were constructed (300 mm and 600 mm respectively), and integrated into the device. This allowed the displacement of the floating breakwater to be altered, whilst maintaining the operational draft, and removed any undesirable phenomena resulting from the subsequent moonpool created.

Table 4.1: OWC device dimensions corresponding to the theoretical diagram presented in Figure 4.1

Variable	Dimension (mm)
s_1	212
s_2	123
s_3	120
s_4	111
t_L	12
W	330
D	160
h	600

The second design requirement was fulfilled by incorporating a recessed area surrounding the OWC device inlets to which either inlet opening frames or shut-off panels could be configured. This allowed for simple and repeatable methods to be employed for OWC device configuration variations, subsequently allowing for a series of different conditions to be compared. For simplicity, each OWC device configuration variation was given an identification label which can be found in Table 4.2.

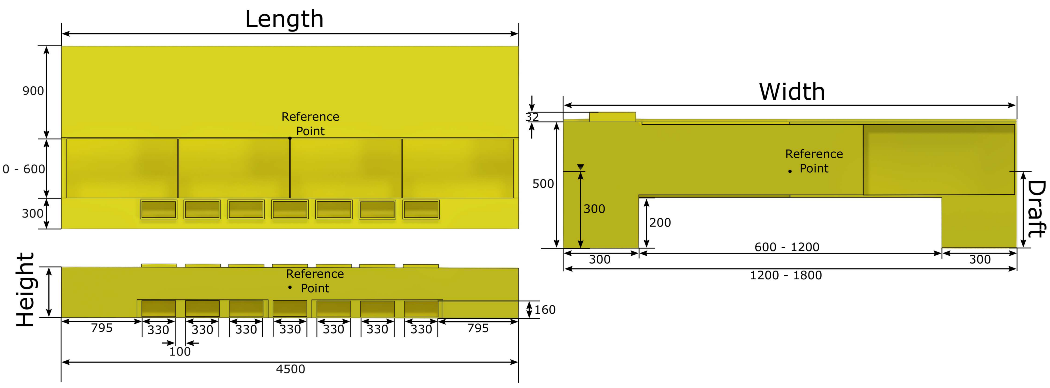

Figure 4.3: AMC Model 18-17 in top, side and front views with dimension orientations and values, all model-scale dimensions in mm

Figure 4.3 displays the dimension and orientation definitions prescribed for the OWC WEC integrated floating breakwater. It should be noted that the width of the device is defined along the bow-to-stern axis, subsequently corresponding to the longitudinal axis of the AMC MTB. This notation was selected to ensure the largest dimension of the structure was denoted as length, which is the transverse measurement of the device. This breakwater dimension and orientation notation correlates with common breakwater naming convention [140, 144].

Table 4.2: OWC device configurations with spacing intervals indicated where applicable. Units in mm.

Device Configuration	**Visual Representation**
Breakwater Only	
Single	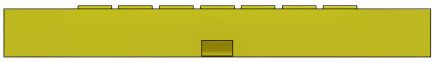
Double	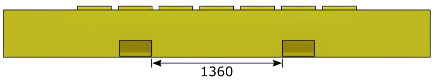
Close	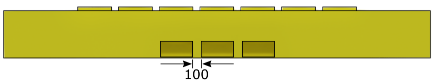
Intermediate	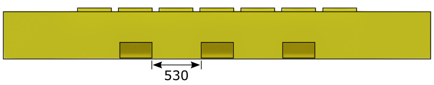
Far	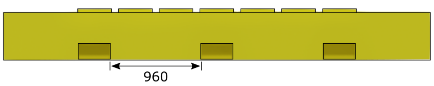
Double-Double	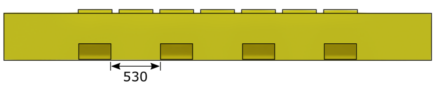

The floating breakwater structure had overall dimensions of 4500 mm length, 500 mm height and width which was varied between 1200 mm, 1500 mm and 1800 mm, as illustrated in Figure 4.3. The operational draft of the device was maintained at 300 mm for all experimental tests. Figure 4.3 also illustrates the dimensions of device, where the OWC chambers had dimensions of 330 mm × 160 mm, with 100 mm of spacing between each device. It should be noted that in Figure 4.3, dimensions that are given a range indicate that they were varied across different conditions during the experimental investigation. Figure 4.4 illustrates the device when installed in the AMC MTB at operational water depth.

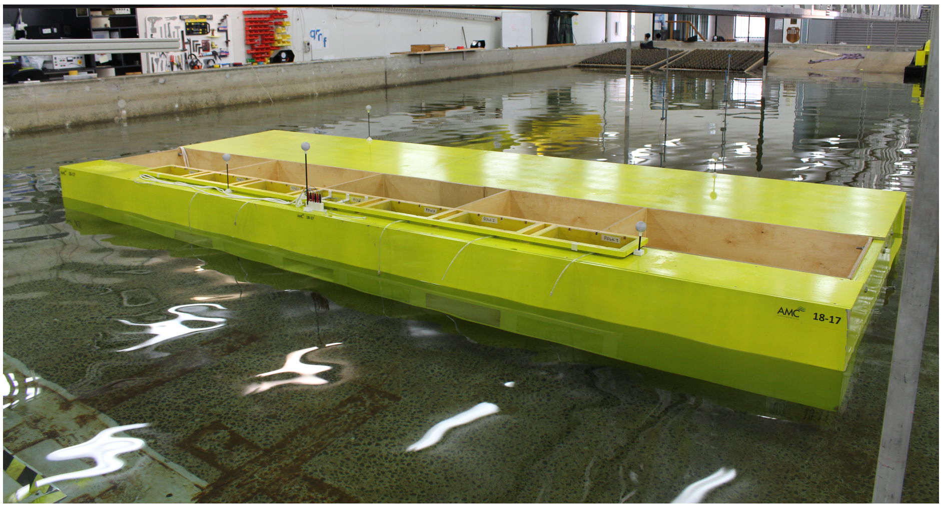

Figure 4.4: AMC Model 18-17 installed in the AMC MTB in the 1800 mm breakwater width configuration

Mooring

During the experimental configuration, the device was moored using two soft mooring assemblies configured on opposite sides of the MTB, such that the hanger/weight assembly which provided the constant force could be utilised from the outside of the basin (see Figure 4.5). Each hanger was outfitted with 6 kg of weight, which provided the necessary constant force to allow the device to operate. It also helped maintain the device's position in the transverse middle of the MTB, and could be easily altered to adjust the device in the event that it shifted position from centre. The mooring lines were then run through the pulley system and connected to the model via pre-installed eyelets located at midships and directly on the waterline. All conditions considered in this chapter had the floating breakwater/WEC device moored in the basin with a heading angle of 0°, such that the front of the model ran perpendicular to the direction of incident wave propagation.

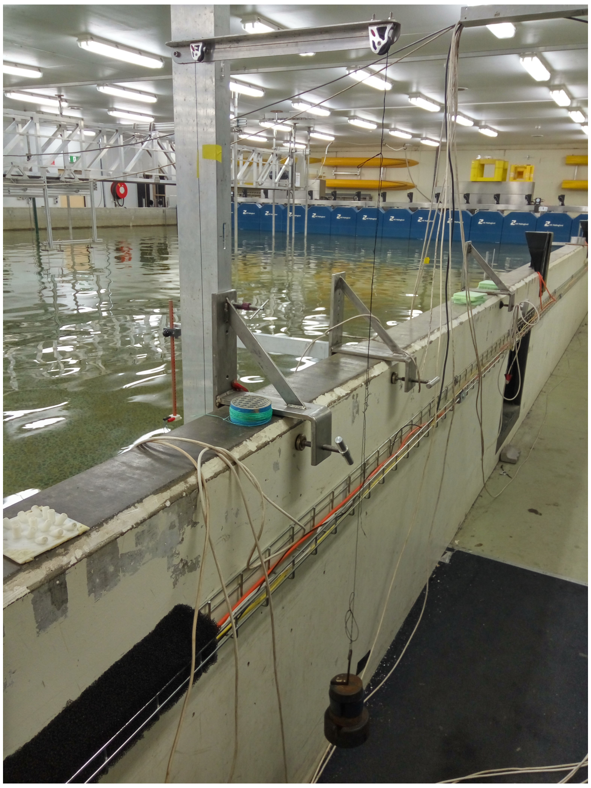

Figure 4.5: Soft mooring assembly with hanger/weight attached as utilised during experiments to provide constant force to model

Power Take-off

The desired linear damping relationship of the PTO was simulated through the use of the porous Enviro-Cloth mesh as discussed in Chapters 2 and 3. The variations in damping were given an abbreviation for simplification purposes, where LDV is the linear damping value. The damping values investigated were achieved through layering sheets of the porous mesh, where additional layers resulted in increased damping applied to the system.

Table 4.3: Pneumatic damping nomenclature and characteristics

Damping Type	Damping I.D	Damping Coefficient (δ) $\left[\frac{kg}{m^4 s}\right]$
Linear	LDV_1	1145
	LDV_2	2382
	LDV_3	3450
	LDV_4	4672
	LDV_5	6410

The damping specifications for each variation can be found in Table 4.3 and Figure 4.6 illustrates an example of the damping characteristics of the mesh for each of the operational chambers. The conditional damping dataset presented in each subplot of Figure 4.6 is the collation of the damping data obtained from all experimental runs conducted for the specified condition, subsequently indicating that the applied damping is frequency independent. Comparing Figures 4.6a, 4.6b and 4.6c with respect to δ derived from the linear assumption, it can be observed there is variation between the obtained values, however these variations are within approximately $\pm$ 5% of the mean value across the chambers. This linearity of the relationship compares well with the approximated damping relationship typically associated with the Wells Turbine (cf. Fig. 5 in [211]), indicating the porous fabric mesh presents a good simulant for modelling the PTO induced damping at model scale.

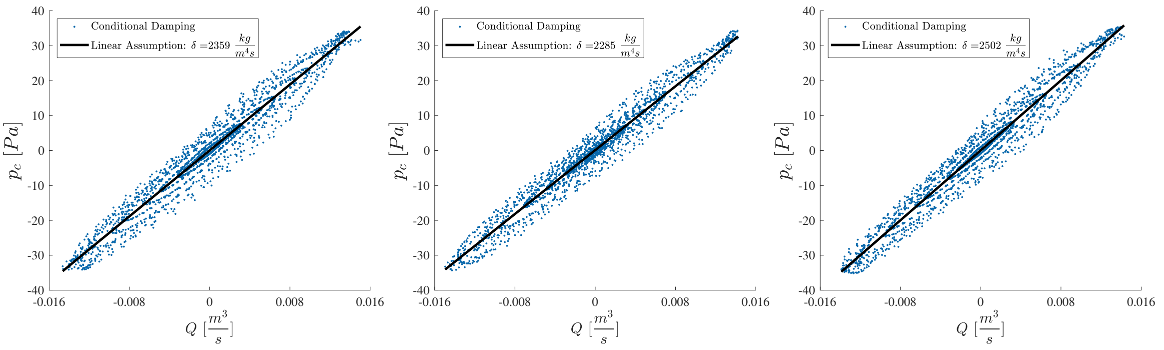

(a) Port Chamber (b) Middle Chamber (c) Starboard Chamber

Figure 4.6: Conditional damping characteristics with linear assumption of δ for each operational OWC chamber in the Far configuration with LDV_2 applied

4.3.4 Instrumentation

Water surface elevation was measured using resistance type wave probes configured to a multi-channel wave probe monitor manufactured by HR Wallingford (cf. Chapter 2). Each probe configured in the wave basin was 300 mm long, and there were a total of seven wave probes in the basin consisting of three reflection probes, two transmission probes and one incident and phase wave probe respectively. The wave probes located in the OWC chambers were custom-built for AMC Model 18-17 and vary in length dependant upon their position in the chambers. The OWC chamber probes were made to be transferable between all chambers, however their positioning within the chamber would vary dependant upon which chamber(s) was operational. The dynamic pressure inside the OWC chambers was measured using pressure sensors (one per chamber) incorporated with a small diffuser that prevented water entering or becoming lodged within the pressure probe tap.

The wave probes were calibrated either daily, or at the change of condition, whichever were to occur first. Each of the basin situated probe ranges was calibrated to $\pm$ 100 mm, whilst the OWC chamber wave probes were calibrated to $\pm$ 130 mm to ensure resonant free surface elevations were sufficiently captured. The OWC chamber pressure probes were calibrated at the change of condition to $\pm$ 300 Pa with a gain setting of 10 and a low-pass filter value of

10 Hz to remove any unwanted noise from the signal. All probes discussed in this chapter were sampled at 200 Hz.

4.3.5 Test Matrix

The experimental investigation into the floating breakwater/WEC device was conducted across two separate sessions in July/August 2018 and January 2019 respectively. The experimental test matrix details 41 varying conditions that were investigated from which data was processed to determine the impact of each conditional change on the performance of the OWC devices. Table 4.4 lists the parameters that were varied throughout the experimental testing, with the right hand column presenting the varying conditions. Note that parameters such as fixing the device, incident wave angle and quadratic damping were not tested for all OWC device configurations, nor breakwater width variations, hence Table A.1 (see Appendix A) should be referred to regarding specifics for conditional information.

All experimental runs were randomised with respect to frequency, sea state (regular and irregular) and wave height (where applicable). This is in compliance with the Design of Experiment guidelines as specified by the International Towing Tank Committee [198, 199].

Table 4.4: Experimental Parameters

Parameters	**Details of 1:20 Scale Experiments**
Water Depth	$h = 0.600$ m
Regular Waves	$H = 0.02$ m, 0.03 m, 0.04 m, 0.05 m, 0.06 m $f = 0.5$ Hz - 1.2 Hz
Breakwater Length	$W_b = 1200$ mm, 1500 mm, 1800 mm
OWC Device Configurations	One Device: Single Two Devices: Double Three Devices: Close, Intermediate, Far Four Devices: Double-Double
Power Take-off	Linear: Fabric Mesh (LDV_1 - LDV_5)
Mooring Arrangement	Soft Mooring
Motion	Fixed and Floating

4.3.6 Data Processing

The sinusoidal nature of the regular wave experimental data collected during the investigation allowed the use of a phase-averaging post processing technique, as discussed in Chapter 3. Phase averaging can be utilised to improve the reliability of data, subsequently reducing experimental uncertainty, without the necessity for repeated runs. Orphin et al. [189] investigated the experimental uncertainty of an OWC WEC using both phase averaging and 10 wave repeat techniques, from which it was concluded that phase averaging could provide experimental uncertainty results comparable with those obtained from the traditional 10 repeat technique.

4.4 Results and Discussion

4.4.1 Uncertainty Analysis

The true value of a measured physical quantity should include both bias and precision errors [212]. An uncertainty analysis can be conducted in order to estimate the magnitude of these errors. As outlined in [89], uncertainty in measurement can be subdivided into three categories: a) standard uncertainty, b) combined uncertainty, and c) expanded uncertainty. Standard uncertainty is a function of two types of uncertainty; Type A uncertainty, which is derived from statistical analysis of repeat observations, and Type B uncertainty, which is evaluated for other considerations such as instrument calibration, quantification of assumptions and other such relevant information pertaining to the experiments. The methodology regarding experimental uncertainty analysis of wave energy converters for this experimental investigation is as presented in [89], the theory of which can be found in Appendix B. As such, notation and equations presented follow that proposed by International Towing Tank Conference guideline 7.5-02-07-03.12 "Uncertainty Analysis for a Wave Energy Converter" [213].

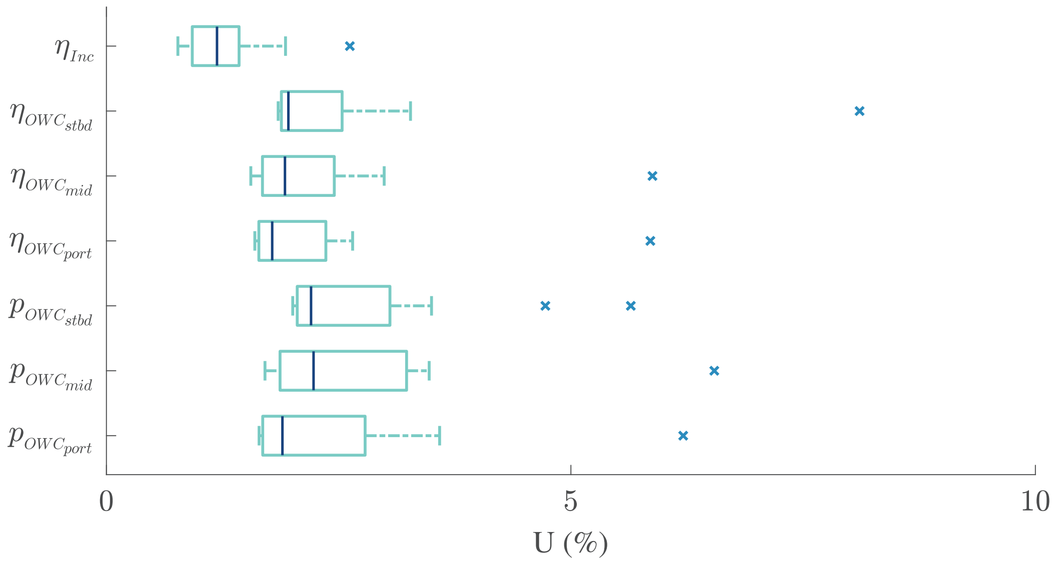

Figure 4.7: Expanded Uncertainty, U, for directly measured variables to a 95% Confidence Interval, with the coverage factor, k, varying depending on the number of repeats of each respective experimental run.

Figure 4.7 presents the expanded uncertainty, U, for each of the variables measured directly via instrumentation during the experimental investigation. The variables measured included the incident wave elevation, OWC chamber free surface elevation and dynamic pressure.

For the purpose of investigating the associated uncertainty, we consider the amplitudes of these quantities, where η_{Inc} is the amplitude of the incident wave, η_{OWC} is the amplitude of the free surface elevation within the OWC chamber, and p_{OWC} represents the amplitude of OWC chamber pressure. As the example provided investigates the uncertainty of the Far OWC configuration, the subscripts *stbd*, *mid* and *port* refer to the respective operational chambers. The expanded uncertainty for the instrument measurements were derived for each incident wave frequency tested, subsequently developing a uncertainty dataset which is presented using traditional box plots. The box plots conform to generic structure where the left and right edges are the first and third quartiles, representing the 25^{th} and 75^{th} percentiles respectively, the central vertical mark indicates the median, and the whiskers extend to the most extreme data points not considered outliers. Outliers, denoted by $\times$, are identified as data points which fall outside the lower and upper bounds governed by Equations 4.4 and 4.5 respectively,

$$LB = Q_1 - (1.5 \times IQR) \tag{4.4}$$

$$UB = Q_3 + (1.5 \times IQR) \tag{4.5}$$

where Q_1 and Q_3 are the first and third quartiles, and IQR is the interquartile range.

As Figure 4.7 illustrates, the expanded uncertainty for all measurements acquired falls below 10%; yet, when outliers are dismissed the uncertainty in measured variables falls below 5%. The largest uncertainty value was derived for the free surface oscillation amplitude in the starboard OWC chamber, $\eta_{OWC_{stbd}}$, indicating a value of approximately 8%, which though relatively large in magnitude, still falls within an acceptable level of experimental uncertainty. On average, the wave probes yield less measurement uncertainty when compared to the pressure probes, which is predominantly attributed to the Type A repeatability uncertainty. Notwithstanding, both instruments present a narrow uncertainty bandwidth of approximately 2% - 4% which provides favourable confidence in the data acquired from the experimental instruments.

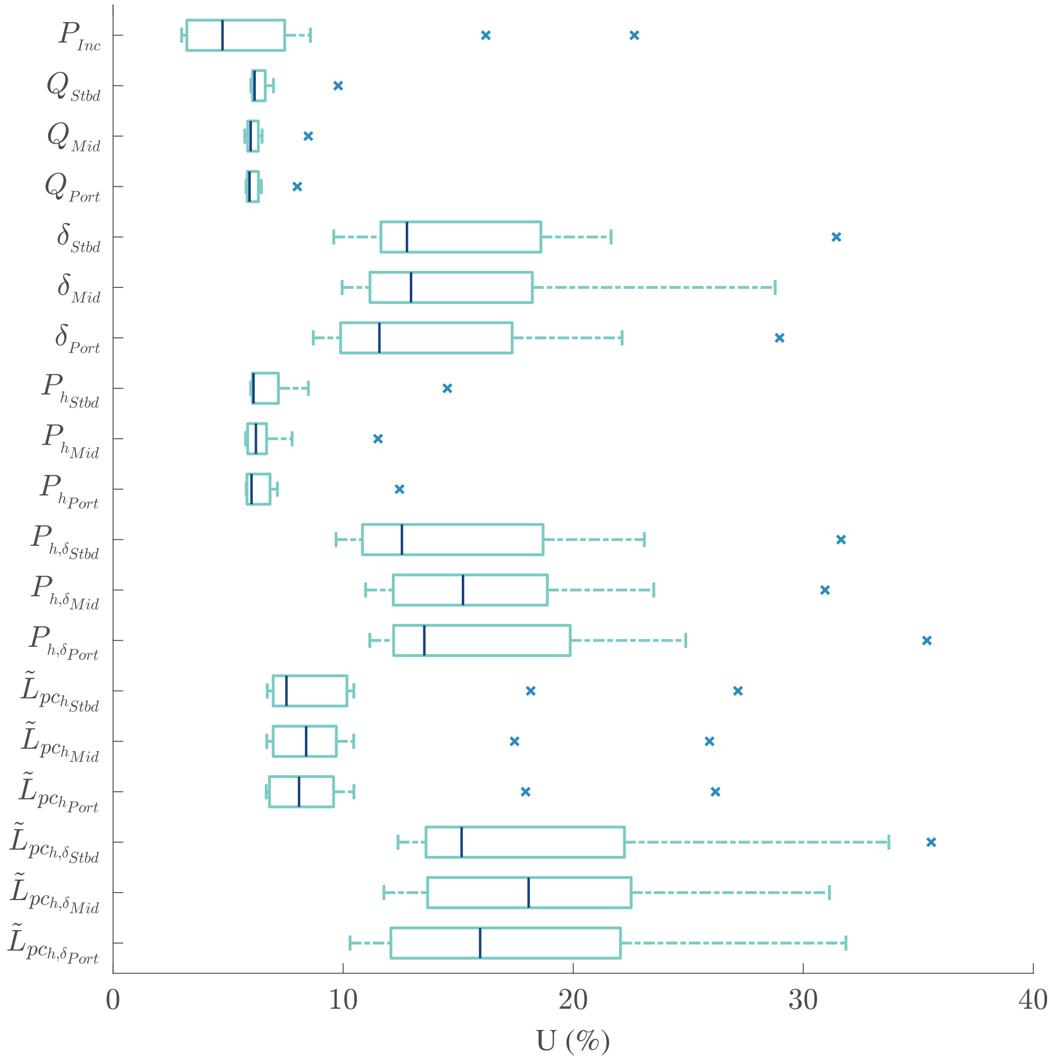

Figure 4.8: Expanded Uncertainty, U, for data reduction equations to 95% Confidence Interval

Figure 4.8 presents the expanded uncertainty of the Data Reduction Equations (DREs) of interest during the experimental investigation, which were found to be of larger magnitude on average than that derived for the measured variables. Similarly to Figure 4.7, the applicable DREs are presented for each operational chamber configured for the analysed condition, where it is observed that there is relatively minimal variation in the experimental uncertainty results across chambers.

As Figure 4.8 highlights, one primary source of uncertainty in the experimental investigation is the pneumatic damping coefficient, δ, as derived from Equation 2.2 in Section 2.1.2. The uncertainty associated with δ, discussed further in Appendix B.2, subsequently propagates into the evaluation of absorbed hydrodynamic power, $P_{h,\delta}$, derived using Equation 2.9, and the non-dimensional capture width following from this derivation of $P_{h,\delta}$, denoted $\tilde{L}_{pc_{h,\delta}}$. Significant contrast is evident in the levels of uncertainty associated with the direct method of evaluating P_h as presented in Equation 2.8 compared to when δ is considered, where the former has expanded uncertainty medians of approximately 8% compared with the approximately 17% corresponding to the δ method.

Using the results for non-dimensional capture width presented in Figure 4.8, a bounds of uncertainty could be applied to the results evaluating the performance of the OWC devices, as found in Figure 4.9. It should be noted that the uncertainty bounds have been linearly interpolated between each experimental data point based on the expanded uncertainty of each experimentally derived value. The results presented in Figure 4.9 provide confidence that the performance evaluations of the OWC devices henceforth are indicative of the true operation of the device, with the experimental uncertainty largest at resonance, and decreasing as the incident wave frequency migrates away from resonance.

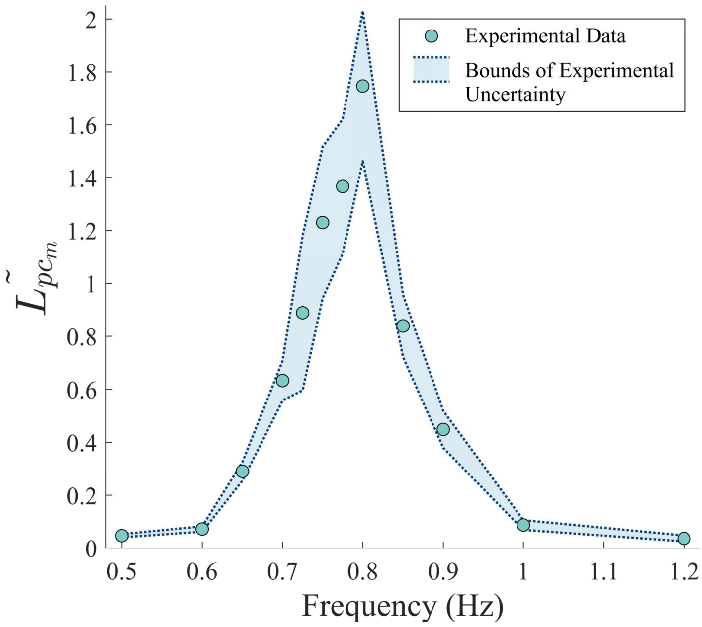

Figure 4.9: Mean non-dimensional capture width, $\tilde{L}_{pc_m}$, with bounds of expanded experimental uncertainty to 95% Confidence Interval for the 1800 mm breakwater configured in the Far OWC device configuration operating in 0.02 m wave heights.

4.4.2 Preliminary Study - LDV_1 Damping

Breakwater Widths

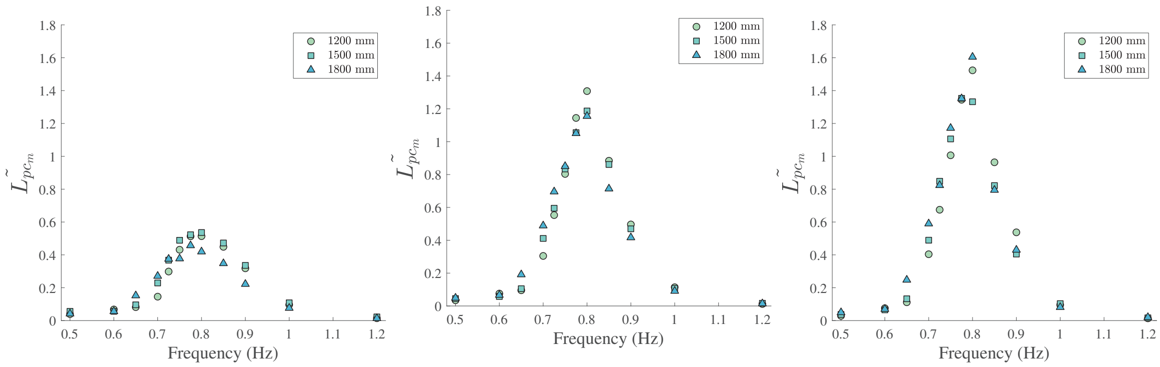

(a) Close Device Configuration (b) Intermediate Device Configuration (c) Far Device Configuration

Figure 4.10: Mean non-dimensional capture width for operational OWC devices in designated device configurations for varying breakwater widths

Evaluation of OWC device performance was determined as the non-dimensional capture width. The subfigures presented in Figure 4.10 illustrate the mean performance of the operational chambers across breakwater width variations for three different device configurations (refer to Table 4.2 for device configuration nomenclature).

From Figure 4.10, it is illustrated that variations to the breakwater width have negligible impact on the performance of the integrated OWC devices. This trend appears consistent across the three device configurations that were varied in breakwater width, with fluctuations in results likely attributed to minor discrepancies in pneumatic damping. The variation in results for each data set within the Figures 4.10a, 4.10b and 4.10c fall within the bounds of experimental uncertainty for this experiment. Similarly, Figure 4.10 indicates that the additional breakwater width has no impact on the overall device performance response (the reasons for which are discussed in Chapter 5). This signifies that device response remains primarily a function of submerged chamber geometry.

The results presented in Figure 4.10 indicate that the additional structure provides no distinct benefit to the performance of the WEC devices integrated. This implies that the breakwater width is not a necessary consideration in the design of the integrated WECs specifically. However, breakwater width will likely be considered with regards to the leeside environmental protection function of the breakwater and the topside infrastructure requirements.

Considering Figures 4.10a, 4.10b and 4.10c sequentially with respect to device configuration, it can be noted that the spacing between devices has a significant impact on the performance of the integrated devices. Each configuration in Figure 4.10 included three operational devices, however the Far configuration in Figure 4.10c displays the greatest extraction capacity which coincides with the largest device spacing, equivalent to approximately 2.9 device widths ($2.9W$).

Device Performance - Individual

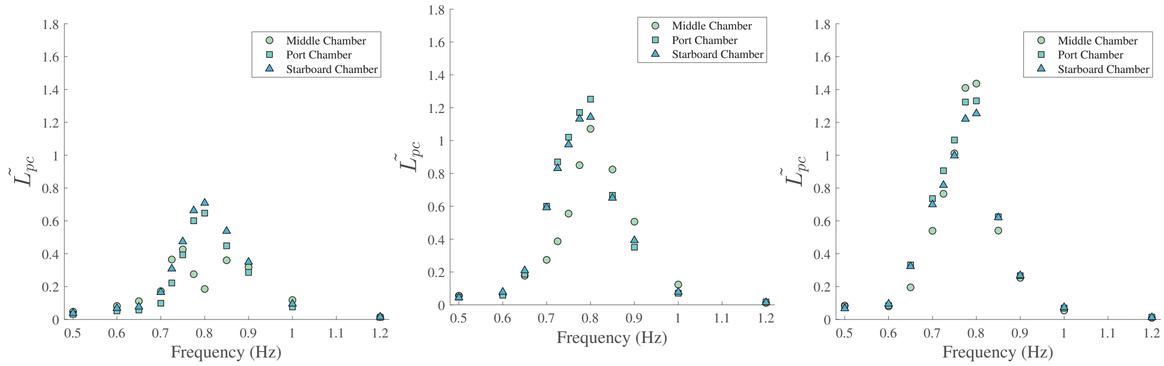

(a) Close Device Configuration

(b) Intermediate Device Configuration

(c) Far Device Configuration

Figure 4.11: Non-dimensional capture width for each operational OWC chamber with the breakwater configured at 1800 mm width operating in 0.02 m regular waves

To further investigate the cause of the performance increase resulting from OWC device spacing presented in Figure 4.10, Figure 4.11 compares the $\tilde{L}_{pc}$ of each operational chamber obtained from configurations in which three devices were operating at varying device spacings. Considering Figure 4.11a which displays the Close OWC configuration equating to device spacing of $0.3W$, it is apparent that the middle chamber is significantly affected as a result of interaction with the port and starboard chambers, most prominently both at, and around the resonance frequency of the devices. This result would indicate that the port and starboard chambers are taking energy from the interior device as their respective capture widths increase at resonance, subsequently leaving less energy available for extraction by the middle chamber. This destructive interaction phenomena is further substantiated in Figure 4.11b for the Intermediate OWC device configuration with device spacing of approximately $1.6W$, which indicates device interaction is present, however at a reduced magnitude relative to that presented in Figure 4.11a, as a reduction in the performance of the middle device is only observable in wave frequencies between 0.7 Hz to 0.8 Hz.

Figure 4.11 also illustrates how device performance is impacted by the reflective structure surrounding the OWC devices. Observing the subplots of Figure 4.11 sequentially, it is evident that increased device spacing, and subsequent increase in reflective structure surrounding each operational device results a substantial increase in device performance. This correlates well with the results presented in Chapter 3, and previous studies regarding breakwater integrated bent duct type OWC devices which presented results indicating that an increase in wave reflection can significantly improve the performance of an OWC device [187]. In particular, Grennell et al. [187] highlighted the importance of the reflective structure immediately around the OWC device, demonstrating the significant reduction in performance caused by lack of reflective structure surrounding the device. A similar phenomena is observed in Figure 4.11a where the outer chambers encroach the reflective surrounding of the middle chamber, significantly limiting its extraction capacities. As device spacing increases, this becomes less discernible up to which point the extraction capacities of all operational devices converge to an equivalent magnitude as found in Figure 4.11c.

As mentioned, Figure 4.11c indicates that the increased device spacing achieved in the Far configuration ($2.9W$) results in negligible interaction effects between devices, with performance variations presented between the individual chambers falling within the bounds of experimental uncertainty. This result would infer that the devices are operating effectively as isolated devices, however due to the multi-device integration, and the subsequent energy sink created, the overall performance of the devices significantly improve relative to that of the single isolated device displayed in Figure 4.12. Overall, these results reiterate the necessity to consider device spacing during the design stage to ensure efficient hydrodynamic extraction occurs without destructive interference due to device interactions.

Device Configuration

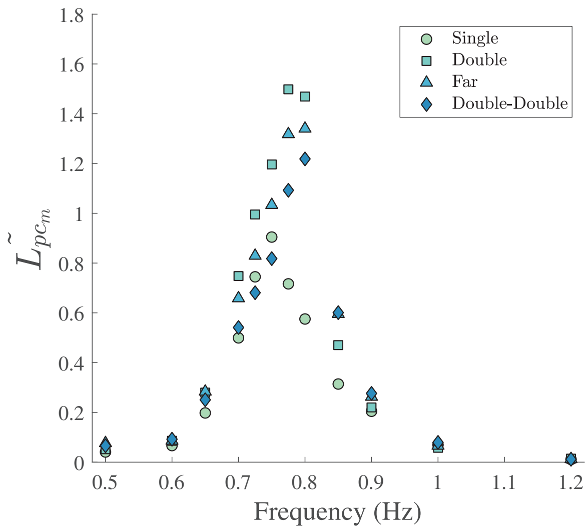

(a) Mean Non-Dimensional Capture Width

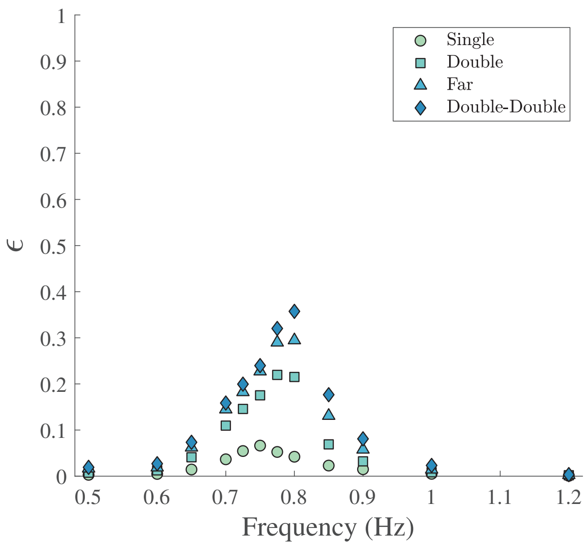

(b) Overall Device Efficiency

Figure 4.12: 1800 mm breakwater width operating in 0.02 m wave height with LDV_1 damping

This device spacing effect is also illustrated in Figure 4.12, which presents the performance of the Single, Double, Far and Double-Double device configurations, having one, two, three and four operational devices respectively. As previously, Figure 4.12a displays the $\tilde{L}_{pc_m}$ of the operational chambers, while Figure 4.12b displays the efficiency, ϵ.

From Figure 4.12a, it can be seen that as the spacing between operational devices increases, the average performance of the chambers subsequently increases, culminating with the Double configuration, having device spacing of approximately $4.1W$, displaying the greatest performance and also largest device spacing. This would indicate that integrated devices are experiencing negative interaction effects as device spacings decrease, reducing extraction capacities and subsequently performing sub-optimally. Significant consideration should therefore be given to device spacing during the design process of multi-device structures in order to avoid any of the ill-effects of device interaction as presented.

With reference to multi-device structures, it is illustrated in Figure 4.12a that multi-device integration results in greater mean chamber performance than that obtained from a solitary integrated device. Considering the Single device configuration, it can be seen that its resonance peak magnitude achieved is approximately 0.9 whilst the mean chamber resonance magnitude for all other configurations is greater than or equal to approximately 1.2, indicating that device performance can be increased through multi-device integration. This relationship may be caused by multiple integrated devices creating a larger 'energy sink' in which the incident wave energy interacts, subsequently improving the absorption capacities of all devices.

Considering Figure 4.12b, it is evident that as the number of devices increase, the overall extraction efficiency of the breakwater increases. This trend is most prominent at the resonance frequency of the OWC devices where the largest variation in ϵ can be observed between the various configurations, while in both the lower and higher tested frequencies, the additional chambers have negligible impact on performance. A significant increase is observed between the Single and Double configurations, whereby introduction of a second OWC device improves extraction efficiency greater than twofold, further highlighting how a multi-device configuration can increase the mean performance for integrated devices as a result of the energy sink created.

Comparing the multi-device configurations at resonance in Figure 4.12b, the Double configuration presents an efficiency of approximately 20%, while the Far configuration presents an efficiency of approximately 30%. This would indicate that the variation in device spacing between the Double and Far configurations has negligible impact on the hydrodynamic performance of the integrated OWC devices as the subsequent performance improvement can be directly attributed to the additional chamber. This trend ceases when comparing the Far configuration to the Double-Double (spacing approximately $1.6W$), as it can be seen that the additional chamber does not improve the overall efficiency equivalently, indicating that interaction effects, combined with the reduction in reflective surrounding structure of the Double-Double compared to the Far configuration negatively impacts the performance of the operational devices. The results from Figure 4.12 indicate that as the device spacing increases to the equivalent of two OWC device inlet widths and greater, the interaction effects appear to be negligible. However, for configurations with device spacing less than this threshold, device interactions are apparent. Hence, during the design stage, emphasis should be placed on the device spacing parameter to ensure optimal device performance, while number of devices will likely be governed by techno-economic drivers. From a techno-economic perspective, multi-device structures present a more attractive concept due to shared costs. Therefore, the evidence to suggest multi-device structures operate more efficiently further contributes to the feasibility of the concept.

Fixed versus Floating

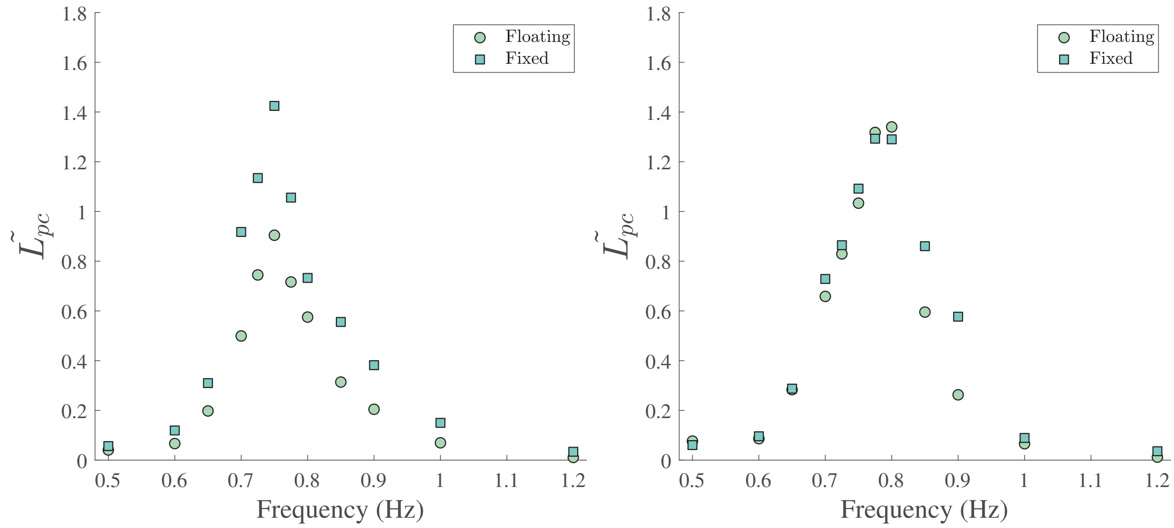

(a) Single OWC Device Configuration

(b) Far OWC Device Configuration

Figure 4.13: Mean non-dimensional capture width for fixed versus floating configurations with breakwater width set to 1800 mm operating in 0.02 m regular waves

The impact of breakwater motion on the performance of the integrated devices was investigated for the Single and Far device configurations, the results of which are presented in Figure 4.13a and 4.13b respectively. Comparison was conducted by rigidly fixing the floating breakwater model, via acrow props, to constrain all six degrees of freedom. The fixed condition was representative of the optimal condition, for both power extraction and wave attenuation (see Chapter 5), as the negative impacts attributed to device motions were eliminated. Firstly examining Figure 4.13a, an apparent increase in device performance is observable when the breakwater is fixed relative to that of its floating counterpart. This trend is evident across the entire frequency bandwidth tested, with the greatest magnitude of variation occurring at resonance, where the fixed configuration experiences approximately 50% increase in performance. This would suggest that motion impacts negatively on integrated OWC device performance when in the floating configuration. The motions have potential to provide positive impact on the OWC device performance subsequently providing added resonance to the system, as is the case for floating-type OWC devices; however, in the present case when out of synchronisation, the negative impact on performance is observed. The results regarding structure motion presented in Chapter 5 indicate that the maximum pitch Response Amplitude Operator (RAO) for the 1800 mm width breakwater variation occurs at approximately 0.65 Hz, while the Heave RAO displays substantial motion in frequencies up to approximately 0.9 Hz. These motion characteristics were obtained with the device constrained using a soft mooring apparatus, effectively replicating a free floating condition. Hence, the introduction of a realistic mooring arrangement may reduce the magnitude of these motions and subsequently mitigate the impact they have on OWC device performance.

The results for the fixed versus floating comparison of the Far configuration presented in Figure 4.13b displays a less discernible performance increase resulting from negation of breakwater motion. As illustrated, the increase in performance is only apparent above the resonance frequency, with the remainder of the tested bandwidth indicative of equivalent performance between the fixed and floating variations. Though the results indicate minimal variation between fixed and floating for the Far configuration, it is likely that motions are negatively impacting device performance, which should be explored with optimal pneumatic damping applied to the devices where performance is amplified.

Taken together, these results suggest there is an association between breakwater motion and integrated device performance, where elimination of device motion improves device performance for the Single configuration, and for most frequencies in the Far configuration. As suggested, further works should be conducted regarding fixed versus floating comparisons at optimal device damping where the effects may be more observable. The implications that these results have on the feasibility of such a concept are with regards to mooring considerations at the design stage. Selecting or designing a mooring system which reduces or constrains motion in specific degrees of freedom would be beneficial for device performance and subsequently device development. However, the feasibility of such a design from an economic perspective will likely be a governing factor in the overall design process.

4.4.3 Damping Variations

To explore the potential for hydrodynamic absorption of the operational devices, pneumatic damping variations were applied to the devices with the aim of establishing optimal damping characteristics of the concept. Figure 4.14 illustrates the $\tilde{L}_{pc_m}$ for the operational chambers in the Far configuration with differing amounts of damping applied (refer to Table 4.3 for damping nomenclature). From the data presented in Figure 4.14, it is apparent that as the pneumatic damping value increased, both the magnitude, and effective performance bandwidth (considered as where $\tilde{L}_{pc_m} \geq 1$) increased. Through pneumatic damping variation, the magnitude of performance of the configuration was effectively doubled at resonance relative to the LDV_1 damping, and the effective bandwidth extended from 0.75 - 0.825 Hz, to approximately 0.65 - 0.9 Hz. It should be noted that, although LDV_5 is specified as the optimal pneumatic damping, it only represents the optimum at resonance. A series of additional tests conducted solely at the resonance frequency of the device provided results to indicate that an increase to the next damping increment (approximately 7000 $\frac{kg}{m^4 s}$) reduced the magnitude of $\tilde{L}_{pc}$, a trend that continued as more damping was applied. The results presented for LDV_5 damping may however be sub-optimum at frequencies above, and below resonance, as such should not be considered the optimum value for overall OWC device performance across the frequency bandwidth tested. Further investigation both numerically and experimentally is recommended in order to comprehensively establish the overall optimal damping characteristics.

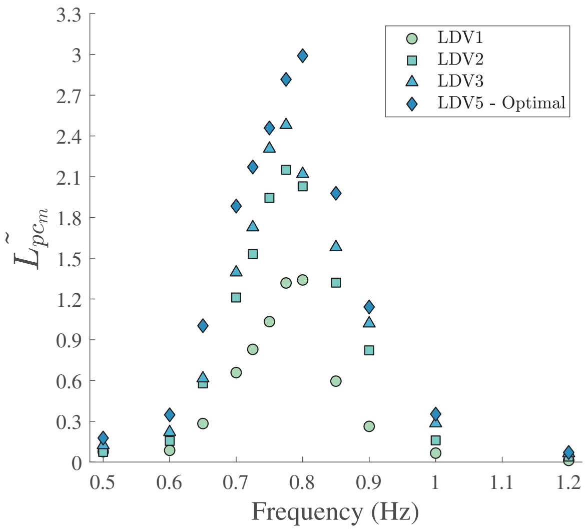

Figure 4.14: Mean non-dimensional capture width for variation in pneumatic damping with the floating structure configured to 1800 mm width and Far OWC device configuration

These results suggest that the damping characteristics of a turbine in the full-scale concept has significant implications on the performance of the device. This parameter should be a key consideration during the design of such a system, in particular, the chamber geometry should be optimised to suit the installed turbine, or vice-versa, to ensure the devices are operating to capacity. This consideration should also take into account the economic viability of a 'custom' turbine or an 'off the shelf' turbine and the damping impact they will impart on the system, as failure to consider these will result in sub-optimal performance.

4.4.4 LDV_5 - Optimal Damping

Device Configuration

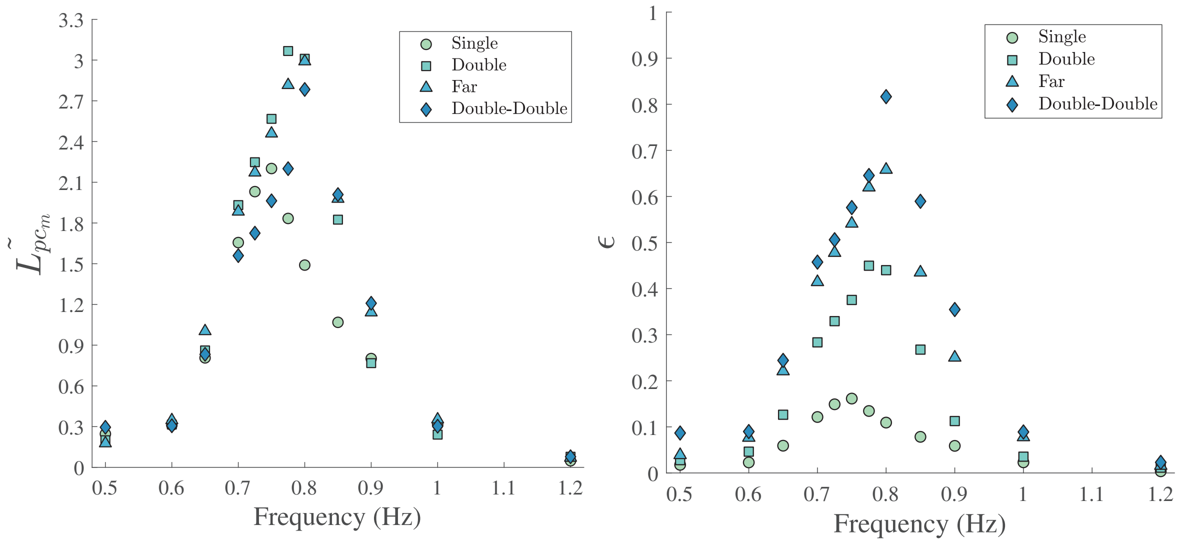

(a) Mean Chamber L_{pc}

(b) Overall Device Efficiency

Figure 4.15: 1800 mm breakwater width operating in 0.02 m wave height with optimal damping (LDV_5)

The results presented in Figure 4.15a and 4.15b illustrate the mean non-dimensional capture width of the operational devices and total efficiency of the OWC device integrated breakwater structure respectively with optimal damping applied. The trends present in Figure 4.15 provide further evidence to support those presented previously in Figure 4.12, which indicate that device spacing, and the subsequent reduction in device-device interaction increases the mean performance of the operational chambers. Similarly, the Double-Double configuration exhibits equivalent negative interaction effects as that of the Intermediate configuration resulting from the $1.6W$ spacing both configurations utilise. Finally, the Double configuration presents the greatest mean device performance, correlating to the largest device spacing.

Figure 4.15 highlights the potential for hydrodynamic absorption of the respective configurations, with Figure 4.15b indicating that the integration of four OWC devices within the breakwater in the Double-Double configuration correlates to approximately 80% of the available incident wave energy interacting with the breakwater to be absorbed at resonance. It is also illustrated that the Far configuration, utilising only three devices, performs equivalently to the four device configuration up to resonance, after which point the benefits of the additional devices become apparent.

The results would suggest that in order to maximise the amount of hydrodynamic energy absorbed, a greater number of devices should be integrated, however the almost 20% increase in performance at resonance with the additional chamber included in the Double-Double relative to the three-device Far configuration may not justify its integration, and subsequently may not be economically viable. A potential solution would be to increase the length of the breakwater to accommodate four devices with similar device spacing to that of the Far configuration, however this would again be driven by economic factors.

It is recommended that in order to develop this concept for an OWC WEC integrated floating breakwater, investigation should be conducted into more realistic sea-states and mooring arrangements. Performance under the influence of irregular waves would further aid in the feasibility of OWC device integration in floating breakwaters, and provide indicative results of expected full-scale hydrodynamic absorption, as is explored in Chapter 6. Similarly, design and integration of realistic mooring arrangements to further explore the impact of motion constraints on device performance would be beneficial in contributing towards the viability of ocean wave energy extraction in deeper waters. Considering the primary role of the breakwater being environmental protection, the impact of device integration on the wave attenuation properties, and structure motions should be investigated to establish the benefits/consequences of device integration. Finally, regarding expansion to full-scale, the impact and potential tuning of air compressibility to optimise device extraction capacity is another important parameter in the development of this concept and should be the focus of future investigations.

Wave Height

With optimal damping applied to the system, the influence of wave height on performance was investigated. Figure 4.16 presents the results of the investigation, in which it can be seen that there is a distinct correlation between wave height and OWC device performance. As the incident wave height decreases, an improvement in both magnitude and effective operation bandwidth is observed for frequencies greater than 0.6 Hz and less than 1.2 Hz, with frequencies outside this range displaying no discernible impact of wave height on performance. These findings are consistent with those found by Elhanafi et al. [88] for an offshore stationary OWC WEC, and similarly for a land-based fixed OWC WEC as presented by Ning et al. [214], in which capture width reduced as a function of wave height. As proposed by Elhanafi et al. [215], the reduction in performance could be attributed to the non-linearities associated with an increase in water sloshing and free surface deformation resulting from larger wave heights. It should be noted that the variation in wave height had no discernible impact on the response curve of the devices, indicating that the wave height parameter has no impact on resonance frequency location within the bandwidth, only the magnitude of performance.

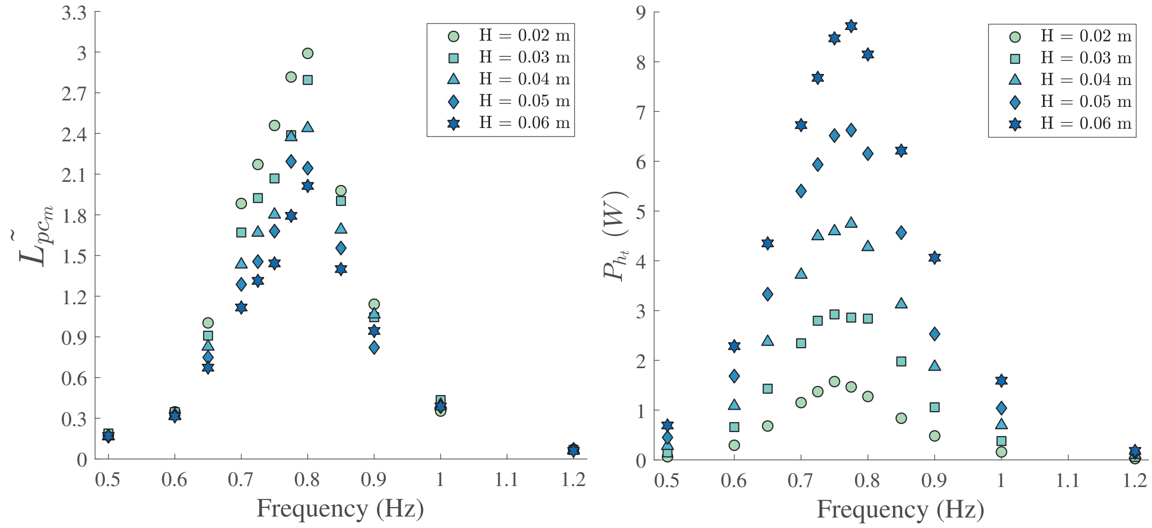

(a) Mean Non-Dimensional Capture Width, $\tilde{L}_{pc_m}$

(b) Mean Power Absorbed, P_{h_t}

Figure 4.16: Mean non-dimensional capture width and mean hydrodynamic power absorbed for wave height variations with structure configured at 1800 mm width in far OWC device configuration

The results presented in Figure 4.16a indicate that as wave height tripled, the performance in terms of L_{pc_m} was reduced by a third at resonance. This would suggest that the operational devices perform better at lower wave heights. However, considering the total hydrodynamic power absorbed as presented in Figure 4.16b, it is evident that although the device is not absorbing energy as effectively in higher wave heights, the total power absorbed increased almost six times at resonance as wave height increased from 0.02 m to 0.06 m. These findings supports the concepts capability to extract ocean wave energy effectively across a number of different wave heights. Consistency in site-specific wave height would allow for more accurate predictions on the performance of the concept, and low wave height conditions will result in more effective conversion due to reduced non-linearities, however as wave height increases greater power absorption is observed. As wave height will affect the device performance, site-specific wave climate analysis should influence the concept at the design stage to ensure optimal energy extraction.

4.4.5 Technology Readiness Levels

The findings in this research contribute towards the Technical Readiness Level of the OWC device integrated floating breakwater concept. Regular wave cases were investigated at small scale to evaluate how physical alterations in the design variables impact device performance. This correlates to the initial protocols recommended for Stage 1 (TRL 1-3) as reported in [165], indicating concept validation should begin with small scale model testing of monochromatic waves within a suitable wave flume. Future works are to include a mooring arrangement investigation to provide realistic constraints to the system, as well as numerical work to investigate parameters including optimum PTO damping, air compressibility and device geometry.

4.5 Conclusions

The present investigation was designed to establish a proof-of-concept for a floating breakwater integrated with OWC wave energy converters, and explore how parameters including device configuration, breakwater width, pneumatic damping and structure motion influence the performance of the integrated devices. The results of this investigation indicate that device configuration, and more importantly device spacing, play significant roles in the overall performance of the structure, as negative device-device interaction was clearly observed as device spacing decreased. The Double-Double configuration was able to absorb approximately 80% of the available wave energy interacting with the breakwater when subjected to LDV_5 damping, however negative device interaction was observable with the device spacing corresponding to this configuration, as such, consideration regarding device configuration should be a function of both performance and economic drivers. Similarly, the integration of multiple devices resulted in improved mean non-dimensional capture width of the operational chambers relative to that of a single integrated device, indicating that multi-device integration is beneficial in the energy extraction capacities of the concept. Additionally, pneumatic damping characteristics and motion constraints were also found to impact the performance of the integrated devices, and should be carefully considered in the design phase of concept development. Finally, breakwater width was found to have no discernible impact on device output, yet this parameters influence on the wave attenuation and motion characteristics of the breakwater is evaluated in Chapter 5, and should subsequently be considered in the design phase. The outcomes obtained from the experimental investigation provide a foundation for future works and development of the concept to continue progression through TRLs.

Chapter 5

Wave Attenuation and Motion Characteristics

5.1 Introduction

This chapter continues the investigation of a floating breakwater/WEC structure for application in the expanding offshore industry. The concept, detailed in Chapter 4, incorporates multiple bent-duct type OWC WECs within a generic Π-type floating breakwater. The device aims to fulfil the environmental protection, energy generation and material/consumable storage likely required of a multi-purpose floating offshore structure. This chapter reports on an investigation regarding the way in which multi OWC device integration impacts the parameters governing floating breakwater performance through model scale hydrodynamic experimentation. To establish a foundational data set, a soft mooring was applied throughout the experimental investigation to simulate a free floating condition. Future works will utilise this foundation to investigate how realistic mooring arrangements can strengthen the results obtained from this analysis. Variations to OWC device configuration, breakwater width, pneumatic damping and motion constraints were used to explore the contributions of each parameter towards overall breakwater performance, with comparisons provided to a generic non-integrated breakwater. Breakwater performance was evaluated as a function of the wave attenuation capacity, specifically the transmission and reflection coefficients, and also structure motions. The scope of the research presented in this chapter focuses exclusively on breakwater performance both with and without OWC devices integrated while interacting with regular incident wave trains. The hydrodynamic performance of the integrated OWC devices in regular waves has been presented in Chapter 4, while the performance of the concept in irregular waves will be presented in Chapter 6.

5.2 Theory

5.2.1 General

The research conducted considers a Π-type floating breakwater 4.5 m in length, 1.2–1.8 m in width, and 0.5 m in height, operating at a draft of 0.3 m as illustrated in Figure 4.3. The aft and forward pontoons are symmetrical and their design is 300 mm in width, and 200 mm in height. The floating breakwater is integrated with seven bent duct type oscillating water column wave energy converters, all of which have identical geometric parameters. Further information on the geometric characteristics of the OWC devices can be found in Chapter 4.

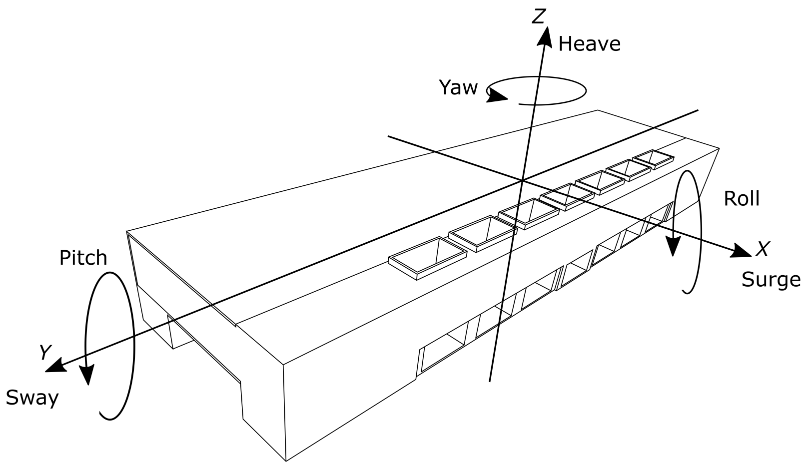

Figure 5.1: Schematic indicating six degree of motion convention for the OWC Device integrated floating breakwater

5.2.2 Wave Attenuation

The wave attenuation characteristics of the breakwater are evaluated using the transmission coefficient, c_T, and the reflection coefficient, c_R, as derived using Equations (5.1) and (5.2) respectively;

$$c_T = \frac{\eta_t}{\eta_0} \tag{5.1}$$

$$c_R = \frac{\eta_r}{\eta_0} \tag{5.2}$$

where η_t represents the amplitude of the transmitted wave, η_0 represents the amplitude of the incident wave, and η_r represents the amplitude of the reflected wave. The transmission coefficient can be derived directly through experimental data acquired from the incident and transmission wave probes configured during testing, while the reflection coefficient utilised the three-probe least squares method proposed by Mansard and Funke [216] for derivation.

5.2.3 Motion

The second major parameter governing floating breakwater performance is motion. For the purpose of this experimental investigation, the motion performance are evaluated using the Response Amplitude Operator (RAO) for the degrees of motion of interest. The RAO indicates the amplitude of structure motion for a given degree of freedom relative to incident wave amplitude, as derived in Equation (5.3),

$$RAO = \frac{A_m}{\eta_0} \tag{5.3}$$

where A_m is the amplitude of the degree of motion of interest. Figure 5.1 displays the six degrees of motion convention for the OWC device integrated floating breakwater, where the incident wave propagates parallel to the x-axis in the negative x direction.

5.3 Experimental Setup and Test Procedures

5.3.1 Model

The geometric properties of the WEC/floating breakwater were presented in Section 4.3.3, while the scale model floating breakwater configured in the basin is pictured in Figure 5.2. All the results presented in this chapter are either in model scale or non-dimensional form. The nominal full-scale dimensions based on the scale factor of 1:20 can be found in Section 4.3.3, however it is possible for other scale factors to be applied.

As was presented in Section 4.3.3, the breakwater width was varied from 1200 mm to 1800 mm in 300 mm increments, which required spacing modules (see Figure 5.2) to fill the void left after separation. To achieve operational draft, ballast was added inside the hull of the floating breakwater in the form of metal weights. Mass was added in order to maintain symmetrical loading, and varied dependent upon the configuration of the OWC devices and the breakwater width, as the mass of water in the operational chambers, and the additional displacement required consideration. The device was moored through use of two soft mooring apparatuses as described in Chapter 4, which employed lump weights to provide the necessary constant force. Additional model information, in conjunction with facility details are presented in Chapter 4.

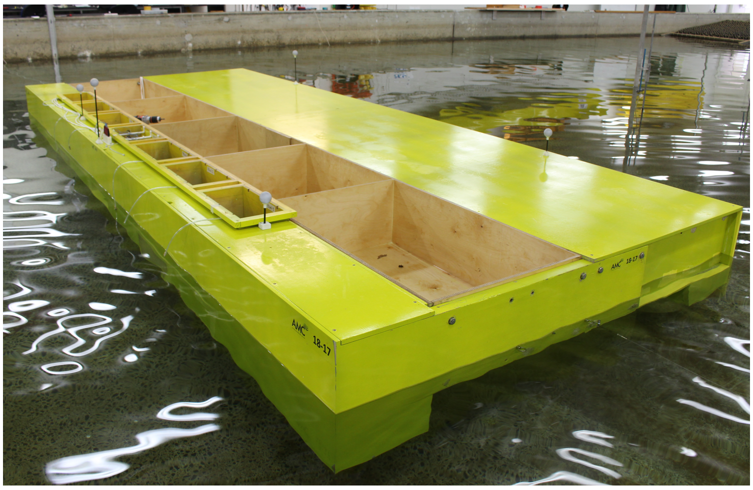

Figure 5.2: The OWC integrated floating breakwater, AMC Model 18-17, installed in the Australian Maritime College Model Test Basin

Table 5.1 presents the specifications for the floating breakwater models investigated. The Far OWC device configuration is displayed to compare the OWC integrated conditions to the breakwater only conditions, as the additional OWC configurations investigated exhibited negligible variation to the values derived for the Far OWC device configuration. It is important to note that when the OWC devices were closed during the breakwater only conditions, the chambers were emptied of water prior to testing to ensure undesirable free surface effects would not impact the data.

Table 5.1: Details of the floating breakwater model investigated during the experimental campaign

Width (mm)	Mass (kg)	Moment of Inertia (kg m^2)	Centre of Gravity (mm)	Pitch Radius of Gyration (mm)
1200				
Breakwater Only	1033	67.4	-0.2, 0, -59.8	255
Far OWC Device Configuration	1009	70.4	-8.3, 0, -59.5	264
1500				
Breakwater Only	1140	163.4	-13.5, 0, -56.5	379
Far OWC Device Configuration	1129	169.4	-19.4, 0, -60.8	387
1800				
Breakwater Only	1269	356.4	-11.9, 0, -59.8	530
Far OWC Device Configuration	1286	361.8	-9.2, 0, 60.0	531

Note: The position of the Centre of Gravity is given as Cartesian coordinates (x, y, z), which are presented relative to the reference point located at the intersection of the transverse and longitudinal midships at the waterline as is displayed in Figure 5.4. The x-axis is the longitudinal axis running aft to forward on the device, the y-axis is the transverse axis running starboard to port, and the z-axis is the vertical axis where up is positive. For all cases investigated, the draft remained constant at 300 mm.

5.3.2 Instrumentation

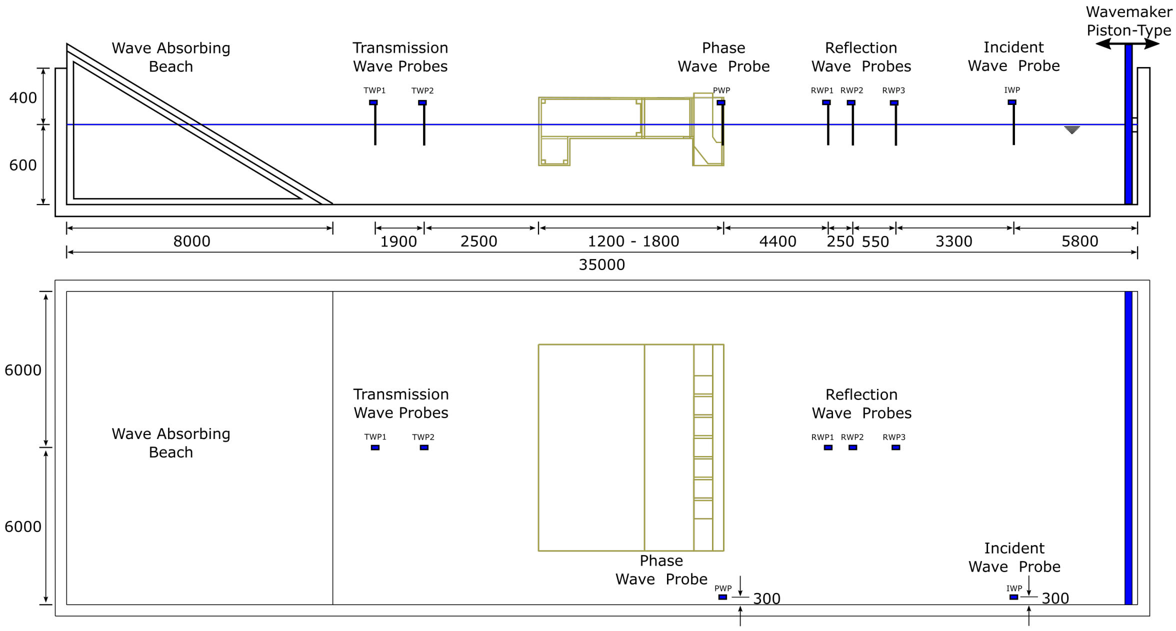

Figure 5.3: Elevation and planar views of experimental test configuration within AMC basin, all units in mm (not to scale)

To measure the instantaneous free surface elevations of the generated waves at different locations within the basin, seven resistive type wave probes were configured as illustrated in the experimental layout in Figure 5.3. The seven basin-situated wave probes included, an incident and phase wave probe (IWP and PWP respectively), three reflection wave probes (RWP1 - RWP3) positioned to comply with governing parameters for reflection analysis as proposed by Mansard and Funke [216], and two transmission wave probes (TWP1 and TWP2). All transmission and reflection wave probes were positioned along the longitudinal axis of the basin (6000 mm from side walls) while the incident and phase wave probes were positioned 300 mm from the side wall of the basin on the starboard side of the device. Details regarding OWC device instrumentation can be found in Chapter 4. All wave probes were calibrated daily, synchronised and sampled at 200 Hz.

The six Degree of Freedom (DOF) rigid body motions of the floating breakwater were acquired through use of an optical motion tracking system (Qualisys). The system utilises eight cameras paired in each corner of the basin to track five passive markers attached to the floating breakwater as illustrated in Figure 5.4. The system tracks each of the installed markers' motions through a time series with respect to a designated reference point on the structure. For the purpose of this investigation, the reference point was designated as the point at which the longitudinal midships, transverse midships and waterline intersect, as illustrated in Figure 5.4.

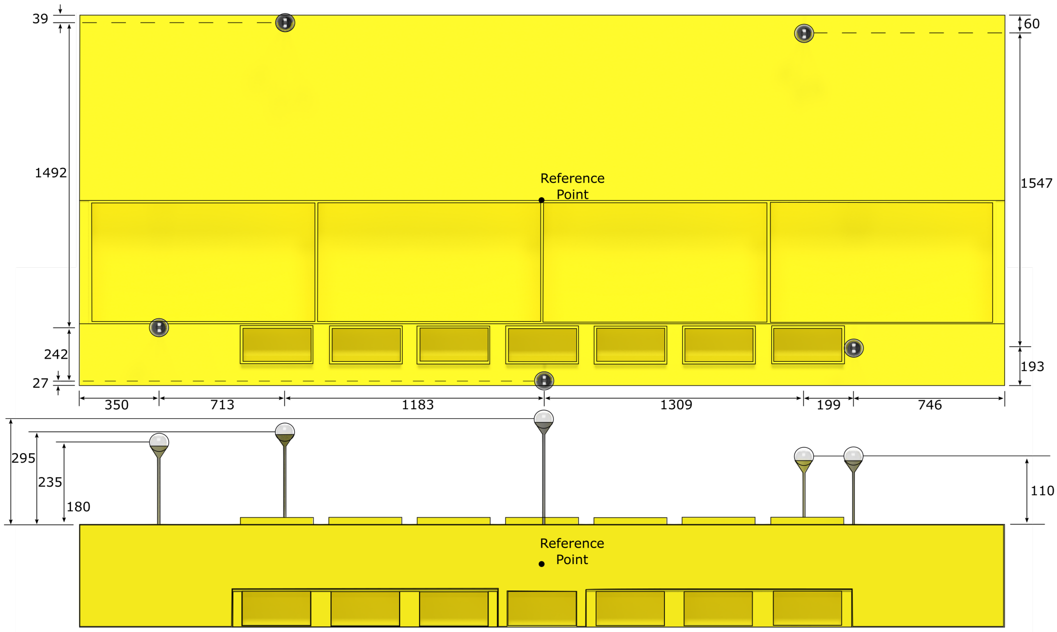

Figure 5.4: Elevation and plan/top view of Qualisys marker location on OWC device integrated floating breakwater, all units in mm (not to scale)

5.4 Results and Discussion

5.4.1 Motion

The main assessment parameters for the performance of floating breakwaters are motion and wave attenuation, both of which are explored with respect to the aforementioned test variables. With applications for this concept targeting multi-use maritime structures in which topside infrastructure is likely to be applied, reduced device motions would be beneficial for increasing the viability. Due to the soft mooring arrangement used during experimental testing, in collaboration with the monochromatic regular wave trains the device was subjected to, the sway, yaw and roll degrees of motion were not considered to be of interest due to minuscule magnitudes, while surge was only constrained through the constant force and was found to subsequently drift. As a soft mooring arrangement was employed, analysis of the surge motion yielded results providing little benefit to the investigation and, thus, are not included. Consequently, the motions of focus for this investigation were heave and pitch. The developers of the Qualisys motion capture system utilised during experimental testing to capture relative motion of the breakwater claim a sensitivity of ± 1 mm and $\pm 0.1°$ [217], which is considered when evaluating the model performance.

Natural Frequency

A preliminary investigation was conducted to experimentally evaluate the natural frequency of each degree of motion (with the exception of sway). A series of decay tests were conducted, of which an example of the time series data can be found in Figure 5.5. The results of the decay test analysis for variations in breakwater width can be found in Table 5.2, while the 1800 mm breakwater both with and without OWC devices integrated are found in Table 5.3. The 'with OWC devices' condition considers the Far OWC device configuration.

Table 5.2: Natural frequencies, f_n, for variations in breakwater width when configured in the breakwater only condition

Degree of Motion	1200 mm Width f_n (Hz)	1500 mm Width f_n (Hz)	1800 mm Width f_n (Hz)
Surge	0.01	0.01	0.01
Heave	0.57	0.51	0.36
Roll	0.62	0.55	0.52
Pitch	0.74	0.67	0.66
Yaw	0.04	0.04	0.04

Table 5.3: Natural frequencies, f_n, as determined through experimental decay tests with model configured in the 1800 mm width condition

Degree of Motion	Without OWC Devices f_n (Hz)	With OWC Devices f_n (Hz)
Surge	0.01	0.01
Heave	0.36	0.35
Roll	0.52	0.48
Pitch	0.66	0.64
Yaw	0.04	0.04

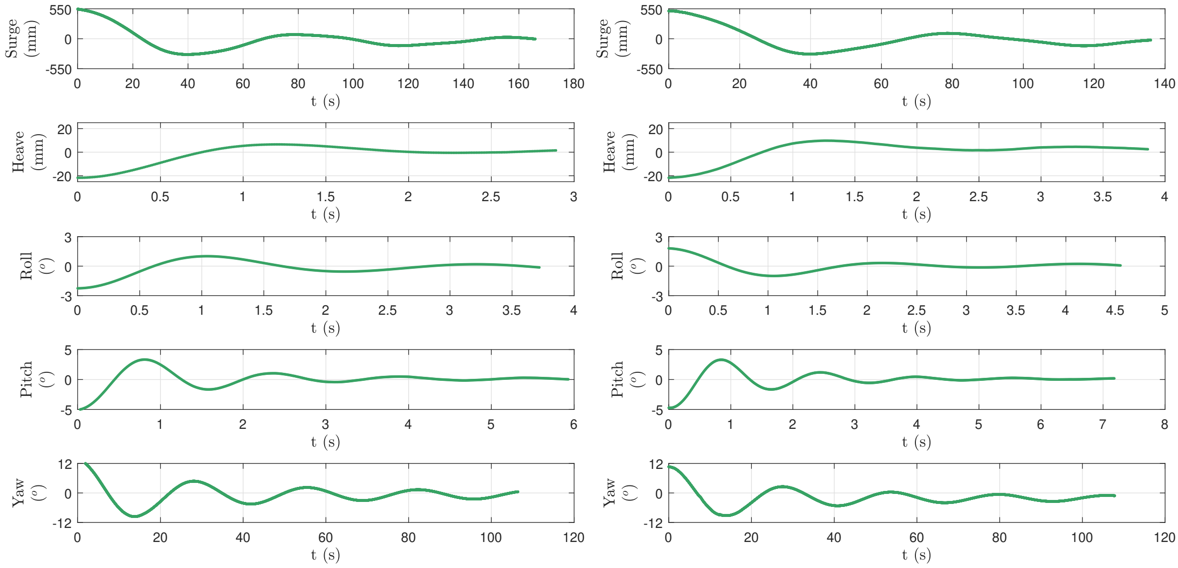

(a) Without OWC Devices

(b) With OWC Devices

Figure 5.5: Time series data for decay tests conducted on the 1800 mm breakwater

Breakwater Width

Conforming to the sequence in which parameters were investigated for wave attenuation performance of the breakwater, the first parameter explored for influence on device motion was breakwater width, the results of which are presented in Figure 5.6 for the breakwater only condition. These results were developed to provide a baseline response for the floating breakwater which could be used to provide comparisons relative to the breakwater integrated cases, as are displayed in Figure 5.7. Comparing Figures 5.6 and 5.7, it can be seen that for the majority of cases investigated, the integration of the OWC WECs resulted in a decrease in the relative motion of the breakwater, most prominently around the resonant frequency of the OWC devices (approximately 0.75 Hz).

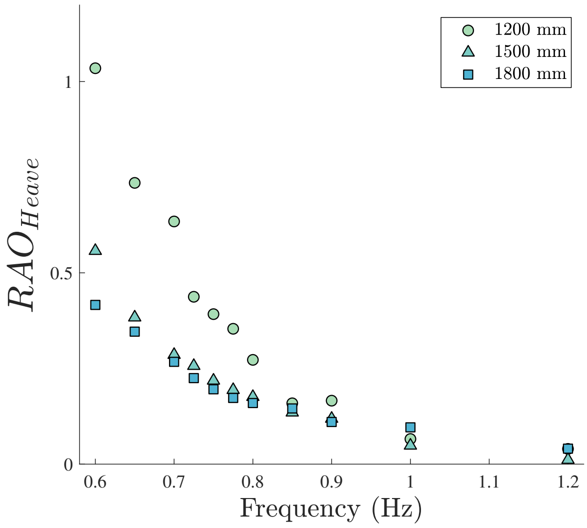

(a) Heave Response Amplitude Operator

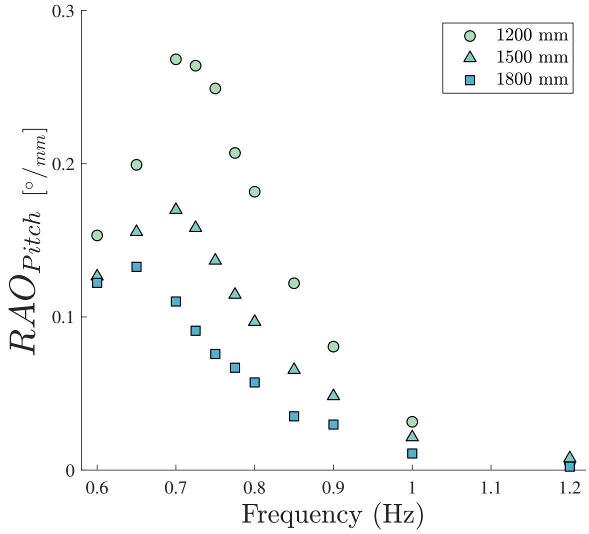

(b) Pitch Response Amplitude Operator

Figure 5.6: Breakwater only configuration operating in 0.02 m wave height

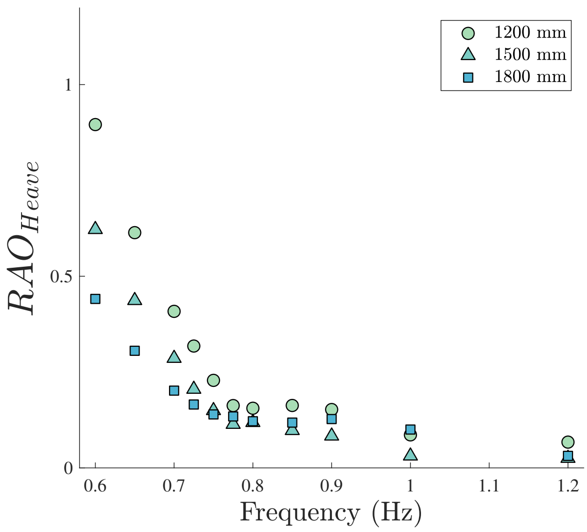

(a) Heave Response Amplitude Operator

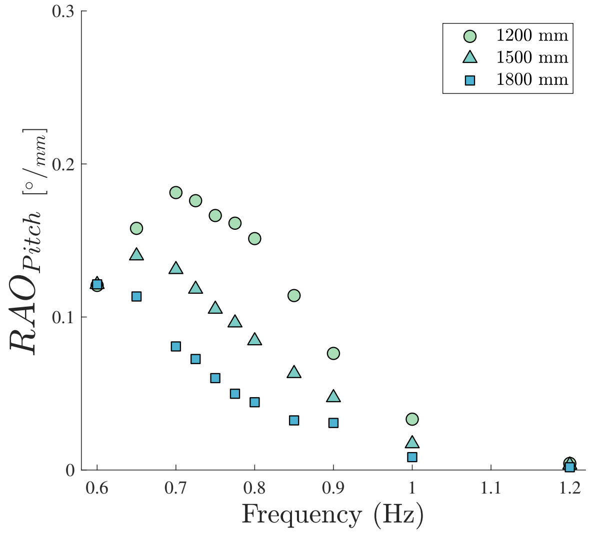

(b) Pitch Response Amplitude Operator

Figure 5.7: Far OWC device configuration operating in 0.02 m wave height

Investigating the breakwater integrated cases further, Figure 5.7a presents the heave response of the WEC integrated floating breakwater under varying breakwater widths, from which an evident trend is displayed indicating that as breakwater width increased the magnitude of heave decreased, most observable in the lower frequencies. As previously established in Table 5.3, the natural frequency of heave motion for the 1800 mm breakwater was determined as approximately 0.35 Hz, which correlates well with the results presented in Figure 5.7a, as it is clear that the heave magnitude continues to rise at the lower end of the test frequency bandwidth, subliminally indicating that the results presented follow the decreasing response typically associated post-resonance. As the incident wave frequency exceeded 0.75 Hz, the response converged to values having less variation and magnitude, at which point the heave magnitude is equivalent to approximately 15% of the incident wave amplitude.

Figure 5.7b presents the pitch response results for the breakwater width variations. Similarly to the heave response, a distinct relationship is presented between breakwater width and pitch response, where it is illustrated that an increase in breakwater width leads to a desirable reduction of pitch magnitude. This trend is observable across the entire frequency bandwidth, where the 1800 mm breakwater exhibits up to approximately 60% less pitching motion compared to the 1200 mm breakwater. Figure 5.7b also illustrates how the pitch resonance period of the breakwater can be manipulated through breakwater width, where as illustrated, the resonance values for the 1200 mm and 1500 mm variations are 0.7 Hz and 0.65 Hz respectively. The pitch natural resonance for the 1800 mm variation correlates well with that determined through decay tests as presented in Table 5.3, which was found to be approximately 0.64 Hz.

The motion results presented in Figure 5.7 illustrate the importance in considering the breakwater width during the design stages of the concept. With the intention at targeting a wave climate correlating to the resonance frequency of the OWC devices (0.75 Hz), it is evident that consideration must be placed on all degrees of motion, as heave variation across breakwater width at this frequency is negligible, however a significant reduction in pitch can be achieved through increased width. The increase in width also presents beneficial attributes in terms of topside area for the incorporation of infrastructure related to the industry application of this concept. This would however be subject to economic considerations, as the increased width will incur additional cost. As minimal relative motion is desirable for a multi-purpose maritime structure such as that considered in this research, all results henceforth will focus on the 1800 mm breakwater width as it possesses the preferred motion characteristics of the configurations tested.

OWC Device Configuration

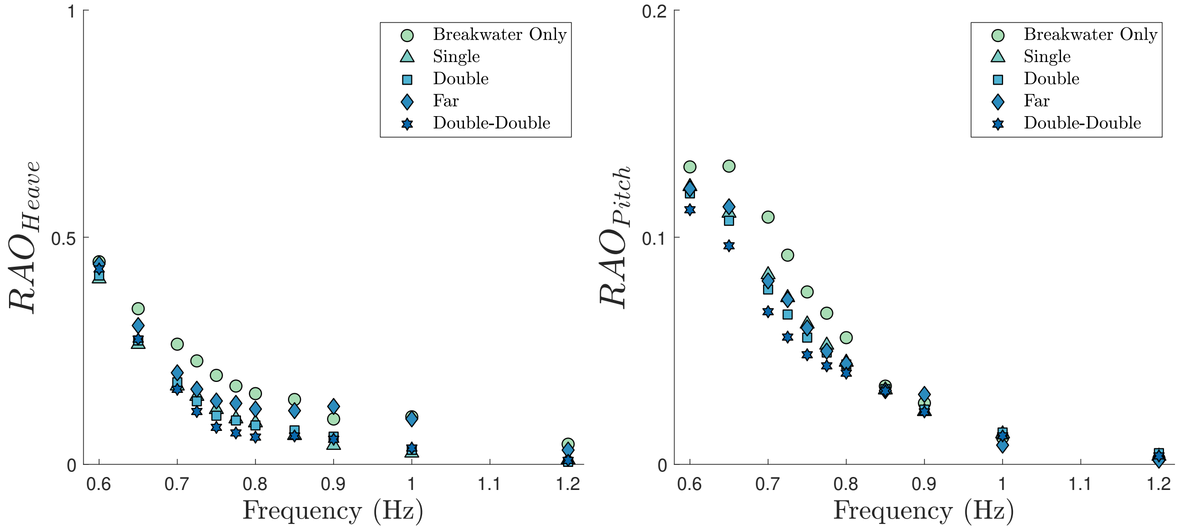

(a) Heave Response Amplitude Operator

(b) Pitch Response Amplitude Operator

Figure 5.8: 1800 mm breakwater width operating in 0.02 m wave height

Figure 5.8 illustrates the results obtained from the investigation regarding the influence of OWC device integration on breakwater motion. Figure 5.8a presents the 1800 mm breakwaters heave response across the five aforementioned device configuration variations, from which the benefits of device integration can be observed. Comparing the breakwater only condition to those in which OWC devices were integrated, a palpable reduction in heave magnitude can be observed, most substantially in the frequencies around the OWC device resonance. In the lower and higher frequencies, the influence of OWC device integration is less discernible, yet it is illustrated that the Double-Double configuration reduces the magnitude of heave response by greater than 50% at select frequencies relative to the breakwater only condition. A similar phenomena is presented in Figure 5.8b, which highlights the considerable reduction in pitch amplitude that is achieved through OWC device integration. At pitch resonance, it can be seen that the addition of OWC chambers substantially reduces the peakedness of the response as well as the magnitude, which continues until 0.8 Hz at which point the results converge and variations are non-discernible.

At select frequencies, it is demonstrated that the magnitude of motion reduction is a function of the number of chambers installed. It is hypothesised that the relative motion of the oscillating column of water within the devices introduces a damping to the system which results in reduction of structure motion. Consequently, as additional chambers are added, the increased mass of water oscillating results in further damping and a subsequent reduction of device motion. As this relationship isn't consistent across all test frequencies, further investigation is recommended to thoroughly establish the influence device integration, and subsequent total power extraction on breakwater motion.

Wave Height

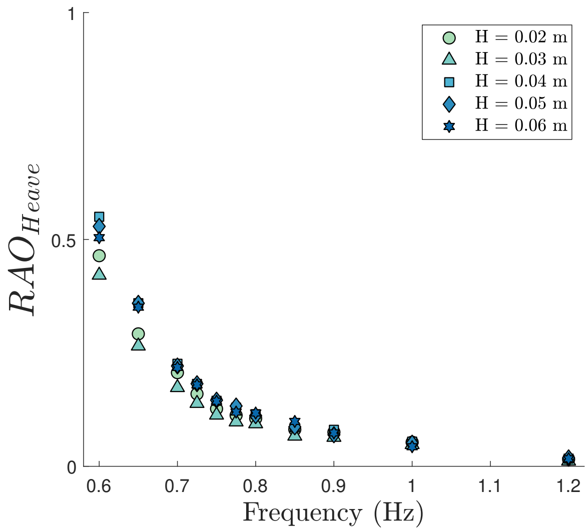

(a) Heave Response Amplitude Operator

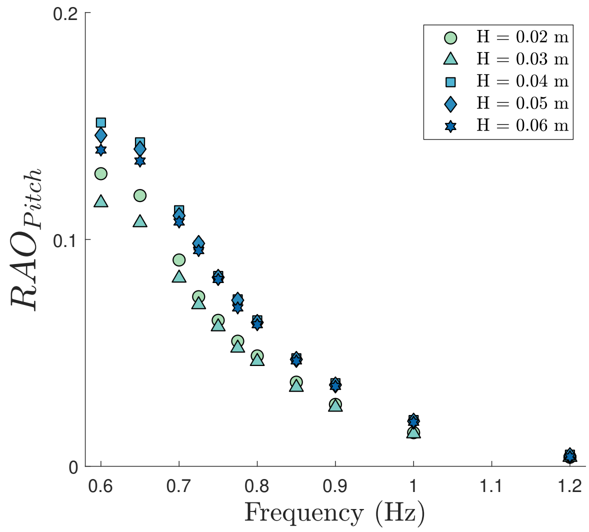

(b) Pitch Response Amplitude Operator

Figure 5.9: 1800 mm breakwater width with Far OWC device configuration operating in varying wave heights

Figure 5.9 presents the motion response of the OWC device integrated floating breakwater in differing incident wave heights. Both Figure 5.9a and 5.9b indicate that for majority of incident wave frequencies tested, the motion response displays a negligible variation as a function of wave height. Examining Figure 5.9b, a non-negligible variation can be found at the pitch resonance of the device, where it can be discerned that the larger wave heights investigated resulted in an increase in pitch relative motion. This relationship is observable in the frequencies immediately prior to, and post resonance, after which the results converge to equivalent relative motion magnitudes for all wave heights. As heave motion resonance was not captured within the test frequency bandwidth, the same relationship could not be definitively ascertained from the experimental investigation, however at the lowest test frequency of 0.5 Hz the relationship can be clearly observed. This is likely the upper bound of the relationship, considered as the equivalent of 0.7 Hz for the pitch relationship.

The cause of this relationship around the motion resonance is hypothesised to be as a result of the response to increasing wave steepness. The floating breakwater structure experiences a rise in motion response due to the increased rate of change of wave amplitude, subsequently increasing the relative motion amplitude. This only occurs at resonance as the motions achieve maximum displacement or rotation at these frequencies. Consequently, the lag generated in lower wave heights results in destructive interference which provides a beneficial trait to the motion response of the breakwater. To further investigate this hypothesis, additional experiments should be carried out across additional wave heights, along with additional frequencies around resonance to provide a more robust analysis of the phenomena. The inclusion of a realistic mooring configuration would also be beneficial in wave height versus motion analysis in order to establish if the relationship found using the soft mooring is transferable. Finally, an investigation into the relationship between loading on the bow face of the breakwater and wave height may provide insight into the relationship observed at resonance in Figure 5.9.

Pneumatic Damping

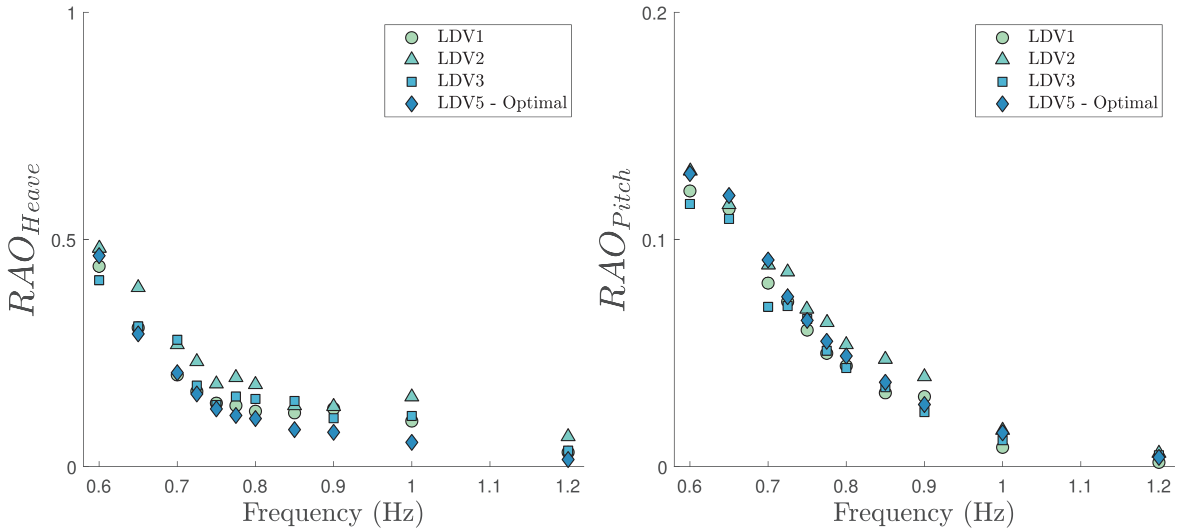

(a) Heave Response Amplitude Operator

(b) Pitch Response Amplitude Operator

Figure 5.10: 1800 mm breakwater width with Far OWC device configuration operating in 0.02 m wave height

Lastly, the OWC device PTO damping was investigated for impact on the breakwater motions, the results of which are presented in Figure 5.10. It was varied from LDV_1, as utilised for all previous results, having a magnitude of 1145 $\frac{kg}{m^4 s}$, through to LDV_5, which had a value of 6410 $\frac{kg}{m^4 s}$. As illustrated, the damping variations investigated had an inconsequential impact on the motion characteristics of the breakwater. With respect to Figure 5.10a, the largest damping, and subsequent largest energy absorption correlates to the lowest relative heave motion. This relationship of damping to motion is not however apparent for the remaining variations, as such it is recommended that further investigation focusing on increased damping characteristics should be explored to establish if any trends emerge. The results for pitch under the influence of pneumatic damping as presented in Figure 5.10b illustrate no distinguishable trends either, with the results for damping variation across frequency randomly distributed in magnitude, whilst following the same response curve.

5.4.2 Wave Attenuation

The primary operational objective for a floating breakwater is environmental protection in terms of leeside wave energy reduction. The wave attenuation characteristics of most floating breakwaters are measured as a function of the transmitted wave and the reflected wave, subsequently providing frequency dependant transmission and reflection coefficients for the structure. As this experimental investigation was considered a proof of concept for the OWC device integrated floating breakwater design, a scaled mooring arrangement was not examined. As such, the results presented regarding wave attenuation performance provide baseline values to which improvements are expected to be made as continual concept development is achieved through future works. For each of the investigated parameters, the transmission and reflection coefficients have been derived for each of the incident wave frequencies to establish the influence of the tested parameters on the relationship between wave period and wave attenuation. As presented in Chapter 4, the experimental uncertainty associated with incident wave elevation during the experiments was approximately $\pm 1\%$, which is considered during the analysis of the transmitted and reflected wave. The results regarding transmission coefficients for the floating breakwater, both with and without OWC devices integrated, produced one unexpected outcome which was values for c_T greater than 1 for a limited number of incident wave frequencies. This occurs across all configurations in which the concept was tested in the free floating condition, but not when the breakwater was fixed. Potential sources of this phenomena are described in Section 5.4.2, such that evaluation of the results thereafter can forgo discussion of the $c_T \geq 1$ values and focus on the relationships between the test variables and the transmission coefficient.

Fixed versus Floating

Figure 5.11 compares the 1800 mm width breakwater arranged in the Far OWC device configuration for both fixed and floating motion conditions. This comparison isolates the amount of energy that is transferred into motions, and the subsequent influence this transfer has on the wave attenuation characteristics of the concept. The transmission characteristics are presented in Figure 5.11a, where it can be observed the fixed case displays significant wave attenuation improvement relative to the floating configuration. The fixed configuration observes a similar general trend to that of the floating condition, in that values for c_T are relatively low for wave frequencies either side of the peak value observed around 0.7 Hz, with the magnitude of the values obtained being the major difference between the two cases. These results indicate that much of the incident wave energy is transferred into breakwater motion when in the floating configuration, subsequently reducing the wave attenuation capacity of the structure. The fixed configuration also observed a significant increase in energy extraction from the OWC devices (see Chapter 4), which likely contributed to the reduction in c_T observed. The incorporation of a realistic mooring arrangement at model scale to provide greater constraint to the motion of the floating breakwater is expected to significantly impact the results presented, as it is clear the floating breakwater motion allows for significant wave attenuation, most prominently in the low frequencies where the wavelength exceeds the width of the breakwater.

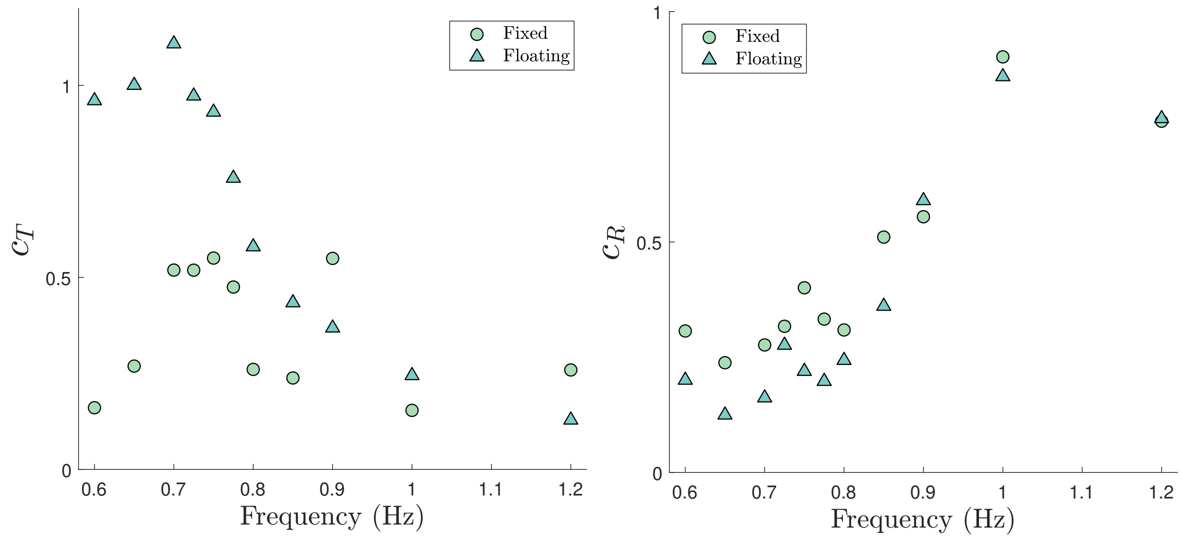

(a) Transmission Coefficient (b) Reflection Coefficient

Figure 5.11: 1800 mm breakwater width with Far OWC device configuration operating in 0.02 m wave height with LDV_1 damping

As presented in Figure 5.11b, a distinct but marginal difference in c_R is observable between the two conditions. It can be seen that the floating breakwater configuration is favourable in almost all incident wave frequencies tested. The general response curve of the two conditions varies little; however, the magnitude of response is evidently reduced through configuration in the floating condition, where a reduction in c_R of up to approximately 50% is observable in the lower frequencies. It is surmised from this result that a significant proportion of the incident wave energy is transferred into device motion while in the floating condition, which curtails the amount of energy available for transferral into the reflected wave.

A considerable inflection in the response curve is observable around 0.725/0.75 Hz for both cases, after which a reduction in reflection is observed until 0.8 Hz (see Figure 5.11b). This bandwidth correlated with the region in which the greatest energy extraction was observed by the integrated OWC devices, as found in Chapter 4. The reduction in reflectivity suggests that the integrated devices absorbed a portion of the incident wave energy which would generally have been be transferred into the reflected wave with a traditional floating breakwater, subsequently improving the performance of the floating breakwater through OWC device integration.

The fixed configuration displayed a greater reduction in reflection at resonance, correlating with the superior energy absorption characteristics identified for the fixed structure relative to the floating configuration (see Chapter 4). This result compares well with previously investigated reflection/absorption characteristics as in Chapter 3 and [187], where the increased reflective structure surrounding the OWC device, and subsequent increase in c_R, results in improved performance. Though these results were expected, they present conclusive evidence of the energy transferral into structure motion for the floating breakwater and presents the benefits of the floating configuration regarding wave reflection, though it was found in Chapter 4 that the increase in reflection is beneficial for OWC device performance. As the two variables are interrelated, it is evident that further research is required to establish a proportionate compromise between the two in order that both energy absorption and wave reflection achieve desired performance characteristics.

High c_T Value Discussion

The following discussion aims to provide insight into potential sources related to the larger than expected values for c_T obtained during the experimental testing, as observed in Figure 5.11. Small scale experimental testing provides an efficient way to acquire performance data across a series of differing sea states and model conditions. It is however subject to laboratory effects, and the subsequent facility bias attributed to physical characteristics and wave generation capabilities of the wave basin. One physical characteristic with the potential to give rise to undesirable laboratory effects is the size of the experimental model relative to the wave tank, which can consequently introduce wave reflection, blockage, radiation and diffraction effects into the acquired data [218, 219].

The diffraction of incident waves around the breakwater was an expected and uncontrollable phenomena present during the experimental testing of the OWC device integrated floating breakwater. Similarly to the reflection of the radiated wave, the diffracted wave likely interfered with the transmitted wave measurement, also increasing the measured value. As diffraction is a function of wave period, the magnitude of diffraction influence on the transmitted wave varied across the test frequency bandwidth. Diffraction diagrams similar to that presented in Figure 5.12 provide approximate diffraction coefficients, k', relating the diffracted wave height to the incident wave height, as presented by Wiegel [220]. Figure 5.12 illustrates a diffraction diagram [221] indicating the location of the transmission wave probe during the experiments. This would suggest that the diffraction coefficient for this particular investigation is approximately k'=0.29; however, this value was not considered accurate due to the constraints associated with the diffraction diagram obtained. As can be observed, the transmission probe is located considerably aft of the breakwater, and visual observation indicated that a much greater sheltering effect closer to the breakwater. Considering real application, it is likely that a number of these modular units would be configured in 'rows', with relatively minor gap between devices, as such, diffracted waves would likely only be of concern in areas near the outermost modules on the end of each of the rows. Validation of this hypothesis would certainly warrant further research.

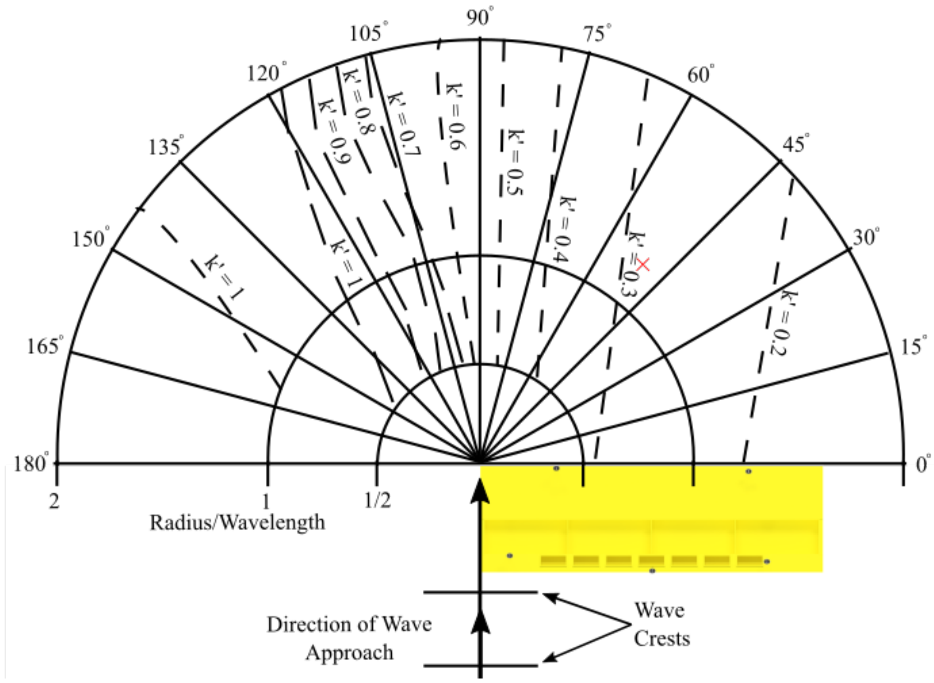

Figure 5.12: A diffraction diagram of wave attack angle 90° as presented in [221] superimposed over the OWC device integrated floating breakwater. The '×' indicates the location of the transmission wave probe having polar coordinates of (1.21,48.01°). The case presented in this figure is with respect to an incident wave frequency of 0.7 Hz.

To the authors knowledge, there is little information available on the diffraction characteristics of detached floating breakwaters, consequently the diffraction diagram presented in Figure 5.12 is applicable to semi-infinite rigid breakwaters whose depth extends to the seafloor. This indicates the inapplicability of correction using the k' value obtained. Much research has been conducted into the diffraction characteristics of this type of breakwater structure, along with diffraction patterns through the gap of two rigid breakwaters, yet little research has been conducted regarding diffraction behind detached breakwaters, and even more specifically detached floating breakwaters. It is hypothesised that the impact of diffraction affected the results obtained for the transmitted wave; however, further research into the phenomena is required to justifiably prove to what degree diffraction influenced the results. Numerical modelling could provide a preliminary synopsis of the diffraction patterns behind the detached floating breakwater, which will be the first step towards identifying the complex wave interaction occurring behind the model. Validation through additional model scale basin testing is recommended for future works to support the hypothesis and results acquired via numerical modelling.

The concept of blockage is relatively well understood for both wind tunnel and towing-tank experiments. The correction factors derived for wind tunnel experiments are not applicable to the current experiment, while towing tank related blockage typically focuses on velocity corrections for towed vessels. Subsequently, given the uncertainty associated with applying blockage correction to the current model, the results were left uncorrected, and the effect of blockage on transmitted wave heights of stationary floating structures is recommended for future works. The blockage parameter for the experimental model was 0.188, derived through the use of Equation 5.4,

$$m = \frac{A_x}{A} \tag{5.4}$$

where m represents the blockage parameter, A_x represents the area of maximum submerged transverse section of the model and A represents the cross sectional area of the basin.

The physical size of the model relative to the basin also likely contributed toward the high c_T values with respect to the radiated wave influence, as described by Chakrabarti [219]. The soft mooring applied provided constant force to the model during the experimental investigation, hence, the relative motions of the floating breakwater were greater than what would be expected if a more realistic model scale mooring arrangement had been applied (for example, multiple catenary mooring lines off each of the four corners to the sea floor). The constraint applied to motion in the fixed case, as illustrated in Figure 5.11, significantly reduced the transmission coefficient of the breakwater for majority of test frequencies, thus it is anticipated that improved constraint to motion by way of a realistic mooring arrangement would contribute towards a reduction in the magnitude of c_T for the floating breakwater.

The under-constrained relative motion of the breakwater, particularly heave, as a repercussion of the soft mooring is predicted to have consequently increased the magnitude of the radiated wave from the model, which accentuates the values obtained for c_T. Numerical and experimental investigations regarding interference from radiated waves reflected from tanks walls have been conducted [222–224], identifying that reflected radiated waves can influence the hydrodynamic properties, particularly added mass coefficients, of the model, subsequently impacting wave radiation. While the degree of the interference from the tank walls is unclear, it is hypothesised that this phenomena contributed to the obtained results.

The time series presented in Figure 5.13 illustrate the magnitude of heave and pitch contributing towards wave radiation at the 0.7 Hz, coinciding with the largest c_T value for the 1800 mm breakwater. Figure 5.13 also illustrates the surge motion of the OWC device integrated floating breakwater indicating the displacement of the structure in the direction of the transmission wave probe during the experimental test. This becomes an issue due to both the proximity of the port and starboard edges of the breakwater to the side walls of the basin, and the floating breakwaters gradual trajectory towards the transmission wave probe. The reflection of the radiated wave off the side walls of the basin is likely to have resulted in interference with the recorded measurements, subsequently increasing the measured value of the transmitted wave. The magnitude to which the results were affected by the radiated wave was not established during testing, and additional experiments are required to establish the contribution of radiated wave reflection on the amplitude of the transmitted wave.

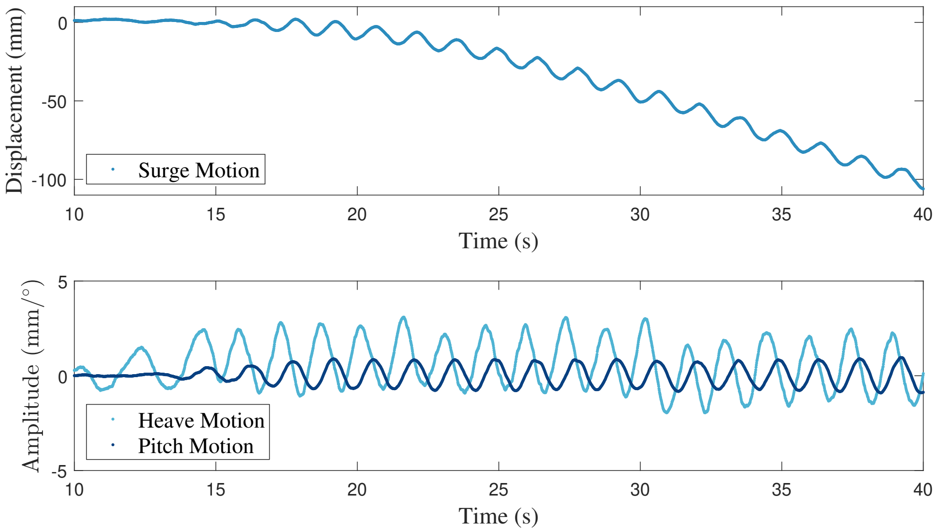

Figure 5.13: Time series of the surge motion (top), and heave and pitch motion (bottom) when subjected to incident waves of 20 mm wave height and 0.9 Hz

The unexpected values obtained where c_T was derived to be greater than one around 0.7 Hz was found consistently throughout the experimental campaign when breakwater was configured in the floating arrangement. Considering the wavelength and the results obtained from the fixed case (see Figure 5.11a), it is hypothesised that the major cause of the effect observed is strong diffraction around the device. In culmination with the strong diffraction, it is suspected that the results were also influenced, and accentuated, due to the radiated waves developed from the heave motion of the breakwater and the subsequent blockage induced by the physical size of the model relative to the basin. Though it is unclear whether the basin walls contributed toward the results, previous investigations indicate that reflected radiated waves can influence the hydrodynamic coefficients of the floating structure which is likely to impact the wave transmission. As a soft mooring arrangement was employed during the experimental investigation, it is expected that introduction of a realistic mooring arrangement with greater motion constraints would significantly reduce the values obtained for transmission, and minimise the discrepancy between the floating and fixed results. The width of the device is a major factor in the design of a floating breakwater structure, and may be a function of multiple units in a row; hence, it should be considered strongly when establishing the protective frequency criteria of the concept. During wave calibration tests without the model present, a comparison of the raw time series data against those with the model present indicate that the presence of the floating breakwater also contributed towards the high c_T values, as illustrated in Figure 5.14. The combination of these sources resulted in the values for transmission coefficient to illogically exceed the value of 1; nonetheless, a series of additional experimental tests and recommendations for future work have been identified to continue with the development of the WEC integrated floating breakwater. These experiments may be conducted in an appropriate wave flume to negate the influence of undesired effects impacting the data.

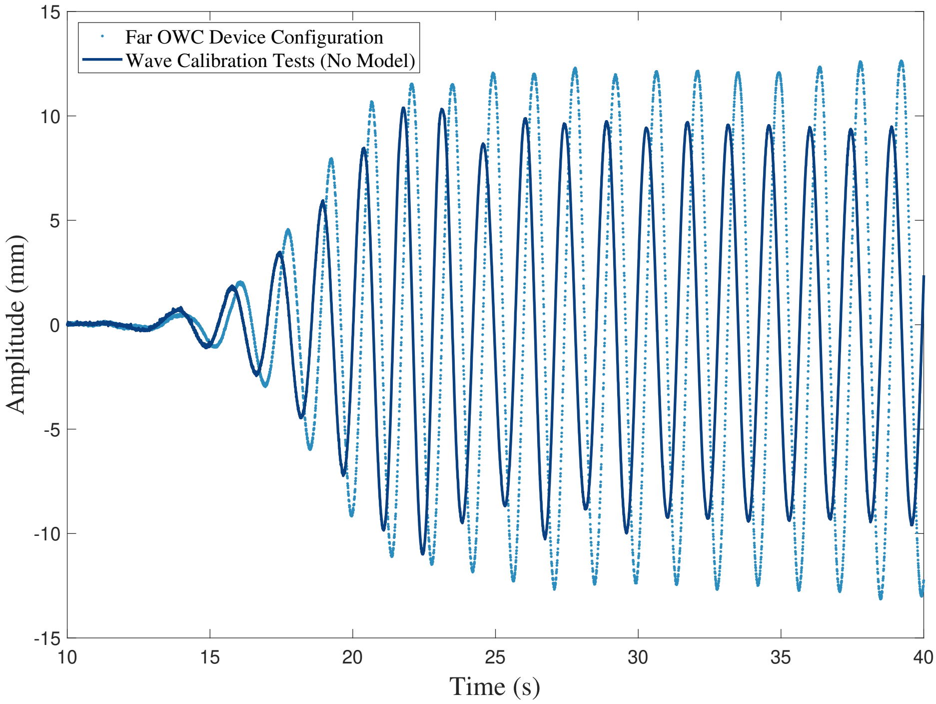

Figure 5.14: Time series comparison of the transmission wave probe amplitudes when subjected to incident waves of 20 mm wave height and 0.9 Hz

Breakwater Width

The results presented in Figure 5.15 illustrate the impact that breakwater width has on the performance parameters of transmission coefficient, c_T, and reflection coefficient, c_R (displayed in Figures 5.15a and 5.15b respectively). Considering firstly the narrowest (1200 mm) breakwater width variation, it is clear that the the response varies significantly from that of the 1500 mm and 1800 mm structures. The wave transmission characteristics of the 1200 mm case corresponds with the expected c_T of the π-type floating breakwater as derived using the equation proposed by Ruol et al. [207, 208], an extension of the equation established by Macagno [225] for transmission coefficients of box-type breakwaters. The theoretical relationship derived by Ruol et al. observes a crest and trough in the response curve when considered with respect to frequency, similarly to that observed in the 1200 mm case. It should be noted that the relationship derived by Ruol et al. considers a chain-moored π-type floating breakwater, consequently the results obtained from the experiments are not directly comparable; however, the general response curve of the structure is. Width is a governing factor of this relationship, subsequently explaining why the crest/trough isn't observed in the two remaining width variations tested, as an increase in breakwater width results in a response shift into the lower frequencies, hence Figure 5.15a solely identifies the crest of the relationship for the 1500 mm and 1800 mm cases.

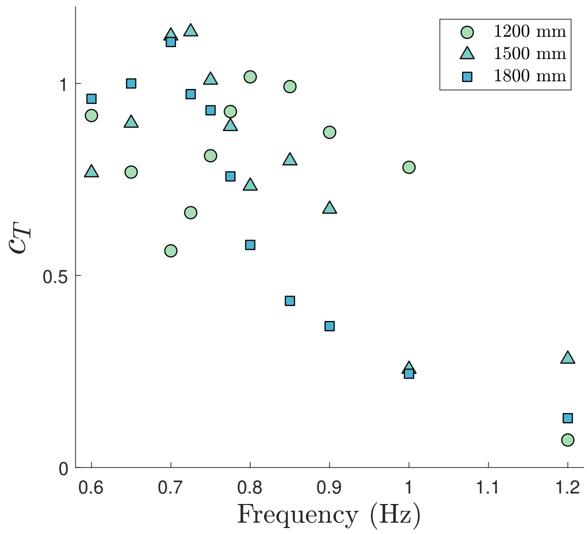

(a) Transmission Coefficient

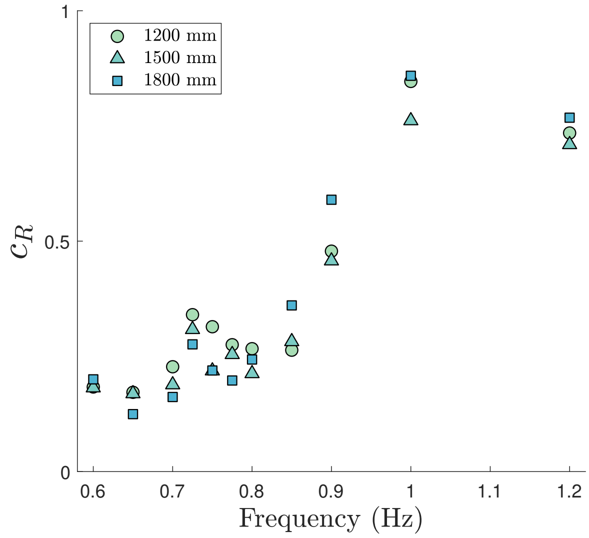

(b) Reflection Coefficient

Figure 5.15: Far OWC device configuration with breakwater in floating condition operating in 0.02 m wave height with LDV_1 damping

Comparing the three width variations, it is illustrated that in the lower frequencies ($\leq$0.75 Hz) the 1200 mm breakwater generally provides the greatest wave attenuation properties, but at higher frequencies the 1800 mm displays significantly better wave attenuation properties than the two alternative structures. As with any floating structure, a number of considerations are required at the design stage, focused around the site specific conditions in which the structure will be operating. Considering the application of this type of concept, the reduced wave transmission of the 1200 mm may be desirable; however, the motion characteristics of the breakwater presented in Figure 5.7, in which the 1200 mm breakwater observes significantly greater relative motion in both heave and pitch, the 1800 mm variation may be more applicable. This compromise is likely to be addressed through tuning of the design so that both performance parameters are optimised for the site-specific sea states.

Evaluating the influence of breakwater width on c_R as Figure 5.15b demonstrates, it is evident that as the frequency increases up to 0.8 Hz, the 1800 mm breakwater width has favourable reflectivity characteristics compared with the 1200 mm and 1500 mm within the same bandwidth. Above 0.8 Hz, there is little difference between the reflectivity characteristics of the 1200 mm and 1500 mm variations; however, the 1800 mm exhibits increased reflectivity as wave length decreases and falls below the width dimension of the breakwater. These results indicate that the majority of variation is within the magnitude of $\pm$ 5%, with a maximum of $\pm$ 15%; however, while there is some variability, no definitive relationship was established between device width and c_R over the entire test frequency bandwidth. The observable variations are likely attributed to the variation in device motion, as discussed in Section 5.4.1.

As with the previous results presented for c_R, the inflection attributed to the OWC device energy absorption is evident for all breakwater width variations. For each case presented, the Far OWC device configuration was employed (refer to Table 4.2 in Chapter 4 for OWC device configurations); thus it was integrated with three OWC devices for each of the width variations.

Device Configuration

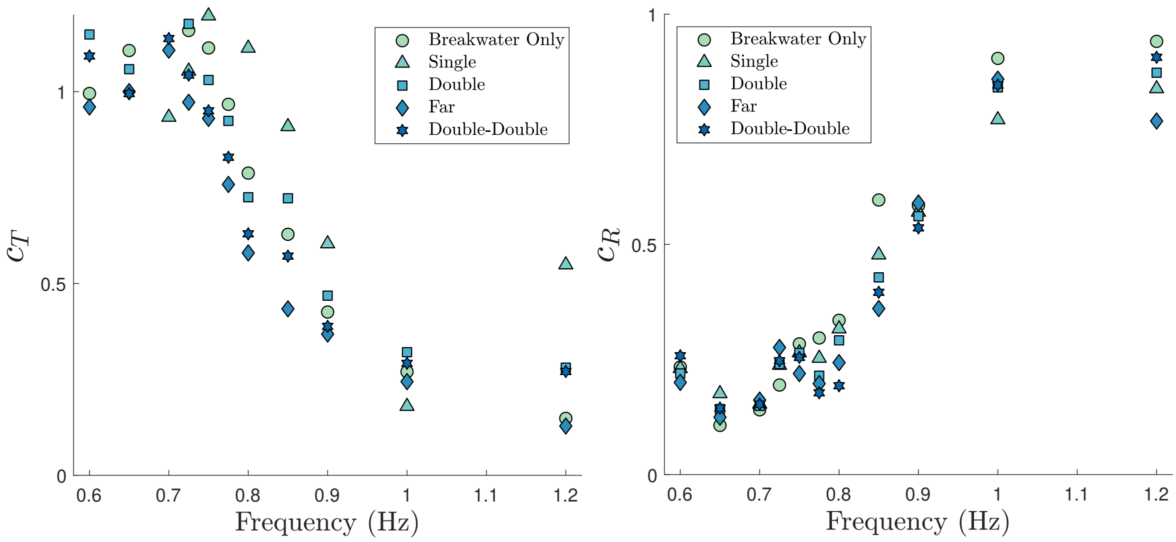

(a) Transmission Coefficient

(b) Reflection Coefficient

Figure 5.16: 1800 mm breakwater width operating in 0.02 m wave height with LDV_1 damping where applicable

In order to investigate the relationship between number of integrated devices and improvement in reflection coefficient, the breakwater was also configured in the Single, Double and Double-Double OWC device configurations as presented in Figure 5.16. Figure 5.16 illustrates the influence of OWC device configuration on the transmission and reflection coefficients of the floating breakwater. Device variations investigated had either 1, 2, 3 or 4 devices operational during the experiments, while the breakwater only condition (represented by the green ○ data points) was also investigated to aid in evaluation of the influence of device integration. Figure 5.16a presents the results illustrating the influence of OWC device configuration on transmission coefficient. Observing the general response with respect to the device configurations, it can be seen that across many of cases the inclusion of OWC devices improved the wave attenuation capacity of the structure, most prominently at the resonance frequency of the OWC devices. The single device configuration response does not follow the general response observed by the other device configurations, to such a degree that a shift in the response appears evident, as such, further investigation into the single configuration is recommended to establish the cause of the response shift. There is no discernible relationship between the number of integrated devices and reduction in c_T; however, it is evident that the integration of multiple OWC devices within the floating breakwater marginally outperforms the generic floating breakwater. As frequency increases ($\geq$ 0.9 Hz) the results begin to converge displaying less variation between the integrated and non-integrated cases, before diverging again at 1.2 Hz, the cause of which requires further investigation. Though the number of devices integrated has no observable relationship to the transmission coefficient, the effects of multi-device configuration on both motion (Figure 5.8) and energy extraction (see Chapter 4) are apparent, subsequently indicating that this parameter requires significant consideration in the development of a WEC integrated floating breakwater.

Focusing on the reflection characteristics presented in Figure 5.16b, it can be observed that the integration of additional OWC devices appears to have had no discernible impact on the general reflection response of the floating breakwater. All variations followed a distinct relationship which varied in magnitude. For both the low and high frequencies tested, there was no clear relationship between number of devices integrated and reflection coefficient, yet in the resonance bandwidth of the integrated OWC devices (approximately 0.775 Hz - 0.8 Hz), it is evident that the increase of devices has a clear influence on the reflection characteristics of the breakwater, as the energy absorption from each additional chamber reduces the energy transferred to the reflected wave. Ideally, OWC device operation will target, and subsequently be tuned to site-specific wave conditions such that the peak frequency of the wave spectra correlates with the resonance frequency of the integrated devices. It can be inferred from the data presented in Figure 5.16b that an expected reduction in breakwater reflection will result, relative to a floating breakwater with no device integration.

Figure 5.16b also directly illustrates the influence of OWC device integration on the reflection response of the floating breakwater. Comparing the breakwater only condition to the remaining conditions in which devices are integrated, further evidence is presented for the aforementioned inflection point, which is observed for all conditions barring the breakwater only condition. This indicates that source of the response inflection is the subsequent incident energy extraction achieved by the installed devices. This presents a beneficial trait of OWC device integrated floating breakwaters which, in collaboration with the energy extraction capacities of the concept, should further the viability of WEC integrated floating breakwater structures for offshore applications.

Wave Height

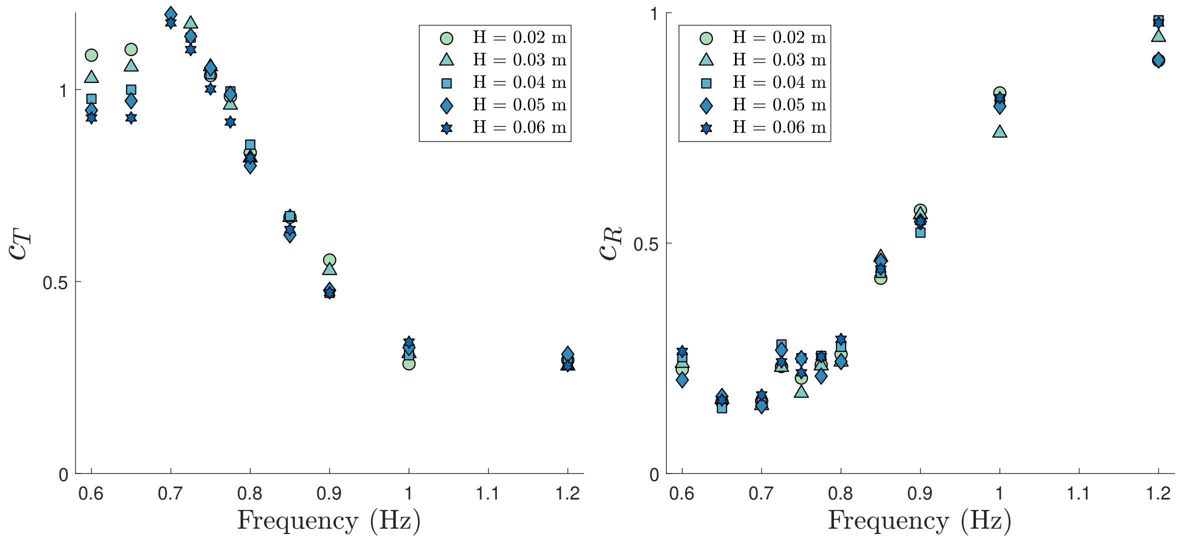

(a) Transmission Coefficient

(b) Reflection Coefficient

Figure 5.17: 1800 mm breakwater width with Far OWC device configuration and LDV_5 damping operating in varying wave heights

The experimental investigation also considered the impact of wave height on the wave attenuation characteristics of the OWC device integrated floating breakwater, the results of which are displayed in Figure 5.17. Figure 5.17a indicates that for frequencies above 0.65 Hz there is a negligible difference in c_T observed relating to wave height variation. Frequencies $\leq$0.65 Hz indicate a distinct trend suggesting as wave height increases, the amplitude of the transmitted wave decreases; however, this is not observed for the remaining frequencies tested. This is hypothesised to be a function of the wave steepness relative to the breakwater width; however, further investigation is required for verification. With regards to Figure 5.17b, it can be observed that, while some variation in the magnitude of results occurs in lower and higher frequencies along with the OWC device resonance bandwidth, there is no discernible variation trend present across the differing wave heights. Focusing more specifically on the OWC device resonance bandwidth, it can be noted that as wave height increases, the magnitude of the inflection decreases. This compares well with the results found in Chapter 4, which illustrated that although a greater amount of energy was absorbed as wave height increased, the proportion of extracted energy to incident wave energy decreased. This translates to a reduction in the c_R inflection, as, although more energy is being absorbed as wave height increases, the proportion of residual incident wave energy available for transfer into reflected wave energy increases.

Pneumatic Damping

The final model variation investigated observed how the Power Take-off pneumatic damping, simulated using the porous linear mesh fabric as specified in Chapter 4, influences the wave transmission and reflection. The results presented in Section 4.4.3 illustrate that increasing the pneumatic damping coefficient, δ, resulted in an increase in OWC device energy absorption, up until the LDV_5 which was found to be the optimal damping at the resonance frequency of the device. Figure 5.18 illustrates the results obtained from experimental testing regarding change in δ and its impact on both c_T and c_R. Figure 5.18a illustrates how transmission coefficient is influenced by pneumatic damping, from which it can be observed that no perceivable relationship can be derived. The general response curves of the damping variation results follow equivalent trends, yet the magnitude of the results vary irregularly for each damping variation across the different test frequencies. These results indicate that the energy extraction of the OWC devices has no distinguishable influence on c_T when configured in the free floating condition.

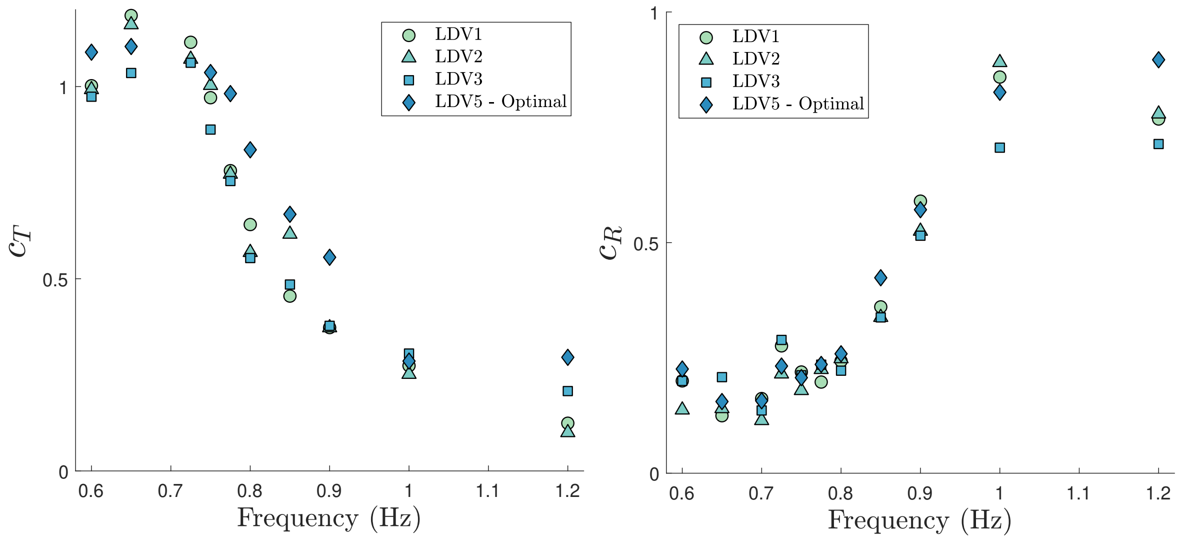

(a) Transmission Coefficient

(b) Reflection Coefficient

Figure 5.18: 1800 mm breakwater width with Far OWC device configuration operating in 0.02 m wave height

Figure 5.18b indicates how c_R for the 1800 mm breakwater width in the Far OWC configuration varies with respect to the pneumatic damping coefficient δ. Similarly to the previously investigated parameters which influence the reflection coefficient, no discernible trend is evident relating PTO damping to magnitude of reflection across the entire test bandwidth, as although the trend remains consistent across all PTO simulant variations, the magnitude varies sporadically. One perceptible product of the increasing damping is observable around the resonance frequency of the OWC devices. It can be seen that the magnitude of the aforementioned inflection point decreases as damping increases in this region, with

LDV_5 exhibiting the greatest reduction of inflection. This phenomena is attributed to the increased energy absorption at frequencies around the resonance frequency resulting from the increased damping. As δ increased (see Figure 4.14 in Chapter 4), it was established that the energy extraction capacities of the installed devices increased in the majority of test frequencies, subsequently resulting in a reduced proportion of the incident wave energy available for reflection and a decrease in c_R.

5.5 Conclusions

The experimental investigation conducted aimed to discern the influence that the integration of multiple OWC devices could have on the performance characteristics of a generic π-type floating breakwater. The proof-of-concept experimental investigation varied a series of design parameters to evaluate the effect each had on the breakwater motion and wave attenuation. From a total of approximately 2200 experimental runs, the following main conclusions can be drawn.

The integration of oscillating water column wave energy converters within the floating breakwater had beneficial impact on both the wave attenuation and motion characteristics. Though no distinct trend was established relating number of installed devices to wave attenuation, it was found that the integration of multiple devices reduced the magnitude of both the transmitted wave for most incident wave frequencies, and the reflected wave most significantly at the resonance frequency of the OWC devices (as found in Chapter 4). Similarly, no observable trend between number of devices and motion was established, however the Double-Double configuration housing 4 operational devices was able to reduce heave and pitch motions by up to approximately 20% relative to the generic, non-integrated breakwater.

The breakwater width plays a significant role in the motion performance of the floating breakwater, where it was established that the 50% increase in breakwater width between the 1200 mm and 1800 mm breakwaters resulted in heave and pitch reductions up to 40% and 50% respectively at select frequencies. The breakwater width also reduced the transmitted wave height in the higher test frequencies evaluated during experimental testing.

Through constraint of the floating breakwater motions, the transmission coefficient was significantly reduced, while an increase was observed in the reflection coefficient. Considering the free floating condition derived from the employed soft mooring, the unexpected results obtained for c_T could be significantly reduced through the incorporation of a realistic mooring arrangement, whilst also providing substantial improvement to the motion and energy absorption characteristics. As such, the utilisation of realistic mooring arrangements for the WEC/breakwater concept are planned for future works.

The experimental investigation conducted provides a foundation for the development of the OWC device integrated floating breakwater concept. The results indicate that device integration has beneficial impacts for both breakwater performance parameters, which in culmination with the energy extraction capabilities of the concept explored in Chapter 4 of this study, aims to further the viability of the concept for application in the offshore industry where the benefits of multi-purpose maritime structures capable of environmental protection, energy production and material/consumable storage solutions are desired.

Chapter 6

Performance in Irregular Seas

6.1 Introduction

A number of physical model scale experimental studies, encompassing both fixed and floating type devices, have been conducted to investigate the performance of OWC WECs in irregular sea states, a few of which can be found in [75, 118, 166, 191, 195, 226]. While most investigations focus on isolated devices, few irregular wave experimental studies have considered floating, multi-device integrated structures. In [227], physical model scale experiments were utilised to investigate the pneumatic conversion efficiency of multiple OWC devices to be installed on Very Large Floating Structures (VLFS). The initial experimental investigation considered only the OWC devices in a fixed configuration to establish the performance in both regular and irregular waves, where it was found that the maximum pneumatic conversion efficiency of the concept was 79% in irregular waves. An extension of this work is presented in [228], which investigated the concept design of the VLFS housing the multiple OWC devices through physical laboratory-scale modelling. More recently in [229], this work was expanded to investigate the performance of the OWC devices when installed on the VLFS in both fixed and floating conditions, with results indicating that the pneumatic conversion efficiency for the floating condition reached 46% in specific irregular wave spectra. In [230], a similar experimental investigation regarding the 'Seabreath' concept was conducted; a floating multi-chamber OWC device designed for application within the Adriatic Sea. Results indicated that the quarter-scale concept for deployment off-shore Riccione would be capable of producing approximately 58 MWh/year, with a full-scale concept expected to potentially produce 7.5 GWh/year.

The following chapter extends previous experimental investigations presented in Chapters 4 and 5, which employed regular waves to analyse the energy extraction, wave attenuation and motion characteristics of a π-type floating breakwater integrated with multiple OWC devices. The studies yielded results to concur with those found in [159, 182, 183], indicating that OWC device integration has beneficial influence on the wave attenuation and motion characteristics of the floating breakwater. Similarly, significant device interaction was observed for multi-device configurations which subsequently impacted device energy extraction capacities. This chapter looks to provide further evidence to support the feasibility of the OWC device integrated floating breakwater as it analyses the performance of energy extraction, wave attenuation and motions in irregular seas. Using various irregular sea states and device configurations, the performance of the concept is evaluated and subsequently compared to those acquired through regular wave testing. The main purpose of this investigation is to subject the concept to more realistic sea states and establish performance matrices both with and without operational OWC devices to increase the feasibility of the concept, and progress further through the TRLs outlined for WEC technology development [165].

6.2 Theory

6.2.1 Theoretical Hydrodynamic Consideration - Regular Waves

Damping

As defined in Section 2.1.2, a linear relationship between volume flux and pressure is considered, as defined in Equation 2.2. The approximations associated with this derivation and the non-negligible errors induced, as detailed in Section 2.1.2, are understood and considered throughout the evaluation.

Performance

OWC device comparisons between regular and irregular waves considered the non-dimensional performance criteria of the amplification factor, $H_{\eta_{AF}}$, which relates the amplitude of chamber free surface oscillation, η_{OWC}, to the incident wave amplitude, η_{Inc}, and is defined in Equation (6.1) for regular waves.

$$H_{\eta_{AF}} = \frac{\eta_{OWC}}{\eta_{Inc}} \tag{6.1}$$

Similarly, breakwater motions were evaluated using Response Amplitude Operators for each degree of freedom of interest. In regular waves, this relates the magnitude of motion to the incident wave amplitude as presented in Equations (6.2) and (6.3) for the heave and pitch motions,

$$RAO_{Heave} = \frac{\eta_{h_{mean}}}{\eta_{Inc}} \tag{6.2}$$

$$RAO_{Pitch} = \frac{\eta_{p_{mean}}}{\eta_{Inc}} \tag{6.3}$$

where $\eta_{h_{mean}}$ and $\eta_{p_{mean}}$ represents the amplitude of motion for heave and pitch respectively.

6.2.2 Theoretical Hydrodynamic Consideration - Irregular Waves

Irregular wave analysis considers JONSWAP spectra, $S_j(\omega)$, defined by significant wave height, H_s, peak frequency, f_p, and peak enhancement factor, γ. The JONSWAP spectra investigated can be considered as Pierson-Moskowitz spectra multiplied by a peak enhancement factor such that,

$$S_j(\omega) = \frac{\alpha g^2}{\omega^5} \exp\left[-\frac{5}{4}\left(\frac{\omega_p}{\omega}\right)^4\right]\gamma^r \tag{6.4}$$

where,

$$r = \exp\left[-\frac{(\omega-\omega_p)^2}{2\sigma^2\omega_p^2}\right] \tag{6.5}$$

and the remaining constants are defined as,

$$\alpha = 0.076\left(\frac{U_{10}^2}{Fg}\right)^{0.22} \tag{6.6}$$

$$\omega_p = 22\left(\frac{g^2}{U_{10}F}\right)^{1/3} \tag{6.7}$$

$$\gamma = 3.3 \tag{6.8}$$

$$\sigma = \begin{cases} 0.07 & \omega \leq \omega_p \\ 0.09 & \omega > \omega_p \end{cases} \tag{6.9}$$

where F represents the fetch, or the unobstructed distance over which the wind blows with constant velocity, g represents gravitational acceleration, and U_{10} represents the wind velocity 10 m above the water surface.

Performance and Power

The performance comparison between regular and irregular waves regarding amplification factor saw $H_{\eta_{AF}}$ defined in irregular waves as,

$$H_{\eta_{AF}} = \frac{S_{\eta_{OWC}}(f)}{S_{\eta_{Inc}}(f)} \tag{6.10}$$

where $S_{\eta_{OWC}}(f)$ and $S_{\eta_{Inc}}(f)$ represent the amplitude spectra for the OWC device free surface elevation and incident wave elevation respectively.

Instantaneous power absorbed by an OWC device as a function of time, $P(t)$, can be derived using Equation (6.11).

$$P(t) = p_c Q \tag{6.11}$$

The time-averaged hydrodynamic power absorbed by the OWC device, P_h, is subsequently derived as,

$$P_h = \frac{1}{t_t}\int_0^{t_t} p_c Q dt \tag{6.12}$$

where t_t represents the time period over which the data is sampled. Performance of the operational OWC devices is accessed in terms of non-dimensional capture width, $\tilde{L}_{pc}$. The average incident wave power per unit crest width in irregular waves can be defined as [231],

$$P_I = \frac{\rho g^2 H_s^2 T_e}{64\pi} \tag{6.13}$$

where the significant wave height , $H_s = 4\sqrt{m_0}$, with $\sqrt{m_0}$ representing the first spectral moment, which equates to one standard deviation of the wave record, and T_e is the energy period defined as,

$$T_e = \frac{m_{\text{-}1}}{m_0} \tag{6.14}$$

where m_{-1} is the first negative spectral moment derived from spectral analysis. As multiple devices are operational during each of the investigated configurations, the energy absorption capacity of the OWC devices considers the mean non-dimensional capture width of the operational devices, as defined in Equation (6.15),

$$\tilde{L}_{pc_{mean}} = \frac{\sum_{i=1}^{n}\tilde{L}_{pc_i}}{n} \tag{6.15}$$

where n represents the number of operational chambers.

Motion

The derivations for RAO_{Heave} and RAO_{Pitch} in irregular waves can be found in Equations 6.16 and 6.17 respectively,

$$RAO_{Heave} = \frac{S_{\eta_{Heave}}(f)}{S_{\eta_{Inc}}(f)} \quad (6.16) \qquad RAO_{Pitch} = \frac{S_{\eta_{Pitch}}(f)}{S_{\eta_{Inc}}(f)} \quad (6.17)$$

where $S_{\eta_{Heave}}(f)$ and $S_{\eta_{Pitch}}(f)$ represent the irregular motion spectra for heave and pitch respectively.

The mean values presented in Section 4.3 were derived such that $RAO_{H_{mean}}$ and $RAO_{P_{mean}}$ represent mean heave and pitch RAO values derived for the designated spectra, defined as,

$$RAO_{H_{mean}} = \frac{H_H}{H_s} \quad (6.18) \qquad RAO_{Pitch} = \frac{H_P}{H_s} \quad (6.19)$$

where H_H and H_P are defined as,

$$H_H = 4\sqrt{m_0} \quad (6.20) \qquad H_P = 4\sqrt{m_0} \quad (6.21)$$

where the first spectral moment of the respective heave and pitch motion spectra is employed.

6.2.3 Linear Superposition

To generate a linear motion spectrum, the encountered wave energy spectrum can be filtered by the appropriate motion transfer function. This approach is valid and appropriate for any motion where the transfer function is normalised by the incident wave amplitude [232]. To calculate the linear motion spectrum, the square of the motion transfer function is multiplied by the corresponding encountered wave spectrum ordinate, as illustrated in Equation 6.22.

$$S_{\eta_m}(f) = S_{\eta_{Inc}}(f)\left(\frac{\eta_{m_{mean}}}{\eta_{Inc}}\right)^2 \quad (6.22)$$

where the subscript m represents the motion being analysed (heave or pitch).

This investigation sought to employ this methodology to derive other linear spectra for quantities normalised by the incident wave amplitude, namely the OWC device wave amplification factor. The linear spectrum for the amplification factor, $S_{\eta_{OWC}}$, was calculated using Equation 6.23.

$$S_{\eta_{OWC}}(f) = S_{\eta_{Inc}}(f)\left(\frac{\eta_{OWC_{mean}}}{\eta_{Inc}}\right)^2 \quad (6.23)$$

To evaluate the accuracy of the linear spectrum estimations relative to the corresponding experimentally measured spectrum, the normalised error, E', was derived for each frequency increment measurement using Equation 6.24.

$$E' = \frac{S_{\eta_{Mes}} - S_{\eta_{Est}}}{max(S_{\eta_{Mes}})} \tag{6.24}$$

where $S_{\eta_{Mes}}$ represents the experimentally measured spectrum, $S_{\eta_{Est}}$ represents the linearly estimated spectrum and $max(S_{\eta_{Mes}})$ is the largest value of the measured spectrum.

6.3 Experimental Setup

6.3.1 Model and Instrumentation

The hydrodynamic performance of the OWC device integrated floating breakwater was evaluated using the results obtained from a suite of experimental investigations conducted in the Model Test Basin of the Australian Maritime College, University of Tasmania, Australia. Details of the experimental set up regarding the hydrodynamic performance of the OWC devices can be found in Chapter 4, while the experimental set up regarding the breakwater motion and wave attenuation characteristics can be found in Chapter 5. For brevity, the details of the instrumentation utilised during the experiments are presented in Table 6.1. For model and experimental configuration details refer to Figure 4.3 in Chapter 4 and Figure 5.3 in Chapter 5 respectively.

The 1:20 scale π-type floating breakwater was integrated with seven OWC devices having uniformity in both dimension and spacing as illustrated in Figure 4.3 in Section 4.3.3, which through the use of a series of shut-off panels allowed a number of various OWC configurations to be investigated. The vertical centre of gravity and the radius of gyration about the assumed pitching axis noted for the device were considered realistic for this multi-purpose floating structure, and are detailed in Chapter 5. The results presented in this article consider three varying OWC device configurations comprising of three operational devices, denoted Close, Intermediate and Far, along with a breakwater only condition, all of which are presented in Table 4.2 with the corresponding spacing dimensions.

The model was moored using a soft mooring arrangement which allowed it to be situated, and operate, within the wave basin through the constant force supplied. Metal lump weights were placed within the hull of the floating breakwater to ballast the system down to operational draft. To avoid any undesirable effects influencing the induced motions of the breakwater, the weights were applied such that symmetrical loading was achieved.

Table 6.1: Experimental instrumentation utilised throughout investigation detailing purpose of use and location within Model Test Basin. All units in mm.

Instrument	Purpose of Measurement	Location (x, y, z)
Incident Wave Probe	Incident Wave Characteristics	
IWP		11700, -5500, 600
Phase Wave Probe	Wave Characteristics at Model	
PWP		3200, -5500, 600
Reflection Wave Probes	Reflected Wave Characteristics	
RWP1		7600, 0, 600
RWP2		7850, 0, 600
RWP3		8400, 0, 600
OWC Chamber Wave Probes$^{\triangle}$	Internal Free Surface Oscillation	
OWCWP1	Characteristics	-120, 60, 600
OWCWP2		-40, 165, 600
OWCWP3		-80, 270, 600
OWC Pressure Probes$^{\triangle}$	Internal Pressure Characteristics	
OWCPP		0, 165, 806
Qualysis Passive Motion Markers	Six Degree of Freedom Motion	
QM1	Characteristics	2931, -1900, 980
QM2		1439, -1187, 1035
QM3		3173, -4, 1095
QM4		1460, 1305, 910
QM5		3007, 1504, 910

Note: The instrument locations consider a Cartesian coordinate system in which the x-axis runs longitudinally along the basin, positive towards the wavemakers, the y-axis runs transversely across the basin, positive to the port side, and the z-axis runs normal to the basin floor, positive above ground level. Locations are referenced from an origin point at the intersection of the longitudinal and transverse midpoints of the basin on the basin floor. The static location of the model measured to the reference point found in Figure 5.4 corresponds to the coordinates 2300, 0, 600.

$^{\triangle}$ The table indicates the number of internally located instruments per operational OWC chamber. Locations of these instruments are referenced to the internal starboard side forward corner of each chamber with the same Cartesian convention previously specified.

To simulate the linear Power Take-Off characteristics typically associated with a Wells type turbine, the outlet of each operational chamber was covered with a porous fabric mesh, previously employed in Chapters 3, 4 and 5. To establish the volume flux of air emanating in and out of the system, the velocity of the internal free surface was numerically derived from the elevation data acquired by the OWC wave probes, the details of which are found in

Chapter 4. Similarly, the uncertainty associated with the OWC devices internal free surface elevation and the assumed linearity of the pneumatic damping coefficient (δ) are presented in Chapter 4, which indicates a mean of $\pm 4\%$ for the free surface elevation, and $\pm 15\%$ for δ when outliers are excluded.

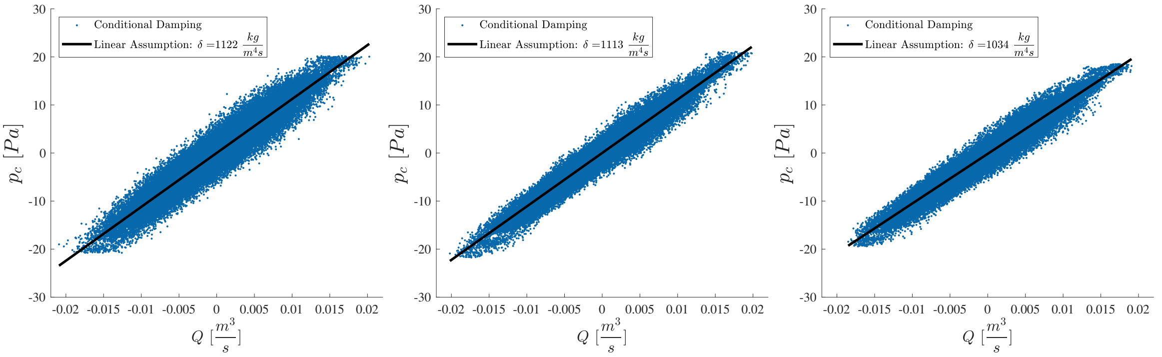

(a) Port Chamber (b) Middle Chamber (c) Starboard Chamber

Figure 6.1: Damping characteristics with linear assumption of δ for each operational OWC chamber in the Far configuration with LDV_1 applied in irregular wave spectrum of $H_s = 0.02$ m and $f_p = 0.75$ Hz.

An example of the linearity of the relationship replicated during the experiments is illustrated in Figure 6.1, where LDV_1 exhibits a mean value of 1089 $\frac{kg}{m^4 s}$ in irregular waves. Regular wave testing conducted in Chapters 3 and 4 identified that the applied pneumatic damping is frequency independent, and can be increased/decreased through the addition/subtraction of layers. An optimal damping value for the model scale testing conducted was 6410 $\frac{kg}{m^4 s}$ as investigated in Chapter 5, which correlates to 10 sheets of mesh, and is referred to as LDV_5.

6.3.2 Experimental Parameters

The current investigation utilised thirteen generic irregular wave spectra in evaluation of the device performance for this proof of concept analysis. The spectra were selected to target wave frequencies found to represent the lower and upper bounds of effective OWC device energy absorption, as well as the resonance frequency of the OWC device. These peak frequencies were then investigated across several significant wave height variations to develop the matrix of test spectra which provided a broad range of wave conditions for analysis. Figure 6.2 illustrates the irregular wave spectra investigated with regards to the peak frequency, f_p, and significant wave height, H_s, and details the generic JONSWAP spectrum inputs for each variation along with the correlating spectrum measured during experiments. Experiments were designed to comply with the Design of Experiment guidelines as specified by the International Towing Tank Committee [198, 199], which requires irregular wave experiments to acquire data equivalent to 30 minutes full-scale, as was achieved during this investigation. Data-processing was achieved through Fast Fourier Transforms using

Welch's method.

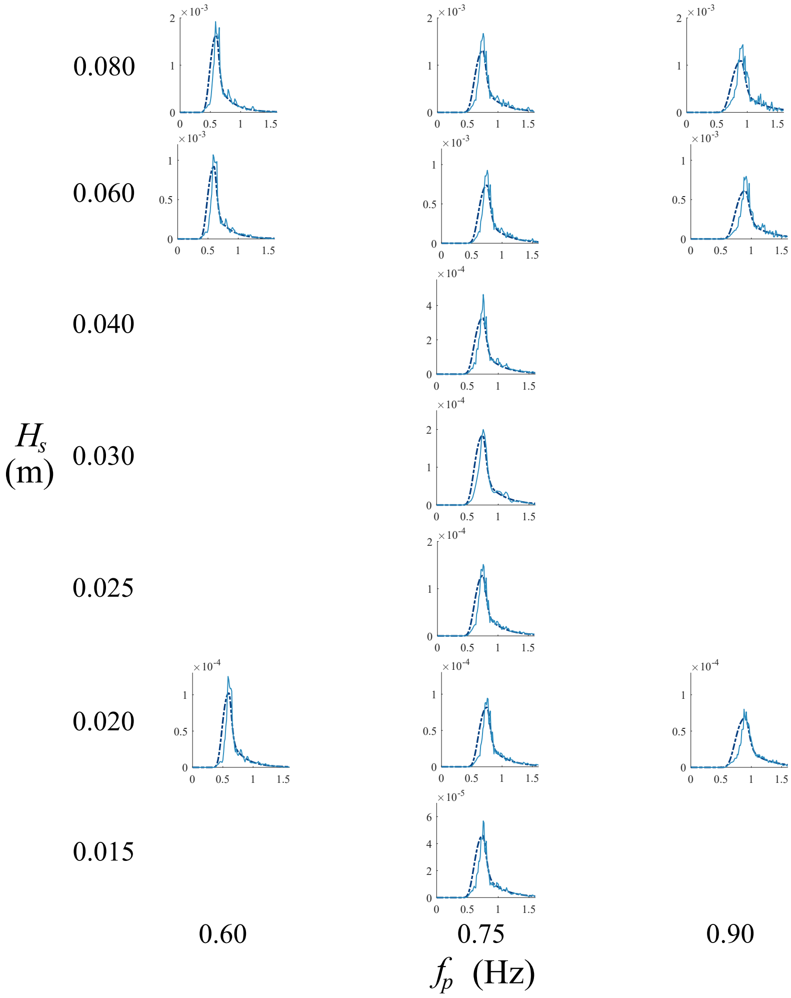

Figure 6.2: H_s versus f_p parameters matrix displaying irregular incident wave spectra investigated. All spectrum plots display the input (dashed) and measured (solid) $S_{\eta_{Inc}}$ (m^2/Hz) with respect to frequency, f, in model scale.

Figure 6.2 indicates that strong correlation between input and measured values for incident wave frequencies greater than the designated peak frequency, indicating the wavemakers could effectively replicate the desired spectrum within this range. At the peak frequency of the spectrum, it can be observed that the magnitudes of the measured spectrum exceed those expected from the input spectrum; however, the target bandwidth for peak frequency is effectively captured by the wavemakers. Frequencies below the peak frequency were not as effectively replicated by the wavemakers as those above the peak frequency, resulting in a lack of longer period waves interacting with the model. This can be observed across all measured spectra, and likely results from the interactions between the incident waves and those reflected from the energy dissipating beach located at the opposing end of the basin.

6.4 Results and Discussion

Results from the experimental investigation described in the previous sections are used to investigate and evaluate the performance of an OWC device integrated floating breakwater in irregular seas. Comparisons of non-dimensional performance parameters are presented for previously investigated regular wave analysis (Chapters 4 and 5), and those acquired through irregular wave testing. Similarly, the results investigate the use of RAO transfer functions derived from regular wave experiments to predict the performance characteristics of the OWC device integrated floating breakwater; including OWC device amplification factor and floating breakwater motions. Finally, the results of the irregular wave experiments have been evaluated to produce performance matrices identifying how parametric variations influence device performance with respect to peak period and significant wave height.

6.4.1 Regular versus Irregular Waves

OWC Performance

To derive comparisons between the hydrodynamic behaviour and performance of the WEC integrated floating breakwater in various configuration, the dimensionless performance parameter of amplification factor, $H_{\eta AF}$, was evaluated for both regular and irregular sea states. The amplification factor is non-dimensionalised with respect to the incident wave height, subsequently any minor variation in wave height across the incident wave frequencies tested is accounted for. Due to the relationship of the non-dimensional character to wave height, all results can be considered a normalisation, which ensures all comparative analyses are true, and variation in results becomes independent of wave height.

Considering first the amplification factor as presented in Figure 6.3, it can be found that there is strong correlation between the results derived from a series of regular wave experiments relative to the spectrum derived from an irregular wave analysis. Figure 6.3a, 6.3b and 6.3c represent the Close, Intermediate and Far OWC device configuations respectively for the WEC/breakwater device, and displays the mean amplification factor measured across the three operational devices in each case.

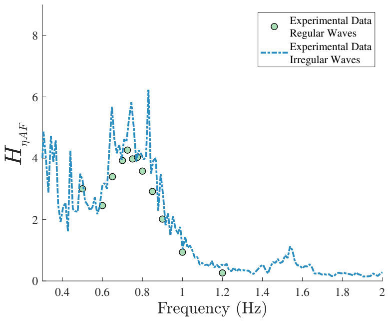

(a) Close Configuration

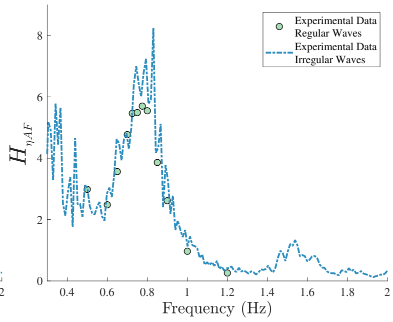

(b) Intermediate Configuration

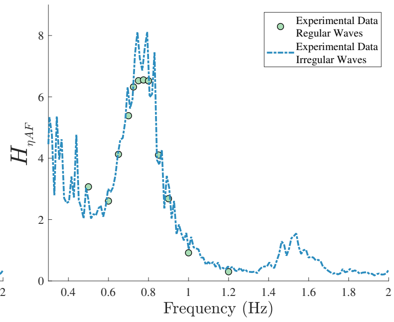

(c) Far Configuration

Figure 6.3: Amplification Factor, $H_{\eta AF}$, for OWC device free surface elevations in the 1800 mm breakwater width with LDV_1 applied operating in 0.02 m wave heights

As Figure 6.3 illustrates, good agreement was found between the amplification factor results derived from the regular and irregular sea state experiments. The results best agree in frequencies both above and below the natural resonance frequency of the OWC devices. The largest variation between the results occurs at resonance, where it can be found that the results obtained from irregular wave experiments marginally over-predict the amplification factors across the three OWC configurations presented. The discrepancy in the results at resonance is likely attributed to the induced non-linearity of the free surface oscillation associated with the resonating devices, whereby the sinusoidal nature of repeating waves probably enhanced the sloshing motions within the chambers. In comparison, the frequency and wave height variation associated with irregular sea states may have more readily regulated the free surface sloshing and allowed the spatially distributed wave probes to more accurately capture the complex dynamics occurring within each chamber. This potential source of variation does however require further investigation for validation.

Figure 6.3 highlights a minor secondary performance peak at a incident wave frequency of approximately 1.5 Hz, likely corresponding a second order response of the OWC device. Though the magnitude is small relative to that experienced at the device's natural frequency, a clear trend is found relating the magnitude of the secondary peak relative to the device spacing, whereby increasing the spacing between the devices results in an increase in magnitude of the response. The experimental frequency bandwidth investigated during regular wave analysis did not extend sufficiently high to capture this phenomena, however investigation into the performance at higher frequencies is included in future research. As an OWC device's performance is a function of its ability to absorb wave energy across a specific frequency bandwidth, exploring variations to pneumatic damping, and manipulation of air compressibility in order to harness this second order response may improve overall device performance.

Figure 6.3 also emphasises the variation in performance based upon the OWC device configuration employed. As found in Chapter 4, destructive interference was observed by devices in regular waves for both the close and intermediate configurations, employing spacing equivalent to approximately 0.3 and 1.6 device widths respectively (edge to edge measurements). As Figure 6.3 demonstrates, the irregular wave spectra investigated was also able to accurately capture the performance differences across all three of the three-device configurations, where the close OWC configuration appears to be significantly impacted by strong device-device interaction causing a substantial reduction in performance relative to the far OWC configuration. As was found with the regular wave experiments, device spacing is a crucial design parameter to be considered in the initial stages of concept development, as it has significant influence on the energy absorption capacities of the devices. The increasingly scattered results for the irregular wave data below approximately 0.5 Hz is attributed to numerically derived errors associated with FFT analysis of the negligibly small incident wave amplitudes in this region, and is common across all irregular wave analyses.

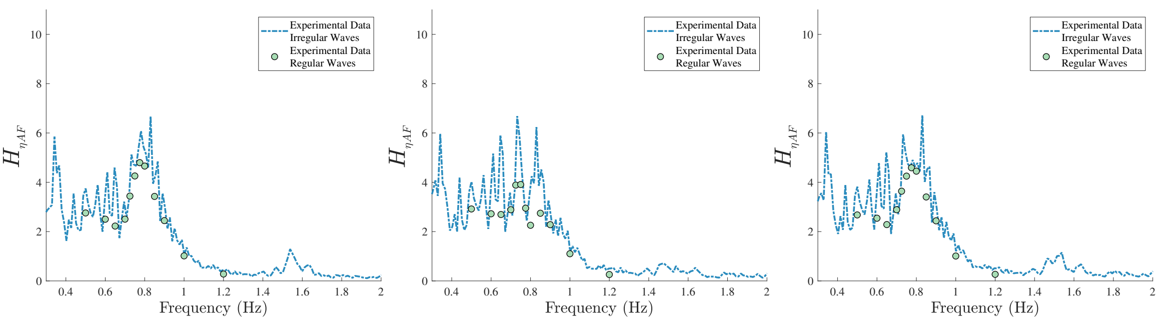

(a) Port Chamber (b) Middle Chamber (c) Starboard Chamber

Figure 6.4: Amplification Factor, $H_{\eta_{AF}}$, for OWC device free surface elevations in the Close configuration with LDV_1 applied operating in 0.02 m wave heights

Investigating the device-device interaction further, Figure 6.4 illustrate the amplification factors observed by the port, middle and starboard chambers whilst in the Close OWC device configuration. As was discovered in Chapter 4, Figure 6.4b shows the considerable reduction in performance observed by the middle chamber around 0.8 Hz, while the two outer chambers display relatively identical performance characteristics. The results from the irregular wave experiments agree well with those obtained from the regular experiments, where the destructive interference is maximum at 0.8 Hz, before rising again at 0.9 Hz to a larger magnitude than observed in the regular wave trials. As explained in Chapter 4, the destructive interference reduced as device spacing, and subsequent reflective structure surrounding the OWC device, increased. This design property has been found to significantly influence the performance of breakwater integrated OWC devices [187], as is displayed in Figure 6.5 where the individual chamber results corresponding to the far configuration can be observed. Figure 6.5 illustrates that as device spacing and reflective surrounding structure increased, the devices observed negligible interference, and subsequently preformed at equivalent capacities much higher than that observed for the close configuration.

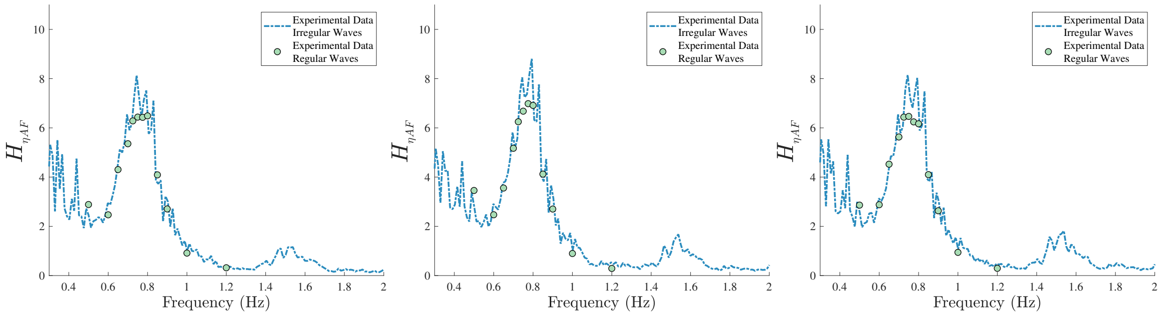

(a) Port Chamber (b) Middle Chamber (c) Starboard Chamber

Figure 6.5: Amplification Factor, $H_{\eta_{AF}}$, for OWC device free surface elevations in the Far configuration with LDV_1 applied operating in 0.02 m wave heights

These results illustrate the potential to forgo the traditional regular wave analysis when establishing the performance characteristics of an OWC device. The mean results obtained from several irregular wave experiments were able to establish comparable results to those obtained through 30+ regular wave tests, and accurately capture complex phenomena including device-device interaction. The benefit of utilising irregular waves not only include the reduction in required experimental time, but also the additional bandwidth of results that can be obtained from a single experimental run, and possible results of interest that may not be observed during regular wave experiments, such as the secondary peak observed as a results of these tests. The measured irregular wave spectra provides high correlation to that of the regular waves investigated; however, it should be noted that the spectra presented thus far had a peak period aligned with the natural period of the OWC devices ($H_s = 0.02$ m and $f_p = 0.75$ Hz). When comparing the results of spectra with peak periods not aligned with the natural period of the OWC devices, the agreement between the irregular and regular results were less favourable. Subsequently, it is suggested that to utilise irregular waves for OWC performance analysis an understanding of the general performance curve, including the resonant period, is required. This may be derived from validated numerical models, as found in Chapter 3.

The impact of the significant wave height increase on the amplification factor is illustrated in Figure 6.6. It can be observed that as the significant wave height of the incident wave spectra increases, the amplification factor tends to decrease in the operational bandwidth of 0.5 Hz - 1.2 Hz, with the most prominent region of reduction around the resonant frequency of the OWC devices ($\approx$ 0.75 Hz - 0.8 Hz). This is most likely attributed to the increased non-linearities observed in the free surface oscillation within the OWC chamber as significant wave height increases, subsequently resulting in a reduction in relative amplitude. While amplification factor decreases, the overall power absorption of the device is likely to increase as incident wave power increases proportional to the square of wave amplitude. Contrarily, the second order response ($\approx$ 1.55 Hz) of the device appears to observe an increase in performance as the significant wave height increases. This may positively influence the evaluation of performance across the observable bandwidth as significant wave height increases, improving the overall extraction capacity of the device. A further peak can be observed around approximately 1.9 Hz, potentially correlating to the presence of a third order response. However, further investigation is required to establish whether this is a function of device performance or simply errors associated with FFT analysis of the incident spectra.

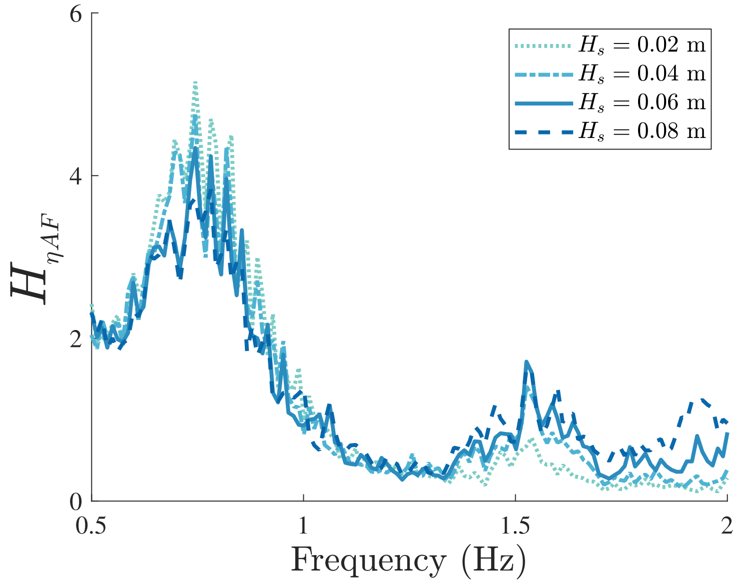

Figure 6.6: Amplification Factor, $H_{\eta_{AF}}$, for OWC device free surface elevations in irregular spectra of $f_p = 0.75$ Hz and varying significant wave heights. The floating breakwater/WEC is in the Far configuration with width of 1800 mm and LDV_5 damping applied.

Motion

Similarly to the comparisons presented for OWC device performance, the following compares the heave and pitch motion RAOs for the WEC/breakwater device in both regular, as found in Chapter 5, and irregular sea states. In Chapter 5 it was established that the integration of OWC WECs within the floating breakwater had a beneficial impact on the motion characteristics relative to a non-integrated structure in regular waves. Alike the OWC device performance parameters, the motion characteristics have been normalised with respect to the incident wave amplitude, hence any subsequent variation in wave height is accounted for.

Examining firstly the heave RAO of the WEC/breakwater device as presented in Figure 6.7a, a strong correlation can be found between both the regular and irregular sea states. As can be observed, for frequencies below 0.5 Hz, and above 1.6 Hz, the irregular results diverge and become more sporadic, which is likely attributed to the relative difference between the negligibly small numerical values within the frequency domain for each respective probe, subsequently amplified during FFT analysis, and is not necessarily representative of the actual motion response. Similarly, good correlation was found for the pitch RAOs of the WEC/breakwater device in both regular and irregular seas, which also captured the natural pitching frequency of the device at approximately 0.64 Hz as found in Chapter 5. As with the heave RAOs, the irregular pitch RAO response curve diverges from the expected results in the low and high frequencies presented in Figure 6.7b, which is also associated with the numerically derived errors linked to FFT analysis of small amplitudes in the incident wave spectra.

Considering both the heave and pitch RAOs presented in Figure 6.7, it can be observed that the second order response found for the OWC device performance is not present for the relative motion. This is attributed to the magnitude of the response, with peak values of approximately 1.25 and 0.15 for heave and pitch respectively. In comparison, the magnitude of peak values for $H_{\eta_{AF}}$ are approximately 8 with LDV_1 applied and 5 with LDV_5 applied. For the multi-purpose floating structure considered, motions are desired to be low; hence, remaining out of the second order response of the structure is a beneficial feature. However, it is recommended that future works include further research conducted to identify additional responses of the floating breakwater/WEC system.

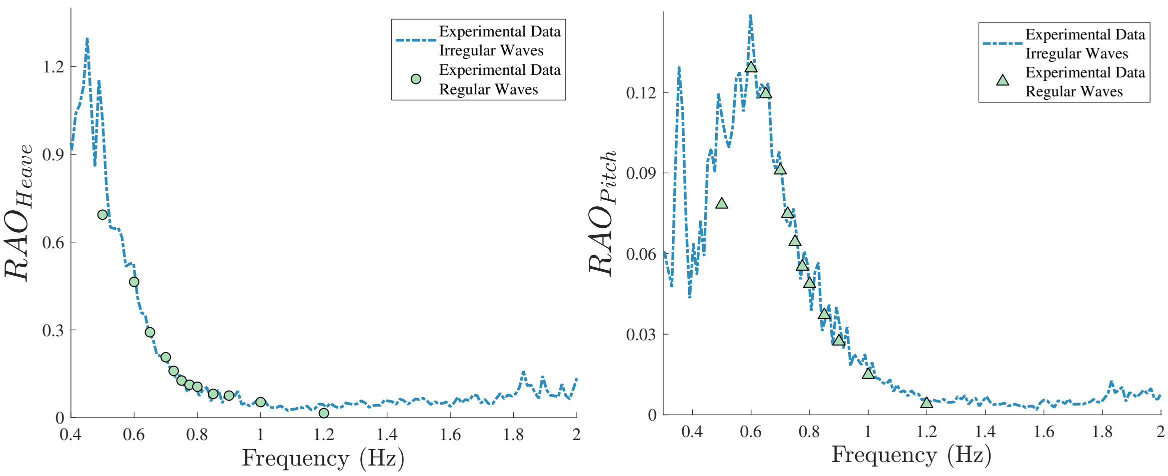

(a) Heave Response Amplitude Operator, RAO_{Heave} (b) Pitch Response Amplitude Operator, RAO_{Pitch}

Figure 6.7: Motion Response Amplitude Operators for regular and irregular sea states with OWC devices in the Far configuration at a breakwater width of 1800 mm.

As was previously discussed regarding the OWC device performance parameters, the high correlation between the regular and irregular wave results suggest the potential to simply conduct irregular wave experimentation and forgo the traditional route of regular wave testing (assuming device properties such as natural frequency are known). Not only does this curtail the temporal constraints typically associated with model scale hydrodynamic experimentation, but also contributes to greater progression through the TRLs associated with WEC technological development [165]. The commonality in the regular and irregular results can also be used contrarily to the aforementioned means, whereby the regular wave RAOs could be used in culmination with the measured irregular incident wave spectra to predict both the OWC device and motion performance characteristics.

6.4.2 Linear Superposition

Through the use of linear superposition as outlined by Lloyd [232], the motion and OWC device performance characteristics for the WEC/breakwater structure could be estimated by utilising the RAOs acquired through regular wave testing. The RAOs are converted into the transfer functions as illustrated in Figure 6.8, which are then multiplied by the incident wave spectra to produce pseudo performance spectra for the parameters of interest. These pseudo spectra were then compared to the measured spectra obtained from the experimental tests conducted, and utilising Equation 6.24 comparisons were derived between the pseudo and measured spectra to determine how accurate the linear superposition method could predict the performance.

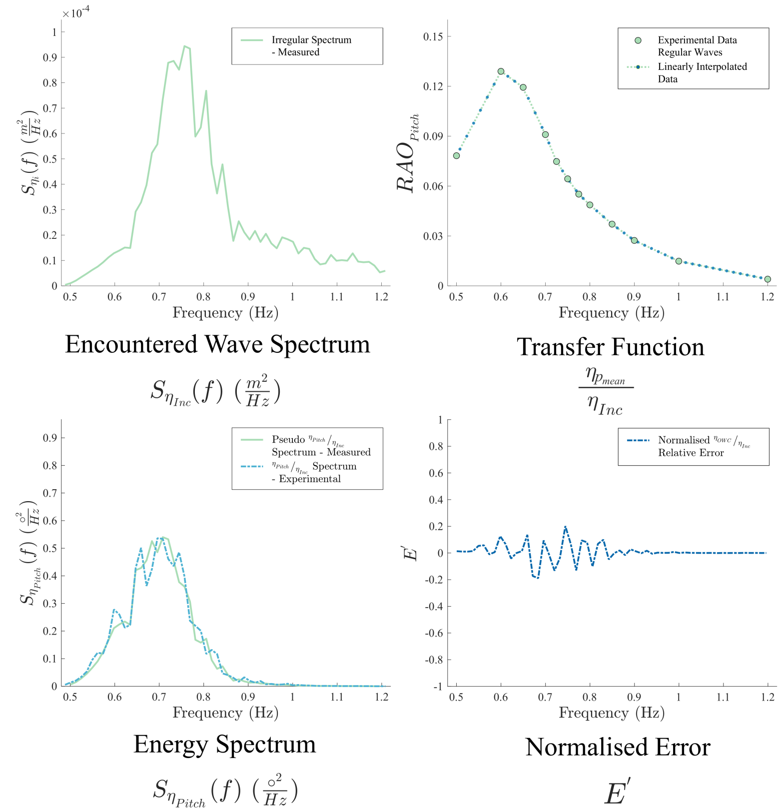

Figure 6.8: Components of linear superposition methodology for pitch RAO with normalised error, E', to indicate variation between pseudo and measured spectra.

Figure 6.8 illustrates an example of the linear superposition process, where the pitch RAO is estimated and compared to the actual measured value in terms of the normalised error. The normalised error presented in the right hand column of Figure 6.8 presents the difference between the pseudo and measured performance results relative to the maximum magnitude of measurement. Subsequently, a positive normalised error result indicates that the pseudo spectra is underestimating the magnitude of performance, and conversely a negative result indicates an over estimation.

By applying the methodology from Section 6.2.3 and Figure 6.8 to heave and pitch and $H_{\eta_{AF}}$, Figure 6.9 was produced to compare how the linear superposition estimations were able to predict the behaviour of the aforementioned performance parameters for incident wave spectra of varying peak period. As can be observed in Figure 6.9, a number of trends are evident in the error obtained from the linear superposition pseudo spectra. Considering the accuracy of the estimations with respect to the peak frequency of the incident wave spectra, Figure 6.9 illustrates that as the peak frequency increased, the estimations for all performance parameters diverged further from the experimentally measured values obtained. The largest errors in the estimations commonly align with the peak frequency of the incident wave spectra, likely a result of the increased wave occurrence. An increase in the error bandwidth is also observable as the peak frequency of the incident spectra increases, where for the $f_p = 0.6$ Hz case majority of the error is contained between 0.5 Hz and 0.85 Hz, while for the $f_p = 0.9$ Hz cases, the errors are evident for all test frequencies. The motion response of the WEC/breakwater concept generate larger discrepancies as peak frequency increases compared to the amplification factors of the OWC devices, which may be a function of the breakwater geometry and increasing wave steepness, however further investigation into the relationship between the two parameters is required for validation.

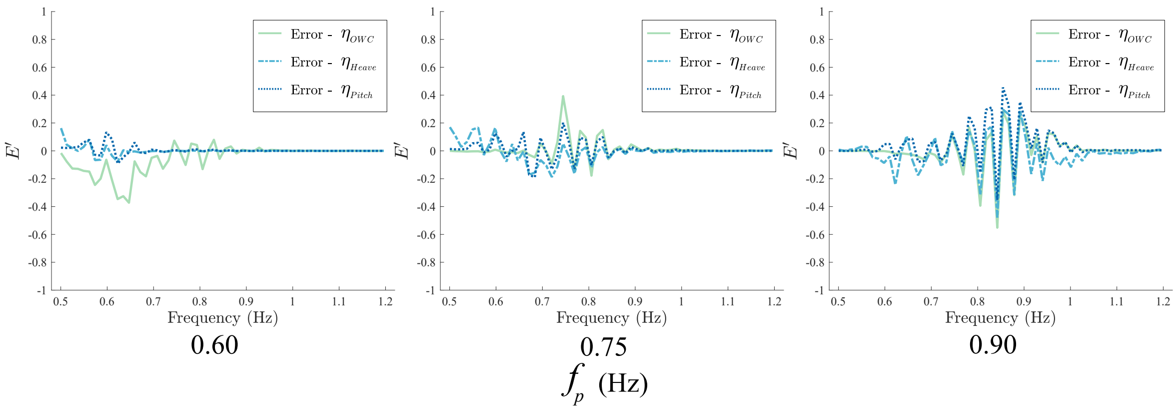

Figure 6.9: Normalised error, E', derived for OWC device free surface elevation, heave motion and pitch motion when comparing the pseudo spectra generated from the linear superposition method to the measured spectra.

While only one significant wave height is presented in Figure 6.9, results were obtained for increasing significant wave heights; however, due to the increasing non-linearities associated with these spectra, the linear superposition method was deemed non-applicable to these incident wave spectra as the estimations derived in the pseudo spectra are less capable of accurately capturing the performance characteristics of the WEC/breakwater device. Figure

6.6 illustrates how the increasing non-linearities impact the relative performance of the device. When this is combined with the sloshing and inertial impacts of increasing water column oscillation within the chamber for both the regular and irregular waves investigated, the results obtained from the pseudo spectra provide in an inaccurate representation of the complex dynamics of the system. Future investigations should investigate whether the small scale of the OWC devices in fact accentuates the sloshing motions, in which case the linear superposition method may be applicable in larger significant wave heights. Similarly, it is suggested that future work exploring the impact of wave steepness on the motion response of the breakwater/WEC be conducted, in conjunction with the influence of water column oscillation on motion characteristics of the breakwater, as this will improve the accuracy of the predictions.

6.4.3 Irregular Sea State Performance Matrices

The irregular wave experimentation allowed for evaluation of the device by comparing the performance characteristics across varying incident wave spectra to produce performance matrices. The following results present matrices for device performance relative to the peak frequency and significant wave height of the incident wave spectra the floating breakwater was subjected to. The values presented in the matrices are the experimentally derived magnitudes for each respective performance parameter which correlate to the tested incident wave spectra defined by the coordinates of the value within the matrix. The grid locations in which no value is presented indicates that an experimental investigation of the corresponding incident wave spectra was not conducted, and has instead been linearly interpolated using an *inpaint_nans* function [233], which adopts a least squares method. These values should be considered as approximations based on the actual values obtained from the experimental investigation.

Non-Dimensional Capture Width ($\tilde{L}_{pc_{mean}}$)

As with previous performance evaluations of OWC devices, the non-dimensional capture width, $\tilde{L}_{pc}$, is considered. As three OWC devices were operational during the irregular wave experiments, the mean non-dimensional capture width, $\tilde{L}_{pc_{mean}}$, of the three operational chambers is presented in Figure 6.10. As Figure 6.10 illustrates, the OWC devices' highest power absorption in the lower wave heights at the natural frequency of 0.75 Hz, where for the 0.02 m case, the mean non-dimensional capture width of the devices is approximately 2.5. An evident trend emerges from the data indicating as significant wave height increases, a subsequent reduction in non-dimensional capture width is observed, which is expected to be associated with the increasing non-linearity related with larger wave interaction. Though a decrease in non-dimensional capture width is observed, performance in terms of power absorbed improves, as wave power increases proportionally to the wave amplitude squared.

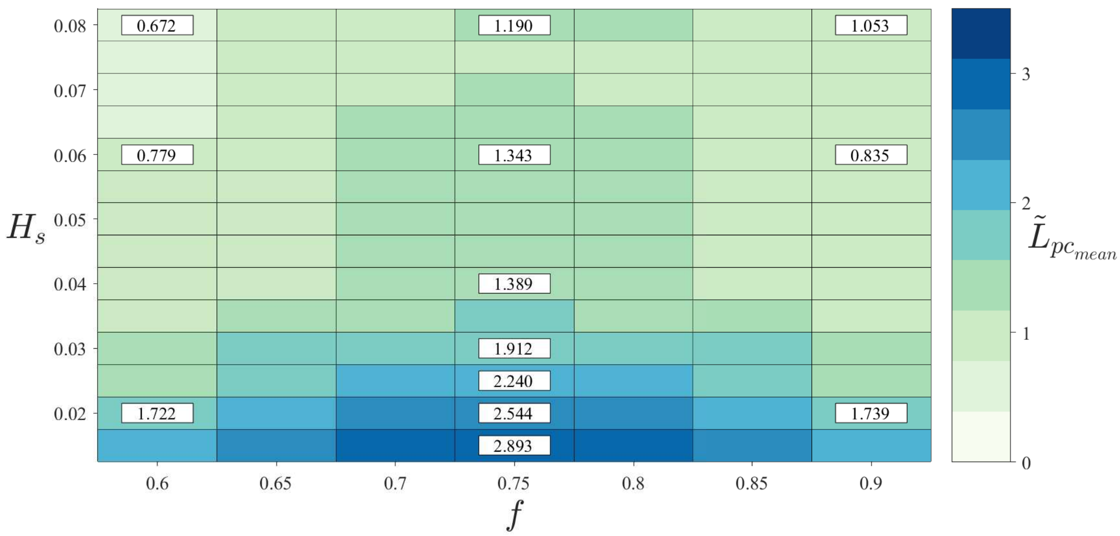

Figure 6.10: Mean non-dimensional capture width, $\tilde{L}_{pc_{mean}}$, for OWC devices in the Far configuration with LDV_5 damping applied with respect to significant wave height, H_s, and peak frequency, f.

For the irregular spectra with peak frequencies that do not correlate to the natural frequency of the OWC devices, the non-dimensional capture width follows the same trend as that discussed; however, the magnitude of the performance is reduced equivalently for both the 0.6 Hz and 0.9 Hz cases. One distinguishing feature is the increase in performance for the 0.9 Hz cases of larger wave height, where the $f_p = 0.9$ Hz, $H_s = 0.08$ m case performs almost equivalently to the corresponding natural frequency case. This increase in performance is potentially attributed to an increase in the pneumatic damping applied by the PTO simulant. This increase in damping in larger significant wave heights may have possibly resulted from heightened free surface oscillations within the OWC chamber causing sloshing, subsequently resulting in the underside of the damping mesh to become wetted. This would decrease permeability of the material and consequently increasing damping; however, further investigation is required to validate this hypothesis.

Motion - Heave

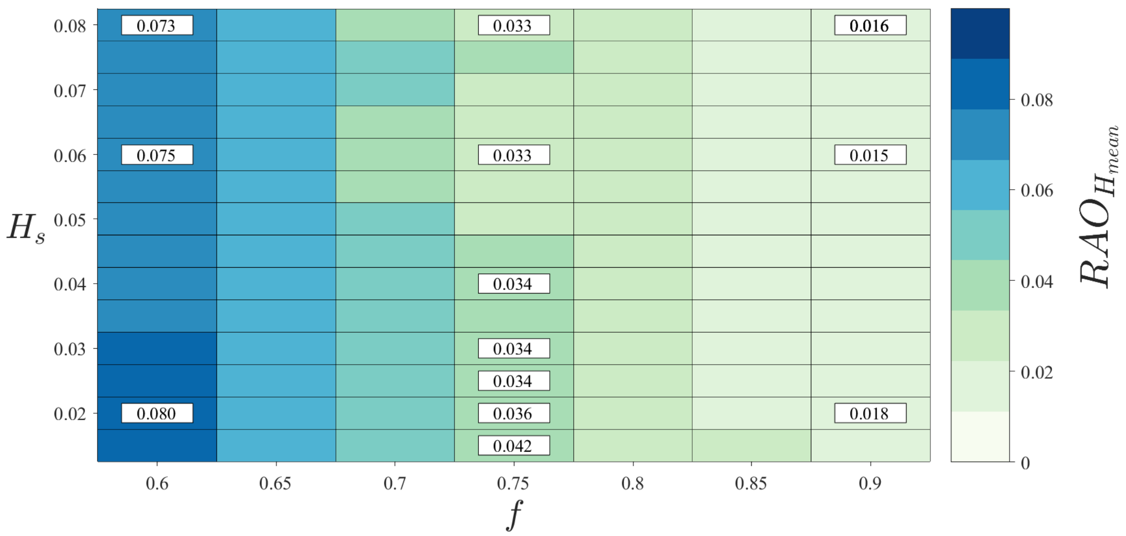

Figure 6.11: Mean Heave Response Amplitude Operators for each wave spectrum experimentally investigated; displayed in terms of the significant wave height, H_s, and peak frequency, f, presented in (m) and (Hz) respectively. The mean Heave RAO was calculated using the mean Heave amplitude for the given spectra, $\eta_{h_{mean}}$, with respect to H_{m0}.

The irregular wave investigation also considered the influence of various incident wave spectra on the motions of the WEC/breakwater concept, in particular the heave and pitch. Figure 6.11 illustrates the mean heave RAO for each incident wave spectra investigated where it can be observed that as peak frequency and significant wave height of the incident spectra increase, the mean heave RAO decreases. This is likely attributed to the higher occurrence of steeper waves associated with incident wave spectra of increasing peak frequency and significant wave height. The variation in the results for spectra of the same peak frequency but varying significant wave height was approximately 10% between the maximum and minimum values, with a consistent trend of decreasing mean heave RAO as significant wave height increased. These results would indicate that the WEC/breakwater device exhibits reduced relative heave motion as wave steepness increases; however, this will likely not be the conditions in which the device will optimally absorb wave energy, as illustrated in Figure 6.10. It is expected that the introduction of a realistic mooring arrangement will significantly reduce the relative motions of the WEC/breakwater device, which will be the focus of future works. The wave steepness will then play a significant role in the design of the mooring arrangement as it has been found that increasing wave steepness elevates the tension experienced by the moorings [140].

A comparison was also conducted to investigate the impact of OWC WEC integration on the relative motions of the breakwater in irregular sea states. The non-integrated breakwater condition was subjected to six irregular spectra, subsequently comparisons were made for the corresponding WEC integrated cases. Table 6.2 details the characteristics of the spectra compared across the integrated and non-integrated configurations, and provides the mean heave RAOs for both cases together with the percentage difference, where a negative result indicates a reduction in relative motion when the devices were integrated. As Table 6.2 indicates, the integration of OWC WECs within the breakwater had a significant beneficial impact on the mean relative heave motion of the breakwater, where all investigated incident spectra observed a reduction, with the average reduction greater than 50%.

Table 6.2: Heave RAO Comparison

			$RAO_{H_{mean}}$		
Spectrum Label	H_s (m)	T_p (s)	Without OWC Devices	With OWC Devices	% Difference
FBOWC_I1	0.020	1.667	0.111	0.080	-27.93
FBOWC_I2		1.333	0.102	0.036	-64.71
FBOWC_I3		1.111	0.067	0.018	-73.13
FBOWC_I4	0.015	1.333	0.097	0.042	-56.70
FBOWC_I5	0.025	1.333	0.089	0.034	-61.80
FBOWC_I6	0.030	1.333	0.077	0.034	-55.84

Motion - Pitch

Relative pitch motion was also investigated across the irregular wave spectra, from which the mean pitch RAOs could be derived. Similarly to that of the heave RAOs, the relative pitch motion observed a trend of decreasing magnitude as peak frequency and significant wave height increased, illustrated in Figure 6.12. The magnitude of the relative pitch motions were far less than that of heave motions; however, these values are expected to be reduced even further with the aforementioned realistic mooring arrangement. The pitching motion of the WEC/breakwater structure was essentially unconstrained as the connection of the soft mooring arrangement to the model acted along the assumed axis of pitch rotation; hence, a simple four point catenary mooring connected at each corner of the breakwater would likely apply greater constraint to the structure and reduce the pitching amplitude. As per the discussion on the effect of wave steepness on heave, it is hypothesised that this also contributes to the reduction in pitch relative motion at the cost of increased slamming on the bow face of the breakwater, which was observable during the experimental investigation. Future research aims to investigate the interrelationship between motion, wave loads, mooring loads and energy absorption of the WEC/breakwater structure to validate the hypotheses presented.

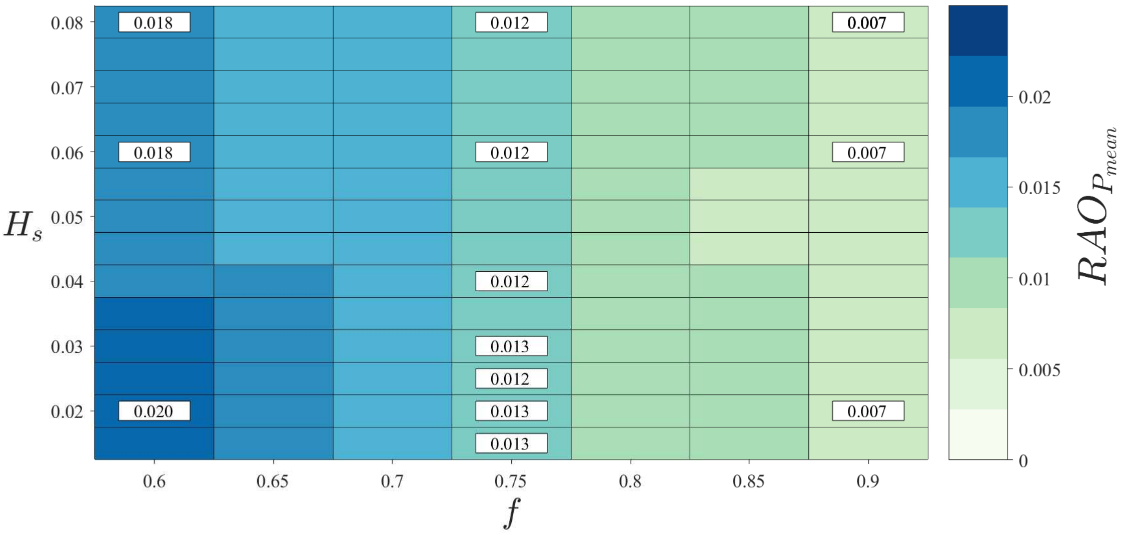

Figure 6.12: Mean Pitch Response Amplitude Operators for each wave spectrum experimentally investigated; displayed in terms of the significant wave height, H_s, and peak frequency, f, presented in (m) and (Hz) respectively. The mean Pitch RAO was calculated using the mean Pitch amplitude for the given spectra, $\eta_{p_{mean}}$, with respect to H_{m0}.

Table 6.3 compares the relative pitch motion for the WEC integrated and non-integrated configurations where it can be observed that, similarly to the relative heave motion, all investigated incident wave spectra exhibited decreased pitch motions when integrated with the OWC devices. The percentage reduction of magnitude for the relative pitching motion was considerably less than that of the heave motion; however, it is evident that the device integration beneficially impacted the pitch motion of the structure, with the average improvement in motion greater than 10%. These results, in culmination with the heave results presented in Table 6.2, indicates that the integration of OWC WECs within the floating breakwater provide an energy sink in which incident wave energy is being absorbed as opposed to transformed into motion as would typically occur with a generic breakwater. The further reductions expected to be experienced as a realistic mooring is applied is likely to add further evidence to support the integration of WECs within floating breakwaters, as the reduced construction and maintenance costs, energy generation and beneficial performance impacts that stem from this multi-purpose maritime structure indicate that ocean wave energy can provide a substantial contribution toward the renewable energy sector.

Table 6.3: Pitch RAO Comparison

			$RAO_{P_{mean}}$		
Spectrum Label	H_s (m)	T_p (s)	Without OWC Devices	With OWC Devices	% Difference
FBOWC_I1	0.020	1.667	0.021	0.020	-4.76
FBOWC_I2		1.333	0.016	0.013	-18.75
FBOWC_I3		1.111	0.008	0.007	-12.50
FBOWC_I4	0.015	1.333	0.016	0.013	-18.75
FBOWC_I5	0.025	1.333	0.015	0.012	-20.00
FBOWC_I6	0.030	1.333	0.015	0.013	-13.33

6.4.4 Technology Readiness Levels

The analysis of performance for varying irregular sea states at small scale is highlighted as a latter component of Stage 1 in the structured development plan of WEC technologies [165], intended to follow the previously established regular wave analysis. The results presented in this chapter provide additional observations regarding the performance of the WEC/breakwater concept, which contributes to the earlier knowledge foundation established through regular wave experimental investigation found in Chapters 4 and 5. The results obtained from the irregular wave analysis indicates the Technology Readiness Level of this concept to be 2-3, with future investigation to be conducted regarding mooring suitability and hull seaworthiness to satisfy the remaining criteria of Stage 1, before development continues to gradually meet the requirements of Stage 2, including survivability for design validation.

6.5 Conclusion

The experimental investigation conducted regarding the performance of the multiple OWC device integrated floating breakwater concept in irregular sea states continues the progression through the WEC technology TRLs. Strong correlation was observed between the non-dimensional performance parameters derived from both regular and irregular wave experimentation indicating that, with knowledge of the OWC device natural frequency, it may be possible to forgo the traditional route of regular wave experimentation and employ targeted irregular wave spectra to derive the performance characteristics. This methodology would allow for investigation over a greater bandwidth of incident wave frequencies with reduced temporal requirements. The correlation between the regular and irregular wave results also presents the converse approach, whereby use of the regular wave RAOs can be used to estimate OWC device and breakwater motion performance. The results of this investigation indicate that for lower wave heights, the linear superposition methodology was able to provide relatively accurate predictions for the breakwater motions; however when wave height increased, the induced non-linearities created divergence from the predicted and measured spectra. The linear superposition methodology was found to be effective for indicating the OWC device performance parameters across all the irregular spectra tested, with the largest estimation errors occurring at resonance.

Over the 13 irregular incident wave spectra tested, the performance in terms of non-dimensional capture width of the integrated OWC devices was found to be equivalent to that observed in regular waves (Chapter 4). As wave height increased, the non-dimensional capture width gradually reduced; however, the increase in available wave power elicited a continual increase in power absorbed. It was established that irregular spectra with peak frequencies aligned with the natural resonance frequency of the devices allowed for greatest performance, with equivalent reduction in performance observed for spectra with peak frequencies either side of the resonant frequency. Breakwater motions in irregular sea states was found to benefit from OWC device integration, with reductions in heave and pitch magnitudes observed for all irregular sea states examined, as was observed during regular wave experimentation (Chapter 5). The results from this investigation contribute to furthering the development of multi-purpose maritime structures as the benefits to the performance of traditional maritime structures are evident, with the additional dividend of renewable energy generation. The continuing progression of this concept validation is set to explore mooring suitability, which is expected to improve the performance of the concept and advance the viability of multi-purpose maritime structures for the ever-expanding blue economy.

Chapter 7

Thesis Conclusions and Future Work

7.1 Conclusions

In this thesis, the integration of oscillating water column wave energy converters within maritime structures was investigated from a hydrodynamic performance perspective through the use of physical scale model experimentation. The development of the project led to the OWC devices being investigated across three distinct configurations;

Isolated
Generic OWC model, whose construction comprised solely of chamber geometry, installed within the wave basin. Representative of the typical arrangement associated with devices installed in WEC farm/array.

Breakwater Integrated - Fixed
Utilised the isolated OWC model, which was then installed within a fixed breakwater model whose depth extended to the basin floor.

Breakwater Integrated - Floating
Multiple bent-duct type OWC devices were integrated within a generic Π-type floating breakwater, which was investigated in a free-floating state.

Initial experimental investigations sought to identify the influence that chamber cross-sectional geometry and breakwater integration (fixed) had on the performance characteristics of the bent-duct type OWC device, the results of which would partially satisfy the first research question posed for this project, as outlined in Section 1.2.2. The experimental results obtained were compared with those acquired from a FEM numerical hydrodynamic model, where the model was validated with good agreement for both the isolated and fixed cases explored. The results from the initial investigation were subsequently utilised to develop the physical scale model for testing during the floating breakwater integrated experiments. The operating conditions of this experiment considered the following main parameters, and sought to explore their impact on both OWC device performance, and floating breakwater performance.

1. Regular and Irregular Waves
2. PTO Damping
3. Breakwater Width
4. OWC Device Configuration
5. Motion Constraints

6. Breakwater Only versus OWC Device Integrated

The following main conclusions can be drawn from the studies completed and presented throughout this thesis:

- The use of the Enviro-Cloth porous fabric mesh as a PTO simulant in physical model scale hydrodynamic investigations can effectively replicate the linear damping relationship typically associated with a Wells type turbine. The damping imparted by the PTO simulant was also determined to be frequency independent, which allowed it to be adopted in both regular and irregular wave investigations [Chapters 3, 4 and 6].
- Comparison of results between cross-sectional geometry of the OWC device chamber (circular and rectangular for this study) indicate that no discernible variation in the potential for power absorption can be attributed to the geometry of the OWC chamber. While this design consideration had negligible impact on the performance, when considering the constructibility and maritime structure integration, the rectangular device presents a more viable design solution [Chapter 3].
- The integration of a generic bent duct OWC device within a fixed, bottom-mounted breakwater provided a significant increase in the potential power absorption of the device compared to the isolated case. Considering the non-dimensional capture width of the device, breakwater integration was found more than double the performance of the device at resonance relative to the equivalent isolated case. Similarly, the performance of the integrated device saw improvement in absorption capacity across almost all incident wave frequencies investigated [Chapter 3].
- The integration of OWC devices within a generic floating Π-type breakwater was able to return non-dimensional performance results that displayed agreement with the fixed breakwater cases, indicating the beneficial influence of breakwater integration. The investigation identified a number of design parameters including PTO damping and motion constraint which could be manipulated to improve the hydrodynamic energy absorption of the integrated devices, while floating breakwater width was found to have no discernible impact on device performance [Chapter 4].
- The integration of multiple devices was found to result in improved mean hydrodynamic absorption for most of the cases relative to that observed by the single integrated device. This is likely attributed to the increased energy sink created as multiple devices resonate, as opposed to the limited sink created by the single device, indicating that multi-device integration is beneficial in the energy extraction capacities of the concept [Chapter 4].

- One of the most important parameters identified for OWC device performance in multi-device configurations is device spacing. Significant device-device interaction was observed as device spacing decreased, resulting in a detrimental impact on the extraction capacities of the integrated devices. While it was found that the Double-Double OWC configuration (4 Devices) was able to extract up to approximately 80% of the available wave energy interacting with the breakwater when PTO damping was optimised, the increase in energy absorbed relative to the the Far (3 Device) configuration was not proportionate to the addition of fourth chamber. This resulted from the device-device interaction reducing the mean performance of each operational device. Subsequently, when considering real world applicability in which CAPEX and OPEX costs are analysed, the Far configuration may present the most feasible solution. [Chapters 4 and 6].

- The integration of multiple OWC WECs within the floating breakwater, when compared to the generic, non-integrated breakwater, was found to reduce the magnitude of the transmitted wave for most incident wave frequencies investigated, while also reducing the reflected wave height most prominently around the resonant frequency of the integrated devices. While no evident trend relating number of devices to wave reduction was observed, it was found that for all multi-device configurations the above-mentioned observations were true. Applying constraint to breakwater motions such that the structure operated fixed further reduced the magnitude of the transmitted wave, but increased the magnitude of the reflected wave, indicating that the incorporation of a realistic mooring arrangement has potential to improve the sheltering capabilities of the concept [Chapter 5].

- Similar to the influence on wave attenuation, the integration of multiple OWC WECs was able to reduce the relative heave and pitch motions of the device by up to 20% in regular waves when compared to the non-integrated breakwater. In irregular waves, the heave motions for the WEC integrated cases were reduced across all incident wave spectra tested relative to the breakwater only cases, with maximum reduction of approximately 73% for specific wave spectra was observed. Furthermore, the pitch motions also decreased for all irregular incident wave spectra tested by up to approximately 20%. No discernible trend was identified relating number of devices to reduction of relative motion across both regular and irregular wave investigations; however, the Double-Double OWC configuration was found to provide the largest reductions across both of the measured motions in regular waves [Chapters 5 and 6].

- Though breakwater width was found to have no impact on the performance of the integrated OWC devices, it played a significant role in the motion performance of the floating breakwater, whereby increasing the width by 50% (1200 mm to 1800 mm) resulted in relative heave and pitch motions being reduced by 40% and 50% respectively. The increase in width also reduced the magnitude of the transmitted wave for some of the higher incident wave frequencies tested during the investigation [Chapter 5].

- The non-dimensional performance parameters of the floating breakwater/WEC concept observed strong correlation between those acquired through both regular and irregular wave investigation. These results suggest that with knowledge of the natural resonance frequency of the integrated OWC devices, it may be possible to forgo traditional regular wave investigation and employ targeted irregular wave spectra to understand the performance characteristics, as this would reduce the temporal constraints of experimental testing, whilst providing a large bandwidth of performance information [Chapter 6].

- Contrary to the aforementioned point, the correlation between the regular and irregular waves also allows for the opposite approach whereby the regular wave RAOs in culmination with the measured irregular spectra can be used to predict the pseudo performance spectra for the concept. The investigation into this methodology indicated that through linear superposition, the reconstructed performance spectra could be closely predicted for the smaller wave heights tested, however as wave height increased, and more non-linearities were induced, the predictions tended to be less accurate.

- The OWC device performance in irregular sea states, in terms of non-dimensional capture width, was found to be equivalent to that in regular waves. Although it was found that increasing significant wave height resulted in a decrease in the mean non-dimensional capture width, the increase in available wave power elicited a continual increase in power absorbed [Chapters 4 and 6].

7.1.1 Concluding Remarks

The results obtained from the final experimental investigation detailed each parameters influence on OWC device hydrodynamic absorption in addition to how OWC device integration impacted the traditional performance criterion of a floating breakwater. Analysis of the results provided answers to all research questions posed for this study, culminating in the development of a proof-of-concept study for a multi-purpose floating offshore structure. To date, the investigations conducted can be considered to have progressed the concept through the technology readiness levels for wave energy converter technology up to TRL 2-3.

The expansion for many blue economy industries into the offshore region has lead to the necessity for development of multi-purpose maritime structures capable of providing environmental protection, topside area for industry specific infrastructure and economically viable source of energy production. The investigation into the WEC/floating breakwater described within this thesis provides promising findings to support future development of the concept to satisfy the increasing demand, with synergistic benefits of OWC device integration evident throughout the works presented. With one of the major challenges facing wave energy being the high associated costs, and subsequent high LCOE, this concept provides a solution which would likely improve the economic feasibility of WEC technology through shared construction and maintenance costs, while also providing improved energy yield relative to the equivalent isolated device array. Although commercial viability remains a distant consideration, the findings of within this thesis provide a stable foundation for ongoing development of multi-purpose maritime structures which harness ocean energy for renewable power generation.

7.2 Future Work

The development of this research culminated in a proof-of-concept investigation for a floating breakwater integrated with multiple OWC WECs. Hence, for further development of the concept and progression through the TRLs associated with WEC technology, a number of studies are considered for future works to assist in satisfying the subsequent development criteria:

- The investigations presented in this thesis regarding the concept considered a free floating condition, which was achieved through use of a soft mooring apparatus, and provided a baseline from which improvements were expected to be made. For future development of the concept, it is necessary to investigate the inclusion of a realistic mooring arrangement at model scale, as to comply with the progression of the concept through the TRLs specified for WEC technology development. The results presented within this thesis indicate that motion restraints produced improved sheltering capacity for the breakwater concept, and also improving the hydrodynamic power absorption properties of the integrated OWC devices. While investigation regarding the influence that a realistic mooring arrangement has on the performance parameters presented throughout this thesis would provide additional data to support the viability of the concept, the optimisation of mooring configuration, material and anchoring system for a multi-purpose maritime structure as is proposed are vital design considerations that warrant analysis as part of future works.
- Conducting further testing in realistic sea states, both for operability and survivability, is essential for the future progression of this proof of concept. The investigations presented within this thesis considered only operational sea states in which the OWC

devices adopted incident headings of 0° and operated in unidirectional waves. Future studies are suggested to expand the scope of operational wave conditions to include oblique waves and short-crested sea states. Research regarding oblique waves and short-crested seas will contribute towards the viability of the concept, and results are expected to dictate deployment considerations including sea state specific positioning and multi-unit configurations. Similarly, survivability is a key design consideration that was beyond the scope of this thesis; however, investigations regarding extreme wave conditions are critical for the advancement of the concept. The survivability of the WEC devices, structure seaworthiness and moorings should be investigated in extreme sea states to provide understanding of the concepts response in survival conditions. The data acquired from such investigations should lead to development of an iterative design methodology which can be employed to optimise the system for both operation in targeted sea-states, and survival in extreme conditions.

- It is necessary to comprehensively investigate the Power Take-Off system for the OWC device integrated floating breakwater concept. As was discussed in Chapter 1, several turbines variations exist for the purpose of bi-directional airflow, and the recent developments regarding vented OWC devices has expanded the scope of available systems for incorporation. Future works should place significant importance on the development of the PTO system, including the relevant PTO control strategies in both operational and survival mode, as the findings of this thesis indicate that the PTO has a substantial impact on the performance of the OWC devices. Sufficient compromise must be established between the influence of the turbine and the economic drivers, as the PTO system represents one of the largest proportions of CAPEX and OPEX associated with WEC technology. Subsequently, governing design based upon a turbine designed specifically for optimal energy conversion, or modifying design to incorporate commercially available sub-optimal PTO systems is an important consideration for future economic feasibility studies.

- The influence of air compressibility, whether to detriment or benefit, was not explicitly explored throughout the investigation into the OWC device integrated maritime structures considered within this thesis. As this is inextricably linked to the PTO system, it is a consideration that must be at the forefront of future development. It is understood that this phenomena has a non-negligible influence on the performance characteristics of OWC devices at full-scale, and should be subsequently considered as the device testing increases in scale. Hence, it is deemed advantageous to conduct future investigations to explore how this effect impacts the device performance as results are extrapolated to full-scale, while also exploring the potential to harness this effect to improve hydrodynamic absorption capacity of the operational devices.

- As discussed in Chapter 5, the modular characteristics of the proof-of-concept floating breakwater/WEC design supports the potential for a multi-unit configurations. Locating multiple units laterally to create rows of multi-purpose platforms would provide significant benefits including; environmental protection, energy generation and topside area, all of which are valuable commodities in the offshore industry. Future works regarding multi-unit arrays of the floating breakwater/WEC concept should consider optimisation of unit configurations, coupling design between units and multi-unit mooring analyses. The results of the aforementioned future investigations should culminate in designs which optimise energy generation, environmental protection capacities and economic considerations, with aim to beneficially support the expanding offshore industry.

Appendix A

Experimental Condition Specifics: Chapters 4, 5 & 6

Table A.1: Condition Parameters for OWC WEC integrated Floating Breakwater Experiments

Condition Number	Breakwater Width (mm)	Device Configuration	Damping Arrangement	Additional Notes
0	N/A	N/A	N/A	Initial Setup and Mooring Check
1	1200	BW Only	N/A	
2	1200	BW Only	N/A	Decay Tests
3	1200	Single	LDV_1	
4	1200	Single	LDV_1	Decay Tests
5	1200	Far	LDV_1	
6	1200	Intermediate	LDV_1	
7	1200	Intermediate	LDV_1	Decay Tests
8	1200	Close	LDV_1	
9	1500	Close	LDV_1	
10	1500	Intermediate	LDV_1	
11	1500	Far	LDV_1	
12	1500	Far	LDV_1	Decay Tests
13	1500	BW Only	N/A	
14	1500	BW Only	N/A	Decay Tests
15	1800	BW Only	N/A	
16	1800	BW Only	N/A	Decay Tests
17	1800	Intermediate	LDV_1	
18	1800	Far	LDV_1	
19	1800	Far	LDV_1	
20	1800	Far	LDV_1	
21	1800	Close	LDV_1	
22	1800	Far	ODV_3	Orifice Plate Used (Quadratic Damping)[1]
23	1800	Far	LDV_2	
24	1800	Far	ODV_2	Orifice Plate Used (Quadratic Damping)[1]
25	1800	Far	LDV_3	
26	1800	Far	ODV_1	Orifice Plate Used (Quadratic Damping)[1]
27	1800	Far	LDV_1	Breakwater Fixed (Motion Constrained)
28	1800	Far	LDV_2	Incident Wave Angle 10°
29	1800	Far	LDV_2	Incident Wave Angle 20°
30	N/A	N/A	N/A	Empty Basin Tests - Incident Wave Baseline
31	1800	Single	LDV_1	
32	1800	Single	LDV_5	
33	1800	Single	LDV_5	Breakwater Fixed (Motion Constrained)
34	1800	Single	N/A	Non-Damped Condition - Breakwater Fixed
35	1800	Single	LDV_1	Breakwater Fixed (Motion Constrained)
36	1800	Far	LDV_5	
37	1800	Far	LDV_1	
38	1800	Double	LDV_1	
39	1800	Double	LDV_5	
40	1800	Double-Double	LDV_1	
41	1800	Double-Double	LDV_5	

[1] ODV represents the Orifice Damping Value which corresponds to orifice plates of area ratios, $\frac{A_{Orifice}}{A_{OWC}}$, equivalent to 0.5%, 1.5% and 5% for ODV_1, ODV_2 and ODV_3 respectively.

Appendix B

Experimental Uncertainty Analysis

B.1 Methodology

Type A uncertainty, $u_{s\text{–}A}$, for a measured quantity is derived through Equations (B.1) and (B.2)

$$\overline{q} = \frac{\sum_{k=1}^{n} q_k}{n} \tag{B.1}$$

where q_k is the k^{th} reading of the repeated observation, n is the total number of observations and $\overline{q}$ is the mean value of the repeated observations. Using Equation (B.1), Type A uncertainty is

$$u_{s\text{–}A} = s(\overline{q}) = \frac{1}{n}\sqrt{\frac{\sum_{k=1}^{n}(q_k - \overline{q})^2}{n-1}} \tag{B.2}$$

where $s(\overline{q})$ is the experimental standard deviation of the mean.

For the purpose of this paper, Type B uncertainty, $u_{s\text{–}B}$, was primarily evaluated for instruments using end-to-end calibration data, from which a linear line of best fit was applied as to follow the methodology outlined in ITTC guideline 7.5-01-03-01 ”Uncertainty Analysis Instrument Calibration” [234]. Another consideration for Type B uncertainty in this investigation was the assumed linearity of the pneumatic damping relationship proposed in Equation (2.2). The uncertainty of this assumed parameter was determined through linear regression analysis, as in [189], defined as the standard error of estimation as given in Equation (B.3)

$$SEE = u_{s\text{–}B} = \sqrt{\frac{(y_j - \widehat{y}_j)^2}{M-2}} \tag{B.3}$$

where M is the number of calibration points, and $y_j - \widehat{y}_j$ presents the magnitude of difference between the calibrated data point and the fitted value.

The standard uncertainty, u_s, of a measurement which is a function of a number of different quantities is equated to the positive square root sum of the terms. For the purpose of this experimental uncertainty analysis, we consider the terms to be Type A and Type B uncertainties as derived through Equations (B.2) and (B.3). Hence, the standard uncertainty is determined in Equation (B.4).

$$u_s = \sqrt{u_{s\text{–}A}^2 + u_{s\text{–}B}^2} \tag{B.4}$$

Generally, the data reduction equation is not directly measured; rather it is determined through N other input quantities (both measured or assumed), for example X_1, X_2, ... , X_N via a functional relationship f. Hence

$$Y = f\left(X_1, X_2, \ldots, X_N\right) \tag{B.5}$$

estimating that,

$$y = f\left(x_1, x_2, \ldots, x_N\right) \tag{B.6}$$

The combined uncertainty, $u_c(y)$, is derived using the law of propagation of uncertainty, which can be considered the positive square root of the combined variance, $u_c^2(y)$, as displayed in Equation (B.7)

$$u_c^2(y) = \sum_{i=1}^{N} \left(\frac{\partial f}{\partial x_i}\right)^2 u_s^2\left(x_i\right) + 2\sum_{i=1}^{N-1}\sum_{j=i+1}^{N} \left(\frac{\partial f}{\partial x_i}\right)\left(\frac{\partial f}{\partial x_j}\right) u_s\left(x_i, x_j\right) \tag{B.7}$$

where $\frac{\partial f}{\partial x_i}$ are the sensitivity coefficients, $u_s(x_i)$ is the standard uncertainty derived for the input estimate x_i, and $u_s(x_i, x_j)$ is the estimated covariance associated with x_i and x_j [89]. It should be noted that in cases where the estimated quantities x_i are not correlated (ie. independent), the second term of Equation (B.7) can be neglected, however in the event that the input estimates are correlated, Pearson's correlation coefficient can be used to determine the degree of correlation between x_i and x_j [235].

Finally, the expanded uncertainty, U, can be determined as the product of the combined uncertainty $u_c(y)$ and a coverage factor k. The coverage factor is determined using a Student's t-distribution for this investigation [236], giving the final expanded uncertainty with a 95% confidence interval. Selecting the correct coverage factor is a function of the effective number of degrees of freedom, which is calculated through the Welch-Satterthwaite formula [237, 238], as presented in Equation (B.8)

$$v_X = \frac{\left(u_c^2\right)^2}{u_{s-A}^2/\nu_{u_{s-A}} + \sum_{i=1}^{M} u_{s-B}^4(x_i)/\nu_{u_{s-B}}(x_i)} \tag{B.8}$$

where v_X represents the effective number of degrees of freedom; $v_{u_{s-A}}$ is given as;

$$\nu_{u_{s-A}} = N - 1 \tag{B.9}$$

and $\nu_{u_{s-B}}(x_i)$ is estimated through Equation (B.10), as recommended by the ISO guide [239]

$$\nu_{u_{s-B}}(x_i) \approx \frac{1}{2}\left(\frac{\Delta u_{s-B}(x_i)}{u_{s-B}(x_i)}\right)^{-2} \tag{B.10}$$

subsequently, the expanded uncertainty is given through evaluation of Equation (B.11).

$$U = ku_c(y) \tag{B.11}$$

B.2 Uncertainty in δ

The high uncertainty associated with δ is predominantly attributed with the assumed linearity of the damping relationship between Q and p_c. This is illustrated in Figure B.1, which presents each components proportional attribution to the overall uncertainty associated with δ, indicating that approximately 50% is associated with the linear assumption. The uncertainty results presented in Section 4.4.1 of Chapter 4 consider LDV_1 damping, which was the lowest of the tested damping. Orphin et al. [89] found that as damping increased, the uncertainty associated with δ consequently decreased as the relationship between p_c and Q became more linear. As such, it is assumed that the uncertainty associated with the optimal damping condition, LDV_5, will be substantially less than that presented for the LDV_1 condition investigated.

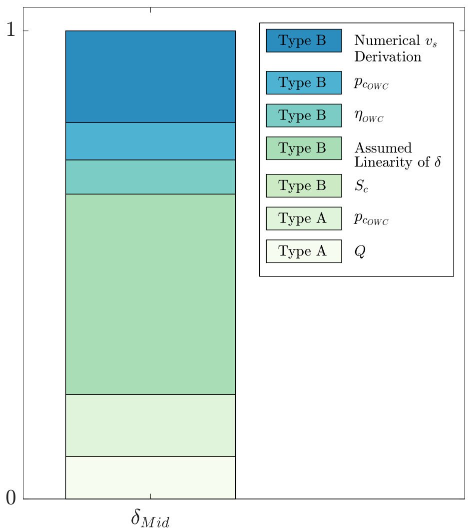

Figure B.1: Uncertainty proportions of variables associated with δ derivation. Considers the δ_{Mid} uncertainty when subjected to an incident wave frequency of 0.8 Hz, correlating to the resonance frequency of the OWC device.

Appendix C

Paper Five: D. Howe, JR. Nader, J. Orphin and G. Macfarlane. "The effect of lip extrusion on performance of a Breakwater Integrated Bent Duct OWC WEC". In: *Proceedings of the 12th European Wave and Tidal Energy Conference.* Vol. 2017. 2017, p. 1–9

This article has been removed for copyright or proprietary reasons.

Appendix D

Paper Six: D. Howe, JR. Nader and G. Macfarlane. "Experimental analysis into the effects of air compressibility in OWC model testing". In: *AWTEC 2018 Proceedings.*. National Taiwan Ocean University, 2018, p. 449

This article has been removed for copyright or proprietary reasons.

Appendix E

Paper Seven: D. Howe, JR. Nader and G. Macfarlane. "Integration of Wave Energy Converters within Floating Offshore Structures". In: *Proceedings of the Australasian Coasts and Ports Conference.* Hobart, Tasmania, 2019.

This article has been removed for copyright or proprietary reasons.

References

[1] EIA. *Annual Energy Outlook 2019 with Projections to 2050*. Report. The U.S. Energy Information Administraction (EIA), 2019.

[2] M. A. H. Baky, M. M. Rahman, and A. S. Islam. "Development of renewable energy sector in Bangladesh: Current status and future potentials". In: *Renewable and Sustainable Energy Reviews* 73 (2017), pp. 1184–1197.

[3] REN21. *Renewables 2019 Global Status Report*. ISBN 978-3-9818911-7-1. Paris: REN21 Secretariat, 2019.

[4] Intergovernmental Panel on Climate Change. *Special Report on Renewable Energy Sources and Climate Change Mitigation*. Cambridge, United Kingdom and New York, NY, USA: Cambridge University Press, 2011.

[5] P. Denholm, M. Hand, M. Jackson, and S. Ong. *Land-Use Requirements of Modern Wind Power Plants in the United States*. Technical Report NREL/TP-6A2-45834. Prepared under Task No. WER9.3550. Golden, Colorado, USA: National Renewable Energy Laboratory (NREL), 2009.

[6] S. Ong, C. Campbell, P. Denholm, R. Margolis, and G. Heath. *Land-Use Requirements for Solar Power Plants in the United States*. Technical Report NREL/TP-6A20-56290. Prepared under Task Nos. SS12.2230 and SS13.1040. Golden, Colorado, USA: National Renewable Energy Laboratory (NREL), 2013.

[7] J. Kaldellis, M Kapsali, E. Kaldelli, and E. Katsanou. "Comparing recent views of public attitude on wind energy, photovoltaic and small hydro applications". In: *Renewable Energy* 52 (2013), pp. 197–208.

[8] S. Bond. "Attitudes towards the development of wind farms in Australia". In: *Environmental Health* 8.3 (2008), p. 19.

[9] J. Firestone, B. Hoen, and J. Rand. "Are public objections to wind farms overblown?" In: *The Conversation* (2018).

[10] J. Cruz. *Ocean wave energy: current status and future prespectives*. Springer Science & Business Media, 2007.

[11] S. Teske, J Muth, S Sawyer, T Pregger, S Simon, T Naegler, M O'Sullivan, S Schmid, J Pagenkopf, B Frieske, et al. *Energy [r]evolution-a sustainable world energy outlook*. Ed. by G. International. Greenpeace International, EREC and GWEC, 2012.

[12] F. d. O. Antonio. "Wave energy utilization: A review of the technologies". In: *Renewable and Sustainable Energy Reviews* 14.3 (2010), pp. 899–918.

[13] A. Babarit. *Ocean wave energy conversion: resource, technologies and performance.* Elsevier, 2017.

[14] N Khan, A Kalair, N Abas, and A Haider. "Review of ocean tidal, wave and thermal energy technologies". In: *Renewable and Sustainable Energy Reviews* 72 (2017), pp. 590–604.

[15] M. Melikoglu. "Current status and future of ocean energy sources: A global review". In: *Ocean Engineering* 148 (2018), pp. 563–573.

[16] W. Krewitt, K. Nienhaus, C. Kleßmann, C. Capone, E. Stricker, W. Graus, M. Hoogwijk, N. Supersberger, U. von Winterfeld, and S. Samadi. "Role and potential of renewable energy and energy efficiency for global energy supply". In: *Climate Change* 18.2009 (2009), p. 336.

[17] A. Lewis, S. Estefen, J. Huckerby, Musial, W., T. Pontes, and J. Torres-Martinez. "Ocean Energy. In IPCC Special Report on Renewable Energy Sources and Climate Change Mitigation [O. Edenhofer, R. Pichs-Madruga, Y. Sokona, K. Seyboth, P. Matschoss, S. Kadner, T. Zwickel, P. Eickemeier, G. Hansen, S. Schlömer, C. von Stechow (eds)]". In: ed. by U. K. Cambridge and U. New York NY. Cambridge University Press, 2011. Chap., pp.

[18] International Energy Agency. *World Energy Outlook 2018*. Ed. by IEA, Paris. IEA, 2018, p. 661. DOI: https://doi.org/https://doi.org/10.1787/weo-2018-en.

[19] K. Gunn and C. Stock-Williams. "Quantifying the global wave power resource". In: *Renewable Energy* 44 (2012), pp. 296–304.

[20] M. Hemer, I. Penesis, K. McInnes, R. Manasseh, and T. Pitman. "Catching the waves: it's time for Australia to embrace ocean renewable energy". In: *The Conversation* (2016).

[21] S. P. Neill and M. R. Hashemi. "Wave power variability over the northwest European shelf seas". In: *Applied Energy* 106 (2013), pp. 31–46.

[22] N. Rascle and F. Ardhuin. "A global wave parameter database for geophysical applications. Part 2: Model validation with improved source term parameterization". In: *Ocean Modelling* 70 (2013), pp. 174–188.

[23] J. Sierra, C Mösso, and D González-Marco. "Wave energy resource assessment in Menorca (Spain)". In: *Renewable Energy* 71 (2014), pp. 51–60.

[24] G. Emmanouil, G. Galanis, C. Kalogeri, G. Zodiatis, and G. Kallos. "10-year high resolution study of wind, sea waves and wave energy assessment in the Greek offshore areas". In: *Renewable Energy* 90 (2016), pp. 399–419.

[25] W. Sasaki. "Changes in wave energy resources around Japan". In: *Geophysical Research Letters* 39.23 (2012).

[26] P. Contestabile, V. Ferrante, and D. Vicinanza. "Wave energy resource along the coast of Santa Catarina (Brazil)". In: *Energies* 8.12 (2015), pp. 14219–14243.

[27] D. G. Mediavilla and H. H. Sepúlveda. "Nearshore assessment of wave energy resources in central Chile (2009–2010)". In: *Renewable Energy* 90 (2016), pp. 136–144.

[28] M. A. Hemer, S. Zieger, T. Durrant, J. O'Grady, R. K. Hoeke, K. L. McInnes, and U. Rosebrock. "A revised assessment of Australia's national wave energy resource".

In: *Renewable Energy* 114 (2017). Wave and Tidal Resource Characterization, pp. 85 –107. ISSN: 0960-1481.

[29] Department of the Environment and Energy. *Australian Energy Statistics, Table O.* Tech. rep. Australian Government, 2019.

[30] Australian Bureau of Statistics. *Interesting Facts about Australia's 25,000,000 population.* Electronic Publication. Aug. 2018. URL: https://www.abs.gov.au/websitedbs/D3310114.nsf/home/Interesting+Facts+about+Australia%E2%80%99s+population.

[31] Australian Bureau of Statistics. *2018 Estimated Residential Population.* Electronic Image. 2019.

[32] Australian Government Department of Environment and Energy. *The Renewable Energy Target (RET) Scheme.* Electronic. (Accessed 16.10.2019). URL: https://www.environment.gov.au/climate-change/renewable-energy-target-scheme.

[33] Clean Energy Council. *Renewable Energy Target.* Electronic. (Accessed 16.10.2019). URL: https://www.cleanenergycouncil.org.au/policy-advocacy/renewable-energy-target.html.

[34] Australian Government Department of Prime Minister and Cabinet. *Australia's 2030 Emission Reduction Target.* Electronic. (Accessed 16.10.2019). 2016. URL: https://www.dpmc.gov.au/sites/default/files/publications/Summary%20Report%20Australias%202030%20Emission%20Reduction%20Target.pdf.

[35] M. Folley and T. Whittaker. "Identifying promising wave energy converter technologies". In: *Renewable Energy in the Service of Mankind Vol I.* Springer, 2015, pp. 279–289.

[36] B. Drew, A. R. Plummer, and M. N. Sahinkaya. "A review of wave energy converter technology". In: *Journal of Power and Energy.* Vol. 223. Part A. Sage Publications Sage UK: London, England, 2009, pp. 887–902.

[37] I. López, J. Andreu, S. Ceballos, I. M. de Alegría, and I. Kortabarria. "Review of wave energy technologies and the necessary power-equipment". In: *Renewable and Sustainable Energy Reviews* 27 (2013), pp. 413–434.

[38] Aquaret. *A guide to aquatic renewable energy technologies.* Electronic Poster. (Accessed 17.10.2019). 2008. URL: http://www.aquaret.com/images/stories/aquaret/pdf/wven_red.pdf.

[39] World Energy Council. *World Energy Perspective: Costs of Energy Technologies.* ISBN 978 0 94612 130 4. Buntingford, England: Regency House, 2013.

[40] Ocean Energy Systems. *International Levelised Cost of Energy for Ocean Energy Technologies.* Tech. rep. International Energy Agency, 2015.

[41] EIA. "Levelized cost and levelized avoided cost of new generation resources in the annual energy outlook 2016". In: *Energy Information Administration, Washington DC* (2016).

[42] E. Rusu and F. Onea. "A review of the technologies for wave energy extraction". In: *Clean Energy* 2.1 (2018), pp. 10–19.

[43] L. Castro-Santos, G. P. Garcia, A. Estanqueiro, and P. A. Justino. "The Levelized Cost of Energy (LCOE) of wave energy using GIS based analysis: The case study of

Portugal". In: *International Journal of Electrical Power & Energy Systems* 65 (2015), pp. 21–25.

[44] A. De Andres, J. Maillet, J. Hals Todalshaug, P. Möller, D. Bould, and H. Jeffrey. "Techno-economic related metrics for a wave energy converters feasibility assessment". In: *Sustainability* 8.11 (2016), p. 1109.

[45] L. Castro-Santos, E. Martins, and C Guedes Soares. "Methodology to calculate the costs of a floating offshore renewable energy farm". In: *Energies* 9.5 (2016), p. 324.

[46] A. d. O. Falcão. "Wave-power absorption by a periodic linear array of oscillating water columns". In: *Ocean Engineering* 29.10 (2002), pp. 1163–1186.

[47] J.-R. Nader, S.-P. Zhu, and P. Cooper. "Hydrodynamic and energetic properties of a finite array of fixed oscillating water column wave energy converters". In: *Ocean Engineering* 88 (2014), pp. 131–148.

[48] J.-R. Nader, S.-P. Zhu, P. Cooper, and B. Stappenbelt. "A finite-element study of the efficiency of arrays of oscillating water column wave energy converters". In: *Ocean Engineering* 43 (2012), pp. 72–81.

[49] A. Babarit. "On the park effect in arrays of oscillating wave energy converters". In: *Renewable Energy* 58 (2013), pp. 68–78.

[50] B. Devolder, V. Stratigaki, P. Troch, and P. Rauwoens. "CFD simulations of floating point absorber wave energy converter arrays subjected to regular waves". In: *Energies* 11.3 (2018), p. 641.

[51] I. Penesis, R. Manasseh, J.-R. Nader, S. De Chowdhury, A. Fleming, G. Macfarlane, and M. K. Hasan. "Performance of ocean wave-energy arrays in Australia". In: *3rd Asian Wave and Tidal Energy Conference (AWTEC 2016)*. Vol. 1. 2016, pp. 246–253.

[52] J.-R. Nader, A. Fleming, G. Macfarlane, I. Penesis, and R. Manasseh. "Novel experimental modelling of the hydrodynamic interactions of arrays of wave energy converters". In: *International Journal of Marine Energy* 20 (2017), pp. 109–124.

[53] A. Fleming and R. Manasseh. "Preliminary experimental observation of surface currents produced by simulating WEC radiation and diffraction wave fields". In: *The 12th European Wave and Tidal Energy Conference*. 2017, pp. 802–1.

[54] A Fleming, J. Nader, G MacFarlane, I Penesis, and R Manasseh. "Experimental investigation of WEC array interactions". In: *Australian Ocean Renewable Energy Symposium (AORES)*. 2016, A20.

[55] P. Troch, V. Stratigaki, T. Stallard, D. Forehand, M. Folley, J. P. Kofoed, M. Benoit, A. Babarit, M. Vantorre, and J. Kirkegaard. "An overview of the WECwakes project: Physical modelling of an array of 25 wave energy converters". In: *Proceedings of the 3rd IAHR Europe Congress, Porto, Portugal*. Vol. 16. 2014.

[56] M. Folley, A. Babarit, B. Child, D. Forehand, L. O'Boyle, K. Silverthorne, J. Spinneken, V. Stratigaki, and P. Troch. "A review of numerical modelling of wave energy converter arrays". In: *ASME 2012 31st International Conference on Ocean, Offshore and Arctic Engineering*. American Society of Mechanical Engineers Digital Collection. 2013, pp. 535–545.

[57] S. Naty, A. Viviano, and E. Foti. "Wave energy exploitation system integrated in the coastal structure of a Mediterranean port". In: *Sustainability* 8.12 (2016), p. 1342.

[58] S. Naty, A. Viviano, and E. Foti. “Feaseability study of a WEC integrated in the port of Giardini Naxos, Italy”. In: *Coastal Engineering Proceedings* 1.35 (2017), p. 22.

[59] Y. Masuda. “Wave-activated generator”. In: *Int. Coll. on the Expositions of the Oceans (Trans.), Bordeaux, France* (1971).

[60] D. Evans. “The oscillating water column wave-energy device”. In: *IMA Journal of Applied Mathematics* 22.4 (1978), pp. 423–433.

[61] D. Evans. “Wave-power absorption by systems of oscillating surface pressure distributions”. In: *Journal of Fluid Mechanics* 114 (1982), pp. 481–499.

[62] A. J. Sarmento and A. d. O. Falcão. “Wave generation by an oscillating surface-pressure and its application in wave-energy extraction”. In: *Journal of Fluid Mechanics* 150 (1985), pp. 467–485.

[63] R Meir. “The development of the oscillating water column”. In: *London-Heathrow 22-23 November 1978* (1978).

[64] M. E. McCormick and W. E. Sheehan. “Positive drift of backward-bent duct barge”. In: *Journal of Waterway, Port, Coastal, and Ocean Engineering* 118.1 (1992), pp. 106–111.

[65] Y. Masuda, L. Xianguang, and G. Xiangfan. “High performance of cylinder float backward bent duct buoy (BBDB) and its use in European seas”. In: *Proceedings of (First) European Wave Energy Symposium*. 1993, pp. 323–37.

[66] Y Masuda, H Kimura, X Liang, X Gao, R. Mogensen, and T Anderson. “Regarding BBDB wave power generation plant”. In: *Proceedings of 2nd European Wave Power Conference*. 1995, pp. 69–76.

[67] D. Hong, S. Hong, and S. Hong. “Numerical study of the motions and drift force of a floating OWC device”. In: *Ocean Engineering* 31.2 (2004), pp. 139–164.

[68] D. Hong, S. Hong, and S. Hong. “Numerical study on the reverse drift force of floating BBDB wave energy absorbers”. In: *Ocean Engineering* 31.10 (2004), pp. 1257–1294.

[69] J.-H. Kim, J.-M. Lew, D.-C. Hong, and S.-W. Hong. “A study on motion and wave drift force of a BBDB type OWC wave energy device”. In: *Journal of Ocean Engineering and Technology* 20.2 (2006), pp. 22–28.

[70] J.-H. Kim, J.-M. Lew, D.-C. Hong, Y.-S. Kim, H.-S. Choi, S.-W. Hong, et al. “A study on motion of a BBDB type OWC wave energy device considering pneumatic damping coefficients in the duct”. In: *The Seventeenth International Offshore and Polar Engineering Conference*. International Society of Offshore and Polar Engineers. 2007.

[71] Y. Masuda and M. E. McCormick. “Experiences in pneumatic wave energy conversion in Japan”. In: *Utilization of Ocean Waves—Wave to Energy Conversion*. ASCE. 1986, pp. 1–33.

[72] A. Babarit, J. Hals, M. Muliawan, A. Kurniawan, T. Moan, and J. Krokstad. “Numerical benchmarking study of a selection of wave energy converters”. In: *Renewable Energy* 41 (2012), pp. 44–63.

[73] J. Lavelle and J. P. Kofoed. *Power Production Analysis of the OE Buoy WEC for the CORES Project.* DCE Technical Reports No. 119. Aalborg: Department of Civil Engineering, Aalborg University, 2011.

[74] T. M. Ferguson, G. Macfarlane, A. Fleming, and I. Penesis. "PIV investigation of 3-dimensional flow within an oscillating water column". In: *International Journal of Marine Energy* 11 (2015), pp. 120–131.

[75] T. M. Ferguson, I. Penesis, G. Macfarlane, and A. Fleming. "A PIV investigation of OWC operation in regular, polychromatic and irregular waves". In: *Renewable Energy* 103 (2017), pp. 143–155.

[76] T. M. Ferguson, A. Fleming, I. Penesis, and G. Macfarlane. "Improving OWC performance prediction using polychromatic waves". In: *Energy* 93 (2015), pp. 1943–1952.

[77] A. Fleming, I. Penesis, G. Macfarlane, N. Bose, and T. Denniss. "Energy balance analysis for an oscillating water column wave energy converter". In: *Ocean Engineering* 54 (2012), pp. 26–33.

[78] A. Fleming, I. Penesis, L. Goldsworthy, G. Macfarlane, N. Bose, and T. Denniss. "Phase averaged flow analysis in an oscillating water column wave energy converter". In: *Journal of Offshore Mechanics and Arctic Engineering* 135.2 (2013), p. 021901.

[79] A. Fleming, I. Penesis, G. Macfarlane, N. Bose, and S. Hunter. "Phase averaging of the velocity fields in an oscillating water column using splines". In: *Proceedings of the Institution of Mechanical Engineers, Part M: Journal of Engineering for the Maritime Environment* 226.4 (2012), pp. 335–345.

[80] A. N. Fleming and G. J. Macfarlane. "Experimental flow field comparison for a series of scale model oscillating water column wave energy converters". In: *Marine Structures* 52 (2017), pp. 108–125.

[81] A. Fleming and G. Macfarlane. "In-situ orifice calibration for reversing oscillating flow and improved performance prediction for oscillating water column model test experiments". In: *International Journal of Marine Energy* 17 (2017), pp. 147–155.

[82] A. Kamath, H. Bihs, and Ø. A. Arntsen. "Numerical modeling of power take-off damping in an oscillating water column device". In: *International Journal of Marine Energy* 10 (2015), pp. 1–16.

[83] I López, B Pereiras, F Castro, and G. Iglesias. "Optimisation of turbine-induced damping for an OWC wave energy converter using a RANS–VOF numerical model". In: *Applied Energy* 127 (2014), pp. 105–114.

[84] I López, B Pereiras, F Castro, and G Iglesias. "Holistic performance analysis and turbine-induced damping for an OWC wave energy converter". In: *Renewable Energy* 85 (2016), pp. 1155–1163.

[85] Z. Liu, B. Hyun, J. Jin, K. Hong, and Y. Lee. "OWC air chamber performance prediction under impulse turbine damping effects". In: *Science China Technological Sciences* 59.4 (2016), pp. 657–666.

[86] A. Thakker, Z. Usmani, and T. Dhanasekaran. "Effects of turbine damping on performance of an impulse turbine for wave energy conversion under different sea conditions using numerical simulation techniques". In: *Renewable Energy* 29.14 (2004), pp. 2133–2151.

[87] I López, B Pereiras, F Castro, and G. Iglesias. "Performance of OWC wave energy converters: influence of turbine damping and tidal variability". In: *International Journal of Energy Research* 39.4 (2015), pp. 472–483.

[88] A. Elhanafi and C. J. Kim. "Experimental and numerical investigation on wave height and power take–off damping effects on the hydrodynamic performance of an offshore–stationary OWC wave energy converter". In: *Renewable Energy* 125 (2018), pp. 518–528.

[89] J. Orphin, I. Penesis, and J.-R. Nader. "Uncertainty analysis for a wave energy converter: the Monte Carlo method". In: *AWTEC 2018 Proceedings* (2018), p. 444.

[90] N Ambli, K Bonke, O Malmo, and A Reitan. "The Kvaerner multiresonant OWC". In: *Proc of the 2nd Int Symposium on Wave Energy Utilisation, Trondheim, Norway, Tapir*. 1982.

[91] O Malmo and A Reitan. "Development of the Kvaerner multiresonant OWC". In: *Hydrodynamics of Ocean Wave-Energy Utilization*. Springer, 1986, pp. 57–67.

[92] A. d. O. Falcão. "The shoreline OWC wave power plant at the Azores". In: *Fourth European Wave Energy Conference, Aalborg, Denmark, Dec*. 2000, pp. 4–6.

[93] A Brito-Melo, F Neumann, A. Sarmento, et al. "Full-scale data assessment in OWC Pico plant". In: *The Seventeenth International Offshore and Polar Engineering Conference*. International Society of Offshore and Polar Engineers. 2007.

[94] A. Pecher, J. Kofoed, I Le Crom, F Neumann, E. d. B. Azevedo, et al. "Performance assessment of the Pico OWC power plant following the EquiMar Methodology". In: *The Twenty-First International Offshore and Polar Engineering Conference*. International Society of Offshore and Polar Engineers. 2011.

[95] A. F. Falcão and J. C. Henriques. "Oscillating-water-column wave energy converters and air turbines: A review". In: *Renewable Energy* 85 (2016), pp. 1391–1424.

[96] T. Whittaker, W Beattie, M Folley, C Boake, A Wright, M Osterried, and T Heath. "The LIMPET wave power project–the first years of operation". In: *Renewable Energy* (2004).

[97] T. Heath, T. Whittaker, and C. Boake. "The design, construction and operation of the LIMPET wave energy converter (Islay, Scotland)[Land Installed Marine Powered Energy Transformer]". In: *European Wave Energy Conference, Aalborg (Denmark)*. 2000, pp. 49–55.

[98] C. B. Boake, T. J. Whittaker, M. Folley, H. Ellen, et al. "Overview and initial operational experience of the LIMPET wave energy plant". In: *The Twelfth International Offshore and Polar Engineering Conference*. International Society of Offshore and Polar Engineers. 2002.

[99] T. Thorpe. *An assessment of the ART OSPREY wave energy device*. ETSU, 1995.

[100] T. W. Thorpe et al. *A brief review of wave energy*. Harwell Laboratory, Energy Technology Support Unit London, 1999.

[101] I. Penesis, G. Macfarlane, S. Hunter, N. Bose, and A. Baghaei. "Wave Energy: an example of collaboration between industry and academia in Australia". In: *Journal of Ocean Technology* 8.1 (2013).

[102] L. D. Appleyard. “Design and Construction of GreenWAVE Energy Converter for Shallow Waters off South Australia”. In: *Journal of Civil Engineering and Architecture* 9 (2015), pp. 1179–1184.

[103] V. Raju, M Ravindran, and P. Koola. “Energy from sea waves-the Indian wave energy programme”. In: *Proc. of the Third Symposium on Ocean Wave Energy Utilisation*. 1991.

[104] A. A. Wells. *Rotary transducers*. US Patent 4,221,538. 1980.

[105] T Setoguchi, M Takao, Y Kinoue, K Kaneko, S Santhakumar, M Inoue, et al. “Study on an impulse turbine for wave energy conversion”. In: *The Ninth International Offshore and Polar Engineering Conference*. International Society of Offshore and Polar Engineers. 1999.

[106] R Curran and L. Gato. “The energy conversion performance of several types of Wells turbine designs”. In: *Proceedings of the Institution of Mechanical Engineers, Part A: Journal of Power and Energy* 211.2 (1997), pp. 133–145.

[107] T.-H. Kim, M. Takao, T. Setoguchi, K. Kaneko, and M. Inoue. “Performance comparison of turbines for wave power conversion”. In: *International Journal of Thermal Sciences* 40.7 (2001), pp. 681–689.

[108] M Torresi, S. Camporeale, P. Strippoli, and G Pascazio. “Accurate numerical simulation of a high solidity Wells turbine”. In: *Renewable Energy* 33.4 (2008), pp. 735–747.

[109] S. H. Salter, J. Taylor, and N. Caldwell. “Power conversion mechanisms for wave energy”. In: *Proceedings of the Institution of Mechanical Engineers, Part M: Journal of Engineering for the Maritime Environment* 216.1 (2002), pp. 1–27.

[110] S. Okuhara, M. Takao, A. Takami, and T. Setoguchi. “Wells turbine for wave energy conversion—improvement of the performance by means of impulse turbine for bi-directional flow”. In: *Open Journal of Fluid Dynamics* 3.02 (2013), p. 36.

[111] A Brito-Melo, L. Gato, and A. Sarmento. “Analysis of Wells turbine design parameters by numerical simulation of the OWC performance”. In: *Ocean Engineering* 29.12 (2002), pp. 1463–1477.

[112] S Raghunathan. “The Wells air turbine for wave energy conversion”. In: *Progress in Aerospace Sciences* 31.4 (1995), pp. 335–386.

[113] J. Henriques, W Sheng, A. Falcão, and L. Gato. “A comparison of biradial and wells air turbines on the Mutriku breakwater OWC wave power plant”. In: *ASME 2017 36th International Conference on Ocean, Offshore and Arctic Engineering*. American Society of Mechanical Engineers Digital Collection. 2017.

[114] M. Folley, R. Curran, and T. Whittaker. “Comparison of LIMPET contra-rotating wells turbine with theoretical and model test redictions”. In: *Ocean Engineering* 33(8-9) (June 2006), pp. 1056–1069.

[115] T. V. Heath. “A review of oscillating water columns.” In: *Philosophical Transactions of the Royal Society A: Mathematical, Physical and Engineering Sciences* 370.1959 (2012), pp. 235–245.

[116] K Kaneko, T Setoguchi, S Raghunathan, et al. "Self-rectifying turbines for wave energy conversion". In: *The First International Offshore and Polar Engineering Conference*. International Society of Offshore and Polar Engineers. 1991.

[117] T. Setoguchi, S Santhakumar, H Maeda, M Takao, and K Kaneko. "A review of impulse turbines for wave energy conversion". In: *Renewable Energy* 23.2 (2001), pp. 261–292.

[118] A. Fleming, G. Macfarlane, S. Hunter, and T. Denniss. "Power performance prediction for a vented oscillating water column wave energy converter with a unidirectional air turbine power take-off". In: *Proceedings of the 12th European Wave and Tidal Energy Conference*. Ed. by EWTEC. 2017, pp. 1204–1.

[119] M. Mustapa, O. Yaakob, Y. M. Ahmed, C.-K. Rheem, K. Koh, and F. A. Adnan. "Wave energy device and breakwater integration: A review". In: *Renewable and Sustainable Energy Reviews* 77 (2017), pp. 43–58.

[120] H Maeda, T Kinoshita, K Masuda, and W Kato. "Fundamental research on oscillating water column wave power absorbers". In: *Journal of Energy Resources Technology* 107.1 (1985), pp. 81–86.

[121] H Ohneda, S Igarashi, O Shinbo, S Sekihara, K Suzuki, H Kubota, H Ogino, and H Morita. "Construction procedure of a wave power extracting caisson breakwater". In: *Proceedings of 3rd Symposium on Ocean Energy Utilization*. 1991, pp. 171–179.

[122] S. Takahashi, H. Nakada, H. Ohneda, and M. Shikamori. "Wave power conversion by a prototype wave power extracting caisson in Sakata port". In: *Coastal Engineering 1992*. American Society of Civil Engineers, 1993, pp. 3440–3453.

[123] E Martins, F. S. Ramos, L Carrilho, P Justino, L Gato, L Trigo, and F Neumann. "CeoDouro project: overall design of an OWC in the new Oporto breakwater". In: *Proceedings of 6th European Wave Tidal Energy Conference*. 2005, pp. 273–80.

[124] P. Boccotti. "Caisson breakwaters embodying an OWC with a small opening—Part I: Theory". In: *Ocean Engineering* 34.5-6 (2007), pp. 806–819.

[125] P. Boccotti, P. Filianoti, V. Fiamma, and F. Arena. "Caisson breakwaters embodying an OWC with a small opening—Part II: A small-scale field experiment". In: *Ocean Engineering* 34.5-6 (2007), pp. 820–841.

[126] H. Martins-Rivas and C. C. Mei. "Wave power extraction from an oscillating water column at the tip of a breakwater". In: *Journal of Fluid Mechanics* 626 (2009), pp. 395–414.

[127] H. Martins-Rivas and C. C. Mei. "Wave power extraction from an oscillating water column along a straight coast". In: *Ocean Engineering* 36.6-7 (2009), pp. 426–433.

[128] Y Torre-Enciso, I Ortubia, L. L. De Aguileta, and J Marqués. "Mutriku wave power plant: from the thinking out to the reality". In: *Proceedings of the 8th European Wave and Tidal Energy Conference, Uppsala, Sweden*. Vol. 710. 2009, pp. 319–329.

[129] E. Medina-Lopez, W. Allsop, A. Dimakopoulos, and T. Bruce. "Conjectures on the Failure of the OWC Breakwater at Mutriku". In: *Proceedings of Coastal Structures and Solutions to Coastal Disasters Joint Conference, Boston, Massachusetts*. 2015.

[130] F.-X. Faÿ, E. Robles, M. Marcos, E. Aldaiturriaga, and E. F. Camacho. "Sea trial results of a predictive algorithm at the Mutriku Wave power plant and controllers assess-

ment based on a detailed plant model". In: *Renewable Energy* 146 (2020), pp. 1725–1745.

[131] F Arena, G Malara, and A Romolo. "A U-OWC wave energy converter in the Mediterranean Sea: Preliminary results on the monitoring system of the first prototype". In: *Renewable Energy Offshore; Guedes Soares, C., Ed.; Taylor & Francis Group: London, UK* (2015), pp. 417–421.

[132] F. Arena, A. Romolo, G. Malara, and A. Ascanelli. "On design and building of a U-OWC wave energy converter in the Mediterranean Sea: a case study". In: *ASME 2013 32nd International Conference on Ocean, Offshore and Arctic Engineering*. American Society of Mechanical Engineers Digital Collection. 2013.

[133] F. Arena, V. Fiamma, V. Laface, G. Malara, A. Romolo, A. Viviano, G. Sannino, and A. Carillo. "Installing U-OWC devices along Italian coasts". In: *ASME 2013 32nd International Conference on Ocean, Offshore and Arctic Engineering*. American Society of Mechanical Engineers. 2013, V008T09A061–V008T09A061.

[134] F Arena, A Romolo, G Malara, V Fiamma, and V Laface. "The first worldwide application at full-scale of the REWEC3 device in the Port of Civitavecchia: Initial energetic performances". In: *Proceedings of the 2nd International Conference on Renewable Energies Offshore (RENEW2016)*. 2016, pp. 303–311.

[135] F Arena, A Romolo, G Malara, V Fiamma, and V Laface. "Validation of the U-Oscillating Water Column model by full-scale experimental data". In: *Proceedings of the 12th European Wave and Tidal Energy Conference*. 2017.

[136] G. Malara, A. Romolo, V. Fiamma, and F. Arena. "On the modelling of water column oscillations in U-OWC energy harvesters". In: *Renewable Energy* 101 (2017), pp. 964–972.

[137] G Malara, R. Gomes, F Arena, J. Henriques, L. Gato, and A. Falcão. "The influence of three-dimensional effects on the performance of U-type oscillating water column wave energy harvesters". In: *Renewable Energy* 111 (2017), pp. 506–522.

[138] G. Malara and F. Arena. "Response of U-Oscillating Water Column arrays: semi-analytical approach and numerical results". In: *Renewable Energy* 138 (2019), pp. 1152–1165.

[139] E Koutandos, P Prinos, and X Gironella. "Floating breakwaters under regular and irregular wave forcing: reflection and transmission characteristics". In: *Journal of Hydraulic Research* 43.2 (2005), pp. 174–188.

[140] L. Z. Hales. *Floating Breakwaters: State-of-the-Art Literature Review*. Tech. rep. Coastal Engineering Research Center Fort Belvoir VA, 1981.

[141] B. H. Adee. "A Review of Developments and Problems in Using Floating Breakwaters". In: *Offshore Technology Conference*. 1976. DOI: 10.4043/2543-MS.

[142] R. C. McGregor and N. S. Miller. "Scrap tyre breakwaters in coastal engineering". In: *Coastal Engineering Proceedings* 1.16 (1978).

[143] J Joly. "On Floating Breakwaters". In: *Scientific Proceedings of the Royal Dublin Society*. Vol. 10. 1905, pp. 378–383.

[144] B. L. McCartney. "Floating breakwater design". In: *Journal of Waterway, Port, Coastal, and Ocean Engineering* 111.2 (1985), pp. 304–318.

[145] A. C. Biesheuvel. “Effectiveness of Floating Breakwaters: Wave attenuating floating structures”. MA thesis. Netherlands: TU Delft, 2013.

[146] J. Dai, C. M. Wang, T. Utsunomiya, and W. Duan. “Review of recent research and developments on floating breakwaters”. In: *Ocean Engineering* 158 (2018), pp. 132–151.

[147] H. Teh. “Hydraulic performance of free surface breakwaters: A review”. In: *Sains Malaysiana* 42.9 (2013), pp. 1301–1310.

[148] J. Mani. “Design of Y-frame floating breakwater”. In: *Journal of Waterway, Port, Coastal, and Ocean Engineering* 117.2 (1991), pp. 105–119.

[149] K Murali and J. Mani. “Performance of cage floating breakwater”. In: *Journal of Waterway, Port, Coastal, and Ocean Engineering* 123.4 (1997), pp. 172–179.

[150] N.-K. Liang, J.-S. Huang, and C.-F. Li. “A study of spar buoy floating breakwater”. In: *Ocean Engineering* 31.1 (2004), pp. 43–60.

[151] H. M. Teh, K. V. John, and A. M. Hashim. “Hydraulic investigation of the H-type floating breakwater”. In: *Oceans 2014-Taipei*. IEEE. 2014, pp. 1–5.

[152] R. Kennedy and J Marsalek. “Flexible Porous Floating Breakwaters”. In: *Coastal Engineering 1968*. ASCE, 1968, pp. 1095–1103.

[153] H. Wang and Z. Sun. “Experimental study of a porous floating breakwater”. In: *Ocean Engineering* 37.5-6 (2010), pp. 520–527.

[154] K.-H. Wang and X. Ren. “Water waves on flexible and porous breakwaters”. In: *Journal of Engineering Mechanics* 119.5 (1993), pp. 1025–1047.

[155] H.-Y. Wang and Z.-C. Sun. “Experimental study on the influence of geometrical configuration of porous floating breakwater on performance”. In: *Journal of Marine Science and Technology* 18.4 (2010), pp. 574–579.

[156] S. Sannasiraj, V Sundar, and R Sundaravadivelu. “Mooring forces and motion responses of pontoon-type floating breakwaters”. In: *Ocean Engineering* 25.1 (1998), pp. 27–48.

[157] A. Williams and A. Abul-Azm. “Dual pontoon floating breakwater”. In: *Ocean Engineering* 24.5 (1997), pp. 465–478.

[158] S. S. Bhat. “Performance of twin-pontoon floating breakwaters”. PhD thesis. University of British Columbia, 1998.

[159] F. He, Z. Huang, and A. W.-K. Law. “An experimental study of a floating breakwater with asymmetric pneumatic chambers for wave energy extraction”. In: *Applied Energy* 106 (2013), pp. 222–231.

[160] J. A. Rea, J. F. Kelly, R. Alcorn, and D. O’Sullivan. “Development and operation of a power take off rig for ocean energy research and testing”. In: *Proceedings of the Ninth EWTEC 2011, Southampton, UK* (2011).

[161] R. Alcorn, A. Blavette, M. Healy, and A. Lewis. “FP7 EU funded CORES wave energy project: a coordinators’ perspective on the Galway Bay sea trials”. In: *Underwater Technology* (2014).

[162] H Hotta, T Miyazaki, Y Washio, and S Ishii. “On the performance of the wave power device Kaimei—the results on the open sea tests”. In: *Proceedings of the 7th International Offshore and Polar Engineering Conference*. 1988, pp. 91–96.

[163] T Miyazaki, Y Masuda, et al. “Tests On The Wave Power Generator ”Kaimei””. In: *Offshore Technology Conference*. Offshore Technology Conference. 1980.

[164] Y. Masuda. “An experience of wave power generator through tests and improvement”. In: *Hydrodynamics of Ocean Wave-Energy Utilization*. Springer, 1986, pp. 445–452.

[165] B Holmes and K Nielson. *Guidelines for the Development & Testing of Wave Energy Systems*. Report T02-2.1. OES-IA Annex II Task 2.1, 2010.

[166] T. Vyzikas, S. Deshoulières, M. Barton, O. Giroux, D. Greaves, and D. Simmonds. “Experimental investigation of different geometries of fixed oscillating water column devices”. In: *Renewable Energy* 104 (2017), pp. 248–258.

[167] S. J. Ashlin, V Sundar, and S. Sannasiraj. “Effects of bottom profile of an oscillating water column device on its hydrodynamic characteristics”. In: *Renewable Energy* 96 (2016), pp. 341–353.

[168] Y. Liu, H. Shi, Z. Liu, and Z. Ma. “Experiment study on a new designed OWC caisson breakwater”. In: *2011 Asia-Pacific Power and Energy Engineering Conference*. IEEE. 2011, pp. 1–5.

[169] Z. Liu, H. Shi, and B.-S. Hyun. “Practical design and investigation of the breakwater OWC facility in China”. In: *Proc. 8th European Wave & Tidal Energy Conf., Uppsala, Sweden*. 2009.

[170] R. Ojima, S. Suzumura, and Y. Goda. “Theory and experiments on extractable wave power by an oscillating water-column type breakwater caisson”. In: *Coastal Engineering in Japan* 27.1 (1984), pp. 315–326.

[171] A. Viviano, S. Naty, E. Foti, T. Bruce, W. Allsop, and D. Vicinanza. “Large-scale experiments on the behaviour of a generalised Oscillating Water Column under random waves”. In: *Renewable Energy* 99 (2016), pp. 875–887.

[172] S. J. Ashlin, S. Sannasiraj, and V Sundar. “Performance of an array of oscillating water column devices integrated with an offshore detached breakwater”. In: *Ocean Engineering* 163 (2018), pp. 518–532.

[173] F. Madhi, M. E. Sinclair, and R. W. Yeung. “The “Berkeley Wedge”: an asymmetrical energy-capturing floating breakwater of high performance”. In: *Marine Systems & Ocean Technology* 9.1 (2014), pp. 5–16.

[174] F. He and Z. Huang. “Hydrodynamic performance of pile-supported OWC-type structures as breakwaters: an experimental study”. In: *Ocean Engineering* 88 (2014), pp. 618–626.

[175] F. He, M. Li, and Z. Huang. “An experimental study of pile-supported OWC-type breakwaters: energy extraction and vortex-induced energy loss”. In: *Energies* 9.7 (2016), p. 540.

[176] D. Ning, X. Zhao, M. Zhao, and H. Kang. “Experimental investigation on hydrodynamic performance of a dual pontoon–power take-off type wave energy converter integrated with floating breakwaters”. In: *Proceedings of the Institution of Mechani-*

cal Engineers, Part M: Journal of Engineering for the Maritime Environment 233.4 (2019), pp. 991–999.

[177] D. Ning, X. Zhao, M. Göteman, and H. Kang. "Hydrodynamic performance of a pile-restrained WEC-type floating breakwater: An experimental study". In: *Renewable Energy* 95 (2016), pp. 531–541.

[178] X. Zhao and D. Ning. "Experimental investigation of breakwater-type WEC composed of both stationary and floating pontoons". In: *Energy* 155 (2018), pp. 226–233.

[179] B Zanuttigh, L Martinelli, M Castagnetti, P Ruol, J. P. Kofoed, and P. Frigaard. "Integration of wave energy converters into coastal protection schemes". In: *Proc ICOE* (2010).

[180] P. Ruol, B. Zanuttigh, L. Martinelli, P. Kofoed, and P. Frigaard. "Near-shore floating wave energy converters: Applications for coastal protection". In: *Coastal Engineering Proceedings* 1.32 (2011), p. 61.

[181] X.-L. Zhao, D.-Z. Ning, and D. Liang. "Experimental investigation on hydrodynamic performance of a breakwater-integrated WEC system". In: *Ocean Engineering* 171 (2019), pp. 25–32.

[182] F. He, Z. Huang, and A. W.-K. Law. "Hydrodynamic performance of a rectangular floating breakwater with and without pneumatic chambers: An experimental study". In: *Ocean Engineering* 51 (2012), pp. 16–27.

[183] F. He, J. Leng, and X. Zhao. "An experimental investigation into the wave power extraction of a floating box-type breakwater with dual pneumatic chambers". In: *Applied Ocean Research* 67 (2017), pp. 21–30.

[184] J.-R. Nader. "Hydrodynamic analysis and performance of a single fixed circular OWC device". In: *11th European Wave and Tidal Energy Conference.* 2015, pp. 1–7.

[185] D. V. Evans and R. Porter. "Efficient Calculation of Hydrodynamic Properties of OWC-Type Devices". In: *Journal of Offshore Mechanics and Arctic Engineering* 119.4 (Nov. 1997), pp. 210–218. ISSN: 0892-7219.

[186] R Porter and D. Evans. "Efficient calculation of hydrodynamic properties of OWC-type devices". In: *Journal of Offshore Mechanics and Arctic Engineering* 119.4 (1997), pp. 210–18.

[187] R. Grennell, D. Howe, J.-R. Nader, and G. Macfarlane. "Performance analysis of an OWC device integrated within a porous breakwater". In: *The 4th Asian Wave and Tidal Energy Conference (AWTEC 2018).* 2018, p. 451.

[188] D. Howe, J.-R. Nader, J. Orphin, and G. Macfarlane. "The effect of lip extrusion on performance of a Breakwater Integrated Bent Duct OWC WEC". In: *12th European Wave and Tidal Energy Conference.* Vol. 2017. 2017, pp. 1–9.

[189] J. Orphin, J.-R. Nader, I. Penesis, and D. Howe. "Experimental uncertainty analysis of an OWC wave energy converter". In: *Proceedings of 12th European Wave and Tidal Energy Conference.* 2017.

[190] R. Gomes, J. Henriques, L. Gato, A. d. O. Falcão, and C Guedes Soares. "Testing of a small-scale model of a heaving floating OWC in a wave channel and comparison with numerical results". In: *Renewable Energies Offshore (ed. C. Guedes Soares)* (2015), pp. 445–454.

[191] A. Sarmento. “Model-test optimization of an OWC wave power plant”. In: *International Journal of Offshore and Polar Engineering* 3.01 (1993).

[192] A. Sarmento. “Wave flume experiments on two-dimensional oscillating water column wave energy devices”. In: *Experiments in Fluids* 12.4-5 (1992), pp. 286–292.

[193] J Nader. “Limitation of the second-order wave theory in low frequencies”. In: *Marine Structures* 43 (2015), pp. 143–147.

[194] D. Howe, J.-R. Nader, and G Macfarlane. “Experimental analysis into the effects of air compressibility in OWC model testing”. In: *AWTEC 2018 Proceedings*. National Taiwan Ocean University, 2018, p. 449.

[195] A. Elhanafi, G. Macfarlane, A. Fleming, and Z. Leong. “Experimental and numerical investigations on the hydrodynamic performance of a floating–moored oscillating water column wave energy converter”. In: *Applied Energy* 205 (2017), pp. 369–390.

[196] S Anand, V Jayashankar, S Nagata, K Toyota, M Takao, and T Setoguchi. “Turbines for wave energy plants”. In: *Proceedings of the 8th International Symposium on Experimental and Computational Aerothermodynamics of Internal Flows*. 2007, pp. 1–7.

[197] O’Gorman, Shannon. “Using mesh material to simulat the Wells turbine damping on an oscillating water column”. Undergrauate Thesis, National Centre for Maritime Engineering and Hydrodynamics, Australian Maritime College. 2014. URL: http://encore.lib.utas.edu.au/iii/encore/record/C__Rb2360348.

[198] T McCombes, C. Johnstone, B Holmes, L. Myers, A. Bahaj, and J. Kofoed. “Best practice for tank testing of small marine energy devices”. In: *EquiMar Project* (2010), pp. 1–48.

[199] ITTC. *Wave Energy Converter Model Test Experiments*. Recommended Procedures and Guidelines 7.5-02-07-03.7. International Towing Tank Conference, 2017.

[200] P. Lange, B Jähne, J Tschiersch, and I Ilmberger. “Comparison between an amplitude-measuring wire and a slope-measuring laser water wave gauge”. In: *Review of Scientific Instruments* 53.5 (1982), pp. 651–655.

[201] J. McKendrick. “NATO School on Instruments and Methods in Air-Sea Interaction 18–27 April 1978, Ustaoset, Norway”. In: *Bulletin of the American Meteorological Society* (1979), pp. 231–233.

[202] R. H. Stewart. “Air-Sea Interaction: Instruments and Methods”. In: ed. by Plenum Press, New York. Springer US, 1980. Chap. Ocean Wave Measurement Techniques, pp. 447–470.

[203] J.-R. Nader, S.-P. Zhu, P. Cooper, and B. Stappenbelt. “A finite element model for efficiency of a moored floating OWC device in regular waves”. In: *ASME 2011 30th International Conference on Ocean, Offshore and Arctic Engineering*. American Society of Mechanical Engineers. 2011, pp. 511–519.

[204] ANSYS®. *Academic Research Release 12.0*.

[205] K Günaydın and M. Kabdaşlı. “Investigation of Π-type breakwaters performance under regular and irregular waves”. In: *Ocean Engineering* 34.7 (2007), pp. 1028–1043.

[206] K Günaydın and M. Kabdaşlı. "Performance of solid and perforated U-type breakwaters under regular and irregular waves". In: *Ocean Engineering* 31.11-12 (2004), pp. 1377–1405.

[207] P. Ruol, L. Martinelli, and P. Pezzutto. "Formula to predict transmission for Π-type floating breakwaters". In: *Journal of Waterway, Port, Coastal, and Ocean Engineering* 139.1 (2012), pp. 1–8.

[208] P. Ruol, L. Martinelli, and P. Pezzutto. "Limits of the new transmission formula for Π-type floating breakwaters". In: *Coastal Engineering Proceedings* 1.33 (2012), p. 47.

[209] P. Ruol, L. Martinelli, and P. Pezzutto. "Experimental and numerical investigation of the effect of mooring stiffness on the behaviour of Π-type floating breakwaters". In: *The Twenty-Second International Offshore and Polar Engineering Conference*. International Society of Offshore and Polar Engineers. 2012.

[210] A. Elhanafi, G. Macfarlane, A. Fleming, and Z. Leong. "Scaling and air compressibility effects on a three-dimensional offshore stationary OWC wave energy converter". In: *Applied Energy* 189 (2017), pp. 1–20.

[211] S Raghunathan. "A methodology for Wells turbine design for wave energy conversion". In: *Proceedings of the Institution of Mechanical Engineers, Part A: Journal of Power and Energy* 209.3 (1995), pp. 221–232.

[212] ITTC. *Guide to the Expression of Uncertainty in Experimental Hydrodynamics*. in 7.5-02-01-01. International Towing Tank Conference, 2014.

[213] ITTC. *Uncertainty Analysis for a Wave Energy Converter*. in 7.5-02-07-03.12. International Towing Tank Conference, 2017.

[214] D.-Z. Ning, R.-Q. Wang, Q.-P. Zou, and B. Teng. "An experimental investigation of hydrodynamics of a fixed OWC Wave Energy Converter". In: *Applied Energy* 168 (2016), pp. 636–648.

[215] A. Elhanafi, A. Fleming, G. Macfarlane, and Z. Leong. "Numerical hydrodynamic analysis of an offshore stationary–floating oscillating water column–wave energy converter using CFD". In: *International Journal of Naval Architecture and Ocean Engineering* 9.1 (2017), pp. 77–99.

[216] E. P. Mansard and E. Funke. "The measurement of incident and reflected spectra using a least squares method". In: *Coastal Engineering Proceedings* 1.17 (1980).

[217] Qualisys Motion Capture Systems. *Marine & Underwater*. Accessed: 09-12-2019. 2019. URL: http://https://www.qualisys.com/applications/engineering/marine-underwater/.

[218] S. A. Hughes. *Physical models and laboratory techniques in coastal engineering*. Vol. 7. World Scientific, 1993.

[219] S. Chakrabarti. *Offshore Structure Modeling*. Vol. 9. World Scientific, 1994.

[220] R. L. Wiegel. "Diffraction of waves by semi-infinite breakwater". In: *Journal of the Hydraulics Division* 88.1 (1962), pp. 27–44.

[221] U.S. Army Coastal Engineering Research Center. *Shore Protection Manual (Fourth Edition)*. Vol. I. U.S. Govt. Printing Office, 1984, p. 652.

[222] R. W. Yeung and S. H. Sphaier. "Wave-interference effects on a truncated cylinder in a channel". In: *Journal of Engineering Mathematics* 23.2 (1989), pp. 95–117.

[223] S. Calisal and T. Sabuncu. “A study of a heaving vertical cylinder in a towing tank”. In: *Journal of Ship Research* 33.2 (1989), pp. 107–114.

[224] J. H. Vazquez and A. N. Williams. “Hydrodynamic Loads on a Three-Dimensional Body in a Narrow Tank”. In: *Journal of Offshore Mechanics and Arctic Engineering* 116.3 (Aug. 1994), pp. 117–121. ISSN: 0892-7219. DOI: 10.1115/1.2920139.

[225] E.-O. Macagno. “Houle dans un canal présentant un passage en charge”. In: *La Houille Blanche* 1 (1954), pp. 10–37.

[226] A. Elhanafi, G. Macfarlane, A. Fleming, and Z. Leong. “Experimental and numerical investigations on the intact and damage survivability of a floating–moored oscillating water column device”. In: *Applied Ocean Research* 68 (2017), pp. 276–292.

[227] I. Crema, I. Simonetti, L. Cappietti, and H. Oumeraci. “Laboratory experiments on oscillating water column wave energy converters integrated in a very large floating structure”. In: *Proceedings of the 11th European Wave and Tidal Energy Conference, Nantes, France.* 2015, pp. 6–11.

[228] L. Cappietti, I. Simonetti, and I. Crema. “Concept Design of Very Large Floating Structures and Laboratory-Scale Physical Modelling”. In: *ASME 2019 38th International Conference on Ocean, Offshore and Arctic Engineering.* American Society of Mechanical Engineers Digital Collection. 2019.

[229] L. Cappietti, I. Simonetti, and I. Crema. “Laboratory experiments on the performance of an OWC-WEC: Fixed condition versus floating platform-embodied condition”. In: *Proceedings of the 13th European Wave and Tidal Energy Conference, Naples, Italy.* 2015, pp. 6–11.

[230] L. Martinelli, P. Pezzutto, and P. Ruol. “Experimentally based model to size the geometry of a new OWC device, with reference to the Mediterranean Sea wave environment”. In: *Energies* 6.9 (2013), pp. 4696–4720.

[231] B. Holmes. *Tank testing of wave energy conversion systems: marine renewable energy guides.* Tech. rep. Orkney: European Marine Energy Centre, 2009.

[232] A. Lloyd. *Seakeeping: ship behaviour in rough weather.* Ellis Horwood, 1989.

[233] J. D’Errico. *inpaint_nans.* Matlab Central File Exchange. Retrieved June 2019. 2012.

[234] ITTC. *Uncertainty Analysis Instrument Calibration.* in 7.5-01-03-01. International Towing Tank Conference, 2014.

[235] JCGM. *Evaluation of measurement data - guide to the expression of uncertainty in measurement.* in JCGM 100:2008. JCGM, 2008.

[236] H. W. Coleman and W. G. Steele. *Experimentation, validation, and uncertainty analysis for engineers.* John Wiley & Sons, 2018.

[237] B. L. Welch. “The generalization of ’student’s’ problem when several different population variances are involved”. In: *Biometrika* 34.1/2 (1947), pp. 28–35.

[238] F. E. Satterthwaite. “An approximate distribution of estimates of variance components”. In: *Biometrics Bulletin* 2.6 (1946), pp. 110–114.

[239] International Organization for Standardization (ISO). *Uncertainty of measurement – Part 3: Guide to the expression of uncertainty in measurement.* in Guide 98-3:2008. Geneva, CH: International Organization for Standardization, 2008.